ENHANCING SOIL CARBON SEQUESTRATION IN BIOENERGY CROPPING SYSTEMS: INTERACTIONS AMONG SOIL STRUCTURE, ROOT TRAITS, AND SOIL CARBON PROCESSING

By

Jin Ho Lee

A DISSERTATION

Submitted to
Michigan State University
in partial fulfillment of the requirements
for the degree of

Crop and Soil Sciences – Doctor of Philosophy

2024

ABSTRACT

Bioenergy cropping systems play a crucial role in reducing carbon (C) emissions, and particularly with perennial vegetation, which enhances soil C sequestration. The fundamental principles of the C sequestration involve stabilizing C within the soil matrix and promoting additional C inputs into the matrix, with soil pores having a key role in creating micro-environments that influence the sequestration. However, without an in-depth understanding of the soil's physical structure and its association with the plant roots and soil C processing, it will be challenging to optimize bioenergy cropping systems to effectively mitigate climate change. The goal of my Ph.D. dissertation research was to explore the complex interactions among plant roots, soil structure, and soil C processing in different perennial vegetation.

In Chapter 1, I evaluated the associations among soil texture, pore structure, and C characteristics in two perennial vegetation, monoculture switchgrass and polyculture restored prairie, across diverse soil types in the Upper Midwest of the USA. This study employed X-ray computed micro-tomography (X-ray μCT) and structural equation modeling to assess their interactions, revealing increases in the volume of medium-sized (50-150 μm diameter) pores and microbial biomass as well as their positive implication on soil C accumulation positive particularly in the prairie vegetation.

In Chapter 2, I examined the pore structure within the detritusphere of soils under the switchgrass and restored prairie vegetation. By investigating soil texture, minerology, and vegetation influences on soil biopores, particulate organic matter (POM) within biopores, and pore structures in close proximity to the POM, this study highlighted that soil texture and mineralogy played a major, while vegetation a modest, role in defining the pore structure in root detritusphere.

In Chapter 3, I focused on the switchgrass, particularly the differences in very fine roots among switchgrass cultivars and their effects on soil pores and C processes. Using flatbed scanner for roots and X-ray μCT for pores, I demonstrated how pore structures altered by very fine roots positively impact increases in soil microbial biomass and C accrual, with their notable variations across different cultivars.

In Chapter 4, I explored belowground C and nitrogen (N) transfer between plants and its association with soil C and N inputs and pore structure formation. This study provided insights into the variation in

root- and mycorrhizae-based C and N transfers by different plant combinations and their implications for potential soil C storage, emphasizing the fine pore (8-30 μm diameter) formation.

In Chapter 5, I investigated how spatial soil N variability, achieved by partial N application or legume planting, alters root distribution and affects belowground C and N transfer and soil pore structure. This study showed that roots grew towards N enriched locations, promoting C and N transfer and their subsequent inputs into soil to those locations, emphasizing the formation of fine pores via root-based transfer mechanism.

My dissertation contributed to the understanding of how two bioenergy cropping systems: monoculture switchgrass and polyculture prairie can be optimized for maximum C sequestration. By elucidating the interactions among roots, soil structure, and C processes, this work provides valuable insights for developing sustainable bioenergy cropping that mitigate climate change and enhance soil health.

ACKNOWLEDGEMENTS

It has been an honor to conduct my doctoral research under the guidance of Dr. Alexandra Kravchenko. Without her patience and unwavering support, I would not have been able to achieve this far. She consistently provided me with the best research opportunities and encouraged collaborations across various disciplines and organizations. I would also like to extend my deepest gratitude to Dr. Andrey Guber. A number of discussions with him have always pushed me to learn more and improve my research positively. His support in designing the experimental setup has been invaluable to my dissertation. I am grateful for Dr. Phil Robertson's generous guidance, expanding my narrow insight into general soil and agricultural sciences while allowing me to maintain my focus on climate change mitigation. His outstanding expertise and experience in soil science have been a significant source of inspiration. I am equally grateful to Dr. Gregory Bonito for helping me to expand my background in soil microorganisms, another crucial driver for soil carbon sequestration. His guidance has been pivotal in understanding the microbial aspects of my research. I appreciate very much that Dr. Yakov Kuzyakov joined my dissertation committee. He has greatly contributed to my understanding of soil carbon cycling processes. His suggestions, numerous papers, and insightful comments have been essential in helping me develop a correct and comprehensive view of soil carbon dynamics. Having such distinguished guidance committee members has been an honor, and I am profoundly thankful for their support, encouragement, and invaluable contributions to my academic and research journey.

I would like to thank all members of the Kravchenko Lab. Maxwell Oerther, who is indispensable to our lab, provided invaluable assistance with fieldwork and all laboratory experiments. His support and friendship were essential to completing the experiments required for this thesis. Dr. Tayler Ulbrich was not only a research collaborator but also one of the best friends I made during the Ph.D. program. My senior, Dr. Alyssa Kim, helped me adjust to the new environment and offered practical advice on surviving Ph.D. life. I am rooting for her new challenge in Korea! I am also grateful to Dr. Archana Juyal, Dr. Maik Lucas, Dr. James O'Sullivan, Dr. Maoz Dor, and Dr. Poulamee Chakraborty, the best postdoctoral researchers in our lab. Special thanks to my fellow doctoral students, Sukhdeep Singh and Goutham Thotakuri, who have

always encouraged me. I also extend special thanks to Dr. Michelle Quigley, Ovya Venkat, and Lizabeth Dotzlaf for their help with X-ray micro-CT scanning and various laboratory experiments. Additionally, I thank Dr. Linh Nguyen, Dr. Hongbing Zheng, Dr. Weiqing Zhang, Dr. Ricardo Bordonal, Dr. Majid Mahmoudabadi, and many other researchers who have passed through the Kravchenko Lab. There are many other colleagues from Kellogg Biological Station and the Great Lakes Biological Research Center, and I appreciate their support and collaboration as well.

I would like to express my deepest gratitude to my wife, Nari Kang. Her unwavering support and understanding have been my greatest source of strength throughout this journey. Her patience and encouragement have been invaluable, allowing me to pursue my dreams with confidence. To my parents, thank you for your unconditional love and for instilling in me the values of perseverance and hard work. Your belief in my abilities has always motivated me to strive for excellence. Thanks to my two brothers, who have supported our parents in my absence. Finally, to my daughter Evelyn Moah Lee, you are my inspiration and my joy. Your smiles and laughter have been a constant reminder of the beauty and purpose in life, driving me to achieve my best. This accomplishment would not have been possible without the love and support of my family, and I am forever grateful for their presence in my life.

TABLE OF CONTENTS

Introduction

Conversion from fossil fuels to bioenergy is a part of the global endeavors of combatting climate change (IPCC, 2014). Considering concerns of food security and land availability, cultivating perennial bioenergy plants on lands unsuitable for food production is a promising option for the bioenergy production (Sang and Zhu, 2011; Mehmood et al., 2017; Robertson et al., 2017). Microbial pathways of sugar catabolism and fermentation produce ethanol from lignocellulosic feedstocks of bioenergy plants (Fortman et al., 2008), and yields of such ethanol from a number of perennial plants are comparable to those of annual crops (Varvel et al., 2008; David and Ragauskas, 2010). Perennial vegetation can also reduce carbon (C) losses due to soil disturbance by tillage, often necessary when growing annual crops, and can lead to soil C gains (Lal, 2001; Mosier et al., 2021). Benefits of the bioenergy cropping can be further amplified if the crops can capture atmospheric carbon dioxide and store it as soil organic matter resulting in soil C sequestration (Robertson et al., 2008; Robertson et al., 2011). Diverse perennial vegetation is particularly promising to enhance soil C accumulation (Lange et al., 2015; Sprunger & Robertson, 2018) and increase overall nitrogen (N) availability (Mulder et al., 2002; Lee et al., 2003; Lange et al., 2019), subsequently improving soil health and fostering plant growth (Lal, 2016). Such beneficial synergies for C accumulation and plant productivity, arising as a function of plant diversity, are often reported in perennial grass mixtures (Thilakarathna et al., 2012; Lange et al., 2015; Yang et al., 2019; Lee et al., 2023).

The fundamental principles of soil C sequestration involve promoting C inputs into the soil and stabilizing added C against immediate losses (Six and Jastrow, 2002), where physical and chemical protections of C within the soil matrix drive soil C stabilization (Clough and Skjemstad, 2000; Six et al., 2002). Plant roots and residues are major sources of soil C, while elevated soil biological activity stimulates C accumulation via the enhanced production and processing of the added C (Lange et al., 2015; Chen et al., 2018).

Pore structure, i.e., shapes, connectivity, size and spatial distributions of soil pores, defines many functions and processes of the soil (Rabot et al., 2018; Lucas, 2022). It regulates availability of O_2, water, and nutrients to soil microorganisms and influences processing of soil organics (Thomsen et al., 1999;

Bouckaert et al., 2013). Pore connectivity is especially important for providing a suitable habitat for soil-dwelling organisms and enabling microorganisms to access soil organic matter (SOM) (Negassa et al., 2015; Rabbi et al., 2016). Pores of different size ranges have differential effects on the activity and abundance of microorganisms. Specifically, micro-environments associated with higher enzyme activities and greater microbial abundance are found in pores ranging from tens to hundreds μm Ø (Kravchenko et al., 2019; Strong et al., 2004). The proximity between nearest pores governs microbial accessibility to C sources located on soil particles and regulates aeration for soil microorganisms (Dungait et al., 2012; Schlüter and Vogel, 2016; Rohe et al., 2021), subsequently influencing their abundance and activity (Ekschmitt et al., 2008; Schlüter et al., 2019).

Switchgrass (*Panicum virgatum* L.) is recognized as a viable biofuel feedstock due to its high biomass yield produced across a wide range of environmental and climatic conditions and thus a greater energy production potential compared to many other native perennial grasses (Parrish and Fike, 2005; Sanderson and Adler, 2008; Gelfand et al., 2020). However, very slow to negligible soil C gains were often reported in this deep-root perennial (Garten Jr. and Wullschleger, 2000; Liebig et al., 2005; Bates et al., 2022). Moreover, a number of recent field experiments have demonstrated that monoculture switchgrass lags behind other candidate perennial bioenergy cropping systems in its C gains, including mixtures of native grasses or restored prairie systems that involve switchgrass as one of the plant species (Yang et al., 2019; Lee et al., 2023; Perry et al., 2023). The goal of my Ph.D. research was to explore possible factors for enhancing switchgrass's capacity for soil C sequestration, comparing its effectiveness to other polyculture perennial bioenergy cropping systems.

REFERENCES

Bates, C.T., Escalas, A., Kuang, J., Hale, L., Wang, Y., Herman, D., Nuccio, E.E., Wan, X., Bhattacharyya, A., Fu, Y., Tian, R., Wang, G., Ning, D., Yang, Y., Wu, L., Pett-Ridge, J., Saha, M., Craven, K., Brodie, E.L., Firestone, M., and Zhou, J. (2022). Conversion of marginal land into switchgrass conditionally accrues soil carbon but reduces methane consumption. *The ISME Journal*, 16: 10–25. doi:10.1038/s41396-021-00916-y

Bouckaert, L., Sleutel, S., Van Loo, D., Brabant, L., Cnudde, V., Van Hoorebeke, L., and De Neve, S. (2013). Carbon mineralisation and pore size classes in undisturbed soil cores. *Soil Research*, 51(1): 14–22. doi: 10.1071/SR12116

Chen, S., Wang, W., Xu, W., Wang, Y., Wan, H., Chen, D., . . . Bai, Y. (2018). Plant diversity enhances productivity and soil carbon storage. *Proceedings of the National Academy of Sciences of the United States of America*, 115(16): 4027-4032. doi:10.1073/pnas.1700298114

Clough, A. and Skjemstad, J. O. (2000). Physical and chemical protection of soil organic carbon in three agricultural soils with different contents of calcium carbonate. *Australian Journal of Soil Research*, 38(5): 1005-1016. doi:10.1071/SR99102

David, K. and Ragauskas, A. J. (2010). Switchgrass as an energy crop for biofuel production: A review of its ligno-cellulosic chemical properties. *Energy and Environmental Science*, 3(9): 1182-1190. doi:10.1039/b926617h

Dungait, J.A.J., Hopkins, D.W., Gregory, A.S., and Whitmore, A.P. (2012). Soil organic matter turnover is governed by accessibility not recalcitrance. *Global Change Biology* 18: 1781–1796. doi:10.1111/j.1365-2486.2012.02665.x

Ekschmitt, K., Kandeler, E., Poll, C., Brune, A., Buscot, F., Friedrich, M., Gleixner, G., Hartmann, A., Kästner, M., Marhan, S., Miltner, A., Scheu, S., and Wolters, V. (2008). Soil-carbon preservation through habitat constraints and biological limitations on decomposer activity. *Journal of Plant Nutrition and Soil Science,* 171: 27–35. doi:10.1002/jpln.200700051

Fortman, J. L., Chhabra, S., Mukhopadhyay, A., Chou, H., Lee, T. S., Steen, E., and Keasling, J. D. (2008). Biofuel alternatives to ethanol: pumping the microbial well. *Trends in Biotechnology*, 26(7): 375-381. doi: 10.1016/j.tibtech.2008.03.008

Garten Jr., C.T. and Wullschleger, S.D. (2000). Soil Carbon Dynamics beneath Switchgrass as Indicated by Stable Isotope Analysis. *Journal of Environmental Quality*, 29: 645–653. doi:10.2134/jeq2000.00472425002900020036x

Gelfand, I., Hamilton, S. K., Kravchenko, A. N., Jackson, R. D., Thelen, K. D., and Robertson, G. P. (2020). Empirical Evidence for the Potential Climate Benefits of Decarbonizing Light Vehicle Transport in the U.S. With Bioenergy from Purpose-Grown Biomass with and without BECCS. *Environmental Science and Technology*, 54 (5): 2961-2974. doi: 10.1021/acs.est.9b07019

IPCC (2014). Technical Summary In Climate Change 2014: Mitigation of Climate Change. Contribution of Working Group III to the Fifth Assessment Report of the Intergovernmental Panel on Climate Change [Edenhofer, O., R. Pichs-Madruga, Y. Sokona, E. Farahani, S. Kadner, K. Seyboth, A. Adler, I. Baum, S. Brunner, P. Eickemeier, B. Kriemann, J. Savolainen, S. Schlömer, C. von

Stechow, T. Zwickel and J. C. Minx (eds.)]. Cambridge University Press, Cambridge, United Kingdom and New York, NY, USA.

Kravchenko, A. N., Guber, A. K., Razavi, B. S., Koestel, J., Blagodatskaya, E. V., and Kuzyakov, Y. (2019). Spatial patterns of extracellular enzymes: Combining X-ray computed micro-tomography and 2D zymography. *Soil Biology and Biochemistry*, 135: 411-419. doi:10.1016/j.soilbio.2019.06.002

Lal, R. (2001). Soil degradation by erosion. *Land Degradation and Development*, 12(6): 519-539. doi:10.1002/ldr.472

Lal, R. (2016). Soil health and carbon management. *Food and Energy Security* 5: 212–222.

Lange, M., Eisenhauer, N., Sierra, C. A., Bessler, H., Engels, C., Griffiths, R. I., Mellado-Vázquez, P. G., Malik, A. A., Roy, J., Scheu, S., Steinbeiss, S., Thomson, B. C., Trumbore, S. E., and Gleixner, G. (2015). Plant diversity increases soil microbial activity and soil carbon storage. *Nature Communications*, 6 doi:10.1038/ncomms7707

Lange, M., E. Koller-France, A. Hildebrandt, Y. Oelmann, W. Wilcke, and G. Gleixner. (2019). Chapter Six - How plant diversity impacts the coupled water, nutrient and carbon cycles. *In* N. Eisenhauer, D. A. Bohan, and A. J. Dumbrell [eds.], Advances in Ecological Research, Mechanisms underlying the relationship between biodiversity and ecosystem function, 185–219. Academic Press.

Lee, J. H., M. Lucas, A. K. Guber, X. Li, and Kravchenko, A. N. (2023). Interactions among soil texture, pore structure, and labile carbon influence soil carbon gains. *Geoderma,* 439: 116675.

Lee, T. D., P. B. Reich, and Tjoelker, M. G. (2003). Legume presence increases photosynthesis and N concentrations of co-occurring non-fixers but does not modulate their responsiveness to carbon dioxide enrichment. *Oecologia* 137: 22–31.

Liebig, M.A., Johnson, H.A., Hanson, J.D., and Frank, A.B. (2005). Soil carbon under switchgrass stands and cultivated cropland. *Biomass and Bioenergy*, 28: 347–354. doi:10.1016/j.biombioe.2004.11.004

Lucas, M. (2022). Perspectives from the fritz-scheffer awardee 2020—The mutual interactions between roots and soil structure and how these affect rhizosphere processes#. *Journal of Plant Nutrition and Soil Science*, 185(1): 8-18. doi:10.1002/jpln.202100385

Mehmood, M. A., Ibrahim, M., Rashid, U., Nawaz, M., Ali, S., Hussain, A., and Gull, M. (2017). Biomass production for bioenergy using marginal lands. *Sustainable Production and Consumption*, 9: 3– 21. doi: 10.1016/j.spc.2016.08.003

Mosier, S., Córdova, S. C., and Robertson, G. P. (2021). Restoring Soil Fertility on Degraded Lands to Meet Food, Fuel, and Climate Security Needs via Perennialization. *Frontiers in Sustainable Food Systems*, 5, doi: 10.3389/fsufs.2021.706142

Mulder, C., A. Jumpponen, P. Högberg, and Huss-Danell, K. (2002). How plant diversity and legumes affect nitrogen dynamics in experimental grassland communities. *Oecologia,* 133: 412–421.

Negassa, W. C., Guber, A. K., Kravchenko, A. N., Marsh, T. L., Hildebrandt, B., and Rivers, M. L. (2015). Properties of Soil Pore Space Regulate Pathways of Plant Residue Decomposition and

Community Structure of Associated Bacteria. *PLOS ONE*, 10(4), e0123999. doi: 10.1371/journal.pone.0123999

Parrish, D. J. and J. H. Fike. (2005). The Biology and Agronomy of Switchgrass for Biofuels. *Critical Reviews in Plant Sciences,* 24: 423–459.

Perry, S., Falvo, G., Mosier, S., and Robertson, G.P. (2023). Long-term changes in soil carbon and nitrogen fractions in switchgrass, native grasses, and no-till corn bioenergy production systems. *Soil Science Society of America Journal*. doi:10.1002/saj2.20575

Rabbi, S. M. F., Daniel, H., Lockwood, P. V., Macdonald, C., Pereg, L., Tighe, M., … Young, I. M. (2016). Physical soil architectural traits are functionally linked to carbon decomposition and bacterial diversity. *Scientific Reports*, 6(1): 33012. doi: 10.1038/srep33012

Rabot, E., Wiesmeier, M., Schlüter, S., and Vogel, H.-J. (2018). Soil structure as an indicator of soil functions: A review. *Geoderma*, 314: 122–137. https://doi.org/10.1016/j.geoderma.2017.11.009

Robertson, G. P., Dale, V. H., Doering, O. C., Hamburg, S. P., Melillo, J. M., Wander, M. M., Parton, W. J., Adler, P. R., Barney, J. N., Cruse, R. M., Duke, C. S., Fearnside, P. M., Follett, R. F., Gibbs, H. K., Goldemberg, J., Mladenoff, D. J., Ojima, D., Palmer, M. W., Sharpley, A., Wallace, L., Weathers, K. C., Wiens, J. A., Wilhelm, W. W. (2008). Agriculture: Sustainable biofuels redux. *Science*, 322(5898): 49-50. doi:10.1126/science.1161525

Robertson, G. P., Hamilton, S. K., Del Grosso, S. J., and Parton, W. J. (2011). The biogeochemistry of bioenergy landscapes: Carbon, nitrogen, and water considerations. *Ecological Applications*, 21(4): 1055-1067. doi:10.1890/09-0456.1

Robertson, G. P., Hamilton, S. K., Barham, B. L., Dale, B. E., Izaurralde, R. C., Jackson, R. D., Landis, D. A., Swinton, S. M., Thelen, K. D., and Tiedje, J. M. (2017). Cellulosic biofuel contributions to a sustainable energy future: Choices and outcomes. *Science,* 356, eaal2324. doi:10.1126/science.aal2324

Rohe, L., Apelt, B., Vogel, H.-J., Well, R., Wu, G.-M., and Schlüter, S. (2021). Denitrification in soil as a function of oxygen availability at the microscale. *Biogeosciences,* 18: 1185–1201. doi:10.5194/bg-18-1185-2021

Sanderson, M. A. and P. R. Adler. (2008). Perennial Forages as Second Generation Bioenergy Crops. *International Journal of Molecular Sciences,* 9: 768–788.

Sang, T. and Zhu, W. (2011). China's bioenergy potential. *Global Change Biology Bioenergy*, 3: 79– 90. doi:10.1111/j.1757-1707.2010.01064.x

Schlüter, S. and Vogel, H.-J. (2016). Analysis of Soil Structure Turnover with Garnet Particles and X-Ray Microtomography. *PLOS ONE*, 11: e0159948. doi:10.1371/journal.pone.0159948

Schlüter, S., Zawallich, J., Vogel, H.-J., and Dörsch, P. (2019). Physical constraints for respiration in microbial hotspots in soil and their importance for denitrification. *Biogeosciences*, 16: 3665–3678. doi:10.5194/bg-16-3665-2019

Six, J. and Jastrow, J. D. (2002). Organic Matter Turnover. In Lal, R. (Eds.), *Encyclopedia of Soil Science* (pp. 936-942), Marcel Dekker, New York.

Sprunger, C. D., and G. Philip Robertson. (2018). Early accumulation of active fraction soil carbon in newly established cellulosic biofuel systems. *Geoderma* 318: 42–51.

Strong, D. T., De Wever, H., Merckx, R., and Recous, S. (2004). Spatial location of carbon decomposition in the soil pore system. *European Journal of Soil Science*, 55(4): 739-750. doi:10.1111/j.1365-2389.2004.00639.x

Thilakarathna, R. M. M. S., Y. A. Papadopoulos, A. V. Rodd, A. N. Gunawardena, S. A. E. Fillmore, and Prithiviraj, B. (2012). Characterizing nitrogen transfer from red clover populations to companion bluegrass under field conditions. *Canadian Journal of Plant Science,* 92: 1163–1173.

Thomsen, I. K., Schjønning, P., Jensen, B., Kristensen, K., and Christensen, B. T. (1999). Turnover of organic matter in differently textured soils: II. Microbial activity as influenced by soil water regimes. *Geoderma*, 89(3): 199–218. https://doi.org/10.1016/S0016-7061(98)00084-6

Varvel, G. E., Vogel, K. P., Mitchell, R. B., Follett, R. F., and Kimble, J. M. (2008). Comparison of corn and switchgrass on marginal soils for bioenergy. *Biomass and Bioenergy*, 32: 18– 21. doi:10.1016/j.biombioe.2007.07.003

Yang, Y., D. Tilman, G. Furey, and Lehman, C. (2019). Soil carbon sequestration accelerated by restoration of grassland biodiversity. *Nature Communications,* 10: 718.

CHAPTER 1: Interactions among soil texture, pore structure, and labile carbon influence soil carbon gains[1]

Abstract

Perennial vegetation with high plant diversity, e.g., restored prairie, is known for stimulation of soil carbon (C) gains, due in part to enhanced formation of pore structure beneficial for long-term C storage. However, the prevalence of this phenomenon across soils of different types remains poorly understood. The aim of the study was to assess the associations between pore structure, soil C, and their differences in monoculture switchgrass and polyculture restored prairie vegetation across a wide range of soils dominating the Upper Midwest of the USA. Six experimental sites were sampled, representing three soil types with texture ranging from sandy to silt loams. The two vegetation systems studied at each site were (i) monoculture switchgrass (*Panicum virgatum* L.), and (ii) polyculture restored prairie, also containing switchgrass as one of its species. X-ray computed micro-tomography (μCT) was employed to analyze soil pore structure. Structural equation modeling and multiple path analyses were used to assess direct and indirect effects of soil texture and pore characteristics on microbial biomass C (MBC), particulate organic matter (POM), dissolved organic C (DOC), short-term respiration (CO_2), and, ultimately, soil organic C (SOC). Across studied sites, prairie increased fractions of medium (50–150 μm Ø) pores by 11–45 %, SOC by 3–69 %, and MBC by 18–59 % (except for one site). The greater were the prairie-induced increases in the medium pore volumes, the greater were the prairie-induced SOC gains. Greater C losses via CO_2 and DOC contributed to slower C accumulation in the prairie soil. We surmise that the interactive feedback loop relating medium pores and soil C acts across a wide range of soil textures and is an important mechanism through which perennial vegetation with high plant diversity, such as restored prairie, promotes rapid SOC gains.

[1] Originally published as: Lee, J. H., Lucas, M., Guber, A. K., Li, X., & Kravchenko, A. N. (2023). Interactions among soil texture, pore structure, and labile carbon influence soil carbon gains. *Geoderma*, 439, 116675. doi: 10.1016/j.geoderma.2023.116675

1.1 Introduction

Cropping systems influence soil pore characteristics (Helliwell et al., 2019, Lucas, 2022) due in part to differences in root architectures and biomass, quantities and qualities of C inputs, and rhizosphere microbial community composition (Pagliai and De Nobili, 1993, Sprunger et al., 2017, Lucas et al., 2022). Of particular relevance for microbial activity and, thus, for processing and protection of the newly added C are the pores in the tens to hundreds micrometer size range, which we will refer to here as medium pores. Such pores are often associated with greater mineralization of newly added C (Strong et al., 2004, Quigley et al., 2018), higher microbial activity (Wright et al., 1995, Kravchenko et al., 2019a, Liang et al., 2019), and faster and greater microbial turnover (Ruamps et al., 2011, Kravchenko et al., 2021). The chemical composition of dissolved organic matter residing in pores of different size ranges also differs, leading to differential decomposition rates (Bailey et al., 2017). Previous work by our team (Kravchenko et al., 2019b) demonstrated that bioenergy cropping systems with high plant diversity developed greater volumes of medium pores than low diversity systems. This finding is important for elucidating the drivers through which diverse assemblages of perennial bioenergy plants can generate significant soil C gains (Sanford, 2014, Sprunger and Philip Robertson, 2018), thus for developing strategies to maximize the climate mitigation benefits of biofuel production. However, Kravchenko et al. (2019b) study was based on only a single soil (sandy loam Alfisol), raising questions regarding universality of the observed phenomenon.

Pore formation and characteristics also depend on inherent soil physical properties, especially soil texture. Generally, the volume and size of pores increases with increasing size of soil particles, as larger particles are likely to give rise to larger pores in-between them (Nimmo, 2013, Ding et al., 2016, Fan et al., 2021). Thus, the formation of medium pores in soils of contrasting textures may differ in their contribution to the decomposition of soil organic matter and plant residues and to the stabilization of the processed C. Indeed, greater decomposition of soil-incorporated root and leaf residues was observed when the residues were surrounded by soil with a greater abundance of > 30 μm Ø pores compared to that of the soil with prevalence of smaller pores (Negassa et al., 2015, Kim et al., 2020). Also, greater amount of the decomposed substrates was found to be occluded and subsequently protected in fine-textured soils than that

in coarse-textured soils (Kölbl and Kögel-Knabner, 2004, Schweizer et al., 2019, Haddix et al., 2020). Furthermore, Shen (1999) found that finer textured soils had a higher capacity for sorption of dissolved organic matter, likely caused by slow water movement and greater microbial processing of the dissolved organic matter (Don and Schulze, 2008, Kaiser and Kalbitz, 2012). Thus, we surmise that soil texture can modify the contribution of plant community composition to formation and size-distribution of soil pores and modulate the importance of pore structure for soil C processing. Modifications in pore structure may subsequently lead to changes in labile organic matter and then influence soil organic C (SOC) contents.

The first objective of this chapter is to compare pore size distributions (PSD), labile C characteristics, and organic C contents of the soils from two bioenergy cropping systems, a monoculture switchgrass and a polyculture restored prairie which includes switchgrass as one of the species after their multiple years of implementation at six experimental sites with disparate soil characteristics. I hypothesize that increases in volumes of medium pores and SOC in prairie vegetation, previously observed in the sandy loam Alfisol soil (Kravchenko et al., 2019b), would also be present across a range of soil types and textures.

The second objective is to explore the joint influences of the cropping systems and pore characteristics on microbial biomass C (MBC) and other forms of labile C (i.e., particulate organic matter (POM), dissolved organic C (DOC), and short-term CO_2 respiration (CO_2)) along with the potential contributions of such influences to the long-term soil C accumulation. I hypothesize that greater formation of medium pores under prairie vegetation will contribute to greater MBC and other labile C forms and will lead to increases in SOC contents.

1.2 Materials and Methods

1.2.1 Experimental design and soil sample collections

The six experimental sites from Great Lakes Bioenergy Center used for this experiment were established in 2013 at Lux Arbor (LA), Lake City (LC), and Escanaba (ES) locations in Michigan and Hancock (HA), Rhinelender (RH), and Oregon (OR) locations in Wisconsin (Table 1) (Kasmerchak and Schaetzl, 2018). In three of the sites, namely LA, ES and OR, the soils belonged to Alifisol, in two, i.e., LC

and RH, to Spodosols, and in HA to Entisol types, and were regarded as overall low fertility soils unsuitable for food production.

Table 1.1. Soil taxonomy, geographical locations, and texture of the six studied sites.

Experimental site	Soil taxonomy	Location (Lat., Long.)	Texture	Sand (%)	Silt (%)	Clay (%)
Oregon (OR), WI	Typic Hapludalf (Alfisol)	42.97, -89.36	Silt loam	9.9[d]	73.3[a]	16.8[a]
Lux Arbor (LA), MI	Typic Hapludalf (Alfisol)	42.48, -85.45	Loam	51.9[c]	38.8[b]	9.3[b]
Escanaba (ES), MI	Inceptic Hapludalf (Alfisol)	45.76, -87.19	Sandy loam	65.9[b]	31.5b[c]	2.6[d]
Rhinelender (RH), WI	Entic Haplorthod (Spodosol)	45.67, -89.22	Sandy loam	65.9[b]	27.4[c]	6.7[c]
Hancock (HA), WI	Typic Udipsamment (Entisol)	44.12, -89.53	Loamy sand	82.3[a]	12.9[d]	4.8[cd]
Lake City (LC), MI	Oxyaquic Haplorthod (Spodosol)	44.30, -85.20	Loamy sand	86.8[a]	9.2[d]	4.0[d]

Note: different letters within the same column indicate significant differences ($p < 0.05$) among the studied sites (OR, LA, ES, and RH sites: n = 4 and HA and LC sites: n = 3).

Two bioenergy cropping systems selected for the study were monoculture switchgrass (*Panicum virgatum* L.) and polyculture restored prairie. The restored prairie consisted of 18 plant species of grasses (including switchgrass), forbs, and legumes. At each site the experiment was set up as a randomized complete block design with four (LA, ES, RH, and OR) or three (LC and HA) replicated blocks. The two cropping systems were randomly assigned to the plots within each block. Both cropping systems shared the same managing and harvesting practices since the establishment of the six sites, that is, both were not fertilized and not tilled. Soil from the first five sites was sampled in November of 2019, and samples from OR site were collected a year later.

Two types of soil samples were collected from each replicated plot. First, three intact soil cores (5 cm in height and 5 cm in diameter) were taken from 5 to 10 cm depth to be further used for μCT scanning. Then, loose soil surrounding the cores was collected for subsequent bulk soil measurements of soil texture and C characteristics. All collected samples were stored at 4 °C until the measurements and scanning.

Two types of soil samples were collected from each replicated plot. First, three intact soil cores (5 cm in height and 5 cm in diameter) were taken from 5 to 10 cm depth to be used for X-ray computed

micro-tomography (μCT) scanning. This specific depth was chosen because it represents the portion of the soil profile most significantly affected by the root systems. The loose soil surrounding the cores was collected for subsequent measurements of soil texture and C characteristics (MBC, POM, DOC, CO_2, and SOC contents). All collected samples were stored at 4 °C until the measurements and scanning.

1.2.2 Soil measurements

The following chemical properties were measured in soil passes through 2-mm sieve at the MSU Soil & Plant Nutrient Laboratory (East Lansing, Michigan, USA): soil pH was measured in a 1:1 soil: water slurry; available phosphorus (Bray-P) was determined by Bray-Kurtz P1 (weak acid) test; concentrations of potassium, calcium, magnesium for cation exchange capacity (CEC), and metals including: zinc (Zn), manganese (Mn), iron (Fe), and copper (Cu) were measured using inductively coupled plasma (ICP) spectrophotometers after extracting these cations from soil samples (Warncke et al., 2009). Soil texture was determined using the hydrometer method (Gee and Or, 2002).

Chloroform fumigation-incubation method was used to determine soil MBC (Paul et al., 1999). Two sets of 10 g soil samples were prepared, and water was added to the samples with a pipette to achieve 50 % of their water holding capacity. Then, the samples were preincubated for five days. After the preincubation, one set of the samples was fumigated for 24 h by ethanol-free chloroform vapor, while the other set of the samples remained unfumigated. After that, both sets of soils were subjected to a ten-day incubation at 20 °C in the dark. Emitted CO_2 was measured using Infrared Photoacoustic Spectroscopy (1412 Photoacoustic multi-gas monitors, INNOVA Air Tech Instruments, Ballerup, Denmark) in the gas circulation mode. Differences between quantities of CO_2 emitted from fumigated and non-fumigated samples were used to calculate MBC. The quantities of CO_2 emitted from unfumigated samples were reported as measures of the short-term respiration. This respiration indicates the amount of decomposed C substrates from soils during the incubation period (Adviento-Borbe et al., 2006, Haney et al., 2008).

Soil POM contents were determined using physical fractionation (53–2000 μm) method (Cambardella and Elliott, 1992). Specifically, 30 g of air-dried soil was passed through 2-mm sieve and dispersed with 70 ml of sodium hexametaphosphate solution. Then, all organic debris including roots in a

53 μm sieve were rinsed by distilled water and collected. The organic debris were oven-dried at 40 °C for two days and weighed. Dried debris were combusted using a benchtop Maffle's Furnace (OMEGA Engineering Inc., Norwalk, USA) at 500 °C for three hours and weighed again. The amount of POM was determined by calculating differences between weights before and after combustion. For SOC, sieved and ground soil samples were analyzed by a CHNSO Elemental Analyzer (Costech Analytical Technologies, Valencia, USA).

Rhizosphere soil was used for the DOC measurements. Plants from both systems were carefully uprooted and manually shaken, and the soil adhering to roots, regarded as rhizosphere soil, was collected. Six grams of the rhizosphere soil was extracted by 30 ml of 0.5 M K_2SO_4 by shaking at 200 rpm for one hour, and the extracts were filtered with Whatman grade 202 filter paper. Concentration of DOC was determined using a vario TOC cube (Elementar Americas Inc., New York, USA). Means of three-year DOC concentrations were used as one of the labile C characteristics in this study, besides MBC, POM, and CO_2.

1.2.3 Soil core scanning and image analysis

Microscale quantification of soil pore size distributions was obtained via X-ray μCT, a tool that can provide visualization of soil in its intact state (Udawatta et al., 2008, Vogel et al., 2010). Prior to X-ray μCT scanning, all soil cores were brought to the matric potential of 28 kPa, which ensured that pores larger than 5 μm Ø were air-filled and thus easily detectable on the μCT images. For that, the cores were first saturated for 24 h in a water filled sand bath, and then transferred to a pressure chamber (5 bar pressure plate extractor, Soilmoisture Equipment Corp., Goleta, CA, USA) and kept there for two days at 28 kPa. Bringing all cores to the same matric potential enabled comparisons of detectable via X-ray μCT pore volumes among experimental sites and plant systems.

The cores were scanned using X-ray μCT instrument (North Star Imaging, X3000, Rogers, USA) at the Department of Horticulture facility, Michigan State University. The scanning resolution and projected energy level were 18.2 μm and 75 kV with 450 μA, respectively. The high resolution was achieved using the Subpi-mode of the scanner, combining four individual scanning's. Scanned images from 3014 projections were reconstructed by efX software (North Star, Rogers, USA).

Image analyses for size distributions of pore volumes were performed using ImageJ-Fiji software (Schindelin et al., 2012) and SimpleITK in Python (Beare et al., 2018). The following image pre-processing steps were conducted to remove artifacts and noises. First, the images were cropped into squares (2.7 cm in length, 2.7 cm in width, and 4.1 cm height corresponded to 1500 × 1500 × 2240 pixels) from the center to exclude sampling artifacts near the soil core walls. Then, 'Remove Background' tool in Xlib/Beat plugin of ImageJ software was used to remove shadowing effects from the images, and removal of ring artifacts was conducted on the image polar domain using a stripe filter of the Xlib/Beat plugin. Finally, 2-D non-local mean filter ($\sigma = 0.1$) was applied to reduce the noise (Darbon et al., 2008, Buades et al., 2011).

The pre-processed grayscale images were segmented into pore and solid binary images. Mean threshold values were obtained by averaging the thresholds derived from eight segmentation methods (Otsu, Kittler, Triangle, Huang, ISO, Li, Renyi, and Moments) using SimpleITK (Lucas et al., 2022a). The rationale for averaging thresholds is to mitigate biases of the individual methods, thus enhancing accuracy in pore threshold calculation (Schlüter et al., 2014). Pore size distributions of 3D stacked images were determined by the 'Local Thickness' approach in ImageJ, based on the maximum inscribed sphere method (Hildebrand and Rüegsegger, 1997, Vogel et al., 2010). The volumes of pores of different size classes were expressed as fractions of the total soil volume (mm^3/mm^3).

Pores larger than 500 μm Ø were not included in further analyses as they were rarely related to soil C cycling (Nunan et al., 2003, Franklin et al., 2021). In accordance with the reported size ranges, we decided to define 50–150 μm Ø as the range of medium pores and consider this range as a potential determinant of labile C characteristics and consequent C accumulation of soil over the studied sites.

1.2.4 Statistical analysis

The effects of the two plant systems at the studied experimental sites were assessed using SAS 9.4 (SAS Institute Inc., NC, USA) procedures of PROC MIXED and PROC GLIMMIX. Since we did not expect that 6–7 years of prairie and switchgrass vegetation growth will influence soil texture, the statistical models for sand, silt, and clay contents included only the experimental sites as the fixed effect. The statistical models for soil C characteristics (MBC, POM, DOC, CO_2, and SOC), volumes of medium pores,

and other soil chemical properties consisted of the fixed effects of plant systems, experimental sites, and their interaction. All models included the random effects of experimental blocks nested within the sites and effects of soil cores nested within plots, plant systems, and sites. The assumptions of normality and variance homogeneity were assessed using normal probability plots, plots of residuals vs. predicted values, and Levene's tests for equal variances.

Linear relationships among the texture variables, e.g., sand content, medium pore volumes, and C characteristics were assessed using Pearson's correlation coefficients. For each of the studied soil properties, except texture, we also calculated the differences between the switchgrass and prairie systems (Δ) within individual experimental blocks of each site. Working with Δ enabled us to focus on the changes generated by vegetation differences, while reducing the influence of the inherent variability among the experimental sites.

1.2.5 Structural equation modeling and path analysis

Complex causal relationships through which soil texture, pores, microbial biomass, and labile C may contribute to SOC required that, in order to address the study's hypotheses, we employed path analysis and structural equation modeling (SEM) (Pérès et al., 2013, Eisenhauer et al., 2015, Zhao et al., 2019, Liao et al., 2022). Path analysis can reveal the causal relationships among a set of observed variables (Grace, 2006, Lange et al., 2015), and SEM uses latent variables, which are hypothetical constructs encompassing comprehensive effects of more than one observed variable on other variables (Grace, 2006, Eisenhauer et al., 2015). The analyses were performed using PROC CALIS procedure of SAS 9.4.

The conceptual structure of the explored models is shown on Fig. S1. Individual percentage of sand and clay contents were used to construct an exogenous latent variable, "soil texture", which directly affects SOC contents, fraction of medium pores, and "labile C" (arrow 1, 2, and 3 on Figure 1.1). Measured MBC, POM, DOC, and CO_2 constructed an endogenous variable, "labile C", affected by the "soil texture" and the fraction of medium pores (arrow 3 and 4 on Figure 1.1). The "labile C" and the fraction of medium pores are also declared to be exogenous variables, with both direct and indirect effects on SOC contents (arrow 4, 5, and 6 on Figure 1.1). The multi-relationships postulated in our model were developed based on and

are supported by the literatures listed in Table 1.3. The models for prairie and switchgrass systems were fitted separately.

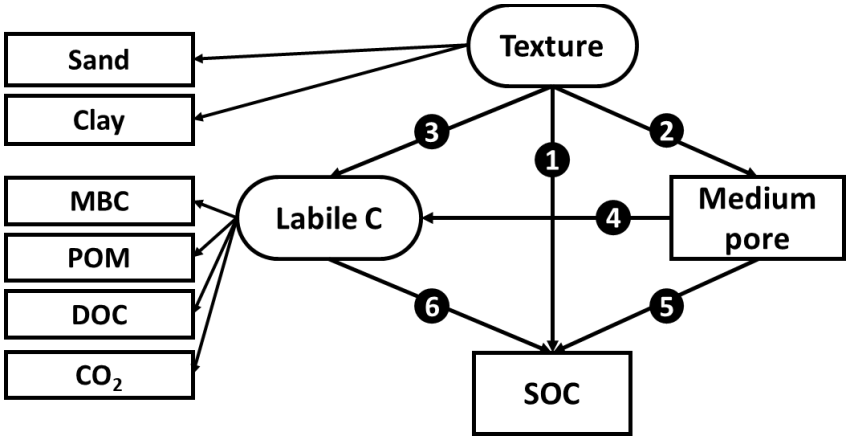

Figure 1.1. Conceptual paths of the structural equation model. The individually numbered paths correspond to the list of hypotheses and supporting literatures reported in Table 1.3.

Table 1.2. List of the path analysis models, table numbers of supporting literatures for the model hypotheses, and corresponding figure numbers.

Models for	Components of the latent variables	Hypotheses listed on	Results reported on
Effects of individual labile C components	MBC in "Labile C"	Table 1.3 and 1.4	Fig. 1.8a
	POM in "Labile C"	Table 1.3 and 1.4	Fig. 1.8b
	DOC in "Labile C"	Table 1.3 and 1.4	Fig. 1.8c
	CO_2 in "Labile C"	Table 1.3 and 1.4	Fig. 1.8d
Effects of Δs of individual labile C components	ΔMBC in "ΔLabile C"	Table 1.3 and 1.4	Fig. 1.10a
	ΔPOM in "ΔLabile C"	Table 1.3 and 1.4	Fig. 1.10b
	ΔDOC in "ΔLabile C"	Table 1.3 and 1.4	Fig. 1.10c
	ΔCO_2 in "ΔLabile C"	Table 1.3 and 1.4	Fig. 1.10d

Note: All models share the same conceptual paths illustrated on Fig. 1.1. Thus, models of path analyses include variables of Sand (sand contents), Medium (volume fractions of medium pores), and SOC (soil organic C), and only individual components of "Labile C" and "ΔLabile C" were different by the models.

Table 1.3. Theoretical supports for the hypothesized paths in the structural equation modeling (Arrows in the conceptual model of Figure 1.1 indicate hypothesized mechanisms of the individually numbered paths).

Paths from		**Paths to**		**Path #**	**Hypotheses under the paths**	**References**
(Latent)	(Observed)	(Latent)	(Observed)	(Fig. 1.1)		
Soil texture	Sand	-	SOC	①	Sandy soils have lower SOC storage capacity, and sand-associated OC has a shorter turnover time than that of clay-associated OC.	Kleber et al., 2007; Singh et al., 2018
	Clay		SOC	①		
	Sand		Pore	②	Sandy soils have greater volume of mid-size pores, since the pore size progressively increases with the size of soil particles forming the pores.	Nimmo, 2013; Ding et al., 2016
	Clay		Pore	②		
	Sand	Labile C	MBC	③	Fine-textured soils have greater microbial biomass due to their greater spatial heterogeneity and better water retention.	Kaiser et al., 1992; Woloszczyk et al., 2020
	Clay		MBC	③		
	Sand		POM	③	Fine-textured soils contain less free POM, since high surface areas of such soils stimulate POM protection and stabilization.	Kölbl & Kögel-Knabner, 2004; Witzgall et al., 2021
	Clay		POM	③		
	Sand		DOC	③	Fine-textured soils contain less free POM, since high surface areas of such soils stimulate POM protection and stabilization.	Shen, 1999; Filep et al., 2022
	Clay		DOC	③		
	Sand		CO_2	③	Sandy soils stimulate C losses as CO_2 because of their lower capability to protect C substrates from decomposition.	Franzluebbers, 1999 Witzgall et al., 2021
	Clay		CO_2	③		
-	Pore	Labile C	MBC	④	Greater volume of medium pores leads to greater microbial biomass by serving as habitats for them.	Strong et al., 2004; Franklin et el., 2021
	Pore		POM	④	Soils with greater volume of medium pores lead to greater contents of POM due to the higher growth of fine roots in the soils.	Bodner et al., 2014; Fukumasu et al., 2022
	Pore		DOC	④	DOC in large pores is less complex and easier stabilized, thus soils dominated by large pores will have lower DOC.	Shen, 1999; Bailey et al., 2017
	Pore		CO_2	④	Soils dominated by large pores may have greater CO_2 respiration, due to greater OC availability to microorganisms and transit of CO_2 from them.	Lennon et al., 2012; Mangalassery et al., 2013
	Pore	-	SOC	⑤	Greater volumes of medium pores lead to greater organic matter processing and more channels for transits and storage of the processed C.	Quigely et al., 2018; Franklin et el., 2021
Labile C	MBC	-	SOC	⑥	Greater soil microbial biomass leads to faster C turnover and consequent C accumulation.	Miltner et al., 2012; Oduor et al., 2013
	POM		SOC	⑥	More POM suggests greater quantities of C which can be potentially processed and stabilized within the soil.	Lavallee et al., 2019; Witzgall et al., 2021
	DOC		SOC	⑥	Greater DOC levels suggest greater quantities of C which can be potentially processed and stabilized within the soil.	Dou et al., 2008; Filep & Rékási, 2011
	CO_2		SOC	⑥	Greater CO_2 respiration is indicative of faster decomposition of newly added C substrates and existing SOC.	Prommer et al., 2020; Witzgall et al., 2021

It should be noted that soil pores and SOC are closely intertwined. SOC accumulation and pore formation are linked in a feedback cycle (Marinari et al., 2000): an increase in one accelerates the increases in the other, and simultaneous examination of both sides of the cycle is not possible. Since our data set includes 6 experimental sites with very different soil textures but rather comparable SOC levels, and texture is the major primary driver for pore formation, in this study we decided to focus on the pores → SOC side of the cycle and to explore the contribution of pores as drivers of SOC accumulation.

An additional model was constructed to examine the effect of texture on the differences (Δs) between prairie and switchgrass systems in terms of the difference in the labile C characteristics (ΔMBC, ΔPOM, ΔDOC, ΔCO_2), fractions of medium pores (ΔMedium), and SOC contents (ΔSOC) that developed during the 6–7 years of system implementations. The values of Δs were calculated as described in the previous section, and the model for Δs used the same conceptual structure of the original model (Figure 1.1). Means of sand and clay contents from both plant systems were used as an exogenous latent variable (arrow 1, 2, and 3 on Figure 1.1), and Δs of the "labile C" components and the pore fractions were defined as endogenous variables under the "soil texture" (arrow 2 and 3 on Figure 1.1). Δs of "labile C" components and the pore fractions were also used as exogenous variables for ΔSOC (arrow 5 and 6 on Figure 1.1).

Multiple path analyses were performed to explore the effect of individual components within the "labile C" on SOC contents and hypothesized causal relationships of it with other observed variables. For that we used the same SEM concepts (Table 1.3) to contract four path analysis models using percentage of sand contents (arrow 1, 2, and 3 on Figure 1.1). We choose to work with sand as opposed to silt content in these path analyses because the relationship between pore volumes and silt contents is known to be less significant compared to that with sand or clay contents (Ding et al., 2016). Because of a very narrow range of clay contents observed in the six studied sites (Table 1.1), path analyses with clay content were also found to be less informative than those with sand. Each of the four models included one of the observed variables from the "labile C" as endogenous variable being affected by sand contents and fractions of medium pores (arrow 3 and 4 on Figure 1.1). Each component of "labile C" was also used as exogenous variable influencing SOC contents (arrow 6 on Figure 1.1). Means of sand content were used to construct

another four models including difference of each observed variable within "labile C" between the two plant systems (ΔMBC, ΔPOM, ΔDOC, ΔCO_2). The list of the path analysis models was attached on Table 1.2, and the hypothesized effects of the individual component of "labile C" were described by additional statements of Table 1.4.

Table 1.4. Theoretical support for the hypothesized effects of individual component within labile C characteristics in the path analyses (Arrows in the conceptual model of Figure 1.1 indicate hypothesized mechanisms of the individually numbered paths).

Fig. #	Path # (Fig. 1.1)	Paths from	Paths across	Paths to	Hypotheses under the paths
1.8a & 1.9a	①	Sand	-	TOC	Sand content determines accessibility of microorganisms to nutrient source, and soil pores function as their habitats. Those affect microbial growth, which relates to C turnover rates and consequent C accumulation.
	②-⑤	Sand	Pore	TOC	
	③-⑥	Sand	**MBC**	TOC	
	②-④-⑥	Sand	Pore - **MBC**	TOC	
1.8b & 1.9b	①	Sand	-	TOC	Sand content and soil pores affect the occlusion and stabilization of POM, and POM functions as an organic C source for soil microorganisms, while the products of its decomposition are stabilized.
	②-⑤	Sand	Pore	TOC	
	③-⑥	Sand	**POM**	TOC	
	②-④-⑥	Sand	Pore - **POM**	TOC	
1.8c & 1.9c	①	Sand	-	TOC	Sand content and soil pores affect retention in and/or loss from soil, and remaining DOC in the soil functions as a major source of soil organic C and/or as an easily decomposed component of the organic C.
	②-⑤	Sand	Pore	TOC	
	③-⑥	Sand	**DOC**	TOC	
	②-④-⑥	Sand	Pore - **DOC**	TOC	
1.8d & 1.9d	①	Sand	-	TOC	Sand content and soil pores determine organic C availability to microorganisms and transit of respired CO_2.Thus, the respiration rates indicate how much newly added C substrates are processed and/or existed soil C is decomposed.
	②-⑤	Sand	Pore	TOC	
	③-⑥	Sand	**CO_2**	TOC	
	②-④-⑥	Sand	Pore - **CO_2**	TOC	

Note: Literatures to support the hypotheses of the paths were listed in Table 1.3.

We followed the two-index presentation strategy for model evaluation suggested by Hu and Bentler (1999). That is, a chi-square test (χ^2) and goodness of fit index (GFI) were used to determine model fitness and adequacy. The indices measure the degree to which the model accounts for the variance and covariance among the observed variables (Bentler, 1990). The models with χ^2 test p values > 0.05 and GFI > 0.90 are regarded as acceptable (Hu and Bentler, 1999, Eisenhauer et al., 2015). Since the observed variables differed in their units and scales, the standardized coefficients were computed using standardized data through PROC CALIS procedure. The computed coefficients were used to compare the relative impact of the initially incommensurable variables and to indicate the strength of the paths (Kwan and Chan, 2011).

1.3. Results

1.3.1 Basic soil properties

Soils of the six sites ranged in texture from silt loam to loamy sand. HA and LC sites were loamy sands with more than 80 % sand content, while silt loam of OR site contained less than 10 % of sand (Table 1.1). The prairie and switchgrass soils within each site did not differ from each other in terms of the soil chemical properties (Table 1.5). The only exception was a tendency for the higher Mn content in prairie soils, which was statistically significant in LC site.

Table 1.5. Soil chemical properties of the prairie and switchgrass bioenergy systems of the six studied sites.

Experimental site	Plant system	pH	Bray P (ppm)	CEC (meq/100 g)	Zn (ppm)	Mn (ppm)	Fe (ppm)	Cu (ppm)
Oregon (OR)	Prairie	5.7	11.5	10.1	5.4	95.9	41.3	3.8
	Switchgrass	5.8	12.3	9.2	5.6	86.9	31.0	3.7
Lux Arbor (LA)	Prairie	6.4	15.8	6.3	2.0	44.3	21.3	2.1
	Switchgrass	6.2	19.5	5.9	1.9	38.7	24.8	1.7
Escanaba (ES)	Prairie	6.4	9.0	7.6	2.8	31.8	20.5	6.2
	Switchgrass	6.4	7.8	7.7	2.6	26.5	20.8	6.8
Rhinelender (RH)	Prairie	4.9	258.8	3.1	2.6	23.7	72.5	11.8
	Switchgrass	5.1	241.3	3.7	1.8	21.8	71.3	10.8
Hancock (HA)	Prairie	6.0	73.7	4.0	3.5	16.3	26.7	1.7
	Switchgrass	6.0	78.3	4.1	3.0	15.3	37.0	1.6
Lake City (LC)	Prairie	5.7	28.3	5.0	4.2	**25.6**	27.5	0.8
	Switchgrass	6.5	40.5	6.2	3.6	**12.0**	18.3	0.7

Note: Bolded values of chemical properties within each site indicate that differences between prairie and switchgrass soil were statistically significant at the $p < 0.05$ level.

1.3.2 SOC and labile C characteristics

The interaction between experimental sites and plant systems in the ANOVA tests were not statistically significant for the studied soil C variables, except for POM (Figure 1.2). Across all studied sites, SOC and MBC were higher in prairie than in switchgrass system ($p < 0.05$) (Figure 1.2a and 1.2b). SOC was higher than that of switchgrass in all sites (Figure 1.2a), and MBC was higher than that of switchgrass in all sites, but LC (Figure 1b). POM was higher in prairie than in switchgrass in four of the sites (Figure 1.2c). There were no significant differences between the two systems in terms of either DOC or short-term respiration (Figure 1.2d and 1.2e).

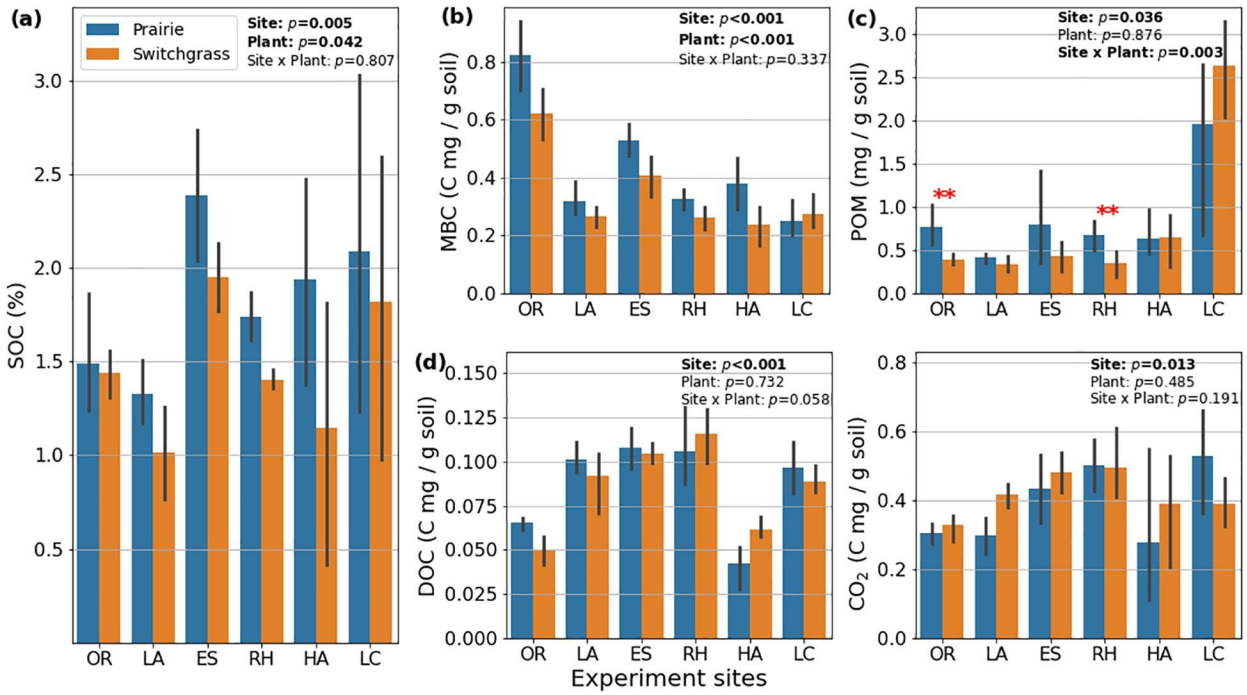

Figure 1.2. Soil C characteristics of the prairie and switchgrass bioenergy systems in the six studied experimental sites (**a**: SOC, **b**: MBC, **c**: POM, **d**: DOC, and **e**: 10-day CO_2 respiration) (OR: Oregon; LA: Lux Arbor; ES: Escanaba; RH: Rhinelender; HA: Hancock; LC: Lake City). Error bars represent standard deviation, and ANOVA test results are shown in the top-right corner of each figure. Symbol ** on Fig. 1.2c denotes statistically significant differences in POM between the two systems in each studied site at the $p < 0.05$ level (POM was the only variable where the Plant*Site interaction was statistically significant). OR, LA, ES, and RH sites: n = 4 and HA and LC sites: n = 3.

1.3.3 Volume of medium pores and its relationship to SOC

The pore-size distributions differed among the studied six sites and between two plant systems (Figure 1.3). Since the pores within 50–150 µm Ø size range were hypothesized to be of the greatest importance for decomposition and protection of the newly added C, the fractions of medium pores were extracted from the entire data set and analyzed separately (Figure 1.4). Prairie system had greater fractions of medium pores than switchgrass across all sites ($p = 0.005$) (Figure 1.4). Examples of distributed pores within this size range in the two systems of Oregon and Lake City sites, having the least and most sand contents (Table 1.1), are provided in Figure 1.5.

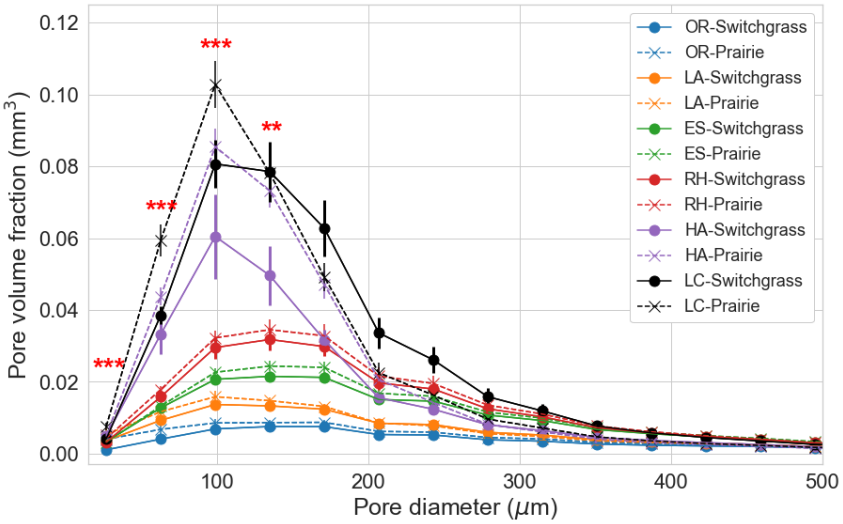

Figure 1.3. Soil pore size distributions in prairie and switchgrass systems of six studied sites (OR: Oregon; LA: Lux Arbor; ES: Escanaba; RH: Rhinelender; HA: Hancock; LC: Lake City). Shown are averages and standard deviations. The ** and *** symbols denote significant differences between the two systems across all sites at $p < 0.01$ and < 0.001 levels, respectively (OR, LA, ES, and RH sites: n = 12 and HA and LC sites: n = 9).

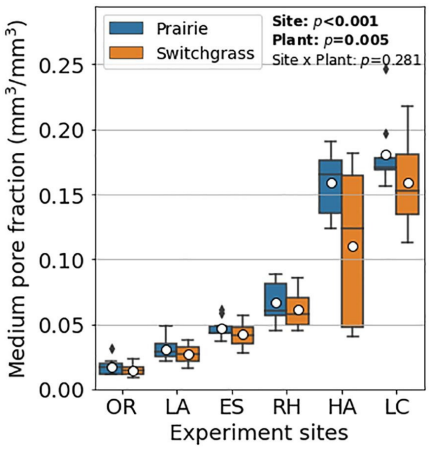

Figure 1.4. Fractions of medium (50–150 µm Ø) pores in intact soil cores from prairie and switchgrass systems of the six studied sites (OR: Oregon; LA: Lux Arbor; ES: Escanaba; RH: Rhinelender; HA: Hancock; LC: Lake City). Means are represented by white circles and medians by horizontal black lines. ANOVA results are shown in the top-right corner (based on 12 scanned soil cores per site from OR, LA, ES, and RH and on 9 cores per site from HA and LC).

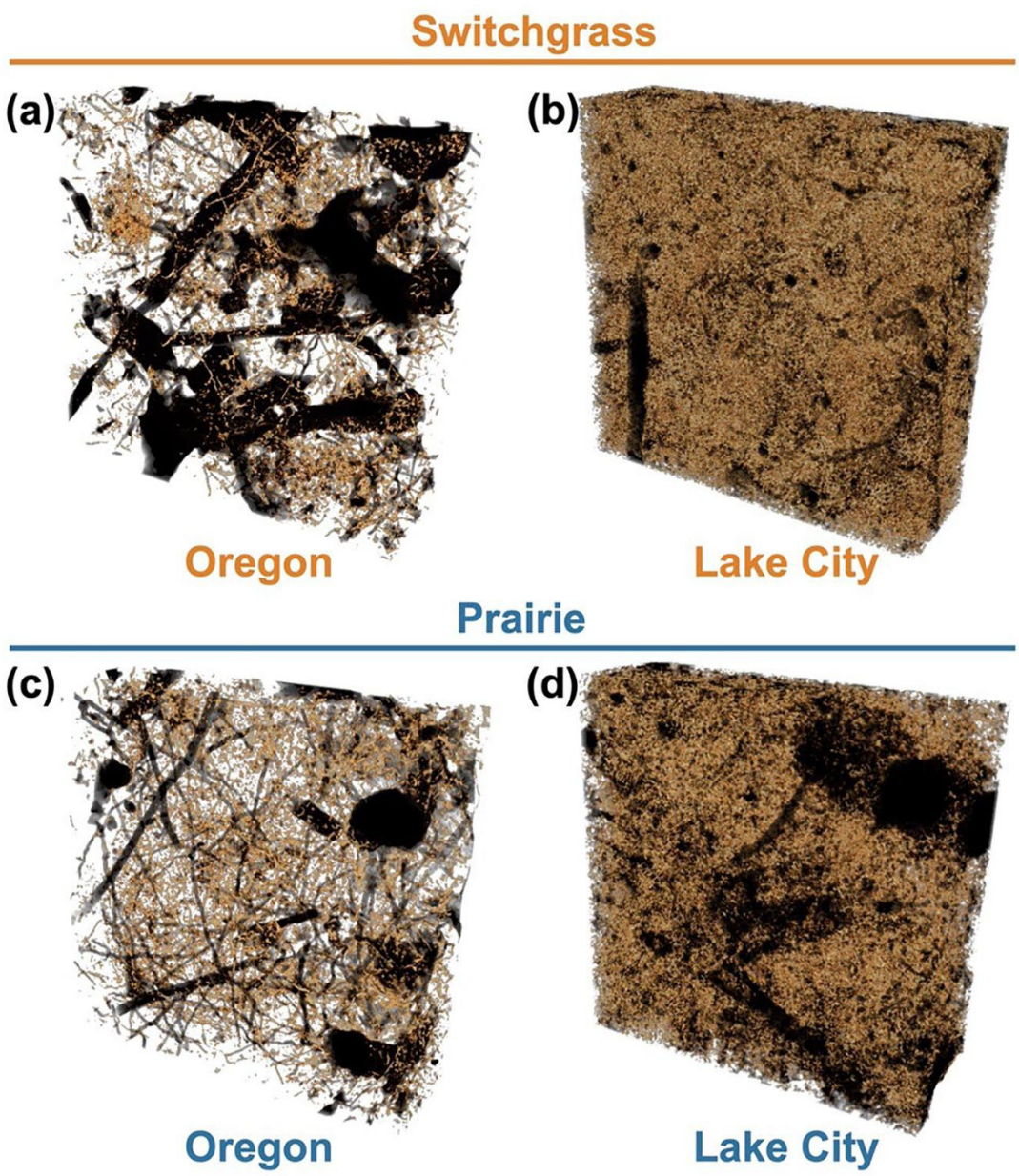

Figure 1.5. Examples of 3D images showing pores (dark to lightbrown) in the intact samples of soils from monoculture switchgrass and restored prairie systems in Oregon, WI (silt loam) and Lake City, MI (loamy sand) experimental sites. Shown are pores visible at the studied X-ray µCT resolution, i.e., > 18.2 µm Ø. Lightbrown marks the medium (50–150 µm Ø) pores.

The fractions of medium pores were not correlated to SOC contents in either prairie (p = 0.19) or switchgrass (p = 0.41) soils (Figure 1.6a and 1.6b). But the differences in SOC contents between prairie and switchgrass soils, ΔSOC, were positively correlated to the respective differences in medium pore fractions, ΔMedium, when assessed across all studied sites (Figure 1.6c).

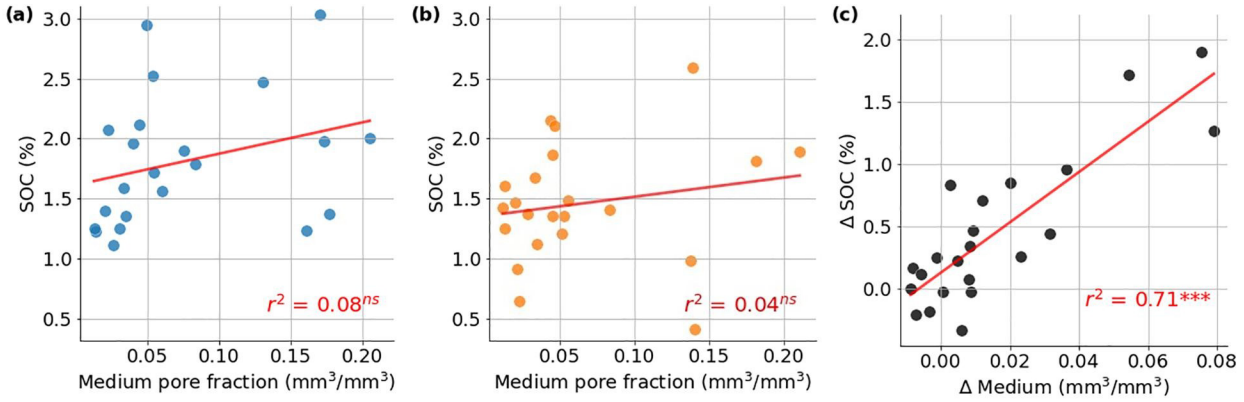

Figure 1.6. Relationships between fractions of medium (50–150 µm Ø) pores and soil organic C (SOC) contents **(a)** in prairie system and **(b)** in switchgrass system as well as **(c)** differences between soils of prairie and switchgrass systems in terms of medium pores (Δ Medium) plotted versus respective differences in SOC contents. The differences developed after 6–7 years of system implementation and were calculated by subtracting the pore fractions and SOC contents of switchgrass system from those of the prairie system. Shown are observations from the six studied sites (dots), the linear regression fitted to the data (red), and the r^2 value for the fitted regression model (in **(a)** and **(b)** $p > 0.05$, in **(c)** $p < 0.001$).

1.3.4 Structural equation modeling

The two plant systems showed similar trends in terms of their paths of direct and indirect effects of soil texture on SOC contents. The texture affected the fraction of medium pores and labile C in both systems (Figure 1.7a), and labile C affected SOC contents (Figure 1.7a). However, the medium pore fractions did not influence either labile C or SOC contents in either of the systems.

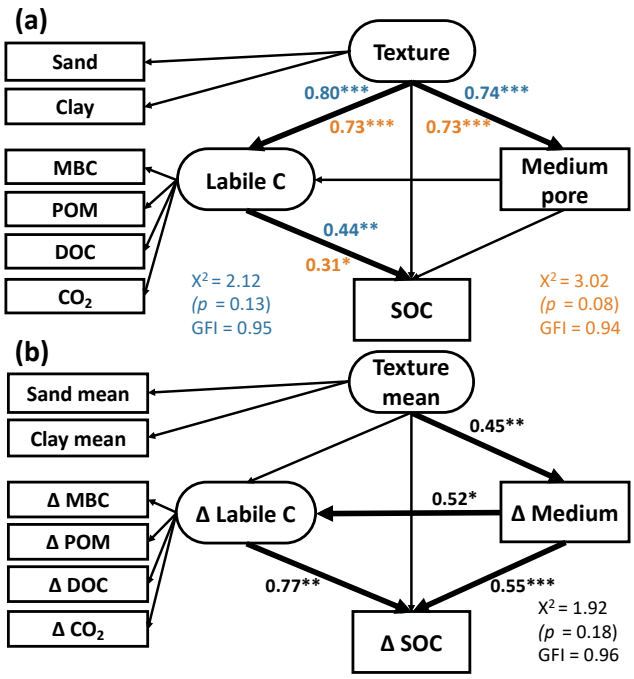

Figure 1.7. Structural equation models examining the hypothesized effects of soil texture, represented by sand and clay contents on **(a)** soil organic C (SOC) and **(b)** on the difference in SOC between soils under either prairie or switchgrass vegetation. We hypothesize that the texture influences the overall formation of medium (50-150 μm Ø) pores **(a)**, as well as their enhanced formation under prairie vegetation **(b)**. Directly and indirectly (through medium pores) it affects soil labile C, while all of them influence the SOC contents **(a)** as well as SOC increases due to diverse vegetation of the prairie system **(b)**. Observed and latent variables are given with rectangular and oval boxes, respectively. Numbers represent standardized path coefficients, and bold arrows (solid for positive and dashed for negative) represent statistically significant effects (*, **, and *** denote statistical significance at $p < 0.05$, < 0.01, and < 0.001 levels, respectively). On **(a)**, orange and blue mark the results from switchgrass and prairie systems, respectively. χ^2 and GFI values are shown under the corresponding models.

The texture influenced the differences between prairie and switchgrass in terms of the fractions of medium pores, which then affected the differences in labile C, ΔLabile C (Figure 1.7b). These prairie-switchgrass differences in the fractions of medium pores along with ΔLabile C, mediated by texture, influenced the prairie-switchgrass differences in SOC contents. Prairie system had greater medium pore fractions and SOC contents compared to switchgrass (Figure 1.2a and 1.4). Thus, the magnitude of the increases due to prairie in medium pore fractions directly and indirectly affected the magnitude of the increases in SOC contents (Figure 1.7b).

1.3.5 Multiple path analyses

Sand contents had a direct negative effect on MBC and direct positive effects on DOC and CO_2 (Figure 1.8a, 1.8c, and 1.8d). There was no direct effect of sand contents on POM in both plant systems, while the fraction of medium pores was the main driver of the positive indirect effect of sand contents on POM (Figure 1.8b). For DOC and CO_2 that indirect effect was negative (Figure 1.8c and 1.8d). Soil MBC and POM had direct positive effects on SOC contents (Figure 1.8a and 1.8b), whereas DOC and CO_2 of the soil had no direct effect on SOC contents in both plant systems (Figure 1.8c and 1.8d). As expected, the effects of clay contents had opposite signs of those of sand content (Figure 1.9).

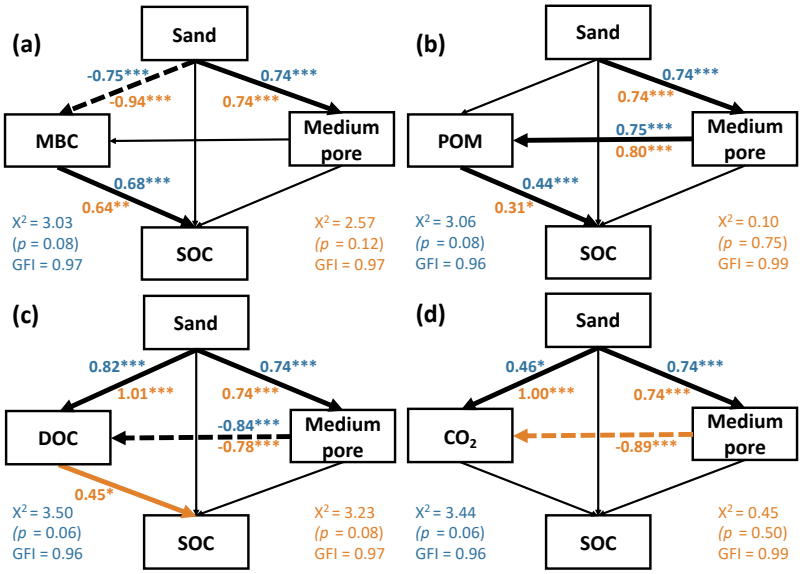

Figure 1.8. Multiple path analyses for direct and indirect effects of sand in the restored prairie and monoculture switchgrass soils in terms of SOC, manifested through medium (50-150 µm Ø) pores and either MBC **(a)**, POM **(b)**, DOC**(c)**, or short-term respiration CO_2 **(d)**. Numbers on the arrows are standardized path coefficients, and arrows (solid for positive and dashed for negative) were bolded when the paths were statistically significant (*, **, and *** denote statistical significance at $p < 0.05$, < 0.01, and < 0.001 levels, respectively). χ^2 and GFI values are shown under the corresponding path analysis models.

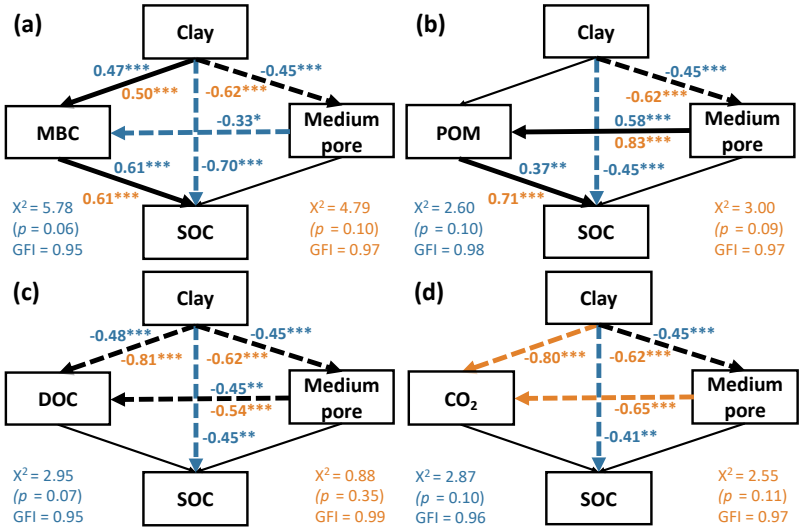

Figure 1.9. Multiple path analyses for direct and indirect effects of clay in the restored prairie and monoculture switchgrass soils in terms of SOC, manifested through medium (50-150 µm Ø) pores and either MBC **(a)**, POM **(b)**, DOC**(c)**, or short-term respiration CO_2 **(d)**. Numbers on the arrows are standardized path coefficients, and arrows (solid for positive and dashed for negative) were bolded when the paths were statistically significant (*, **, and *** denote statistical significance at $p < 0.05$, < 0.01, and < 0.001 levels, respectively). χ^2 and GFI values are shown under the corresponding path analysis models.

The fraction of medium pores was higher in prairie compared to switchgrass system (Figure 1.4), and the increases in fractions of such pores due to prairie system (ΔMedium) were positively influenced by soil sand content (Figure 1.10). Sand content negatively, while clay content positively (Figure 1.11), influenced the magnitude of increases in MBC due to prairie system (ΔMBC), but it did not affect either ΔDOC or ΔPOM (Figure 1.10a, 1.10c, and 1.10d). The ΔMedium led to greater ΔMBC and ΔSOC (Figure 1.10a). While increase in MBC due to prairie (ΔMBC) positively influenced ΔSOC (Figure 1.10a), the contributions of ΔDOC and ΔCO_2 were negative (Figure 1.10c and 1.10d).

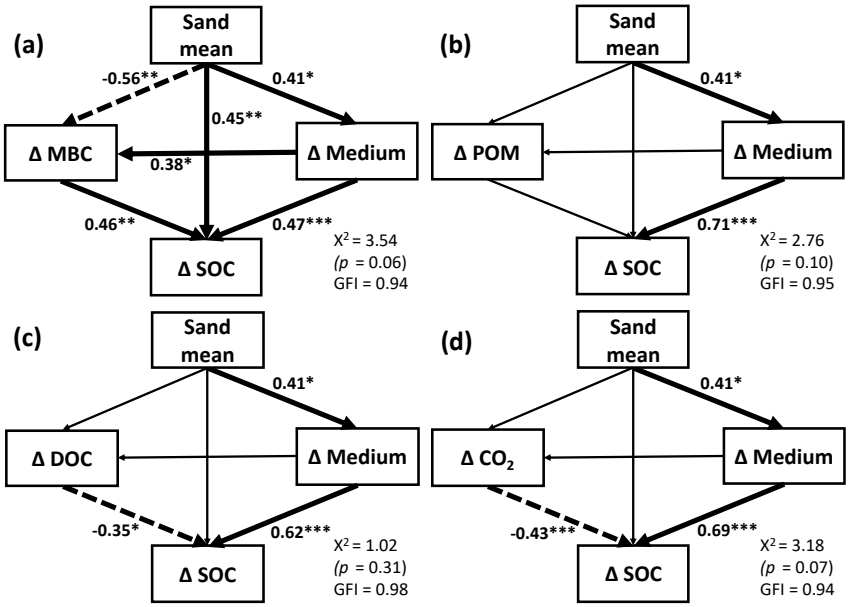

Figure 1.10. Multiple path analyses for direct and indirect effects of sand on differences between the restored prairie and monoculture switchgrass soils in terms of SOC, manifested through the differences in medium (50-150 μm Ø) pores and either MBC **(a)**, POM **(b)**, DOC**(c)**, or short-term respiration CO_2 **(d)** differences. Numbers on the arrows are standardized path coefficients, and arrows (solid for positive and dashed for negative) were bolded when the paths were statistically significant (*, **, and *** denote statistical significance at $p < 0.05$, < 0.01, and < 0.001 levels, respectively). χ^2 and GFI values are shown under the corresponding path analysis models.

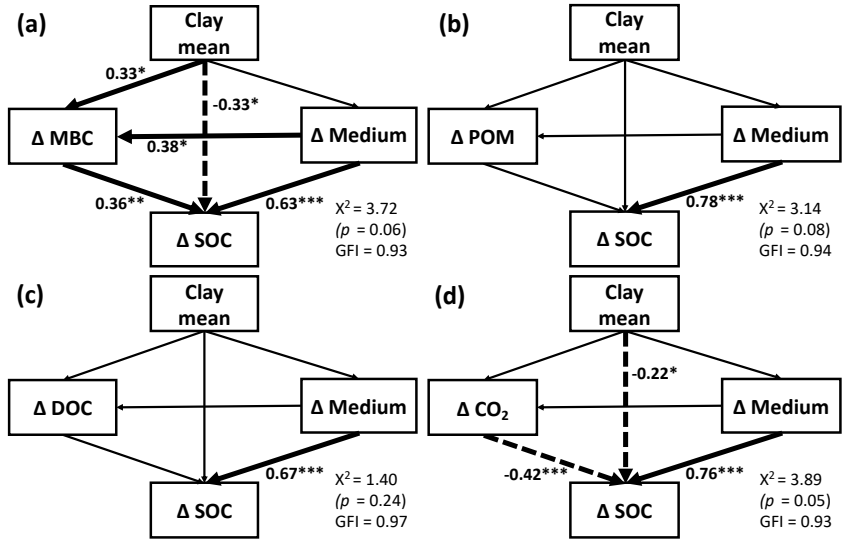

Figure 1.11. Multiple path analyses for direct and indirect effects of clay on differences between the restored prairie and monoculture switchgrass soils in terms of SOC, manifested through the differences in medium (50-150 μm Ø) pores and either MBC **(a)**, POM **(b)**, DOC**(c)**, or short-term respiration CO_2 **(d)** differences. Numbers on the arrows are standardized path coefficients, and arrows (solid for positive and dashed for negative) were bolded when the paths were statistically significant (*, **, and *** denote statistical significance at $p < 0.05$, < 0.01, and < 0.001 levels, respectively). χ^2 and GFI values are shown under the corresponding path analysis models.

1.4 Discussion

After polyculture restored prairie and monoculture switchgrass systems were in place for several (6–7) years their soils diverged in terms of the volumes of medium (50–150 μm Ø size range) pores, as well as in terms of the soil MBC and SOC contents. The results supported our hypotheses that prolonged prairie vegetation leads to greater formation of medium pores which further stimulate soil C gains across a range of soil textures and types. When the effects of sand content and changes in the volume of medium pores were accounted for, the increases in MBC due to prairie vegetation led to increases in SOC contents over those of monoculture switchgrass, while the increases in DOC contents and short-term respiration led to SOC decreases.

1.4.1 Monoculture switchgrass system is slower in soil C accrual than restored prairie

The finding that long-term implementation of polyculture prairie system increased SOC contents as compared to monoculture switchgrass (Figure 1.2a) is in agreement with other published studies, which consistently observed greater soil C in polyculture system than in monoculture. High plant diversity positively affected soil C accumulation in bioenergy cropping systems of the US Midwest (Fornara and Tilman, 2008, Sanford, 2014, Sprunger and Philip Robertson, 2018), and increasing the number of plant species directly promoted soil C gains and soil microbial biomass (Prommer et al., 2020). Increases in soil C contents were positively correlated with the plant species richness in grasslands of UK and Central Europe (De Deyn et al., 2011, Lange et al., 2015).

Plant systems with highly diverse perennial vegetation stimulate soil C accrual via several mechanisms. Among them are greater inputs of active C into rhizosphere, faster rates of microbial growth and turnover (Lange et al., 2015, Eisenhauer et al., 2017, Sprunger and Robertson, 2018), and greater nitrogen use efficiency in cases of joint presence of C4 grasses and legumes (Lange et al., 2015). Greater microbial activity is another recognized driver of soil C gains in diverse plant communities vs. monocultures (Lange et al., 2015), but this does not seem to be the case for monoculture vs. polyculture switchgrass system (Jesus et al., 2016, Zhang et al., 2017).

Greater above- and belowground productivity is yet another driver of soil C gains suggested by large scale *meta*-analysis (Chen et al., 2018) and experimental work (Furey and Tilman, 2021). However, switchgrass monoculture cropping system appears to be an exception, because its root biomass and aboveground productivity are massive, yet the soil C gains are very slow to non-existent (McLaughlin and Kszos, 2005, Chimento et al., 2016, Sprunger et al., 2020). Indeed, when working with soils of LA experimental site of this study, Gelfand et al. (2020) reported lower root biomass in the prairie than in the switchgrass system, while harvested aboveground biomass was more than twice that in the switchgrass as in the prairie. Significantly greater aboveground productivity of switchgrass was observed compared to that of prairie in all other experimental sites reported in our study, i.e., OR, ES, RH, HA, and LC (Li et al., 2022), as well as in yet another low fertility soil of the U.S. Midwest (Cooney et al., 2023). Another experiment in the direct vicinity of our LA site (Lei et al., 2021) reported no statistically significant differences in root biomass between the restored prairie and the monoculture switchgrass system. Thus, contrary to the expectations, our results and published studies suggest that the productivity does not always serve as a significant determinant of soil C accumulation.

Faster C accrual in the prairie than in the switchgrass soil was related to greater formation of medium pores (Figure 1.4). Changes in the pore systems, e.g., volumes of medium pores, likely responded to the differences in the root systems of the plant communities (Pagliai and De Nobili, 1993, Lucas et al., 2022). We surmise that the volume of fine roots is the key contributor to the formation of medium pores (Bodner et al., 2014, Koebernick et al., 2017). Prairie vegetation has greater densities of fine (<2mm Ø) roots as compared to monoculture switchgrass (Sprunger et al., 2017), and even fine roots of the prairie tend to be thinner than those of the switchgrass. For example, only 35–71 % of switchgrass fine roots had their diameters within < 0.5 mm size range, while a number of other native grasses had more than 80 % of their fine roots in the < 0.5 mm Ø size class (De Graaff et al., 2013, Liu et al., 2022).

1.4.2 Contributions of soil texture and medium pores to SOC gains under prairie vegetation

The advantages of the prairie over monoculture switchgrass in terms of soil C accrual appeared to be much more pronounced in the coarse- than in the fine-textured soils of this study. For example, the SOC

content of the prairie system was ~ 3 % higher than that of the switchgrass in the silt loam soil (OR), while it was 15–69 % higher in the coarser textured soils (Figure 1.2a). Consistent with our findings, Juyal et al. (2021) reported only minor differences in soil C between prairie and monoculture switchgrass systems in fine-textured soils of topographic depressions, while substantially higher C in prairie than in switchgrass in the coarse-textured soils of uphill areas. Kasanke et al. (2021) reported that soil C contents under switchgrass vegetation even decreased after 6 years of growth on sandy soils.

According to our hypotheses (Table 1.2), the influence of the soil texture on the magnitude of increases in SOC contents under prairie vegetation was manifested through the texture's contribution to formation of soil pores, to MBC, and to C protection on mineral surfaces. Soil texture drives the size distribution of soil pores (Nimmo, 2013, Ding et al., 2016, Fan et al., 2021). Higher sand content was associated with greater presence of the medium pores in the studied soils, in both plant systems (Figure 1.8). Medium sized pores are easily accessible to fine roots and root hairs (Koebernick et al., 2017, Lucas, 2022). Thus, it can be surmised that prolific fine roots of prairie vegetation readily explored the existing medium pores in the sandier soils of this study, while still contributing to the formation of new ones. Bulkier switchgrass roots might have been at a disadvantage since they did not have as much access to the already existing medium size pore space.

Pores determine access to the soil organic matter by microorganisms and thus its processing and protection (Strong et al., 2004, Negassa et al., 2015). Medium pores are known to function as optimal microbial habitats, supporting high microbial activity (Wright et al., 1995, Nunan et al., 2003, Xia et al., 2022). They ensure high oxygen and water availability, yet do not limit the accessibility of microorganisms to organic matter substrates (Rawlins et al., 2016, Keiluweit et al., 2018). They were also reported as the primary locations of rhizodeposition inputs (Quigley and Kravchenko, 2022), thus providing C and nutrients for the resident microorganisms. A diversity of C inputs from polyculture prairie vegetation probably stimulated development of high species diversity in the microbial communities. The resultant greater microbial activity in such pores could lead to faster processing of new C additions and potentially

to generation of more microbial decomposition products and necromass, which then can be protected within the soil matrix (Strong et al., 2004, Quigley et al., 2018, Guidi et al., 2021).

Our study does not allow us to directly examine the utilization of the medium pores by the roots of the two studied systems. However, it is reasonable to assume that if the medium pores were less used by the switchgrass with its thicker roots, they did not receive as much new C inputs and were not as attractive to microorganisms as they were in the prairie systems. It is important to emphasize that it is not just the volume of the medium pores *per se* that stimulates SOC gains, but the volume of such pores that are supplied with new C. Indeed, the observed SOC contents were not related to the fractions of medium pores (Figure 1.6a and 1.6b). Yet, the differences between the two systems, i.e., ΔMedium and ΔSOC, were positively associated with each other (Figure 1.6c), suggesting that formation of such pores, which in prairie system was likely accompanied by C inputs, went hand-in-hand with soil C gains.

This explanation is further supported by our MBC results. Consistent with other reports (Kaiser et al., 1992, Franzluebbers et al., 1996), MBC decreased with increasing sand contents in this study, thus was negatively correlated with the volume fractions of the medium pores (Figure 1.12). However, the increase in the medium pores due to prairie vegetation, ΔMedium, promoted MBC increases, ΔMBC (Figure 1.10a). Thus, extra formation of such pores via prairie vegetation, likely accompanied by the rhizodeposits and other C inputs into them, stimulated microorganisms. Consistent with our expectations (Table 1.3) and literatures (Miltner et al., 2012, Oduor et al., 2018, Prommer et al., 2020), the ΔMBC positively influenced ΔSOC, likely through greater quantities of living microorganisms and their necromass accumulation.

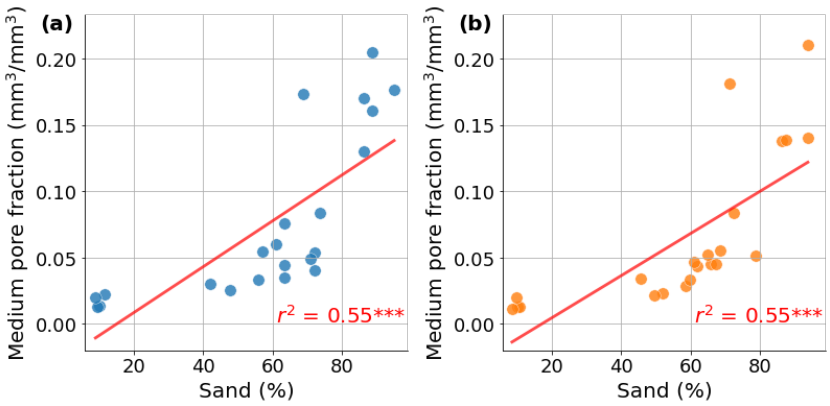

Figure 1.12. Relationships between sand contents and medium (50-150 µm Ø) **(a)** in prairie system and **(b)** in switchgrass system. Shown are observations from the six studied sites (dots), the linear regression fitted to the data (line), and the r^2 values for the fitted regression models (*** denote coefficient levels at the $p < 0.001$ level).

MBC, POM, DOC, and short-term respiration are often found to be positively correlated to each other and to the SOC contents (Franzluebbers, 1999, Dou et al., 2008, Oduor et al., 2018). Such correlations reflect joint common effects of soil texture, management practices or land use changes on soil C inputs and protection, which simultaneously drive root growth and subsequent POM inputs (Rasse et al., 2005, Ontl et al., 2015), abundance of microorganisms (Anderson and Domsch, 1989, Jinbo et al., 2006), and subsequent DOC and CO_2 production in a course of microbial activity (Jinbo et al., 2006, Mavi et al., 2012, Woloszczyk et al., 2020). Similarly, when examined across the range of the studied soils, path analysis of this study demonstrated that greater MBC, POM, and DOC is related to an overall greater SOC (Figure 1.8).

Yet, analysis of the differences between the two systems enabled unraveling some of the co-variations between these labile C characteristics and offered us an opportunity to assess the mechanisms of their individual impacts on SOC gains. Prairie-induced increases in DOC and short-term respiration negatively influenced ΔSOC (Figure 1.10c) – the result consistent with the expectation that greater C losses as either CO_2 or DOC slow down SOC gains. Greater DOC suggests that there is more organic C available for immediate microbial decomposition or possible loses with outflowing water into deeper soil layers (Kalbitz and Kaiser, 2008, Andrews et al., 2011), and coarse-textured soils tended to retain less DOC than

the fine-textured ones (Shen, 1999, Filep et al., 2022). C mineralization from newly added C substrates can be more rapid in coarse-textured soils compared to that in fine-textured soils (Franzluebbers, 1999).

Even though other studies, e.g., Fukumasu et al. (2022) found positive associations between volumes of 30–100 μm Ø pores and POM contents, suggestive that the abundance of such pores was likely to be associated with higher growth of fine roots, the POM effect was not significant in our study. That likely was due to substantial variability of our POM data (Figure1.2).

1.5 Conclusions

Multiple years of prairie vegetation led to greater volume fractions of medium pores compared to monoculture switchgrass across several soils of the U.S. Upper Midwest (Alfisol, Spodosol, and Entisol). The magnitude of the formation of such pores tended to be greater in coarse- than in fine-textured soils. Stimulation of such pore formation by prairie system led to greater microbial biomass, which, in turn, led to greater SOC contents compared to monoculture switchgrass system. The more prairie vegetation promoted development of such pores, the higher were its SOC contents as compared to the monoculture switchgrass. On the contrary, potentially higher C losses via CO_2 respiration and DOC in the prairie system contributed to slower soil C accumulation. The study provides an evidence that the interactive feedback loop connecting soil physical characteristics of texture and pore structure with microbial activity, and C accumulation acts across a wide range of soils and is an important mechanism of C gains in polyculture prairie vegetation.

1.6 Acknowledgements

I would like to thank Michelle Quigley from Michigan State University for conducting X-ray μCT scanning, Jenie Gil Lugo and Maxwell Oerther for assistance with sample collection, and the Kellogg Biological Station and Great Lakes Bioenergy Research Center team for agronomic management of the field experiment. This research was funded by the Great Lakes Bioenergy Research Center, U.S. Department of Energy, Office of Science, Office of Biological and Environmental Research under Award Number DE-SC0018409. The work was also supported by the NSF LTER Program (DEB 1027253) at Kellogg Biological Station and by Michigan State University's AgBioResearch.

REFERENCES

Adviento-Borbe, M. A. A., Doran, J. W., Drijber, R. A., & Dobermann, A. (2006). Soil electrical conductivity and water content affect nitrous oxide and carbon dioxide emissions in intensively managed soils. *Journal of Environmental Quality*, 35 (6), 1999 – 2010. doi: 10.2134/jeq2006.0109

Anderson, T. -H., & Domsch, K. H. (1989). Ratios of microbial biomass carbon to total organic carbon in arable soils. *Soil Biology and Biochemistry*, 21(4), 471-479. doi:10.1016/0038-0717(89)90117-X

Andrews, D. M., Lin, H., Zhu, Q., Jin, L., & Brantley, S. L. (2011). Hot spots and hot moments of dissolved organic carbon export and soil organic carbon storage in the shale hills catchment. *Vadose Zone Journal*, 10(3), 943-954. doi:10.2136/vzj2010.0149

Bailey, V. L., Smith, A. P., Tfaily, M., Fansler, S. J., & Bond-Lamberty, B. (2017). Differences in soluble organic carbon chemistry in pore waters sampled from different pore size domains. *Soil Biology and Biochemistry*, 107, 133-143. doi:10.1016/j.soilbio.2016.11.025

Beare, R., Lowekamp, B., and Yaniv, Z. (2018). Image segmentation, registration and characterization in R with SimpleITK. J. Stat. Softw. 86, 1–35. doi: 10.18637/jss.v086.i08

Bentler, P. M. (1990). Comparative fit indexes in structural models. *Psychological Bulletin*, 107(2), 238-246. doi:10.1037/0033-2909.107.2.238

Bodner, G., Leitner, D., & Kaul, H. -P. (2014). Coarse and fine root plants affect pore size distributions differently. *Plant and Soil*, 380(1), 133-151. doi:10.1007/s11104-014-2079-8

Buades, A., Coll, B., & Morel, J -M. (2011). Non-Local Means Denoising, *Image Processing On Line*, 1, 208–212. doi:10.5201/ipol.2011.bcm_nlm

Cambardella, C. A., & Elliot, E. T. (1992). Particulate soil organic-matter changes across a grassland cultivation sequence. *Soil Science Society of America Journal*, 56(3), 777-783. doi:10.2136/sssaj1992.03615995005600030017x

Chen, S., Wang, W., Xu, W., Wang, Y., Wan, H., Chen, D., . . . Bai, Y. (2018). Plant diversity enhances productivity and soil carbon storage. *Proceedings of the National Academy of Sciences of the United States of America*, 115(16), 4027-4032. doi:10.1073/pnas.1700298114

Chimento, C., Almagro, M., & Amaducci, S. (2016). Carbon sequestration potential in perennial bioenergy crops: the importance of organic matter inputs and its physical protection. *GCB Bioenergy*, 8(1), 111-121. doi:10.1111/gcbb.12232

Clough, A., & Skjemstad, J. O. (2000). Physical and chemical protection of soil organic carbon in three agricultural soils with different contents of calcium carbonate. *Australian Journal of Soil Research*, 38(5), 1005-1016. doi:10.1071/SR99102

Cooney, D. R., Namoi, N., Zumpf, C., Lim, S. -H., Villamil, M., Mitchell, R., & Lee D. K. (2023). Biomass Production and Nutrient Removal by Perennial Energy Grasses Produced on a Wet Marginal Land. *Bioenergy Research*, 16(2), 886-897. doi: 10.1007/s12155-022-10488-0

Darbon, J., Cunha, A., Chan, T. F., Osher, S., & Jensen, G. J. (2008). Fast nonlocal filtering applied to electron cryomicroscopy. Paper presented at the 2008 5th IEEE International Symposium on Biomedical Imaging: From Nano to Macro, Proceedings, ISBI, 1331-1334. doi:10.1109/ISBI.2008.4541250

David, K., & Ragauskas, A. J. (2010). Switchgrass as an energy crop for biofuel production: A review of its ligno-cellulosic chemical properties. *Energy and Environmental Science*, 3(9), 1182-1190. doi:10.1039/b926617h

De Deyn, G. B., Shiel, R. S., Ostle, N. J., Mcnamara, N. P., Oakley, S., Young, I., Freeman, C., Fenner, N., & Bardgett, R. D. (2011). Additional carbon sequestration benefits of grassland diversity restoration. *Journal of Applied Ecology*, 48(3), 600-608. doi:10.1111/j.1365-2664.2010.01925.x

De Graaff, M. A., Six, J., Jastrow, J. D., Schadt, C. W., & Wullschleger, S. D. (2013). Variation in root architecture among switchgrass cultivars impacts root decomposition rates. *Soil Biology and Biochemistry*, 58, 198-206. doi:10.1016/j.soilbio.2012.11.015

Ding, D., Zhao, Y., Feng, H., Peng, X., & Si, B. (2016). Using the double-exponential water retention equation to determine how soil pore-size distribution is linked to soil texture. *Soil and Tillage Research*, 156, 119-130. doi:10.1016/j.still.2015.10.007

Don, A., & Schulze, E. -D. (2008). Controls on fluxes and export of dissolved organic carbon in grasslands with contrasting soil types. *Biogeochemistry*, 91(2-3), 117-131. doi:10.1007/s10533-008-9263-y

Dou, F., Wright, A. L., & Hons, F. M. (2008). Sensitivity of labile soil organic carbon to tillage in wheat-based cropping systems. *Soil Science Society of America Journal*, 72(5), 1445-1453. doi:10.2136/sssaj2007.0230

Eisenhauer, N., Bowker, M. A., Grace, J. B., & Powell, J. R. (2015). From patterns to causal understanding: Structural equation modeling (SEM) in soil ecology. *Pedobiologia*, 58(2-3), 65-72. doi:10.1016/j.pedobi.2015.03.002

Eisenhauer, N., Lanoue, A., Strecker, T., Scheu, S., Steinauer, K., Thakur, M. P., & Mommer, L. (2017). Root biomass and exudates link plant diversity with soil bacterial and fungal biomass. *Scientific Reports*, 7 doi:10.1038/srep44641

Fan, Z., Hu, C., Zhu, Q., Jia, Y., Zuo, D., & Duan, Z. (2021). Three-dimensional pore characteristics and permeability properties of calcareous sand with different particle sizes. *Bulletin of Engineering Geology and the Environment*, 80(3), 2659-2670. doi:10.1007/s10064-020-02078-1

Filep, T., & Rékási, M. (2011). Factors controlling dissolved organic carbon (DOC), dissolved organic nitrogen (DON) and DOC/DON ratio in arable soils based on a dataset from hungary. *Geoderma*, 162(3-4), 312-318. doi:10.1016/j.geoderma.2011.03.002

Filep, T., Zacháry, D., Jakab, G., & Szalai, Z. (2022). Chemical composition of labile carbon fractions in hungarian forest soils: Insight into biogeochemical coupling between DOM and POM. *Geoderma*, 419 doi:10.1016/j.geoderma.2022.115867

Fornara, D. A., & Tilman, D. (2008). Plant functional composition influences rates of soil carbon and nitrogen accumulation. *Journal of Ecology*, 96(2), 314-322. doi:10.1111/j.1365-2745.2007.01345.x

Franklin, S. M., Kravchenko, A. N., Vargas, R., Vasilas, B., Fuhrmann, J. J., & Jin, Y. (2021). The unexplored role of preferential flow in soil carbon dynamics. *Soil Biology and Biochemistry*, 161 doi:10.1016/j.soilbio.2021.108398

Franzluebbers, A. J., Haney, R. L., Hons, F. M., & Zuberer, D. A. (1996). Active fractions of organic matter in soils with different texture. *Soil Biology and Biochemistry*, 28(10-11), 1367-1372. doi:10.1016/S0038-0717(96)00143-5

Franzluebbers, A. J. (1999). Potential C and N mineralization and microbial biomass from intact and increasingly disturbed soils of varying texture. *Soil Biology and Biochemistry*, 31(8), 1083-1090. doi:10.1016/S0038-0717(99)00022-X

Fukumasu, J., Jarvis, N., Koestel, J., Kätterer, T., & Larsbo, M. (2022). Relations between soil organic carbon content and the pore size distribution for an arable topsoil with large variations in soil properties. *European Journal of Soil Science*, 73(1) doi:10.1111/ejss.13212

Furey, G. N., & Tilman, D. (2021). Plant biodiversity and the regeneration of soil fertility. *Proceedings of the National Academy of Sciences of the United States of America*, 118(49) doi:10.1073/pnas.2111321118

Gelfand, I., Hamilton, S. K., Kravchenko, A. N., Jackson, R. D., Thelen, K. D., Robertson, G. P. (2020). Empirical Evidence for the Potential Climate Benefits of Decarbonizing Light Vehicle Transport in the U.S. With Bioenergy from Purpose-Grown Biomass with and without BECCS. *Environmental Science and Technology*, 54 (5), 2961-2974. doi: 10.1021/acs.est.9b07019

Grace, J.B. (2006). *Structural Equation Modeling and Natural Systems*. Cambridge University Press, Cambridge, United Kingdom and New York, NY, USA.

Gee, G. W., & Or, D. (2002). *2.4 particle-size analysis*. In J. H. Dane, & C. G. Topp (eds.), *Methods of soil analysis: Part 4 physical methods* (pp. 255– 293). Madison, WI: Soil Science Society of America, American Society of Agronomy.

Guidi, P., Falsone, G., Wilson, C., Cavani, L., Ciavatta, C., & Marzadori, C. (2021). New insights into organic carbon stabilization in soil macroaggregates: An in situ study by optical microscopy and SEM-EDS technique. *Geoderma*, 397 doi:10.1016/j.geoderma.2021.115101

Haddix, M. L., Gregorich, E. G., Helgason, B. L., Janzen, H., Ellert, B. H., & Francesca Cotrufo, M. (2020). Climate, carbon content, and soil texture control the independent formation and persistence of particulate and mineral-associated organic matter in soil. *Geoderma*, 363 doi:10.1016/j.geoderma.2019.114160

Haney, R. L., Brinton, W. H., & Evans, E. (2008). Estimating soil carbon, nitrogen, and phosphorus mineralization from short-term carbon dioxide respiration. *Communications in Soil Science and Plant Analysis*, 39 (17-18), 2706 – 2720. doi: 10.1080/00103620802358862

Helliwell, J. R., Sturrock, C. J., Miller, A. J., Whalley, W. R., & Mooney, S. J. (2019). The role of plant species and soil condition in the structural development of the rhizosphere. *Plant Cell and Environment*, 42(6), 1974-1986. doi:10.1111/pce.13529

Hildebrand, T. & Rüegsegger, P. (1997). A new method for the model-independent assessment of thickness in three-dimensional images. *Journal of Microscopy*, 185(1), 67-75. doi:10.1046/j.1365-2818.1997.1340694.x

Hu, L. -T. & Bentler, P. M. (1999). Cutoff criteria for fit indexes in covariance structure analysis: Conventional criteria versus new alternatives. *Structural Equation Modeling*, 6(1), 1-55. doi:10.1080/10705519909540118

IPCC (2014). Technical Summary In Climate Change 2014: Mitigation of Climate Change. Contribution of Working Group III to the Fifth Assessment Report of the Intergovernmental Panel on Climate Change [Edenhofer, O., R. Pichs-Madruga, Y. Sokona, E. Farahani, S. Kadner, K. Seyboth, A. Adler, I. Baum, S. Brunner, P. Eickemeier, B. Kriemann, J. Savolainen, S. Schlömer, C. von Stechow, T. Zwickel and J. C. Minx (eds.)]. Cambridge University Press, Cambridge, United Kingdom and New York, NY, USA.

Jesus, E. D., Liang, C., Quensen, J. F., Susilawati, E., Jackson, R. D., Balser, T. C., & Tiedje, J. M. (2016). Influence of corn, switchgrass, and prairie cropping systems on soil microbial communities in the upper Midwest of the United States. *GCB Bioenergy*, 8(2), 481-494. doi: 10.1111/gcbb.12289

Jinbo, Z., Changchun, S., & Wenyan, Y. (2006). Land use effects on the distribution of labile organic carbon fractions through soil profiles. *Soil Science Society of America Journal*, 70(2), 660-667. doi:10.2136/sssaj2005.0007

Juyal, A., Guber, A., Oerther, M., Quigley, M., & Kravchenko, A. (2021). Pore architecture and particulate organic matter in soils under monoculture switchgrass and restored prairie in contrasting topography. *Scientific Reports*, 11(1) doi:10.1038/s41598-021-01533-7

Kaiser, E. A., Mueller, T., Joergensen, R. G., Insam, H., & Heinemeyer, O. (1992). Evaluation of methods to estimate the soil microbial biomass and the relationship with soil texture and organic matter. *Soil Biology and Biochemistry*, 24(7), 675-683. doi:10.1016/0038-0717(92)90046-Z

Kaiser, K., & Kalbitz, K. (2012). Cycling downwards - dissolved organic matter in soils. *Soil Biology and Biochemistry*, 52, 29-32. doi:10.1016/j.soilbio.2012.04.002

Kalbitz, K., & Kaiser, K. (2008). Contribution of dissolved organic matter to carbon storage in forest mineral soils. *Journal of Plant Nutrition and Soil Science*, 171(1), 52-60. doi:10.1002/jpln.200700043

Kasanke, C. P., Zhao, Q., Bell, S., Thompson, A. M., & Hofmockel, K. S. (2021). Can switchgrass increase carbon accrual in marginal soils? the importance of site selection. *GCB Bioenergy*, 13(2), 320-335. doi:10.1111/gcbb.12777

Kasmerchak, C.S. & Schaetzl, R. (2018). Soils of the GLBRC Marginal Land Experiment (MLE) sites. *Kellogg Biological Station Long term Ecological Research Special Publication*, Zenodo, doi:10.5281/zenodo.2578238.

Keiluweit, M., Gee, K., Denney, A., & Fendorf, S. (2018). Anoxic microsites in upland soils dominantly controlled by clay content. *Soil Biology and Biochemistry*, 118, 42-50. doi:10.1016/j.soilbio.2017.12.002

Kim, K., Guber, A., Rivers, M., & Kravchenko, A. (2020). Contribution of decomposing plant roots to N2O emissions by water absorption. *Geoderma*, 375 doi:10.1016/j.geoderma.2020.114506

Kleber, M., Sollins, P., & Sutton, R. (2007). A conceptual model of organo-mineral interactions in soils: Self-assembly of organic molecular fragments into zonal structures on mineral surfaces. *Biogeochemistry*, 85(1), 9-24. doi:10.1007/s10533-007-9103-5

Koebernick, N., Daly, K. R., Keyes, S. D., George, T. S., Brown, L. K., Raffan, A., Cooper, L. J., Naveed, M., Bengough, A. G., Sinclair, I., Hallett, P. D., & Roose, T. (2017). High-resolution synchrotron imaging shows that root hairs influence rhizosphere soil structure formation. New Phytologist, 216(1), 124-135. doi:10.1111/nph.14705

Kölbl, A., & Kögel-Knabner, I. (2004). Content and composition of free and occluded particulate organic matter in a differently textured arable cambisol as revealed by solid-state 13C NMR spectroscopy. *Journal of Plant Nutrition and Soil Science*, 167(1), 45-53. doi:10.1002/jpln.200321185

Kravchenko, A. N., Guber, A. K., Razavi, B. S., Koestel, J., Blagodatskaya, E. V., & Kuzyakov, Y. (2019a). Spatial patterns of extracellular enzymes: Combining X-ray computed micro-tomography and 2D zymography. *Soil Biology and Biochemistry*, 135, 411-419. doi:10.1016/j.soilbio.2019.06.002

Kravchenko, A. N., Guber, A. K., Razavi, B. S., Koestel, J., Quigley, M. Y., Robertson, G. P., & Kuzyakov, Y. (2019b). Microbial spatial footprint as a driver of soil carbon stabilization. *Nature Communications*, 10(1) doi:10.1038/s41467-019-11057-4

Kravchenko, A., Guber, A., Gunina, A., Dippold, M., & Kuzyakov, Y. (2021). Pore-scale view of microbial turnover: Combining 14C imaging, μCT and zymography after adding soluble carbon to soil pores of specific sizes. *European Journal of Soil Science*, 72(2), 593-607. doi:10.1111/ejss.13001

Kwan, J. L. Y., & Chan, W. (2011). Comparing standardized coefficients in structural equation modeling: A model reparameterization approach. *Behavior Research Methods*, 43(3), 730-745. doi:10.3758/s13428-011-0088-6

Lal, R. (2001). Soil degradation by erosion. *Land Degradation and Development*, 12(6), 519-539. doi:10.1002/ldr.472

Lange, M., Eisenhauer, N., Sierra, C. A., Bessler, H., Engels, C., Griffiths, R. I., Mellado-Vázquez, P. G., Malik, A. A., Roy, J., Scheu, S., Steinbeiss, S., Thomson, B. C., Trumbore, S. E., & Gleixner, G. (2015). Plant diversity increases soil microbial activity and soil carbon storage. *Nature Communications*, 6 doi:10.1038/ncomms7707

Lavallee, J. M., Soong, J. L., & Cotrufo, M. F. (2020). Conceptualizing soil organic matter into particulate and mineral-associated forms to address global change in the 21st century. *Global Change Biology*, 26(1), 261-273. doi:10.1111/gcb.14859

Lei, C., Abraha, M., Chen, J., & Su, Y. -J. (2021). Long-term variability of root production in bioenergy crops from ingrowth core measurements. *Journal of Plant Ecology*, 14(5), 757-770. doi: 10.1093/jpe/rtab018

Lennon, J. T., Aanderud, Z. T., Lehmkuhl, B. K., & Schoolmaster Jr., D. R. (2012). Mapping the niche space of soil microorganisms using taxonomy and traits. *Ecology*, 93(8), 1867-1879. doi:10.1890/11-1745.1

Li, X., Petipas, R. H., Antoch, A. A., Liu, Y., Stel, H. V., Bell-Dereske, L., Smercina, D. N., Bekkering, C., Evans, S. E., Tiemann, L. K., Friesen, M. L. (2022). Switchgrass cropping systems affect soil carbon and nitrogen and microbial diversity and activity on marginal lands. *GCB Bioenergy*, 14 (8), 918 – 940. doi:10.1111/gcbb.12949

Liang, A., Zhang, Y., Zhang, X., Yang, X., McLaughlin, N., Chen, X., Guo, Y., Jia, S., Zhang, S., Wang, L., & Tang, J. (2019). Investigations of relationships among aggregate pore structure, microbial biomass, and soil organic carbon in a mollisol using combined non-destructive measurements and phospholipid fatty acid analysis. *Soil and Tillage Research*, 185, 94-101. doi:10.1016/j.still.2018.09.003

Liao, H., Hao, X., Zhang, Y., Qin, F., Xu, M., Cai, P., Chen, W., & Huang, Q. (2022). Soil aggregate modulates microbial ecological adaptations and community assemblies in agricultural soils. *Soil Biology and Biochemistry*, 172 doi:10.1016/j.soilbio.2022.108769

Liu, Y. -F., Meng, L. -C., Huang, Z., Shi, Z. -H., & Wu, G. -L. (2022). Contribution of fine roots mechanical property of Poaceae grasses to soil erosion resistance on the Loess Plateau. *Geoderma*, 426 doi:10.1016/j.geoderma.2022.116122

Lucas, M., Nguyen, L. T. T., Guber, A., & Kravchenko, A. N. (2022a). Cover crop influence on pore size distribution and biopore dynamics: Enumerating root and soil faunal effects. *Frontiers in Plant Science*, 13 doi:10.3389/fpls.2022.928569

Lucas, M. (2022b). Perspectives from the fritz-scheffer awardee 2020—The mutual interactions between roots and soil structure and how these affect rhizosphere processes#. *Journal of Plant Nutrition and Soil Science*, 185(1), 8-18. doi:10.1002/jpln.202100385

Mangalassery, S., Sjögersten, S., Sparkes, D. L., Sturrock, C. J., & Mooney, S. J. (2013). The effect of soil aggregate size on pore structure and its consequence on emission of greenhouse gases. *Soil and Tillage Research*, 132, 39-46. doi:10.1016/j.still.2013.05.003

Marinari, S., Masciandaro, G., Ceccanti, B., & Grego, S. (2000). Influence of organic and mineral fertilisers on soil biological and physical properties. *Bioresource Technology*, 72(1), 9-17. doi:10.1016/S0960-8524(99)00094-2

Mavi, M. S., Sanderman, J., Chittleborough, D. J., Cox, J. W., & Marschner, P. (2012). Sorption of dissolved organic matter in salt-affected soils: Effect of salinity, sodicity and texture. *Science of the Total Environment*, 435-436, 337-344. doi:10.1016/j.scitotenv.2012.07.009

McLaughlin, S. B., & Kszos, L. A. (2005). Development of switchgrass (*Panicum virgatum*) as a bioenergy feedstock in the United States. *Biomass & Bioenergy*, 28(6), 515-535. doi: 10.1016/j.biombioe.2004.05.006

Mehmood, M. A., Ibrahim, M., Rashid, U., Nawaz, M., Ali, S., Hussain, A., & Gull, M. (2017). Biomass production for bioenergy using marginal lands. *Sustainable Production and Consumption*, 9, 3–21. doi: 10.1016/j.spc.2016.08.003

Miltner, A., Bombach, P., Schmidt-Brücken, B., & Kästner, M. (2012). SOM genesis: Microbial biomass as a significant source. Biogeochemistry, 111(1-3), 41-55. doi:10.1007/s10533-011-9658-z

Negassa, W. C., Guber, A. K., Kravchenko, A. N., Marsh, T. L., Hildebrandt, B., & Rivers, M. L. (2015). Properties of soil pore space regulate pathways of plant residue decomposition and community structure of associated bacteria. *PLoS ONE*, 10(4) doi:10.1371/journal.pone.0123999

Nimmo J. R. (2013). Porosity and Pore Size Distribution, *Reference Module in Earth Systems and Environmental Sciences*, Elsevier, 27-Sep-13 doi: 10.1016/B978-0-12-409548-9.05265-9.

Nunan, N., Wu, K., Young, I. M., Crawford, J. W., & Ritz, K. (2003). Spatial distribution of bacterial communities and their relationships with the micro-architecture of soil. *FEMS Microbiology Ecology*, 44(2), 203-215. doi:10.1016/S0168-6496(03)00027-8

Oduor, C. O., Karanja, N. K., Onwonga, R. N., Mureithi, S. M., Pelster, D., & Nyberg, G. (2018). Enhancing soil organic carbon, particulate organic carbon and microbial biomass in semi-arid rangeland using pasture enclosures. *BMC Ecology*, 18(1) doi:10.1186/s12898-018-0202-z

Ontl, T. A., Cambardella, C. A., Schulte, L. A., & Kolka, R. K. (2015). Factors influencing soil aggregation and particulate organic matter responses to bioenergy crops across a topographic gradient. *Geoderma*, 255-256, 1-11. doi:10.1016/j.geoderma.2015.04.016

Pagliai, M., & De Nobili, M. (1993). Relationships between soil porosity, root development and soil enzyme activity in cultivated soils. *Geoderma*, 56(1-4), 243-256. doi:10.1016/0016-7061(93)90114-Z

Paul, E. A., Harris, D., Klug, M. J. & Ruess, R. W. (1999). *Standard Soil Methods for Long-term Ecological Research*. In Robertson, G. P., Coleman, D. C., Bledsoe, C. S. & Sollins, P. (Eds.) (Ch. 15, pp. 291–317), Oxford University Press, Oxford, UK.

Pérès, G., Cluzeau, D., Menasseri, S., Soussana, J. F., Bessler, H., Engels, C., Habekost, M., Gleixner, G., Weigelt, A., Weisser, W. W., Scheu, S., & Eisenhauer, N. (2013). Mechanisms linking plant community properties to soil aggregate stability in an experimental grassland plant diversity gradient. *Plant and Soil*, 373(1-2), 285-299. doi:10.1007/s11104-013-1791-0

Prommer, J., Walker, T. W. N., Wanek, W., Braun, J., Zezula, D., Hu, Y., Hofhansl, F., & Richter, A. (2020). Increased microbial growth, biomass, and turnover drive soil organic carbon accumulation at higher plant diversity. *Global Change Biology*, 26(2), 669-681. doi:10.1111/gcb.14777

Quigley, M. Y., Negassa, W. C., Guber, A. K., Rivers, M. L., & Kravchenko, A. N. (2018). Influence of pore characteristics on the fate and distribution of newly added carbon. *Frontiers in Environmental Science*, 6(JUN) doi:10.3389/fenvs.2018.00051

Quigley, M. Y., & Kravchenko, A. N. (2022). Inputs of root-derived carbon into soil and its losses are associated with pore-size distributions. *Geoderma*, 410 doi:10.1016/j.geoderma.2021.115667

Rawlins, B. G., Wragg, J., Reinhard, C., Atwood, R. C., Houston, A., Lark, R. M., & Rudolph, S. (2016). Three-dimensional soil organic matter distribution, accessibility and microbial respiration in macroaggregates using osmium staining and synchrotron X-ray computed tomography. *Soil* 2, 659–671. doi:10.5194/soil-2016-32

Rasse, D. P., Rumpel, C., & Dignac, M. -F. (2005). Is soil carbon mostly root carbon? mechanisms for a specific stabilisation. *Plant and Soil*, 269(1-2), 341-356. doi:10.1007/s11104-004-0907-y

Ruamps, L. S., Nunan, N., & Chenu, C. (2011). Microbial biogeography at the soil pore scale. *Soil Biology and Biochemistry*, 43(2), 280-286. doi:10.1016/j.soilbio.2010.10.010

Robertson, G. P., Dale, V. H., Doering, O. C., Hamburg, S. P., Melillo, J. M., Wander, M. M., Parton, W. J., Adler, P. R., Barney, J. N., Cruse, R. M., Duke, C. S., Fearnside, P. M., Follett, R. F., Gibbs, H. K., Goldemberg, J., Mladenoff, D. J., Ojima, D., Palmer, M. W., Sharpley, A., Wallace, L., Weathers, K. C., Wiens, J. A., Wilhelm, W. W. (2008). Agriculture: Sustainable biofuels redux. *Science*, 322(5898), 49-50. doi:10.1126/science.1161525

Robertson, G. P., Hamilton, S. K., Del Grosso, S. J., & Parton, W. J. (2011). The biogeochemistry of bioenergy landscapes: Carbon, nitrogen, and water considerations. *Ecological Applications*, 21(4), 1055-1067. doi:10.1890/09-0456.1

Sanford, G. R. (2014). Perennial grasslands are essential for long term SOC storage in the Mollisols of the North Central USA. In Hartemink, A. & McSweeney, K. (Eds.), Soil carbon (pp. 281– 288), *Progress in soil science*, Springer International, Switzerland.

Sang, T., & Zhu, W. (2011). China's bioenergy potential. *Global Change Biology Bioenergy*, 3, 79– 90. doi:10.1111/j.1757-1707.2010.01064.x

Schindelin, J., Arganda-Carreras, I., Frise, E., Kaynig, K., Longair, M., Pietzsch, T., Preibisch, S., Rueden, C., Saalfeld, S., Schmid, B., Tinevez, J. -Y., White, D. J., Hartenstein, V., Eliceiri, K., Tomancak, P., & Cardona, A. (2012). Fiji: an open-source platform for biological-image analysis. *Nature Methods,* 9, 676–682 doi:10.1038/nmeth.2019

Schulte, L. A., Niemi, J., Helmers, M. J., Liebman, M., Arbuckle, J. G., James, D. E., . . . Witte, C. (2017). Prairie strips improve biodiversity and the delivery of multiple ecosystem services from corn–soybean croplands. *Proceedings of the National Academy of Sciences of the United States of America*, 114(42), 11247-11252. doi:10.1073/pnas.1620229114

Schlüter, S., Sheppard, A., Brown, K., & Wildenschild, D. (2014). Image processing of multiphase images obtained via X-ray microtomography: A review. *Water Resources Research*, 50(4), 3615-3639. doi:10.1002/2014WR015256

Schweizer, S. A., Bucka, F. B., Graf-Rosenfellner, M., & Kögel-Knabner, I. (2019). Soil microaggregate size composition and organic matter distribution as affected by clay content. *Geoderma*, 355 doi:10.1016/j.geoderma.2019.113901

Shen, Y. -H. (1999). Sorption of natural dissolved organic matter on soil. *Chemosphere*, 38(7), 1505-1515. doi:10.1016/S0045-6535(98)00371-3

Singh, M., Sarkar, B., Sarkar, S., Churchman, J., Bolan, N., Mandal, S., et al. (2018). Stabilization of soil organic carbon as influenced by clay mineralogy. *Advances in Agronomy*, 148, 33– 84. doi:10.1016/bs.agron.2017.11.001

Six, J., Conant, R. T., Paul, E. A., & Paustian, K. (2002). Stabilization mechanisms of soil organic matter: Implications for C-saturation of soils. *Plant and Soil*, 241(2), 155-176. doi:10.1023/A:1016125726789

Six, J. & Jastrow, J. D. (2002). Organic Matter Turnover. In Lal, R. (Eds.), *Encyclopedia of Soil Science* (pp. 936-942), Marcel Dekker, New York.

Sprunger, C. D., Oates, L. G., Jackson, R. D., & Robertson, G. P. (2017). Plant community composition influences fine root production and biomass allocation in perennial bioenergy cropping systems of the upper midwest, USA. *Biomass and Bioenergy*, 105, 248-258. doi:10.1016/j.biombioe.2017.07.007

Sprunger, C. D., & Philip Robertson, G. (2018). Early accumulation of active fraction soil carbon in newly established cellulosic biofuel systems. *Geoderma*, 318, 42-51. doi:10.1016/j.geoderma.2017.11.040

Sprunger, C. D., Martin, T., & Mann, M. (2020). Systems with greater perenniality and crop diversity enhance soil biological health. *Agricultural & Environmental Letters*, 5(1), e20030. doi: 10.1002/ael2.20030

Strong, D. T., De Wever, H., Merckx, R., & Recous, S. (2004). Spatial location of carbon decomposition in the soil pore system. *European Journal of Soil Science*, 55(4), 739-750. doi:10.1111/j.1365-2389.2004.00639.x

Udawatta, R. P., Anderson, S. H., Gantzer, C. J., & Garrett, H. E. (2008). Influence of prairie restoration on CT-measured soil pore characteristics. *Journal of Environmental Quality*, 37(1), 219-228. doi:10.2134/jeq2007.0227

Varvel, G. E., Vogel, K. P., Mitchell, R. B., Follett, R. F., & Kimble, J. M. (2008). Comparison of corn and switchgrass on marginal soils for bioenergy. *Biomass and Bioenergy*, 32, 18– 21. doi:10.1016/j.biombioe.2007.07.003

Vogel, H. -J., Weller, U., & Schlüter, S. (2010). Quantification of soil structure based on minkowski functions. *Computers and Geosciences*, 36(10), 1236-1245. doi:10.1016/j.cageo.2010.03.007

Warncke, D., Dahl, J., & Jacobs, L. (2009). Nutrient recommendations for field crops in Michigan. *MSU Extension Bulletin E2904*, Michigan State University, East Lansing, USA. Available at: http://tinyurl.com/kgyvr6h

Witzgall, K., Vidal, A., Schubert, D. I., Höschen, C., Schweizer, S. A., Buegger, F., Pouteau, V., Chenu, C., & Mueller, C. W. (2021). Particulate organic matter as a functional soil component for persistent soil organic carbon. *Nature Communications*, 12(1) doi:10.1038/s41467-021-24192-8

Woloszczyk, P., Fiencke, C., Elsner, D. -C., Cordsen, E., & Pfeiffer, E. -M. (2020). Spatial and temporal patterns in soil organic carbon, microbial biomass and activity under different land-use types in a long-term soil-monitoring network. *Pedobiologia*, 80 doi:10.1016/j.pedobi.2020.150642

Wright, D. A., Killham, K., Glover, L. A., & Prosser, J. I. (1995). Role of pore size location in determining bacterial activity during predation by protozoa in soil. *Applied and Environmental Microbiology*, 61(10), 3537-3543. doi:10.1128/aem.61.10.3537-3543.1995

Xia, Q., Zheng, N., Heitman, J. L., & Shi, W. (2022). Soil pore size distribution shaped not only compositions but also networks of the soil microbial community. *Applied Soil Ecology*, 170 doi:10.1016/j.apsoil.2021.104273

Zhang, B. Z., Penton, C. R., Xue, C., Quensen, J. F., Roley, S. S., Guo, J. R., Garoutte, A., Zheng, T. L., & Tiedje, J. M. (2017). Soil depth and crop determinants of bacterial communities under ten biofuel cropping systems. *Soil Biology and Biochemistry*, 112, 140-152. doi: 10.1016/j.soilbio.2017.04.019

Zhao, W., Zhang, R., Cao, H., & Tan, W. (2019). Factor contribution to soil organic and inorganic carbon accumulation in the loess plateau: Structural equation modeling. *Geoderma*, 352, 116-125. doi:10.1016/j.geoderma.2019.06.005

CHAPTER 2: Pore structure in detritusphere of soils under switchgrass and prairie vegetation[2]

Abstract

Root detritusphere, i.e., the soil in vicinity of decomposing root residues, plays an important role in soil microbial activity and C sequestration. Pore structure (size distributions and connectivity of soil pores) in the detritusphere serves as a major driver for these processes and, in turn, is influenced by physical characteristics of both soil and roots. This study compared pore structure characteristics in root detritusphere of soils of contrasting texture and mineralogy subjected to >6 years of two contrasting vegetations: monoculture switchgrass and polyculture prairie systems. Soil samples were collected from five experimental sites in the US Midwest representing three soil types. Soil texture and mineralogy were measured using hydrometer and X-ray powder diffraction, respectively. The intact cores were scanned with X-ray computed micro-tomography to identify visible soil pores, biopores, and particulate organic matter (POM). We specifically focused on pore structure within the detritusphere around the POM of root origin. Results showed that the detritusphere of coarser-textured soils, characterized by high sand and quartz contents, had lower porosity in the vicinity of POM compared to finer-textured soils. POM vicinities in finer soils had high proportions of large (>300 μm Ø) pores, and their pores were better connected than in coarser soils. Lower porosity in outer (>1 mm) parts of detritusphere of switchgrass than of prairie suggested soil compaction by roots, with the effect especially pronounced in coarser soils. The results demonstrated that soil texture and mineralogy play a major, while vegetation a more modest, role in defining the pore structure in root detritusphere.

[2] Originally submitted as: Lee, J. H., Lucas, M., Guber, A. K., & Kravchenko, A. N. (2023). Pore structure in detritusphere of soils under switchgrass and restored prairie vegetation community, *Land degradation & Development*. (*Under review*)

2.1 Introduction

Plant roots are a major driver of soil pore formation and a source of soil organic matter (SOM) (Bodner et al., 2014; Sokol et al., 2019). After the root senesces, its residues remain in the soil as detritus, and a several millimeters thick region that surrounds these decaying residues is called the detritusphere (Gaillard et al., 1999; Védère et al., 2020). Soil pore structure within the detritusphere is distinct from that of the bulk soil due to past activity of live roots as well as due to biological and physical changes after roots' senescence. For example, rearrangement of soil particles or micro-aggregates during root growth (Mitchell and Soga, 2005) may lead to an increase in porosity adjacent to the root (Helliwell et al., 2017), while soil compaction can occur near growing roots (Lucas et al., 2019a). However, upon root senescence pore spaces can be partially or completely refilled by soil particles during the decomposition of root residues (Phalempin et al., 2022). Since the detritusphere is a main arena of microbial activity and carbon (C) processing (Kuzyakov and Blagodatskaya, 2015), characteristics of pore structure within detritusphere likely play a special role for the whole soil volume.

Properties of the detritusphere pore structure depend on a number of factors, including but not limited to: (i) inherent characteristics of soil particles that influence pore formation, such as soil texture and mineralogy; (ii) inherent pore characteristics, i.e., the pore structure within that specific location prior to the root growth within it; (iii) composition of the soil microbial community; (iv) morphological, chemical, and physical characteristics of the roots that generate the detritus.

The structural stability of the detritusphere pores is affected by sand content and abundance of quartz, both known to decrease stability of soil aggregation (Almajmaie et al., 2017; Rivera and Bonilla, 2020), likely due to the large size and low surface area of sand grains as well as the absence of negative charges (Bazzoffi et al., 1995; Six et al., 2000). Moreover, soils dominated by quartz tend to be more easily dispersed than kaolinitic clays due to their lower binding capacity (Buhmann et al., 1996; Neaman et al., 1999), thus such soils are prone to be easily disaggregated under disruptive forces such as rainfall (Wakindiki and Ben-Hur, 2002).

Inherent soil characteristics affect root growth patterns and thus formation of root-derived pores. Root systems have been shown to grow more extensively in loose than in compact soil (Croser et al., 1999; Bengough et al., 2006), as well as in an undisturbed soil than in that homogenized by sieving and packing (Phalempin et al., 2021b). The roots preferably utilize existing pore spaces, and indeed, the rhizosphere can be more porous than the bulk soil when roots are able to grow into a highly connected pore system (Lucas et al., 2019a). The established soil biopores that have been frequently and continuously used by roots are more likely to be stable due to root exudate and mucilage inputs (Traoré et al., 2000), likely maintaining their structure upon the root senescence and residue decomposition.

Vegetation type directly affects pore structure via differences in root types and characteristics. For example, the presence of coarse root systems increased the volume of > 70 μm diameter (Ø) pores by 30%, whereas plant species with dense fine root systems generated larger volume of < 30 μm Ø pores (Bodner et al., 2014). Total volumes of soil biopores, i.e., the pores formed by the activity of living organisms such as roots, in Ø < 0.2 mm and 0.2–0.5 mm size classes significantly differed among the plant species with different root system characteristics (Lucas et al., 2022). The differences in pore structure generated by plants with contrasting root systems are expected to be more pronounced in the direct vicinity of roots (Helliwell et al., 2019), thus, carried later into the properties of the detritusphere. After a plant dies, the root residues located in the biopores are decomposed, and the difference in the magnitude of decomposition is likely to be affected by the detritusphere's pore structure. Variations in residue decomposition can result in variations in the size of the gap between the residues and soil particles, potentially leading to further alterations of the pore structure.

While the structure of pores within the rhizosphere under different soil texture and contrasting vegetation has been actively explored (Helliwell et al., 2017; Helliwell et al., 2019; Phalempin et al., 2022, 2021b), very little information is available on pore structure of detritusphere. For example, Helliwell et al. (2017) observed micro-scale structural changes in pores surrounding growing root systems in uniformly packed soils and found increases in porosity at the interface between roots and soil as roots grow into loamy sand and clay loam soils. However, it is still unclear what happens to the pores surrounding roots once the

roots die and decomposition begins. As the detritusphere is one of the most important microbial hotspots (Kuzyakov and Blagodatskaya, 2015), the lack of such information in the pore structure limits progress in understanding mechanisms of soil C cycling and sequestration.

The objective of this chapter is to characterize the pore structure in the root detritusphere of soils of two contrasting vegetation systems: monoculture switchgrass (*Panicum virgatum* L.), where root detritus originated from switchgrass roots, and polyculture restored prairie, where root residues originated from a variety of herbaceous plant species. The two systems have been in place for over six years, generating differences in soil C contents (Sanford, 2014; Sprunger and Robertson, 2018), pore structures (Juyal et al., 2021), and microbial characteristics (Jesus et al., 2016; Li et al., 2022). We compared pore connectivity and size distribution within the detritusphere of the two systems at five experimental sites representing three soil types with contrasting texture and mineralogy.

2.2 Materials and Methods

2.2.1 Experimental design and soil sample collections

Two of the experimental sites used for this study were located in Wisconsin (Oregon and Hancock) and three in Michigan (Lux Arbor, Lake City, and Escanaba), and those sites are parts of the Marginal Land Experiment in Great Lake Bioenergy Research Center. The soils of Oregon, Lux Arbor, and Escanaba sites are Alfisols, and of Hancock and Lake City sites are Entisols and Spodosols, respectively. At each site a randomized complete block design experiment with 3 (Hancock) or 4 (the rest of the sites) replications has been established in 2013. Details on the research sites and soil descriptions have been reported by Kasmerchak and Schaetzl (2018) and Lee et al. (2023), and soil properties are described in chapter 1.

The two studied vegetation systems were: (1) non-fertilized monoculture switchgrass; and (2) restored prairie, which consisted of 18 plant species of grasses (including switchgrass), forbs, and legumes, which are listed in https://lter.kbs.msu.edu/wp-content/uploads/2012/05/GLBRC-Species.pdf. Soil sampling was conducted in 2020 (Oregon site) and 2019 (the other 4 sites). Two types of soil samples were collected from each of four replicated plots in each site. First, three intact soil cores (5 cm height and 5 cm Ø) were collected from 5 to 10 cm depth for X-ray computed micro-tomography (μCT) scanning. Then,

the loose soil surrounding the cores was also collected for measurements of soil texture and mineralogy. All samples were stored at 4 °C until scanning and measurements.

2.2.2 Measurements of soil porosity, texture, and mineralogy

Soil porosity was calculated from bulk and particle densities of the collected samples (i.e., density-based total porosity), and texture was determined using the hydrometer method (Gee and Or, 2002) in all replicated plots of all sites. Soil mineralogy composition was measured using X-ray powder diffraction (XRD) carried out at the Illinois State Geological Survey (Champaign, Illinois, USA). Because of the high costs of XRD analyses only three replicated samples from each system in each site were subjected to these measurements. Prior to XRD analyses, the samples were cleaned, dried in a vacuum oven, and ground to < 44 μm. Then, one subset of the prepared sample was powdered by the McCrone mill (MBP) (McCrone Accessories & Components, Westmont, IL, USA) for quantification of non-clay minerals (quartz, clay, K-feldspar, P-feldspar, calcite, dolomite, siderite, and pyrite/marcasite), and the other was fractionized into < 2 μm powder for clay minerals (smectite, mica, kaolinite, and chlorite). The two types of powders were then spread on a glass slide and analyzed using a Siemens/Bruker D5000 X-ray Powder Diffraction instrument (Billerica, MA, USA). JADE™ software (Newtown Square, PA, USA) was used to identify percentages of constituents in each powdered sample from XRD patterns.

2.2.3 Soil core scanning and image analysis

Pore structure assessments were performed via X-ray μCT. Soil cores were drained at -28 kPa using a 5-bar pressure plate extractor (Soilmoisture Equipment Corp., Goleta, CA) prior to μCT scanning to remove water from pores Ø >10 μm and to increase the contrast between the solids and air on X-ray μCT images. Then, the cores were scanned using X-ray μCT machine (North Star Imaging, X3000, Rogers, MV, USA) at the Department of Horticulture facility, Michigan State University. The energy settings were 75 kV and 450 μA. The scanning resolution of 18 μm was achieved using the Subpix-mode of the scanner, combining four individual scans shifted half pixel in vertical and horizontal directions. Scanned images of 3014 projections were reconstructed by efX software (North Star, Rogers, MN, USA).

A schematic summary of the steps involved in the image processing for this study is outlined in Figure 2.1. The image pre-processing was conducted using ImageJ-Fiji software (Schindelin et al., 2012) to remove artifacts and noise. First, to exclude sampling artifacts near the soil core walls, images were centered and cropped into prisms (1500 × 1500 × 2240 pixels corresponded to 2.7 cm length, 2.7 cm width, and 4.1 cm height). Then, 'Remove Background' tool in Xlib/Beat plugin was used to remove shadowing effects from the images, followed by the removal of ring artifacts on the image's polar domain using a stripe filter of the Xlib/Beat plugin. After that, a 3D non-local mean filter ($\sigma = 0.1$) implemented in scikit-image (Walt et al., 2014) was used to reduce the noise (Darbon et al., 2008; Buades et al., 2011). The pre-processing steps dropped the resolution of images from 18 to 36 µm.

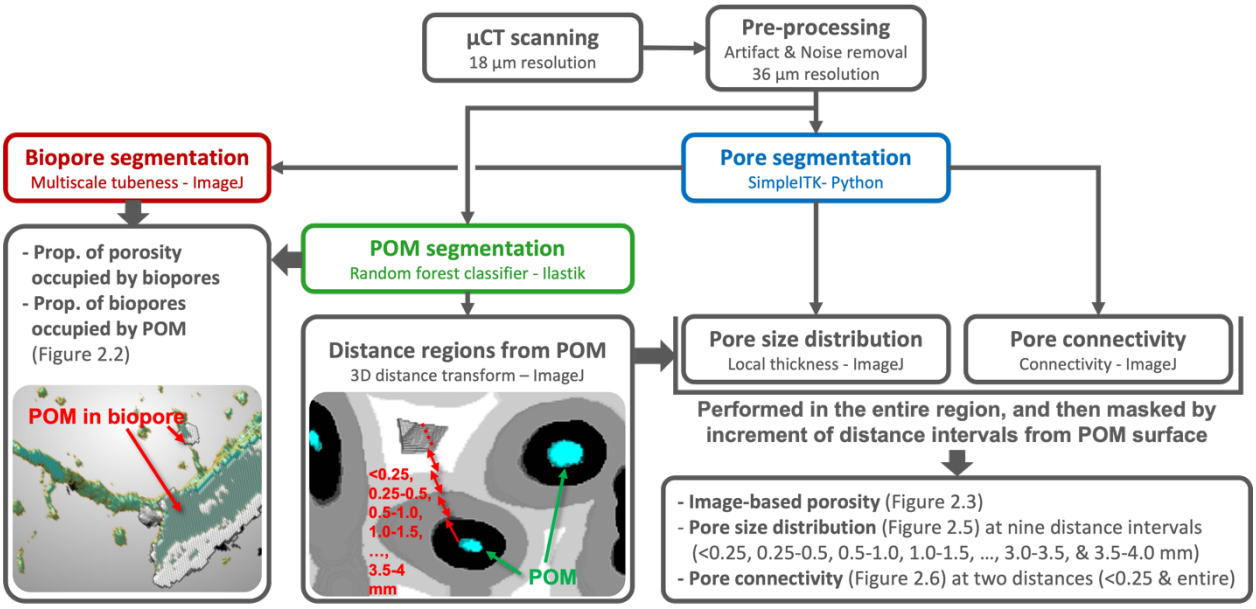

Figure 2.1. Schematic representation of the steps of the image analysis procedure. Intact soil cores were scanned, and images were pre-processed to remove artifacts and noises. Then, POM and pores were segmented using Ilastik software and SimpleITK in Python, respectively. After that, biopores were segmented from the pores using Tubeness of ImageJ in multiple scales; POM fractions located within the biopores were measured; and pore size distributions were obtained. Nine masks corresponding to nine distance intervals (<0.25, 0.25-0.5, 0.5-1.0, 1.0-1.5, …, 3.0-3.5, and 3.5-4.0 mm) away from the segmented POM were created using 3D distance transform in ImageJ. Pore connectivity was calculated separately within <0.25 interval and entire image stacks using Connectivity tool in ImageJ.

Root residues, which we will refer to as particulate organic matter (POM), were segmented from the filtered images with Ilastik software, a machine learning-based tool (Berg et al., 2019). A random forest classifier was used on a multi-dimensional feature space of the filtered gray scale images. The classifier

was trained using two cores from each combination of different vegetation and sites (20 of 114 cores) and then applied on entire cores. The training dataset produced out-of-bag error rate estimates less than 1.8% overall, and all segmented POM images were visually inspected to ensure the accuracy and integrity of the segmentation process. The outcome of POM segmentation was denoised by removing objects smaller than four voxels in diameter from the images.

Segmentation of the filtered grayscale images into pore and solid binary images was performed to identify the pores visible at the image resolution, referred further on as image-based pores. For each sample the segmentation threshold was estimated as an ensemble of six segmentation methods (i.e., Otsu, Triangle, Huang, IsoData, Li, and Moments). The global thresholds for the stack of images in each individual core, estimated using the six segmentation methods, were averaged and applied to that stack to separate the solid and air-filled voxels in the images using SimpleITK in Python (Beare et al., 2018; Lucas et al., 2022). Obtained images were used to compute pore size distributions using 'Local Thickness' tool, an approach based on the maximum inscribed sphere method (Hildebrand and Rüegsegger, 1997; Vogel et al., 2010).

Biopores were identified as described by Lucas et al. (2022). Specifically, to employ tubular-shaped features of biopores in differentiating them from other irregularly shaped pores, we used the Tubeness plugin in ImageJ-Fiji for shape detection. As rising σ-values significantly increased the computational time, binary images were scaled down to 50% and 20% for Tubeness filtering with σ-values ranging from 1-4 and 2-30, for each scale respectively, with a step size of 1. Gaussian blurring was applied to the entire binary image with varying σ-values in order to efficiently identify biopores of various diameters. The resulting tubular channels were slightly smaller than the root channel itself due to the exclusion of rough surface on biopore walls. Thus, to better capture the actual width of biopores, 3D dilation steps were employed as a postprocessing measure. After combining all elongated objects, misclassified objects were removed (Phalempin et al., 2021a). Proportions of biopores in the entire pore system were calculated. After that, proportions of biopores occupied by POM were computed by first calculating the volume of POM located in biopores and then dividing this volume by the entire volume of biopores.

Nine masks corresponding to interval regions nine distances away from the segmented POM (0-0.25, 0.25-0.5, 0.5-1.0, 1.0-1.5, 1.5-2.0, 2.0-2.5, 2.5-3.0, 3.0-3.5, and 3.5-4.0 mm) were created using 3D distance transform in ImageJ-Fiji. Then, masks of interval regions were applied to the pore-solid segmented image and to the pore size distribution image of the entire sample to calculate the porosities and the size distributions individually for each interval region. Contributions of pores of different size classes to image-based porosity of the distance interval regions were expressed as pore fractions (%). We considered three pore size classes, namely 36-150 μm, 150-300 μm, and > 300 μm Ø. The 36 μm Ø corresponded to the smallest pore size that could be reliably detected on the studied images. Pores < 150 μm Ø are known to have especially high microbial activity and strongly contribute to the C processing (Strong et al., 2004; Kravchenko and Guber, 2017; Kravchenko et al., 2019), and pores < 300 μm Ø function as the secondary pathways for water and nutrient supplies to resident microorganisms (Franklin et al., 2021).

A Connectivity tool of BoneJ plugin in the ImageJ-Fiji was used for the pore connectivity calculations: first, Euler numbers (χ) were computed, and the numbers were divided by the total volume of corresponding regions (V) (Odgaard and Gundersen, 1993; Vogel and Roth, 2001):

$$\chi_v = \frac{N - C + H}{V} \quad (1)$$

where N is the number of isolated objects, C is the number of redundant connections or loops, and H is the number of completely enclosed cavities, which are typically negligible in soil pore systems (Vogel, 2002; Lucas et al., 2021). The minimum size of the object was 2 × 2 × 2 voxel. Higher, e.g., positive, χ_V values calculated via Eq. (1) correspond to lower connectivity, while lower, e.g., negative, to the higher connectivity. To simplify the presentation of the connectivity data we report the results as negative values of χ_V, that is, the high values of $-\chi_V$ correspond to high connectivity while the low values to low connectivity.

Since pore connectivity can be affected by the volume of the soil in which it is calculated, we did not assess it at the same distance intervals as those that were used for the image-based porosity and pore size distributions described above. Instead, we only calculated it in immediate vicinity of the residue, i.e.,

the region of 0-0.25 mm away from the POM, and for the entire soil volume. The resultant two estimates of the connectivity were used for comparisons among the five experimental sites and plant systems.

2.2.4 Statistical analysis

The data were analyzed using SAS 9.4 (SAS Institute Inc., NC, USA) procedures of PROC MIXED and PROC GLIMMIX. Since we did not expect that 6-7 years of disparate vegetation influenced soil texture and mineralogy, the statistical models for texture and mineralogy characteristics included only the fixed effects of the experimental sites. For the other soil properties, the statistical models included the fixed effects of sites, plant systems, and their interactions. Statistical models for analyses of image-based porosity data at different distances from POM additionally included the same fixed effects as the soil properties and individually tested by distance intervals, as the interactions among the sites, plant systems, and distances were significant. All models included the random effects of experimental blocks nested within the sites and, when necessary, the random effects of cores nested within the blocks, plant systems, and sites. The latter were used as an error term for testing the plant system effects. The assumptions of normality and variance homogeneity were assessed using normal probability plots, plots of residuals vs. predicted values, and Levene's tests for equal variances.

Additionally, we grouped the sites into two soil texture classes for comparing pore size distributions and connectivity between finer-textured soils and coarser-textured soils. The first group included Oregon, Lux Arbor, and Escanaba sites, the three soils with < 66 % sand content, and the second group consisted of Hancock and Lake City sites with > 82 % sand content (Table 2.1). Models for analysis of pore size distribution data within each distance interval and of connectivity data within 0-0.25 mm distance and entire image stack included the fixed effects of plant systems, soil groups, and their interaction, and random effects of experimental sites nested within soil groups, blocks nested within the sites, and cores nested within the blocks, plant systems, sites, and groups.

Table 2.1. Proportion (%) of the components in soil texture, McCrone mill powder (MBP) mineralogy, and clay mineralogy in the five studied experimental sites.

	Components	Oregon, WI Alfisol	Lux Arbor, MI Alfisol	Escanaba, MI Alfisol	Hancock, WI Entisol	Lake City, MI Spodosol
Soil texture	Sand	10^{D}	52^{C}	66^{B}	82^{A}	87^{A}
	Silt	73^{A}	39^{B}	31^{B}	13^{C}	9^{C}
	Clay	17^{A}	9^{B}	3^{C}	5^{C}	4^{C}
MBP mineralogy	Quartz	77.6^{B}	81.4^{B}	79.1^{B}	92.1^{A}	88.7^{A}
	Clay	2.0^{A}	1.7^{A}	1.2^{AB}	0.7^{B}	1.0^{AB}
	K-feldspar	6.9^{B}	6.3^{B}	11.7^{A}	3.2^{C}	5.0^{BC}
	P-feldspar	10.3^{A}	7.5^{A}	4.2^{B}	2.7^{C}	3.5^{BC}
	Calcite	0.3^{AB}	0.4^{AB}	0.6^{A}	0.2^{B}	0.3^{AB}
	Dolomite	0.8^{AB}	0.9^{A}	0.9^{A}	0.3^{C}	0.5^{B}
	Siderite	1.6^{A}	1.2^{A}	1.3^{A}	0.5^{B}	0.6^{B}
	Pyrite/Marcasite	0.5^{AB}	0.6^{AB}	1.0^{A}	0.3^{B}	0.4^{B}
Clay mineralogy	Smectite	16.0^{A}	10.1^{A}	15.0^{A}	19.7^{A}	16.6^{A}
	Mica	67.1^{A}	62.3^{A}	63.1^{A}	54.9^{A}	67.2^{A}
	Kaolinite	8.1^{A}	10.3^{A}	11.2^{A}	12.5^{A}	6.9^{A}
	Chlorite	8.8^{B}	17.3^{A}	10.6^{AB}	12.9^{AB}	9.3^{B}

Note: different letters within the same row indicate significant differences ($p < 0.05$) among the studied sites (Oregon, Lux Arbor, Escanaba, and Lake City sites: n = 4 and Hancock site: n = 3).

Linear relationships among soil texture variables, mineralogical and clay mineralogy variables, proportions of biopores and POM in biopores, and the distance-based porosities and connectivity were assessed using Pearson's correlation coefficients.

2.3 Results

2.3.1 Soil texture and mineralogy in the studied sites

Sand content varied greatly among the studied sites, with Oregon having the lowest content at 10% and Lake City having the highest at 87% (Table 2.1). The silt content was the highest in Oregon at 73% and the lowest in Lake City at 9%, and the site with the highest clay content was also Oregon at 17%. In all five sites, quartz was the dominant mineral (78-92%) with 6-16% of K-feldspars and P-feldspars, and < 2% contents of other minerals. Hancock and Lake City had higher contents of quartz and lower contents of K-feldspars and P-feldspars compared to Oregon, Lux Arbor, and Escanaba sites. Mica dominated the clay fraction of all studied soils (55-67%), while smectite, kaolinite, and chlorite were present at < 20%, and did not differ among the sites.

Quartz was positively correlated with sand content, while silt and clay contents were positively correlated with feldspars, dolomites, and siderites across all studied sites (Table 2.2). Interestingly, contents of smectite and kaolinite were positively correlated with sand contents, while mica was negatively correlated with sand but positively with silt and clay (Table 2.2).

Table 2.2. Correlation coefficient between soil texture and components in McCrone mill powder (MBP) and clay mineralogy across all experimental sites and both systems.

	MBP mineralogy							
Soil texture	Quartz	Clay	K-feldspar	P-feldspar	Calcite	Dolomite	Siderite	Pyrite/Marcasite
Sand	**0.86*** **	**-0.94*** **	**-0.44*** **	**-0.98*** **	-0.11	**-0.80*** **	**-0.91*** **	**-0.22***
Silt	**-0.88*** **	**0.95*** **	**0.49*** **	**0.98*** **	0.05	**0.82*** **	**0.93*** **	**0.26***
Clay	**-0.71*** **	**0.88*** **	**0.21** **	**0.93*** **	-0.14	**0.64*** **	**0.80*** **	0.02
	Clay mineralogy							
Soil texture	Smectite		Mica		Kaolinite		Chlorite	
Sand	**0.48*** **		**-0.61*** **		**0.39** **		-0.08	
Silt	**-0.51*** **		**0.63*** **		**-0.37** **		0.09	
Clay	**-0.34** **		**0.48*** **		**-0.43*** **		-0.00	

Note: Bolded values indicate statistical significances at $p < 0.05$, and the marked *, **, and *** denote coefficient levels at the $p < 0.05$, < 0.01, and < 0.001 level, respectively.

2.3.2 Bioporosity and POM located within biopores

The soils of Oregon had the lowest total and image-based porosity, measuring at around 21% and 10% in both plant systems, respectively (Figure 2.2A). In soils of Lux Arbor and Escanaba, both types of porosities were higher than those of Oregon. The soils of Hancock and Lake City had the greatest total and image-based porosity, while lower bioporosity than the other three sites (Figure 2.2A). There were no significant differences observed in total porosities, image-based porosities, and bioporosities between the two plant systems, with the exception of the bioporosity of Lux Arbor site (Figure 2.2A). Proportions of the image-based porosity occupied by biopores were also the greatest in soils of Oregon and Lux Arbor compared to those of Hancock and Lake City soils under both plant systems (Figure 2.2C). The significant difference in the proportions occupied by biopores between the two plant systems was found only in Lux Arbor site, where biopores constituted 19% and 24% of the image-based porosities of prairie and switchgrass systems, respectively (Figure 2.2C). The proportion of pore space occupied by biopores was negatively correlated with sand content and quartz, while positively correlated to silt, clay and P-feldspar (Table 2.3).

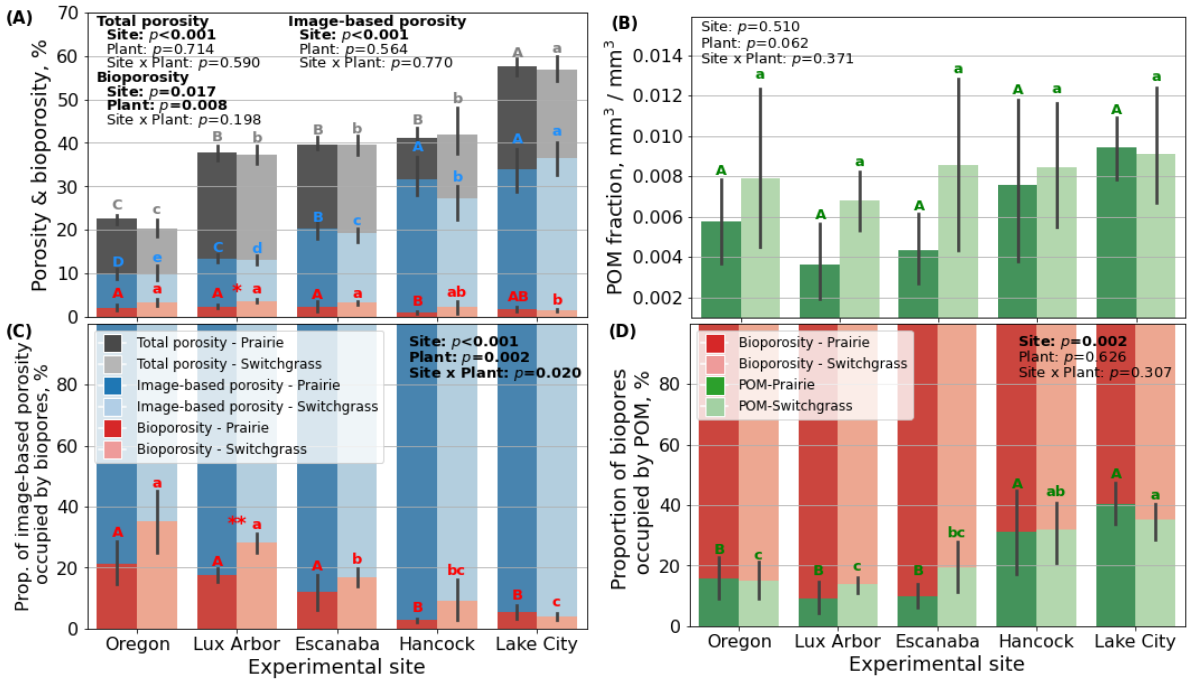

Figure 2.2. Pore and particulate organic matter (POM) characteristics in the soils of the five studied sites under switchgrass and prairie systems: **(A)** Total and image-based porosity (> 36 µm Ø) and bioporosity, expressed as % of the total soil volume, **(B)** POM, expressed as fraction of the total soil volume, **(C)** proportion of image-based porosity occupied by biopores, and **(D)** proportion of biopores occupied by POM. Error bars represent standard deviations, and ANOVA F-test results are shown in the top corner of each figure. Different uppercase and lowercase letters indicate significant differences ($p < 0.05$) among the experimental sites within prairie and switchgrass systems, respectively. * and ** denote significant differences between the two systems within each studied site at the $\alpha < 0.05$ and < 0.01 level, respectively.

Table 2.3. Correlation coefficients between soil texture, selected components of McCrone mill powder (MBP) and clay mineralogy and proportion (Prop.) of image-based porosity occupied by biopores and proportion of biopores occupied by POM, across all experimental sites.

		Prop. of porosity occupied by biopores	Prop. of biopores occupied by POM
Soil texture	Sand	**-0.71*** **	**0.46***
	Silt	**0.68*** **	**-0.46***
	Clay	**0.74*** **	**-0.38***
MBP mineralogy	Quartz	**-0.52****	**0.57****
	K-feldspar	0.08	**-0.47***
	P-feldspar	**0.69*** **	**-0.41***
Clay mineralogy	Smectite	-0.33	0.30
	Mica	0.15	-0.08
	Kaolinite	0.10	-0.17
	Chlorite	0.12	-0.16

Note: Bolded values indicate statistical significances at $p < 0.05$, and the marked *, **, and *** denote coefficient levels at the $p < 0.05$, < 0.01, and < 0.001 level, respectively.

Neither the two plant systems nor the five studied sites showed significant differences in POM fractions (Figure 2.2B). However, proportions of biopores occupied by POM varied among the studied soils (Figure 2.2D). In the soils of Hancock and Lake City, POM occupied >30% of the bioporosity, while in Oregon and Lux Arbor it was <20% (Figure 2.2D). The bioporosity occupied by POM was positively correlated with sand and quartz contents and negatively correlated with silt, clay, K- and P-feldspar contents (Table 2.3).

2.3.3 Pore structure changes with the distance from POM

Image-based porosity decreased with the distance from the POM surface in all soil cores (Figure 2.3). In both systems, at < 0.25 mm distance from POM the image-based porosity tended to be higher in finer-textured soils of Oregon, Lux Arbor, and Escanaba than in the coarser-textured soils of Hancock and Lake City (Figure 2.3). These pores are shown as examples in Figure 2.4. However, the differences in the porosity among the sites at < 0.25 mm distance faded at 0.25-0.5 mm interval, and upon distance reaching the 0.5-1.0 mm the image-based porosity of Hancock and Lake City exceeded that of the Oregon, Lux Arbor, and Escanaba. The image-based porosities at < 0.25 mm distance were negatively correlated with

sand content and quartz, while total image-based porosities were positively correlated with them (Table 2.5). The total porosities were negatively correlated with silt, clay, and P-feldspar.

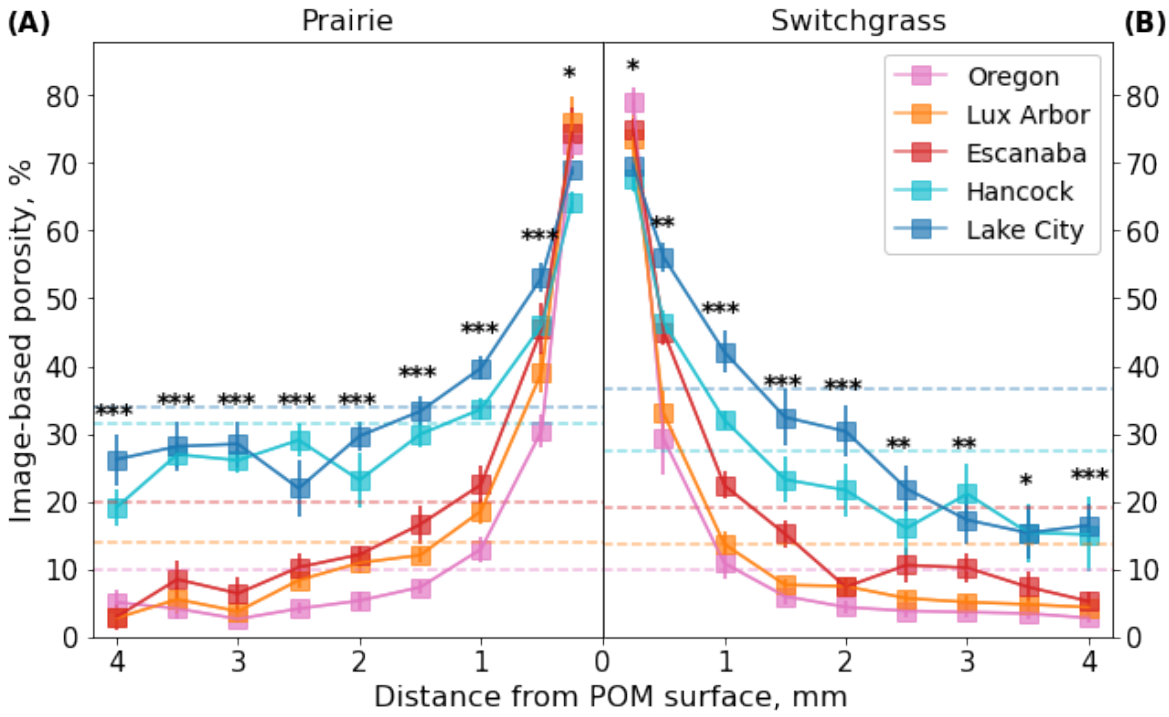

Figure 2.3. Image-based porosity (> 36 µm Ø) by distance intervals (<0.25, 0.25-0.5, 0.5-1.0, 1.0-1.5, …, 3.0-3.5, and 3.5-4.0 mm) from POM under **(A)** prairie and **(B)** switchgrass systems. Error bars represent standard deviation. The dashed lines of each figure indicate image-based porosities of entire soil volumes. *, **, and ** denote significant differences among 5 studied sites of each interval at the $\alpha < 0.05$, <0.01, and < 0.001 level, respectively. Statistical differences between two plant systems and comparisons among the studied sites within each interval and region are shown on Table 2.4.

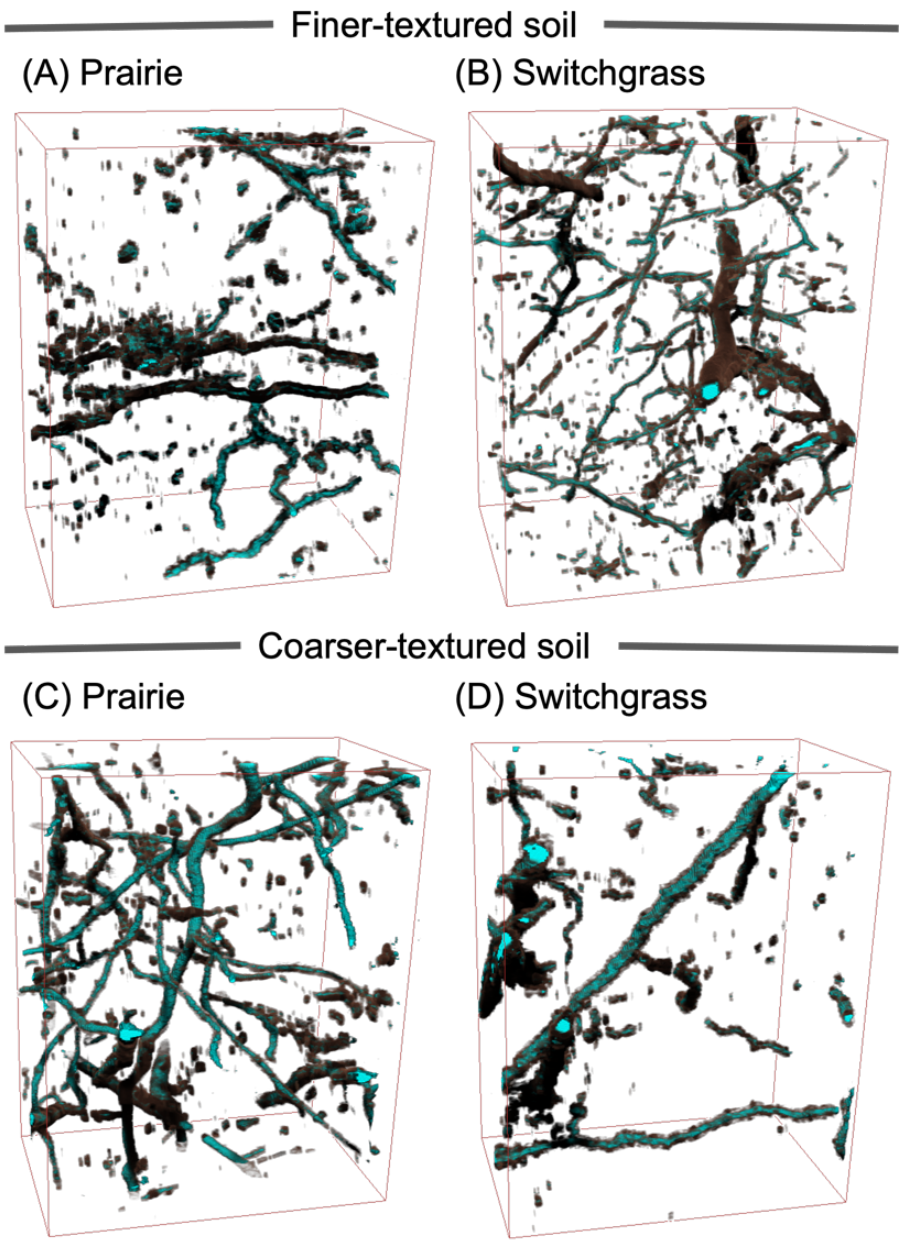

Figure 2.4. Examples of 3D images showing pores at < 0.25 mm distances from the segmented POM of switchgrass and prairie systems in finer- (Oregon, Lux Arbor, and Escanaba sites) and coarser-textured (Hancock and Lake City) soils. Solid green and semi-transparent brown colored area indicate POM and pores, respectively.

Table 2.4. Image-based porosity (> 36 μm Ø) by distance intervals (<0.25, 0.25-0.5, 0.5-1.0, 1.0-1.5, …, 3.0-3.5, and 3.5-4.0 mm) from POM under switchgrass and prairie systems in five studied sites.

Intervals (mm)	Plant system	Image-based porosity (%)					ANOVA results (*p* value)		
		Oregon	Lux Arbor	Escanaba	Hancock	Lake City	Site	Plant	Site*Plant
<0.25	Prairie	72.72^{AB}	76.01^{A}	74.48^{AB}	64.14^{C}	68.89^{BC}	**0.003**	0.247	0.426
	Switchgrass	78.52^{A}	72.72^{AB}	75.14^{AB}	66.99^{B}	69.41^{B}			
0.25-0.5	Prairie	30.47^{D}	39.14^{C}	45.53^{BC}	46.06^{B}	53.12^{A}	**<0.001**	0.521	0.547
	Switchgrass	28.36^{B}	32.94^{B}	44.77^{A}	46.66^{A}	56.60^{A}			
0.5-1.0	Prairie	13.07^{C}	18.58^{BC}	22.58^{B}	33.70^{A}	39.66^{A}	**<0.001**	0.189	0.285
	Switchgrass	10.30^{D}	13.95^{CD}	21.82^{C}	31.71^{B}	43.15^{A}			
1.0-1.5	Prairie	7.34^{C}	**12.08^{BC}**	16.63^{B}	**29.93^{A}**	33.33^{A}	**<0.001**	**0.032**	0.575
	Switchgrass	5.90^{D}	**7.81^{CD}**	15.05^{BC}	**23.01^{B}**	33.00^{A}			
1.5-2.0	Prairie	5.36^{D}	10.94^{CD}	12.16^{C}	23.16^{B}	29.66^{A}	**<0.001**	0.201	0.845
	Switchgrass	4.40^{C}	7.50^{C}	7.39^{C}	21.67^{B}	30.37^{A}			
2.0-2.5	Prairie	4.18^{C}	8.38^{C}	10.29^{C}	**29.08^{A}**	21.95^{B}	**<0.001**	**0.048**	0.067
	Switchgrass	3.78^{C}	5.80^{C}	10.57^{BC}	**16.16^{AB}**	21.61^{A}			
2.5-3.0	Prairie	2.61^{B}	3.84^{B}	6.16^{B}	**26.27^{A}**	**27.86^{A}**	**<0.001**	0.192	**0.301**
	Switchgrass	3.65^{C}	2.48^{C}	10.20^{BC}	**21.10^{A}**	**17.15^{AB}**			
3.0-3.5	Prairie	4.20^{B}	5.56^{B}	8.51^{B}	**27.15^{A}**	**27.62^{A}**	**<0.001**	**0.003**	0.518
	Switchgrass	3.43^{B}	4.87^{B}	7.38^{AB}	**15.16^{A}**	**15.38^{A}**			
3.5-4.0	Prairie	5.16^{B}	2.79^{B}	2.95^{B}	19.25^{A}	26.18^{A}	**<0.001**	0.102	0.194
	Switchgrass	2.82^{B}	4.38^{B}	5.28^{B}	15.13^{A}	16.49^{A}			

Note: different letters within the same row indicate the differences ($p < 0.05$) among the studied sites (Oregon, Lux Arbor, Escanaba, and Lake City sites: n = 4 and Hancock site: n = 3). Differences between the two systems that were different from zero ($p < 0.05$) and significant effects in ANOVA table are shown in bold. Since distance interval 2.5-3.0 mm away from POM surface was the only distance where Site*Plant interaction was statistically significant, differences between two plant systems at each site were additionally shown.

Table 2.5. Three classes of pore fractions at each distance interval (<0.25, 0.25-0.5, 0.5-1.0, 1.0-1.5, …, 3.0-3.5, and 3.5-4.0 mm) from POM under switchgrass and prairie systems in finer- and coarser-textured soils.

Intervals (mm)	Pore sizes (μm Ø)	Finer-textured		Coarser-textured		ANOVA results (*p* value)		
		Prairie	Switchgrass	Prairie	Switchgrass	Texture	Plant	Texture *Plant
<0.25	36-150	5.1^{a}	3.9^{a}	13.8^{a}	8.0^{b}	**0.007**	**<0.001**	**0.020**
	150-300	22.0^{BC}	17.3^{C}	36.5^{A}	27.6^{B}	**0.005**	**0.012**	0.429
	> 300	72.9^{A}	78.8^{A}	49.7^{B}	64.3^{A}	**0.003**	**0.005**	0.222
0.25-0.5	36-150	21.0^{C}	17.7^{C}	54.1^{A}	43.1^{B}	**0.003**	**0.005**	0.125
	150-300	30.4^{B}	28.2^{B}	36.5^{A}	40.2^{A}	**0.007**	0.679	0.109
	> 300	48.6^{A}	54.1^{A}	9.4^{C}	16.6^{B}	**<0.001**	**0.049**	0.822
0.5-1.0	36-150	33.9^{C}	33.5^{C}	68.4^{A}	57.5^{B}	**0.003**	**0.037**	0.077
	150-300	31.0^{A}	31.9^{A}	28.2^{A}	35.0^{A}	0.996	0.057	0.109
	> 300	35.1^{A}	34.6^{A}	3.4^{B}	7.5^{B}	**0.003**	0.643	0.565
1.0-1.5	36-150	41.8^{a}	44.1^{a}	73.7^{a}	63.7^{b}	**0.004**	0.227	**0.048**
	150-300	31.5^{A}	33.3^{A}	24.2^{B}	31.5^{A}	0.128	**0.009**	0.119
	> 300	26.7^{A}	22.6^{A}	2.1^{B}	4.8^{B}	**0.004**	0.852	0.328
1.5-2.0	36-150	48.9^{C}	50.3^{C}	76.1^{A}	66.7^{B}	**0.004**	0.276	0.059
	150-300	33.2^{A}	33.4^{A}	22.3^{B}	29.4^{A}	**0.032**	**0.013**	0.096
	> 300	17.9^{A}	16.3^{A}	1.4^{B}	3.9^{B}	**0.014**	0.727	0.603
2.0-2.5	36-150	49.8^{a}	52.1^{a}	78.0^{a}	68.1^{b}	**0.003**	0.220	**0.046**
	150-300	32.3^{A}	32.9^{A}	20.9^{B}	28.3^{A}	**0.013**	**0.025**	0.070
	> 300	17.9^{A}	15.0^{A}	1.1^{B}	3.5^{B}	**0.005**	0.925	0.374
2.5-3.0	36-150	52.3^{C}	53.4^{C}	78.5^{A}	68.8^{B}	**0.003**	0.161	0.081
	150-300	32.5^{A}	33.4^{A}	20.5^{B}	28.1^{A}	**0.011**	**0.028**	0.095
	> 300	15.2^{A}	13.2^{A}	1.0^{B}	3.1^{B}	**0.008**	0.974	0.495
3.0-3.5	36-150	53.2^{B}	57.1^{B}	78.2^{A}	70.3^{A}	**0.006**	0.617	0.093
	150-300	32.9^{A}	31.6^{A}	20.8^{B}	26.5^{AB}	**0.035**	0.373	0.149
	> 300	13.9^{A}	11.3^{A}	1.0^{B}	3.2^{B}	**0.021**	0.948	0.433
3.5-4.0	36-150	57.8^{B}	57.5^{B}	79.9^{A}	67.0^{AB}	**0.028**	0.145	0.163
	150-300	29.8^{A}	32.4^{A}	19.3^{A}	28.6^{A}	0.115	0.064	0.311
	> 300	12.4^{A}	10.1^{A}	0.8^{A}	4.4^{A}	0.073	0.852	0.452

Note: different letters within the same row indicate the differences ($p < 0.05$) among two plant systems in two soil groups (Finer-textured soils: n = 12 and coarser-textured soils: n = 7). Significant effects in ANOVA table are shown in bold. Since distance intervals of < 0.25, 1.0-1.5, and 2.0-2.5 mm away from POM surface for 36-150 μm Ø pores were the only three distances where Texture*Plant interaction was statistically significant, different lowercase letters indicate that the differences ($p < 0.05$) between two plant systems within each textured soil groups.

The vegetation also affected the imaged-based porosity. From 0.1-1.5 mm distance interval in Hancock and 2.5-3.0 mm in Lake City, the image-based porosity was greater in the prairie than that in switchgrass system, while the porosity in switchgrass was numerically greater at <0.25 distance (Figure 2.3 and Table 2.4).

The contribution of the three pore-size classes into the visible porosity changed with the distance from POM. In the region at < 0.25 mm away from the POM, pore group within 36-150 μm Ø size range accounted for 4% of the total porosity in finer-textured soils and 11% in coarser-textured soils (Figure 2.5). Meanwhile, relatively larger pores (> 300 μm Ø) contributed to 75% and 58% of the porosity in finer- and coarser-textured soil of the same distance region, respectively. The contributions of 36-150 μm pores in both textured groups of soils increased with the distance from POM, while that of the larger pores decreased. Notably, the increases in the fractions of smaller pores were more drastic in coarser-textured soils compared to that in finer-textured soils (Figure 2.5). Pores in the coarser soils were mostly represented by finer size pores (36-300 μm Ø) beyond 1.0 mm distance from POM, whereas the finer soils still had 35% and 11 % of the larger pores at 1.0 mm and at 4.0 mm distances from POM, respectively. In coarser-textured soils, prairie system had a greater fraction of smaller size pores within interval regions from 0 to 3.0 mm than the switchgrass system (Figure 2.5C and 2.5D), while the fractions of such pores did not differ between two systems in finer-textured soils (Figure 2.5A and 2.5B).

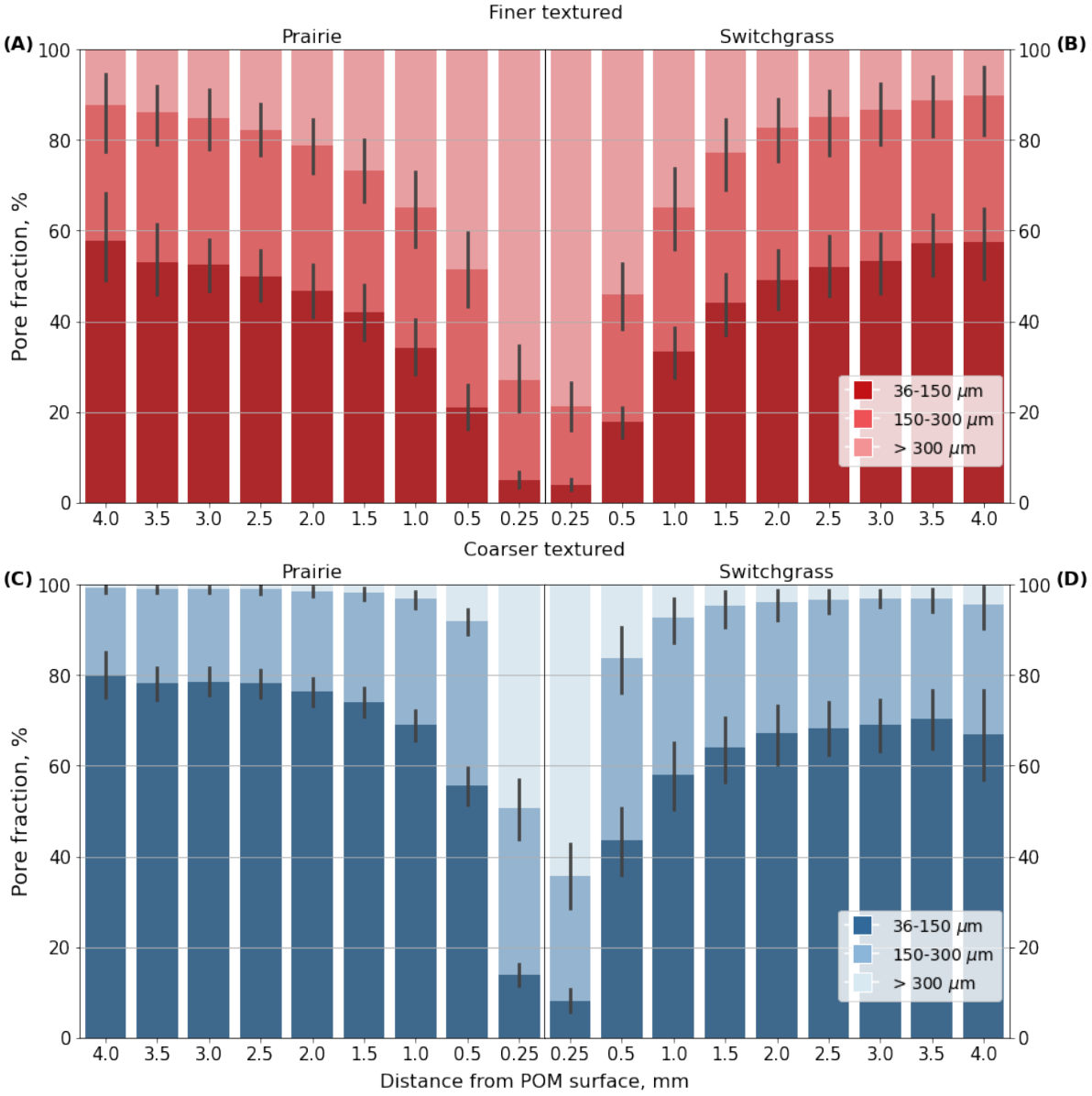

Figure 2.5. Proportion of pore fractions by distance intervals (<0.25, 0.25-0.5, 0.5-1.0, 1.0-1.5, …, 3.0-3.5, and 3.5-4.0 mm) from POM under **(A and C)** prairie and **(B and D)** switchgrass systems in finer- **(A and B)** and coarser-textured **(C and D)** soils. Error bars represent standard deviations, and statistical differences between two textured soil groups and two plant systems within each interval and region were shown on Table 2.5.

In both plant systems, in the immediate vicinity of POM (<0.25 mm away from POM), pore connectivity was greater in finer-textured than in coarser-textured soils. However, when examined across the entire soil volumes, the connectivity was lower in finer-textured than in coarser-textured soils (Figure 2.6). The connectivity in the vicinity of POM was negatively correlated with sand, quartz, and smectite contents, while it was positively correlated with silt, clay, and P-feldspar contents (Table 2.6). However, the total connectivity showed the opposite trend, being positively correlated with sand, quartz, and smectite contents.

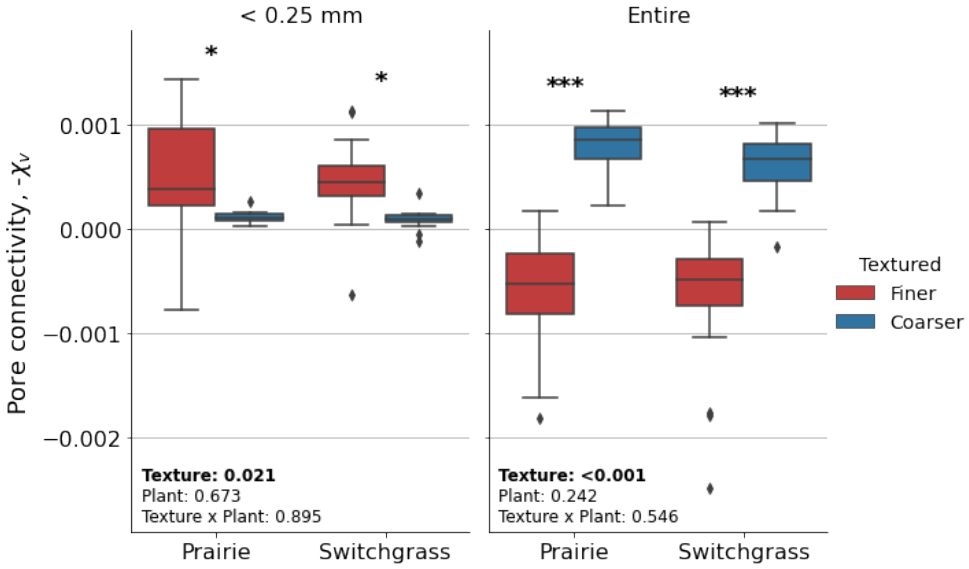

Figure 2.6. Pore connectivity at the region <0.25 mm away from POM and entire image stack. High pore connectivity values indicate pores were more connected, as Euler numbers (χ) were inverted. ANOVA F-test results are shown in the bottom of each figure. * and *** denote significant differences between finer- and coarser-textured soils of each region at the $\alpha < 0.05$ and < 0.001 level, respectively (Finer-textured soils: n = 12 and coarser-textured soils: n = 7).

Table 2.6. Correlation coefficients between soil texture, selected McCrone mill powder (MBP) components, and clay mineralogy with image-based porosity and pore connectivity of < 0.25 mm distance and entire images across five experimental sites.

		Image-based porosity (%)		Pore connectivity ($-\chi_v$)	
		<0.25mm	Entire	<0.25mm	Entire
Soil texture	Sand	**-0.43****	**0.86*****	**-0.71*****	**0.67*****
	Silt	**0.47****	**-0.86*****	**0.67*****	**-0.66*****
	Clay	0.18	**-0.68*****	**0.72*****	**-0.57*****
MBP mineralogy	Quartz	**-0.47***	**0.76*****	**-0.46***	**0.67****
	K-feldspar	0.16	-0.32	-0.06	-0.27
	P-feldspar	**0.53***	**-0.82*****	**0.78*****	**-0.72*****
Clay mineralogy	Smectite	-0.34	0.41	**-0.45***	**0.56***
	Mica	0.12	-0.21	-0.41	-0.35
	Kaolinite	0.11	-0.09	-0.15	-0.05
	Chlorite	0.18	-0.14	0.02	-0.18

Note: Bolded values indicate statistical significances at $p < 0.05$, and the marked *, **, and ** denote coefficient levels at the $p < 0.05$, <0.01, and < 0.001 level, respectively.

2.4 Discussion

Results demonstrat that soil pore structure in the root detritusphere and in the whole soil volumes were affected by both soil texture and plants. Coarser-textured soils had much higher image-based porosity, yet fewer pores of biological origin than finer-textured soils. The biopores of fine-textured soils were numerous and constituted a significantly greater portion of the overall pore space, yet did not hold as much remaining POM as those in the coarse-textured soils. Pore-size distributions in detritusphere as well as their spatial distribution trends with distance from the decomposing roots also markedly differed between the finer- and coarser-textured soils. Pores in the immediate vicinity of POM were better connected in finer-textured soils than in coarser-textured soils in both plant systems. While switchgrass soil had more biopores than prairie, its detritusphere pores consisted of relatively large size pores than those of the prairie, especially in coarser-textured soils.

2.4.1 Influences of soil texture on detritusphere pores

The greatest porosities found at < 0.25 mm away from the POM in soils of both plant systems indicated that the vicinity of the POM was mostly air-filled (Figure 2.3). This “POM gap” between soil

particles and root residues can be explained by incomplete filling of existing pores by roots during their growth and decrease of roots' volume due to shrinking upon drying and/or their decomposition (De Gryze et al., 2006). Consistent with this explanation, roots of *Agave deserti* were found to shrunk by 34% in 24 days of natural drought in a greenhouse study (North and Nobel, 1997), and transpiration shrank roots of *Lupinus albus* (Koebernick et al. 2018). Decreases in POM volume due to decomposition were both visually observed and quantified using X-ray μCT images of intact soil samples (Kim et al., 2020; Juyal et al., 2021).

Our findings of inherent texture and mineralogy characteristics influencing the contribution of biopores to the overall soil porosities (Figure 2.2C and Table 2.1) were consistent with expectations and previous reports. In relatively sandy soils the biopores formed by roots were partially or completely refilled by sand grains after root decomposition, while in loamy soils the biopores that the roots left behind maintained their structure (Phalempin et al., 2022). Sand grains have high volume-to-surface area ratios, and quartz on grain surfaces often lacks negative charge (Bazzoffi et al., 1995; Schrader and Zhang, 1997), resulting in low stability of particle arrangements (Almajmaie et al., 2017). Thus, the subsidence and displacement of the dispersed sand grains near decaying POM residues is likely among the reasons for the lower contributions of biopores to overall porosities in coarser-textured soils (Hancock and Lake City sites) compared to that in finer-textured soils (Oregon, Lux Arbor, and Escanaba sites) (Figure 2.2C) and for the greater proportions of biopore space occupied by POM (Figure 2.2D). The lower pore connectivity near the POM in coarser-textured than in finer-textured soils (Figure 2.6) is another outcome of low stability. Finer, i.e., lower sand and quartz contents, soil particles are expected to facilitate maintenance of the structure by pores around POM, as compared to that of pores in coarser-textured soils.

The other two contributors to the observed differences in biopore volumes and in POM presence within the biopores are the inherent differences between coarser- and finer-textured soils in terms of (i) root growth and (ii) root residue decomposition rates. The volume of biopores and their occupation by roots might be overall lower in coarser-textured soils due to poorer root growth conditions (Dodd and Lauenroth, 1997; Sainju et al., 2017). POM in soils with high sand contents might decompose slower than that in the

soils with low sand contents due to lower microbial activity at organo-mineral surfaces of sand grains (Kaiser et al., 1992; Kögel-Knabner et al., 2008; Haddix et al., 2020). Indeed, a negative correlation between sand contents and microbial biomass C was found across our experimental sites in a parallel study (Lee et al., 2023). Thus, in coarser-textured soils, the size of POM residues might not be decreasing as quickly as in the finer-textured soils, and the region around the POM may not be completely empty yet (Figure 2.3).

However, if the differences in plant growth and decomposition rates had indeed played a significant role in generating the observed differences in the biopore occupation by POM (Figure 2.2D), we would expect to also detect the differences in terms of POM occupation between the two plant systems. Soils of restored prairie have developed higher SOM (Sanford, 2014; Sprunger and Robertson, 2018), thus better plant growth conditions, and much more active and abundant microbial communities (Lange et al., 2015), e.g., significantly higher microbial biomass C (Lee et al., 2023), than those of the monoculture switchgrass. Yet, there were no significant differences between the two systems in terms of POM occupation of the biopores (Figure 2.2D) as well as the porosity in the detritusphere at least 1.0 mm away from POM (Table 2.4), ruling out the importance of these contributors. Thus, we conclude that the loss of structure and collapsing of biopores in coarser-textured soils is the main reason of the observed effects and is likely a wide-spread phenomenon.

The larger proportion of 36-150 μm Ø pores in close proximity (< 0.25 mm distance) to POM in coarser-textured soils (Figure 2.5) is consistent with lower soil porosity at the same distance (Figure 2.3). Sand grains dominating coarser-textured soils can sporadically fill the POM gaps (Phalempin et al., 2022; Schrader and Zhang, 1997), and the filling by the grains may fragment the space of the gaps into finer pores. Indeed, porosities within the <0.25 mm distance to POM were negatively correlated with sand contents (Table 2.6). However, coarser-textured soils had larger contribution of such pores in intervals of > 0.25 mm compared to finer-textured soils, showing positive correlations between sand contents and porosities of the entire volume (Table 2.6). Typically, in such regions beyond the root-influenced zone – areas where root-induced pores are negligible – the porosity tends to increase with higher sand content (Nimmo, 2013; Ding et al., 2016; Fan et al., 2021). Indeed, gaps between sand particles are likely to primarily consist of pores

that range between 50-200 μm Ø (Bantralexis et al., 2023). Therefore, the contrasting contributions of finer pores by distances are an indication of a localized effect (~ 0.25 mm) of roots on the pore structure, beyond which the porosity was mostly controlled by the soil texture.

2.4.2 Influences of vegetation on detritusphere pores

The overall influence of the studied plant systems, 5-6 years after their establishment, on the pore characteristics of detritusphere was much lower than that of the inherent soil characteristics, i.e., texture and mineralogy. An important exception was the image-based porosity in remote portions of detritusphere (> 1.0 mm): it tended to be greater in the soils of restored prairie than in those of switchgrass (Figure 2.3 and Table 2.4). Switchgrass roots often reuse existing biopores (Lucas et al., 2023), and their thick roots were likely responsible for soil compaction and low porosity at >1 mm distances (Aravena et al., 2011; Liu et al., 2022). On the contrary, finer and heavily branching roots of many plant species of restored prairie likely promoted formation of finer pore networks throughout the entire detritusphere, stabilizing them via root exudates and rhizodeposits (Hairiah et al., 2020; Smith et al., 2021). We surmise that these very fine roots rapidly decomposed after soil sampling and thus could not be detected as POM in the current study.

2.5 Conclusions

Soil pore structure both in the entire soil volume and in the root detritusphere was significantly influenced by soil texture and minerology. Coarse-textured quartz-rich soils had higher porosity but lower bioporosity than fine-textured soils, as well as a greater proportions of biopore spaces occupied by POM. There were clear differences between fine- and coarse-textured soils in spatial patterns of pore size distributions as a function of distance from POM. In the immediate vicinity of POM. Finer-textured soils had higher porosity in close proximity of POM, that is greater POM-gap, consisting mainly of large pores (>300 μm Ø) as well as better pore connectivity compared to those of the coarser-textured soils. Despite known differences in the root characteristics of the studied plant systems, i.e., monoculture switchgrass and restored prairie, their impact on detritusphere pore structure was relatively minor. Lack of plant system effect suggests that the observed differences in detritusphere pore structure between finer- and coarser-

textured soils are of primarily physical/mineralogical origin, e.g., due to loss of structure and collapsing of biopores in the latter, and the phenomenon present across a wide range (Alfisols, Entisols, and Spodosols) of soil types. The study provides an insight into the relationship among soil texture, mineralogy, and detritusphere pore structure, which serves as an important arena for microbial activity and soil C processing.

2.6 Acknowledgements

I would like to thank Michelle Quigley from Michigan State University for conducting X-ray μCT scanning, Martin Pentrak from University of Illinois-Champaign for conducting X-ray powder diffraction, Jenie Gil Lugo and Maxwell Oerther for assistance with sample collection, and the Kellogg Biological Station and Great Lakes Bioenergy Research Center team for agronomic management of the field experiment. This research was funded by the Great Lakes Bioenergy Research Center, U.S. Department of Energy, Office of Science, Office of Biological and Environmental Research under Award Number DE-SC0018409. The work was also supported by the NSF LTER Program (DEB 1027253) at Kellogg Biological Station, by Michigan State University's AgBioResearch, and by NC Regional Multistate Project 1187.

REFERENCES

Almajmaie, A., Hardie, M., Doyle, R., Birch, C., and Acuna, T. (2017). Influence of soil properties on the aggregate stability of cultivated sandy clay loams. *Journal of Soils and Sediments*, 17(3): 800–809. doi: 10.1007/s11368-016-1568-1

Aravena, J. E., Berli, M., Ghezzehei, T. A., and Tyler, S. W. (2011). Effects of Root-Induced Compaction on Rhizosphere Hydraulic Properties—X-ray Microtomography Imaging and Numerical Simulations. *Environmental Science & Technology*, 45(2): 425–431. doi: 10.1021/es102566j

Bantralexis, K. E., Markou, I. N., and Zografos, G. I. (2023). Use of sand pore-size distribution to predict cement suspension groutability. *Developments in the Built Environment*, 14: 100138. doi: 10.1016/j.dibe.2023.100138

Bazzoffi, P., Mbagwu, J. S. C., and Chukwu. W. I. E. (1995). Statistical models for predicting aggregate stability from intrinsic soil components. *International Agrophysics*, 9.

Beare, R., Lowekamp, B., and Yaniv, Z. (2018). Image Segmentation, Registration and Characterization in R with SimpleITK. *Journal of Statistical Software*, 86: 8. doi: 10.18637/jss.v086.i08

Bengough, A. G., Bransby, M. F., Hans, J., McKenna, S. J., Roberts, T. J., and Valentine, T. A. (2006). Root responses to soil physical conditions; growth dynamics from field to cell. *Journal of Experimental Botany*, 57(2): 437–447. doi: 10.1093/jxb/erj003

Berg, S., Kutra, D., Kroeger, T., Straehle, C. N., Kausler, B. X., Haubold, C., … Kreshuk, A. (2019). ilastik: Interactive machine learning for (bio)image analysis. *Nature Methods*, 16(12): 1226–1232. doi: 10.1038/s41592-019-0582-9

Bodner, G., Leitner, D., and Kaul, H.-P. (2014). Coarse and fine root plants affect pore size distributions differently. *Plant and Soil*, 380(1–2): 133–151. doi: 10.1007/s11104-014-2079-8

Buades, A., Coll, B., and Morel, J.-M. (2011). Non-Local Means Denoising. *Image Processing On Line*, 1: 208–212. doi: 10.5201/ipol.2011.bcm_nlm

Buhmann, C., Rapp, I., and Laker, M. (1996). Differences in mineral ratios between disaggregated and original clay fractions in some South African soils as affected by amendments. *Soil Research*, 34(6): 909. doi: 10.1071/SR9960909

Croser, C., Bengough, A. G., and Pritchard, J. (1999). The effect of mechanical impedance on root growth in pea (Pisum sativum). I. Rates of cell flux, mitosis, and strain during recovery. *Physiologia Plantarum*, 107(3): 277–286. doi: 10.1034/j.1399-3054.1999.100304.x

Darbon, J., Cunha, A., Chan, T. F., Osher, S., and Jensen, G. J. (2008). Fast nonlocal filtering applied to electron cryomicroscopy. *2008 5th IEEE International Symposium on Biomedical Imaging: From Nano to Macro*, 1331–1334. Paris, France: IEEE. doi: 10.1109/ISBI.2008.4541250

De Gryze, S., Jassogne, L., Six, J., Bossuyt, H., Wevers, M., and Merckx, R. (2006). Pore structure changes during decomposition of fresh residue: X-ray tomography analyses. *Geoderma*, 134(1): 82–96. doi: 10.1016/j.geoderma.2005.09.002

Ding, D., Zhao, Y., Feng, H., Peng, X., and Si, B. (2016). Using the double-exponential water retention equation to determine how soil pore-size distribution is linked to soil texture. (*National Agricultural Library*).

Dodd, M. B., and Lauenroth, W. K. (1997). The influence of soil texture on the soil water dynamics and vegetation structure of a shortgrass steppe ecosystem. *Plant Ecology*, 133(1): 13–28. doi: 10.1023/A:1009759421640

Fan, Z., Hu, C., Zhu, Q., Jia, Y., Zuo, D., and Duan, Z. (2021). Three-dimensional pore characteristics and permeability properties of calcareous sand with different particle sizes. *Bulletin of Engineering Geology and the Environment*, 80(3): 2659–2670. doi: 10.1007/s10064-020-02078-1

Franklin, S. M., Kravchenko, A. N., Vargas, R., Vasilas, B., Fuhrmann, J. J., and Jin, Y. (2021). The unexplored role of preferential flow in soil carbon dynamics. *Soil Biology and Biochemistry*, 161: 108398. doi: 10.1016/j.soilbio.2021.108398

Gaillard, V., Chenu, C., Recous, S., and Richard, G. (1999). Carbon, nitrogen and microbial gradients induced by plant residues decomposing in soil. *European Journal of Soil Science*, 50(4): 567–578. doi: 10.1046/j.1365-2389.1999.00266.x

Gee, G. W., and Or, D. (2002). 2.4 Particle-Size Analysis. In Methods of Soil Analysis (pp. 255–293). John Wiley & Sons, Ltd. doi: 10.2136/sssabookser5.4.c12

Haddix, M. L., Gregorich, E. G., Helgason, B. L., Janzen, H., Ellert, B. H., and Francesca Cotrufo, M. (2020). Climate, carbon content, and soil texture control the independent formation and persistence of particulate and mineral-associated organic matter in soil. *Geoderma*, 363: 114160. doi: 10.1016/j.geoderma.2019.114160

Hairiah, K., Widianto, W., Suprayogo, D., and Van Noordwijk, M. (2020). Tree Roots Anchoring and Binding Soil: Reducing Landslide Risk in Indonesian Agroforestry. *Land*, 9(8): 256. doi: 10.3390/land9080256

Helliwell, J. R., Sturrock, C. J., Mairhofer, S., Craigon, J., Ashton, R. W., Miller, A. J., … Mooney, S. J. (2017). The emergent rhizosphere: Imaging the development of the porous architecture at the root-soil interface. *Scientific Reports*, 7(1): 14875. doi: 10.1038/s41598-017-14904-w

Helliwell, Jon R., Sturrock, C. J., Miller, A. J., Whalley, W. R., and Mooney, S. J. (2019). The role of plant species and soil condition in the structural development of the rhizosphere. *Plant, Cell & Environment*, 42(6): 1974–1986. doi: 10.1111/pce.13529

Hildebrand, T., and Rüegsegger, P. (1997). A new method for the model-independent assessment of thickness in three-dimensional images. *Journal of Microscopy*, 185(1): 67–75. doi: 10.1046/j.1365-2818.1997.1340694.x

Jarvis, N. J. (2007). A review of non-equilibrium water flow and solute transport in soil macropores: Principles, controlling factors and consequences for water quality. *European Journal of Soil Science*, 58(3): 523–546. doi: 10.1111/j.1365-2389.2007.00915.x

Jesus, E. da C., Liang, C., Quensen, J. F., Susilawati, E., Jackson, R. D., Balser, T. C., and Tiedje, J. M. (2016). Influence of corn, switchgrass, and prairie cropping systems on soil microbial

communities in the upper Midwest of the United States. *GCB Bioenergy*, 8(2): 481–494. doi: 10.1111/gcbb.12289

Juyal, A., Guber, A., Oerther, M., Quigley, M., and Kravchenko, A. N. (2021). Pore architecture and particulate organic matter in soils under monoculture switchgrass and restored prairie in contrasting topography. *Scientific Reports*, 11(1): 21998. doi: 10.1038/s41598-021-01533-7

Kaiser, E. A., Mueller, T., Joergensen, R. G., Insam, H., and Heinemeyer, O. (1992). Evaluation of methods to estimate the soil microbial biomass and the relationship with soil texture and organic matter. *Soil Biology and Biochemistry*, 24(7): 675–683. doi: 10.1016/0038-0717(92)90046-Z

Kasmerchak, C. S., and Schaetzl, R. (2018). Soils of the GLBRC Marginal Land Expeirment (MLE) Sites. doi: 10.5281/ZENODO.2578238

Kim, K., Guber, A. K., Rivers, M., and Kravchenko, A. N. (2020). Contribution of decomposing plant roots to N2O emissions by water absorption. *Geoderma*, 375: 114506. doi: 10.1016/j.geoderma.2020.114506

Koebernick, N., Schlüter, S., Blaser, S. R. G. A., and Vetterlein, D. (2018). Root-soil contact dynamics of Vicia faba in sand. *Plant and Soil*, 431(1): 417–431. doi: 10.1007/s11104-018-3769-4

Kögel-Knabner, I., Guggenberger, G., Kleber, M., Kandeler, E., Kalbitz, K., Scheu, S., … Leinweber, P. (2008). Organo-mineral associations in temperate soils: Integrating biology, mineralogy, and organic matter chemistry. *Journal of Plant Nutrition and Soil Science*, 171(1): 61–82. doi: 10.1002/jpln.200700048

Kravchenko, A. N., Guber, A. K., Razavi, B. S., Koestel, J., Blagodatskaya, E. V., and Kuzyakov, Y. (2019). Spatial patterns of extracellular enzymes: Combining X-ray computed micro-tomography and 2D zymography. *Soil Biology and Biochemistry*, 135: 411–419. doi: 10.1016/j.soilbio.2019.06.002

Kravchenko, A. N., Guber, A. K., Razavi, B. S., Koestel, J., Quigley, M. Y., Robertson, G. P., and Kuzyakov, Y. (2019). Microbial spatial footprint as a driver of soil carbon stabilization. *Nature Communications*, 10(1): 3121. doi:10.1038/s41467-019-11057-4

Kravchenko, A. N., and Guber, A. K. (2017). Soil pores and their contributions to soil carbon processes. *Geoderma*, 287: 31–39. doi: 10.1016/j.geoderma.2016.06.027

Kuzyakov, Y., and Blagodatskaya, E. (2015). Microbial hotspots and hot moments in soil: Concept & review. *Soil Biology and Biochemistry*, 83: 184–199. doi: 10.1016/j.soilbio.2015.01.025

Lange, M., Eisenhauer, N., Sierra, C. A., Bessler, H., Engels, C., Griffiths, R. I., … Gleixner, G. (2015). Plant diversity increases soil microbial activity and soil carbon storage. *Nature Communications*, 6(1): 6707. doi: 10.1038/ncomms7707

Lee, J. H., Lucas, M., Guber, A. K., Li, X., & Kravchenko, A. N. (2023). Interactions among soil texture, pore structure, and labile carbon influence soil carbon gains. *Geoderma*, 439: 116675. doi: 10.1016/j.geoderma.2023.116675

Li, X., Petipas, R. H., Antoch, A. A., Liu, Y., Stel, H. V., Bell-Dereske, L., … Friesen, M. L. (2022). Switchgrass cropping systems affect soil carbon and nitrogen and microbial diversity and activity on marginal lands. *GCB Bioenergy*, 14(8): 918–940. doi: 10.1111/gcbb.12949

Liu, Y.-F., Meng, L.-C., Huang, Z., Shi, Z.-H., and Wu, G.-L. (2022). Contribution of fine roots mechanical property of Poaceae grasses to soil erosion resistance on the Loess Plateau. *Geoderma*, 426: 116122. doi: 10.1016/j.geoderma.2022.116122

Lucas, M. (2022). Perspectives from the Fritz-Scheffer Awardee 2020—The mutual interactions between roots and soil structure and how these affect rhizosphere processes #. *Journal of Plant Nutrition and Soil Science*, 185(1): 8–18. doi: 10.1002/jpln.202100385

Lucas, M., Nguyen, L. T. T., Guber, A., and Kravchenko, A. N. (2022). Cover crop influence on pore size distribution and biopore dynamics: Enumerating root and soil faunal effects. *Frontiers in Plant Science*, 13: 928569. doi: 10.3389/fpls.2022.928569

Lucas, M., Santiago, J. P., Chen, J., Guber, A., and Kravchenko, A. N. (2023). The soil pore structure encountered by roots affects plant-derived carbon inputs and fate. *New Phytologist*, 240(2): 515–528. doi: 10.1111/nph.19159

Lucas, M., Schlüter, S., Vogel, H.-J., and Vetterlein, D. (2019a). Roots compact the surrounding soil depending on the structures they encounter. *Scientific Reports*, 9(1): 16236. doi: 10.1038/s41598-019-52665-w

Lucas, M., Schlüter, S., Vogel, H.-J., and Vetterlein, D. (2019b). Soil structure formation along an agricultural chronosequence. *Geoderma*, 350: 61–72. doi: 10.1016/j.geoderma.2019.04.041

Lucas, M., Vetterlein, D., Vogel, H.-J., and Schlüter, S. (2021). Revealing pore connectivity across scales and resolutions with X-ray CT. (*National Agricultural Library*).

Mitchell, J. K., and Soga, K. (2005). Fundamentals of Soil Behavior. In Fundamentals of Soil Behavior. John Wiley and Sons, Inc.

Neaman, A., Singer, A., and Stahr, K. (1999). Clay mineralogy as affecting disaggregation in some palygorskite containing soils of the Jordan and Bet-She'an Valleys. *Soil Research*, 37(5): 913. doi: 10.1071/SR98118

Negassa, W. C., Guber, A. K., Kravchenko, A. N., Marsh, T. L., Hildebrandt, B., and Rivers, M. L. (2015). Properties of Soil Pore Space Regulate Pathways of Plant Residue Decomposition and Community Structure of Associated Bacteria. *PLOS ONE*, 10(4), e0123999. doi: 10.1371/journal.pone.0123999

Nimmo, J. R. (2013). Porosity and Pore Size Distribution. In Reference Module in Earth Systems and Environmental Sciences (p. B9780124095489052659). Elsevier. doi: 10.1016/B978-0-12-409548-9.05265-9

North, G. B., and Nobel, P. S. (1997). Root–soil contact for the desert succulent Agave deserti in wet and drying soil. *The New Phytologist*, 135(1): 21–29. doi: 10.1046/j.1469-8137.1997.00620.x

Odgaard, A., and Gundersen, H. J. G. (1993). Quantification of connectivity in cancellous bone, with special emphasis on 3-D reconstructions. *Bone*, 14(2), 173–182. doi: 10.1016/8756-3282(93)90245-6

Phalempin, M., Landl, M., Wu, G.-M., Schnepf, A., Vetterlein, D., and Schlüter, S. (2022). Maize root-induced biopores do not influence root growth of subsequently grown maize plants in well aerated, fertilized and repacked soil columns. *Soil and Tillage Research*, 221: 105398. doi: 10.1016/j.still.2022.105398

Phalempin, M., Lippold, E., Vetterlein, D., and Schlüter, S. (2021a). An improved method for the segmentation of roots from X-ray computed tomography 3D images: Rootine v.2. *Plant Methods*, 17(1): 39. doi: 10.1186/s13007-021-00735-4

Phalempin, M., Lippold, E., Vetterlein, D., and Schlüter, S. (2021b). Soil texture and structure heterogeneity predominantly governs bulk density gradients around roots. *Vadose Zone Journal*, 20(5). doi: 10.1002/vzj2.20147

Rivera, J. I., and Bonilla, C. A. (2020). Predicting soil aggregate stability using readily available soil properties and machine learning techniques. *CATENA*, 187: 104408. doi: 10.1016/j.catena.2019.104408

Sainju, U. M., Allen, B. L., Lenssen, A. W., and Ghimire, R. P. (2017). Root biomass, root/shoot ratio, and soil water content under perennial grasses with different nitrogen rates. *Field Crops Research*, 210: 183–191. doi: 10.1016/j.fcr.2017.05.029

Sanford, G. R. (2014). Perennial Grasslands Are Essential for Long Term SOC Storage in the Mollisols of the North Central USA. In A. E. Hartemink & K. McSweeney (Eds.), *Soil Carbon* (pp. 281–288). Cham: Springer International Publishing. doi: 10.1007/978-3-319-04084-4_29

Schindelin, J., Arganda-Carreras, I., Frise, E., Kaynig, V., Longair, M., Pietzsch, T., … Cardona, A. (2012). Fiji: An open-source platform for biological-image analysis. *Nature Methods*, 9(7): 676–682. doi: 10.1038/nmeth.2019

Schrader, S., and Zhang, H. (1997). Earthworm casting: Stabilization or destabilization of soil structure? Soil Biology and Biochemistry, 29(3): 469–475. doi: 10.1016/S0038-0717(96)00103-4

Six, J., Elliott, E. T., and Paustian, K. (2000). Soil Structure and Soil Organic Matter II. A Normalized Stability Index and the Effect of Mineralogy. *Soil Science Society of America Journal*, 64(3): 1042–1049. doi: 10.2136/sssaj2000.6431042x

Smith, D. J., Wynn-Thompson, T. M., Williams, M. A., and Seiler, J. R. (2021). Do roots bind soil? Comparing the physical and biological role of plant roots in fluvial streambank erosion: A mini-JET study. *Geomorphology*, 375: 107523. doi: 10.1016/j.geomorph.2020.107523

Sokol, N. W., Kuebbing, S. E., Karlsen-Ayala, E., and Bradford, M. A. (2019). Evidence for the primacy of living root inputs, not root or shoot litter, in forming soil organic carbon. *New Phytologist*, 221(1): 233–246. doi: 10.1111/nph.15361

Sprunger, C. D., and Robertson, G. P. (2018). Early accumulation of active fraction soil carbon in newly established cellulosic biofuel systems. *Geoderma*, 318: 42–51. doi: 10.1016/j.geoderma.2017.11.040

Strong, D. T., Wever, H. D., Merckx, R., and Recous, S. (2004). Spatial location of carbon decomposition in the soil pore system: Spatial location of carbon decomposition. *European Journal of Soil Science*, 55(4): 739–750. doi: 10.1111/j.1365-2389.2004.00639.x

Traoré, O., Groleau-Renaud, V., Plantureux, S., Tubeileh, A., and Boeuf-Tremblay, V. (2000). Effect of root mucilage and modelled root exudates on soil structure. *European Journal of Soil Science*, 51(4): 575–581. doi: 10.1111/j.1365-2389.2000.00348.x

Védère, C., Vieublé Gonod, L., Pouteau, V., Girardin, C., and Chenu, C. (2020). Spatial and temporal evolution of detritusphere hotspots at different soil moistures. *Soil Biology and Biochemistry*, 150: 107975. doi: 10.1016/j.soilbio.2020.107975

Vogel, H.-J. (2002). Topological Characterization of Porous Media. In K. Mecke & D. Stoyan (Eds.), Morphology of Condensed Matter: Physics and Geometry of Spatially Complex Systems (pp. 75–92). Berlin, Heidelberg: Springer. doi: 10.1007/3-540-45782-8_3

Vogel, H.-J., and Roth, K. (2001). Quantitative morphology and network representation of soil pore structure. *Advances in Water Resources*, 24(3–4): 233–242. doi: 10.1016/S0309-1708(00)00055-5

Vogel, H.-J., Weller, U., and Schlüter, S. (2010). Quantification of soil structure based on Minkowski functions. *Computers & Geosciences*, 36(10): 1236–1245. doi: 10.1016/j.cageo.2010.03.007

Wakindiki, I. I. C., and Ben-Hur, M. (2002). Soil Mineralogy and Texture Effects on Crust Micromorphology, Infiltration, and Erosion. *Soil Science Society of America Journal*, 66(3): 897–905. doi: 10.2136/sssaj2002.8970

Walt, S. van der, Schönberger, J. L., Nunez-Iglesias, J., Boulogne, F., Warner, J. D., Yager, N., … Yu, T. (2014). scikit-image: Image processing in Python. *PeerJ*, 2, e453. doi: 10.7717/peerj.453

CHAPTER 3: Root size distributions of switchgrass cultivars, soil pores, and implications for soil carbon processes[3]

Abstract

Switchgrass (*Panicum virgatum* L.) is a promising feedstock for biofuel production, with diverse cultivars representing several ecotypes adapted to different environmental conditions within the contiguous USA. Multiple field studies have demonstrated that monoculture switchgrass cultivation leads to slow to negligible soil carbon (C) gains, an outcome unexpected for such a deep-rooted perennial. We hypothesize that different switchgrass cultivars have disparate impacts on soil C gains, and one of the reasons is variations in physical characteristics of their roots, where roots directly and indirectly influence formation of soil pores. We tested this hypothesis at Great Lakes Bioenergy Research Center's research site in Michigan using two lowland cultivars (Alamo and Kanlow) and four upland cultivars (Southlow, Cave-in-Rock, Blackwell, and Trailblazer). Three types of soil samples were collected: 20cm diameter (Ø) intact cores used for root analyses; 5cm Ø intact cores subjected to X-ray computed tomography scanning at 18μm resolution used for pore characterization; and disturbed soil samples used for microbial biomass C (MBC) and soil C measurements. Path analysis was used to explore interactive relationships among roots, soil pores, and their impact on MBC, and ultimately, on soil C contents across six cultivars. The abundance of very fine roots (<200μm Ø) was positively associated with fractions of pores in the same size range, but negatively with distances to pores and particulate organic matter. Higher abundance of such roots also led to greater MBC, while greater volumes of medium pores (50-200μm Ø) and shorter distances to pores led to greater MBC. Results suggest that the greater proportion of very fine roots is a trait that can potentially stimulate soil C gains, with pore characteristics serving as links for the relationship between such roots and C gains. However, seven years of cultivation led to no significant C gains in any of the studied cultivars.

[3] Originally submitted as: Lee, J. H., Ulbrich, T. C., Lucas, M., Robertson, G. P., Guber, A. K., & Kravchenko, A. N. (2024). Very Fine Roots Differ Among Switchgrass (*Panicum Virgatum* L.) Cultivars and Differentially Affect Soil Pores and Carbon Processes, *Soil Biology and Biochemistry*. (*Under review*)

3.1 Introduction

Switchgrass (*Panicum virgatum* L.) is a phenotypically diverse species with genetic variation among divergent ecotypes and across environmental gradients of eastern North America (Casler et al., 2004, 2007; Lovell et al., 2021). Lowland ecotype switchgrass originates from the southern U.S., which has a warm and mesic climate, while the upland ecotype originates from more northern areas with a drier and colder climate (Vogel et al., 2005; Zhang et al., 2011). Switchgrass cultivars of both lowland and upland ecotypes have been selected for various bioenergy-related traits including biomass yield, winter mortality, and drought tolerance (Haque et al., 2009; Mitchell et al., 2012; Lowry et al., 2019). We surmise that within-species diversity may also give rise to differences in soil C accrual, though Mosier et al. (2024) failed to find cultivar differences in the C accrual.

The plant's root system plays a critical role in plant contributions to soil C gains, and indeed, root characteristics of switchgrass cultivars differ substantially (de Graaff et al., 2013; Ulbrich et al., 2021; Mosier et al., 2024). Their direct contribution is to transfer organic C to the soil through turnover of roots and the released rhizodeposits and exudates (Liang et al., 2018; Sokol et al., 2019; Panchal et al., 2022). The chemical composition of rhizodeposits and exudates is known to vary among different plant genotypes (Huang et al., 2014; Semchenko et al., 2021). In switchgrass, An et al. (2013) found that the concentration of exudates differed among 11 cultivars, and Li et al., (2022) found distinct differences in concentrations of exudates between lowland and upland ecotypes. Such disparate root-derived C sources can have different influences on soil microorganisms (Emmett et al., 2017; Jiang et al., 2017), and several studies have documented varied impacts of different switchgrass cultivars on soil microbial biomass, microbial diversity, and microbial community composition (Sawyer et al., 2019; Roley et al., 2021; Ulbrich et al., 2021; da Costa et al., 2022).

Fine roots are particularly important for soil C cycling, contributing substantially to soil organic matter through their rapid turnover and subsequent decomposition; and their persistent C inputs can constitute 30-80% of soil C across various ecosystems (Ruess et al., 2003; Kalyn and Van Rees, 2006). Switchgrass roots <0.5 mm diameter (Ø) contributed to approximately 70% of the total root density at the

0-20 cm soil depth (An et al., 2022), where C processing actively occurred (Henneron et al., 2022), and such fine roots led to lower priming effect and greater soil C accumulation compared to coarser roots (de Graaff et al., 2013; Adkins et al., 2016). Since the biomass and length of such fine roots were found to differ among various switchgrass cultivars (de Graaff et al., 2013; Liu et al., 2016), we hypothesize that such differences can be an important cause leading to their distinct contributions to soil C processing and gains.

Roots also play a role in the formation of soil pore structure, leading to distinct size distributions and spatial locations of pores within the soil matrix (Bodner et al., 2014; Bacq-Labreuil et al., 2019; Helliwell et al., 2019; Lucas et al., 2022). That occurs both through direct impacts on arrangement of soil particles and penetration of soil aggregates, and through water extraction (Angers and Caron, 1998; Bengough et al., 2016; Oburger and Schmidt, 2016). The size of the impact varies depending on root characteristics (Mahannopkul and Jotisankasa, 2019), because roots determine the water extraction strength (Assadollahi and Nowamooz, 2020).

Pores in tens to hundreds of μm diameter (Ø) size range are especially relevant for microbial abundance and activity, and consequently, for the processing and protection of the newly added C (Strong et al., 2004; Kravchenko et al., 2019a; Franklin et al., 2021). Plants with a higher density of fine roots tend to form pore structures dominated by fine pores compared to plants with coarser roots (Bengough et al., 2016; Bodner et al., 2021). The proximity between nearest pores governs microbial accessibility to C sources located on soil particles and regulates aeration for soil microorganisms (Dungait et al., 2012; Schlüter and Vogel, 2016; Rohe et al., 2021), subsequently influencing their abundance and activity (Ekschmitt et al., 2008; Schlüter et al., 2019). The complex web of fine roots can reduce the distance between soil pores, forming such pores throughout their root area (Gyssels et al., 2005; Reubens et al., 2007).

The abundance of soil microorganisms promoted by optimal habitats with accessible supplies of C can consequently lead to soil C accumulation upon their life and death. Microbially processed organic matter can be more easily stabilized by soil mineral surfaces than that of plant-originated C compounds

(Grandy and Neff, 2008; Miltner et al., 2012). Microbial necromass also contributes significantly to C accumulation, being transformed and stabilized within the soil (Six et al., 2006; Miltner et al., 2012; Kallenbach et al., 2015; Liang et al., 2019).

Objectives of this chapter are to quantify cultivar-level variations (i) in size distributions of switchgrass roots, (ii) in size distributions of soil pores and spatial patterns of pores and particulate organic matter (POM), and (iii) to estimate the impact of roots and pores on soil microbial biomass C (MBC), and ultimately, on soil C gains. I hypothesize that differences in root sizes among switchgrass cultivars lead to differences in sizes and spatial distributions of soil pores and POM fragments and consequently different MBC and soil C contents.

3.2 Materials and Methods

3.2.1. Experimental site and plant and soil sampling

The Great Lake Bioenergy Research Center's Switchgrass Variety Experiment used in this study is located at W.K. Kellogg Biological Station (42°23'N, 85°22'W), Michigan, United States. The soil of the experimental site belongs to the Kalamazoo series (fine-loamy, mixed, active, mesic Typic Hapludalf). For several years prior to the experiment's establishment, the field was in an alfalfa-soybean-maize rotation. In 2009, 12 switchgrass cultivars were established in a randomized complete block design with plots 4.6 m × 12.2 m arranged in four replicated blocks. After the establishment year, all plots were annually fertilized with 56 kg ha^{-1} of nitrogen as dry urea (46-0-0 NPK), and annually harvested post-frost following typical practices (Sanford et al., 2016).

Four upland (Southlow, Cave-in-Rock, Blackwell, and Trailblazer) and two lowland (Alamo and Kanlow) cultivars were selected for this study. We conducted two soil sampling campaigns. First, three intact soil cores (20 cm depth and 2 cm Ø), which we will refer to as tall cores, were collected within 10 cm from crowns of three randomly selected plants in each block. These tall cores were used for root scanning. Prior to root washing and scanning the tall cores were kept at -20 °C.

Second, two intact soil cores (5 cm depth and 5 cm Ø), which will be referred to as short cores, and surrounding bulk soil were collected within 10 cm from crowns of randomly selected plants of each block. The short cores were subjected to X-ray computed micro-tomography (µCT) scanning, and the bulk soil was used for measurements of MBC and soil C. Simultaneously, a set of six short cores was collected from the reference agricultural field adjacent to the Switchgrass Variety Experiment site. The agricultural field was in chisel-plowed corn-soybean-wheat rotational cropping system. We used these samples as representative of soil characteristics prior to switchgrass establishment. All short cores were stored at 4 °C until µCT scanning.

3.2.2 Root analyses

Detailed description of the processing of the tall cores are provided in Ulbrich et al. (2021). Briefly, soils of the tall cores were wet sieved (2 mm) with Nanopure (0.2 µM) water to separate roots from soil, and all visible roots were procured with tweezers. The cleaned roots were scanned with an Epson perfection V600 scanner (Epson America Inc., Long Beach, CA, USA) in a glass scanning bed with 200 ml of Nanopure water. Scanning resolution of root images was 75 µm.

Using RhizoVision software (version 2.0.3), binary images for roots and background were obtained. Then, non-root object filtering and hole filling were conducted to remove background noise and fill unsegmented holes in root portions of images, respectively. Tools in RhizoVision allowed us to identify different size Ø of roots using distance transformation and skeletonization of the root portions (Felzenszwalb and Huttenlocher, 2012). Upon the given scanning resolution, the minimum Ø size of detectable roots was 75 µm, thereby roots classified as the 75 µm size group is assumed to represent ~75-113 µm roots, and the 150 µm size group represents ~113-187 µm roots. Root volumes for each skeletal 2D root of the different Ø groups were calculated by multiplying the length of the root by the cross-sectional area (Seethepalli et al., 2021). Subsequently, volumes were used to determine size distributions of root volume fractions (mm3) in different Ø groups per total core (root + soil) volume (mm3). Root size groups finer than 500 µm Ø were only used in further analyses as such roots, which are generally defined as fine roots, are particularly important for soil C cycling (Ruess et al., 2003; Kalyn and Van Rees, 2006; de Graaff

et al., 2013), contributing more than 70% of the total root density and 67% of the root biomass at the sampling depth of this study (Sprunger et al., 2017; An et al., 2022).

3.2.3 X-ray μCT scanning and image analyses

Soil pore characteristics were measured using short cores via X-ray μCT, a tool that allows for visualization of soil structure in its intact state (Udawatta et al., 2008; Vogel et al., 2010). Prior to X-ray μCT scanning, all short cores were brought to the matric potential of -28 kPa to ensure that >5 μm Ø pores were filled with air so easily detectable in the images. Thus, cores were first saturated for 24 hours on a water filled sand bath and then kept in a pressure chamber for two days at -28 kPa. The cores were scanned using an X-ray μCT instrument (North Star Imaging, X3000, Rogers, MN, USA) at the Horticulture Department of Michigan State University. The scanning resolution was 18 μm, achieved using the Subpix-mode of the scanner, and the projected energy level was 75 kV with 450 μA. Images from 3014 projections were reconstructed by the efX software (North Star, Rogers, MN, USA).

A schematic summary of the steps for image pre-processing and analyses is outlined in Figure 3.1. First, image pre-processing steps were conducted to remove artifacts and noise from 3D stacked soil images using ImageJ-Fiji software (Schindelin et al., 2012). In order to exclude sampling artifacts near the soil core walls, the images were cropped into 2.7 x 2.7 x 4.1 cm (1500 × 1500 × 2240 pixels) centrally located parallelograms. Then, we removed ring artifacts on the image polar domain using a stripe filter of the Xlib/Beat plugin. Finally, a 3D non-local mean filter ($\sigma = 0.1$) was applied to reduce the noise using scikit-image in Python (Darbon et al., 2008; Buades et al., 2011).

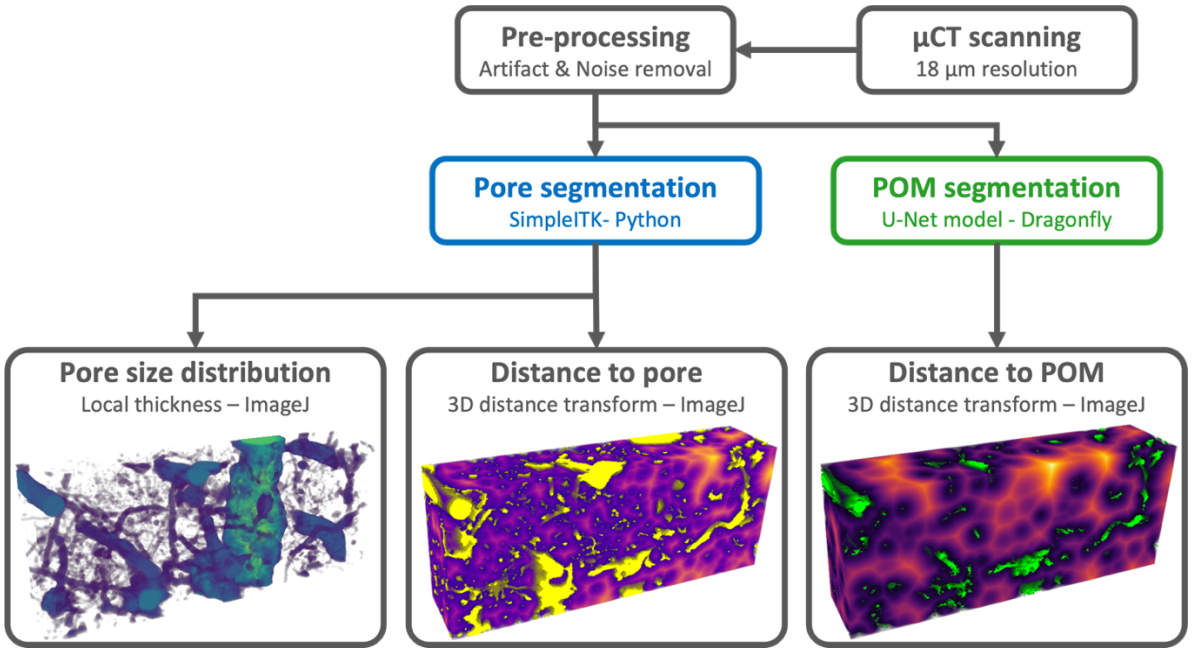

Figure 3.1. Schematic representation of the image analysis procedure. Intact soil cores were scanned with 18 µm resolution, and images were pre-processed to remove artifacts and noises. After that, soil pores and POM were segmented using SimpleITK toolkit in Python and U-Net (convolutional neural network) model in Dragonfly software, respectively. Then, distances from soil solid material to the nearest pores and to the nearest POM fragments and size distributions of the pores were analyzed using 3D distance transform and Local thickness in ImageJ, respectively. Image examples from the soil in one of switchgrass cultivars showing on the bottom left: size distributions of small pores (dark blue) and large pores (light blue); on the bottom center: locations of pores (yellow) and distances to the nearest pores ranging from minimum (dark blue) to maximum (light orange); and on the bottom right: locations of POM fragments (green) and distances to the nearest POM surfaces ranging from minimum (dark blue) to maximum (light orange).

The pre-processed grayscale images were segmented into pore and solid binary images for size distributions and spatial locations of pores. Mean threshold values for the segmentation were obtained by averaging the thresholds between pore and solid phases derived from six segmentation methods (Otsu, Triangle, Huang, ISO, Li, and Moments) using SimpleITK in Python (Beare et al., 2018; Lucas et al., 2022). The rationale for averaging thresholds is to mitigate biases of the individual methods, thus enhancing accuracy in pore threshold calculation (Schlüter et al., 2014). The resolution level and steps of image-processing applied in this study allow us to reliably identify pores larger than 36 µm Ø.

POM segmentation was carried out with a U-Net (convolutional neural network) model under the deep learning engine pre-built in Dragonfly software (Ronneberger et al., 2015; Abadi et al., 2016; Makovetsky et al., 2018). The model was trained using two cores randomly selected from each experimental block (eight of total 48 cores) for switchgrass cultivars and one of six cores from the reference agricultural

field. Seven frames with representative POM fragments in each of the selected cores were used as input, and two slices directly below and above the selected frames were also considered for generating segmentation outcomes. Then, the trained model was applied on the entire number of 54 cores. Segmented POM images were visually inspected to ensure the integrity and accuracy of the process. The outcome of POM segmentation was de-noised by removing clusters < 4 voxels from the images. Then, distances from the locations of the segmented soil solid materials to the nearest pores and from such locations to the nearest POM fragments were determined using the 'Distance Transform 3D' approach in ImageJ-Fiji (Borgefors, 1996). Size distributions of pores in 3D binary images were determined by the 'Local Thickness' approach, based on the maximum inscribed sphere method (Hildebrand and Rüegsegger, 1997; Vogel et al., 2010) in ImageJ-Fiji.

To assess the relationships between size distributions of pores and roots based on volumes at comparable scales, pore Ø sizes were grouped into interval classes as similar as possible to the calculated Ø sizes of root fractions. For example, the 75 µm size group represents the ~36-108 µm pores and the 150 µm size group – the ~108-180 µm pores, etc. Then, pore fractions of each size group were determined by dividing the segmented pore volumes (mm^3) by the total cropped soil (pore + solid) volumes (mm^3). The > 500 µm Ø pores were not quantitatively assessed in this study because of high uncertainty of their estimation in relatively small and short cores.

3.2.4 Soil microbial biomass and total carbon measurements

I measured MBC by the chloroform fumigation-incubation method (Paul et al., 1999). Two sets of 10 g soil samples were prepared by adding sufficient water to reach 50% water holding capacity. The samples were pre-incubated for five days, after which one set was fumigated with ethanol-free chloroform vapor for 24 hours, while the other set remained unfumigated. Both sets were then incubated for 10 days in the dark at 20 °C. The emitted CO_2 was measured using Infrared Photoacoustic Spectroscopy (INNOVA Air Tech Instruments, Ballerup, Denmark) in the gas circulation mode. The difference in CO_2 emissions between the fumigated and non-fumigated samples was used to calculate the MBC. For soil C analysis,

sieved and ground soil samples were analyzed using a CHNSO Elemental Analyzer (Costech Analytical Technologies, Valencia, CA, USA).

3.2.5 Statistical analysis

The differences in soil pores, root traits, MBC, and soil C contents were evaluated among six switchgrass cultivars and between two ecotypes using PROC MIXED procedure of SAS 9.4 (SAS Institute Inc., Cary, NC, USA). All statistical models for comparisons among the six cultivars included fixed effects of cultivars and random effects of experimental blocks. The models for the analyses of the distance to pore and distance to POM data additionally included the random effects of soil cores nested within the blocks. For comparisons between two ecotypes, cultivars were considered as a random factor nested within the corresponding ecotypes. Models for root and pore size distributions included fixed effects of cultivars, root/pore size groups, and their interactions and another random effect of the cores nested within the blocks and cultivars. Root/pore size groups were treated as a repeated measure factor, and cores nested within cultivars were used as an error term for testing the cultivar effect and as a subject of the repeated measurement. The statistical models for comparisons between two ecotypes were similar to those used for cultivar comparisons, except that cultivars were treated as a random effect nested within the ecotype and contributing to the error term for testing for the ecotype effect.

For all datasets, normality of the residuals and homogeneity of the residual variances were assessed by examining histograms, normal probability plots, and side-by-side box plots of the residuals, and by conducting Levene's test for variances. Residuals were found to be normally distributed in all studied variables. Since residual variances among six cultivars or between two ecotypes were not significantly different at $a = 0.1$ level in Levene's test, equal variance models were used in subsequent data analyses. Multiple comparisons among the cultivars or between the ecotypes were conducted using t-test.

A separate analysis was conducted for assessing the differences between the data from the switchgrass cultivar experimental site and the data from the adjacent reference agricultural field. Since the reference agricultural field was not a formal randomized component of the switchgrass cultivar trial, we

used Dunnett's comparison-with-control test as a conservative tool for comparing each cultivar with the reference soils.

Post-hoc power analysis was conducted to identify how many replications should have been taken to be able to detect as statistically significant differences in soil C contents among the six switchgrass cultivars (Stroup, 2002; Kravchenko and Robertson, 2011). The variance component, which was the estimate of block variance in this randomized complete block design, was estimated from the observed soil C contents. The size of the hypothesized difference used in the power analysis was 0.26% of soil C content. Then, the number of samples needed for statistical significance was calculated based on 0.05 probability of Type I error using PROC MIXED procedure in SAS.

Relationships among root and pore fractions within each individual size group, MBC, and soil C contents across all six cultivars were assessed using Pearson's correlation coefficients (r) via the PROC CORR procedure in SAS. The correlation analysis enabled us to assess the hypotheses that (1) roots of certain size groups contribute to the formation of soil pores of the same size range, (2) roots of certain size groups contribute to increases in MBC and soil C contents, and (3) pores of certain size groups contribute to increases in MBC and soil C contents. Correlations were subsequently used for path analysis.

3.2.6 Path analysis

Path analysis is a statistical approach that can infer causal relationships allowing for examination of direct and indirect effects among observed variables based on the theoretical model hypothesized by the researcher (Schumacker and Lomax, 1996; Grace, 2006). Indirect effects in path analysis are identified by estimating the relationship between two variables that is mediated by one or more intervening variables (Preacher and Hayes, 2004). Thus, we used it in this study to address hypotheses regarding relationships among root and pore traits and their direct and indirect contributions to soil MBC and C contents. Since the model for path analysis is constructed based on causal hypotheses between variables, the theoretical and empirical basis for these hypotheses should be provided by peer-reviewed literatures. Overall, we hypothesized that greater abundance of fine roots can lead to soil C gains by releasing more accessible C substrates, and by stimulating the formation of pores, which in turn supports more abundant microbial

communities and facilitates greater soil C stabilization. Detailed descriptions of the individual hypotheses, along with the literature supporting their path formulation, are provided in Table 3.1.

The PROC CALIS procedure of SAS software was used for path analysis. A two-index presentation strategy was utilized for the path analysis model evaluation (Hu and Bentler, 1999). Model fitness and adequacy were determined through a chi-square test (χ^2) and goodness of fit index (GFI) (Bentler, 1990), and acceptable models are characterized by χ^2 test p values >0.05 and GFI >0.90 (Hu and Bentler, 1999; Eisenhauer et al., 2015). The strength of the paths was indicated using standardized coefficients (β). The rationale for using standardized coefficients is to facilitate comparisons of relative impacts upon the initially incommensurable variables (Kwan and Chan, 2011).

Table 3.1. Empirical support for the hypothesized effects in path analysis.

Path from	Path to	Hypothesized effects	References
Fine root	Medium pore	Plants having greater fine roots form soil structure where pores align in size with those fine roots. Such fine-sized pores will be referred to medium pores.	Bengough et al., 2016; Bodner et al., 2021
Fine root	Distance to pore	Higher density of fine roots leads to shorter distance between soil pores by creating more intricate network of pores in soil.	Gyssels et al., 2005; Reubens et al., 2007
Fine root	Distance to POM	Higher density of fine roots leads to the shorter distance between POM by leaving their root residues throughout the soil.	Bengough et al., 2016; Bodner et al., 2021
Fine root	MBC	Plants with fine root system release more C substrates readily accessible to soil microorganisms than plants with coarse root system.	Xu & Juma, 1994; Paterson & Sim, 1999
Fine root	SOC	C substrates released by fine roots come in closer contact with soil surfaces for potential protection than plants with coarse root system.	McCully, 1999; Panchal et al., 2022
Medium pore	MBC	Greater volume of medium pores provides increases the size of optimal habitats available for soil microorganisms.	Strong et al., 2004; Franklin et el., 2021
Distance to pore	MBC	Shorter distance to pores from solid phase promotes microbial access and aeration to C sources within the phase, thereby leading to microbial abundance.	Dungait et al., 2012; Rohe et al., 2021
Distance to POM	MBC	Shorter distance to POM indicates higher proximity between soil microorganisms and C residues, which in turn promotes microbial abundance.	Raynaud and Nunan, 2014; Bickel and Or, 2023
Medium pore	SOC	Greater volumes of medium pores lead to greater organic matter processing and more channels for transits and storage of the processed C.	Quigely et al., 2018; Franklin et el., 2021
Distance to pore	SOC	Shorter distance to pores increases chances that soil surface contacts with labile C flows through pores, enhancing soil C stabilization.	Schlüter et al., 2022; Bickel and Or, 2023
Distance to POM	SOC	Shorter distance to POM contributes more to soil C accumulation, allowing easier translocation of the processed C into surrounding soil matrix.	Védère et al., 2020; Schlüter et al., 2022
MBC	SOC	Greater microbial biomass consequently leads to soil C gains through microbial decomposition products and microbial necromass.	Miltner et al., 2012; Liang et al., 2019

3.3. Results

3.3.1 Root and pore size distributions

There were significant differences in the root fraction of very fine size groups (75 and 150 µm Ø) among the studied switchgrass cultivars, while at sizes >200 µm Ø, there were no significant differences (Figure 3.2A). Specifically, Kanlow and Cave-in-Rock had the highest fraction of very fine roots, i.e., 0.0009 ±0.0001 mm^3/mm^3 in soil, followed by Southlow, Alamo, and Blackwell, while Trailblazer had the smallest fraction of very fine roots, i.e., 0.0005 ±0.0001 mm^3/mm^3 (Table 3.2).

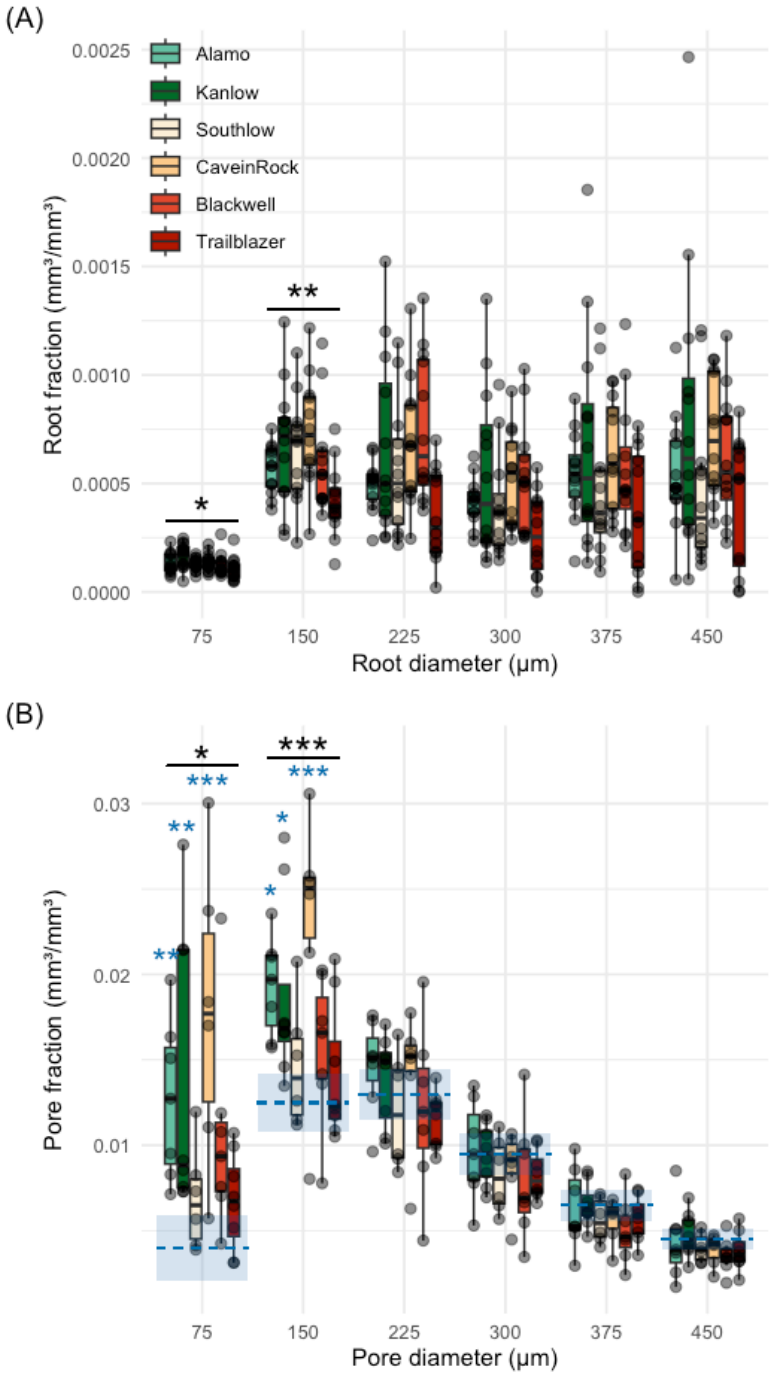

Figure 3.2. (A) Root size distribution determined from flatbed scanned images and (B) pore size distribution determined from µCT scanned images across all six studied switchgrass cultivars. Black marks *, **, and *** indicate statistical differences among cultivars with p<0.05, <0.01, and <0.001, respectively. The blue dashed lines in (B) indicate pore size distribution in the agricultural soil adjacent to this switchgrass variety experiment, assumed to be representative of the soil conditions prior to switchgrass cultivation, and shaded area indicate its 95% confidence interval. Blue marks *, **, and *** on bars indicate significant differences of individual cultivars in pore fractions compared to the agricultural soil at the p <0.05, <0.01, and <0.001 level, respectively.

Table 3.2. Mean values of root and pore fractions (mm^3/mm^3) at the two smallest root and pore size groups. The groups were referred to as 75 μm and 150 μm, which were further summed and defined as very fine roots and medium pores. The ranges of root and pore diameters representing 75 μm size group are 75-113 and 36-108 μm, respectively. The ranges of root and pore diameters representing 150 μm size group are 113-187 and 108-180 μm, respectively.

		Root fraction (mm^3/mm^3)							
Size group	Range of diameters (μm)	Cultivars						Ecotypes	
		Alamo	Kanlow	Southlow	CaveinRock	Blackwell	Trailblazer	Lowland	Upland
75	75-113	0.00014^{BC}	0.00017^{A}	0.00013^{BC}	0.00014^{B}	0.00012^{BC}	0.00011^{C}	0.00016^{A}	0.00013^{B}
150	113-187	0.00057^{B}	0.00073^{A}	0.00066^{AB}	0.00074^{A}	0.00055^{BC}	0.00042^{C}	0.00065^{A}	0.00059^{A}
Very fine root (75+150)	75-187	0.00071^{AB}	0.00090^{A}	0.00079^{AB}	0.00088^{A}	0.00067^{B}	0.00053^{C}	0.00081^{A}	0.00072^{B}
		Pore fraction (mm^3/mm^3)							
		Alamo	Kanlow	Southlow	CaveinRock	Blackwell	Trailblazer	Lowland	Upland
75	36-108	0.0123^{B}	0.0138^{AB}	0.0062^{C}	0.0159^{A}	0.0106^{B}	0.0067^{C}	0.0131^{A}	0.0098^{B}
150	108-180	0.0194^{AB}	0.0190^{AB}	0.0150^{C}	0.0205^{A}	0.0159^{BC}	0.0141^{C}	0.0192^{A}	0.0164^{B}
Medium pore (75+150)	36-180	0.0317^{A}	0.0328^{A}	0.0212^{B}	0.0364^{A}	0.0265^{B}	0.0208^{B}	0.0323^{A}	0.0262^{B}

Note: different letters within each size group mark significant differences (p <0.05) among six cultivars (Root fraction: n = 12 and pore fraction: n = 8) or between two ecotypes.

Consistent with the root size results, soil pore fractions in medium size groups (75 and 150 µm Ø) also significantly differed among the cultivars (Figure 3.2B) and, likewise, no differences were observed among cultivars in coarse (>200 µm Ø) pore size groups (Figure 3.3B). Soil under Cave-in-Rock had the greatest fraction of medium pores, i.e., 0.04 ±0.006 mm^3/mm^3 in soil, followed by Kanlow, Alamo, and Blackwell, with Southlow and Trailblazer having the smallest fractions with 0.02 ±0.005 mm^3/mm^3 (Table 3.2). The fractions of 75 and 150 µm pores in soils under Alamo, Kanlow, and Cave-in-Rock were, respectively, ~70 % and ~35 % greater than those of the adjacent reference agricultural soil (Figure 3.2B).

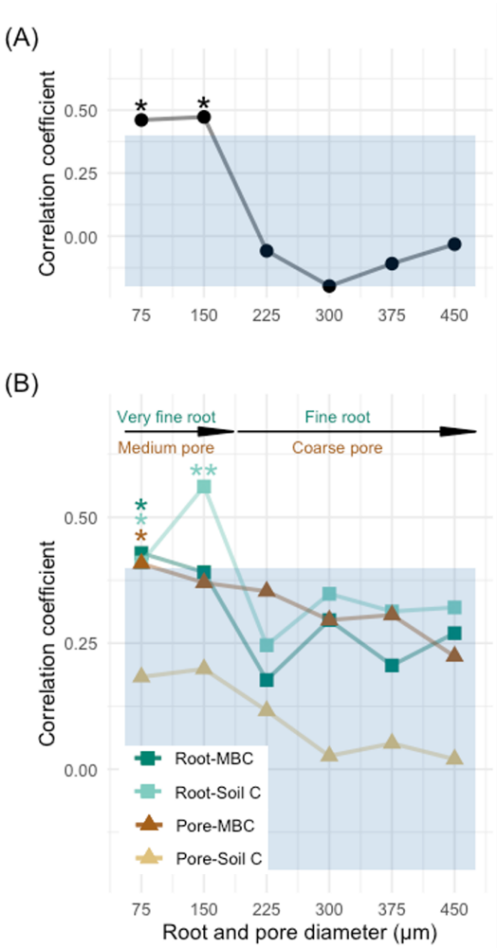

Figure 3.3. (A) Correlation coefficients between root and pore fractions within each size group, and (B) correlation coefficients between root fractions of each size and contents of MBC (Root-MBC) and soil C contents (Root-Soil C) and between pore fractions of each size class and MBC (Pore-MBC) and soil C contents (Pore-Soil C) across switchgrass cultivars. Roots and pores finer than 200 µm diameter were defined as very fine root and medium pore, and coarser than such diameter were as fine root and coarse pore, respectively. Blue shaded area denotes the range of correlation coefficients that are not significantly different from zero (p >0.05). Marks * and ** placed next to and on corresponding coefficient values indicate the significance of the correlation at p <0.05 and <0.01 level, respectively.

Root fractions in very fine size groups were significantly positively associated with pore fractions of medium size groups (r^2 = 0.21 in 75 μm and 0.22 in 150 μm Ø size group, respectively; p <0.05 in both size groups), while no significant correlations were observed between roots and pores of any other size groups (Figure 3.3A).

3.2.2 Distance to pores and POM

The average distance to pores was the largest in the soil under the Trailblazer cultivar, equal to 0.34 ±0.08 mm, while soils under the other five cultivars had similar distances to pores of 0.19 mm on average (Figure 3.4A). The distances under the five cultivars were also similar to that under the adjacent reference agricultural field. Overall, distances to pores in the soils under upland ecotype cultivars were 34% greater than those of lowland ecotype cultivars.

The average distance to POM fragments was also the largest in the soil under Trailblazer, i.e., 0.82 ±0.12 mm, while Cave-in-Rock and two lowland cultivars, Alamo and Kanlow, had the lowest distances to POM of 0.54 ±0.17, 0.62 ±0.14, and 0.60 ±0.12 mm, respectively (Figure 3.4B). The distance to POM in the reference agricultural field was similar to that in the soils under all studied switchgrass cultivars except for Trailblazer. Overall, there were no statistically significant differences in distances to POM between upland and lowland cultivars (Figure 3.4B).

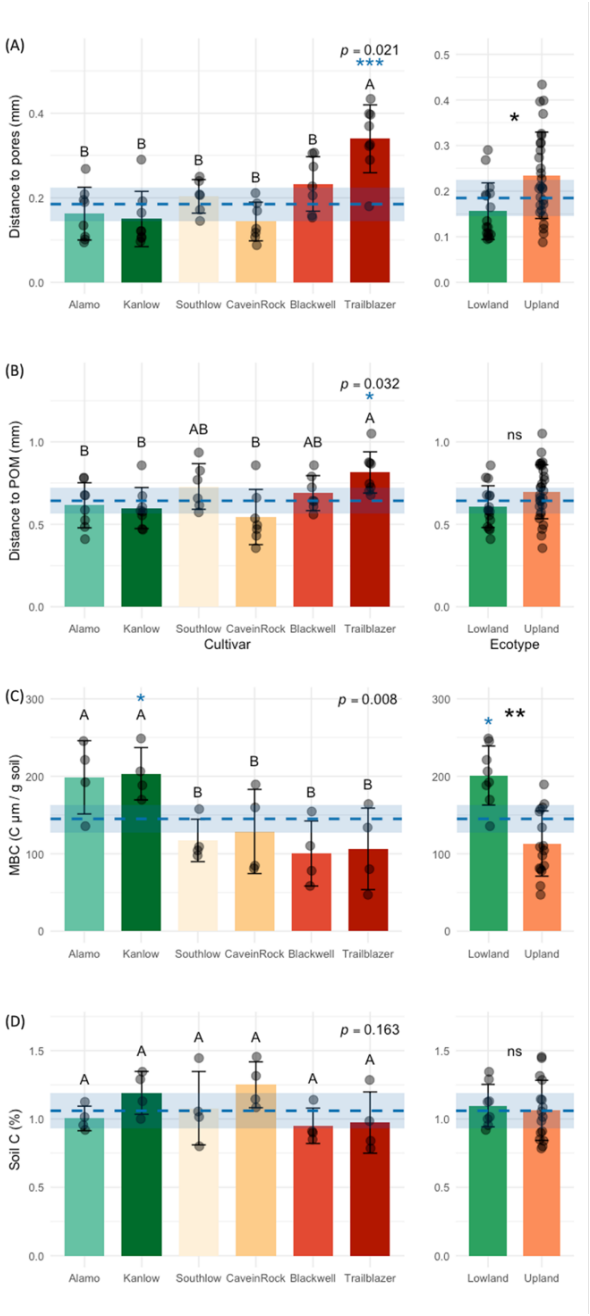

Figure 3.4. (A) Microbial biomass C (MBC), (B) soil C contents, (C) distance to pores, and (D) distance to POM of six switchgrass cultivars individually and grouped by two ecotypes. Error bars represent standard deviation, and dots represent individual data points. Different letters indicate significant differences at p <0.05 among six cultivars (MBC and soil C: n = 4 and distance to pores and POM: n = 8). Since difference in soil C contents was not statistically significant (p >0.05), letters on the bars were same across the cultivars. Letter 'ns' indicates no significant difference between two ecotypes, and black marks * and ** indicate significant differences with p <0.05 and <0.01, respectively. The blue dashed lines mark the average values of MBC, soil C, and the distance to pores and POM in the agricultural soil adjacent to this switchgrass variety experiment, assumed to be representative of the conditions prior to switchgrass cultivation, and shaded area indicate their 95% confidence intervals. Blue marks * and *** on bars indicate significant differences of individual cultivars and ecotypes in MBC and the distances compared to the agricultural soil at the p <0.05 and <0.001 level, respectively.

3.3.3 Soil microbial biomass and carbon

MBC in the soils under Alamo and Kanlow, the two lowland switchgrass cultivars, was ~50-100% higher than under the other four cultivars; in particular MBC under Kanlow was 29% higher than that in the adjacent reference agricultural field (Figure 3.4C). MBC in soils under the cultivars of the lowland ecotype was 44% and 29% higher than that of the upland cultivars and the reference agricultural field, respectively. On the other hand, soil C contents of the cultivars were not different either from each other or from that of the reference agricultural soil (Figure 3.4D). The difference in the C contents between the two ecotypes was also not significant and not different from that in the reference agricultural soil.

MBC across all six cultivars was positively associated with 75 μm Ø roots (r^2 = 0.19; p <0.05) and with 75 μm Ø pores (r^2 = 0.17; p <0.05), while MBC was not correlated with any other size groups of roots and pores >75 μm Ø (Figure 3.3B). MBC was negatively associated with the distance to pores (r^2 = 0.13; p <0.05), whereas not associated with the distance to POM fragments (Table 3.3). Soil C was also positively associated with 75 and 150 μm Ø roots (r^2 = 0.17 and 0.31; p <0.05 and 0.01, respectively), while no significant correlations were observed with any size groups of pores (Figure 3.3B). Soil C was negatively associated with the distance to POM fragments (r^2 = 0.18; p <0.05), whereas not associated with the distance to pores (Table 3.3). Notably, soil C was positively associated with MBC across all six cultivars (r^2 = 0.18; p <0.05).

Table 3.3. Correlation coefficients among very-fine roots, medium pores, distance (Dist.) to pore and POM, microbial biomass C (MBC), and soil C contents across six switchgrass, two lowland, and four upland cultivars.

		Very fine root	Medium pore	Dist. to pore	Dist. to POM	MBC	SOC
All cultivars (n=24)	Very fine root						
	Medium pore	**0.41***					
	Dist. to pore	**-0.49***	**-0.60****				
	Dist. to POM	**-0.52****	**-0.59****	**0.55****			
	MBC	**0.43***	**0.37***	**-0.36***	-0.20		
	Soil C	**0.65*****	0.19	-0.33	**-0.43***	**0.43***	
Lowland cultivars (n=8)	Very fine root						
	Medium pore	0.01					
	Dist. to pore	-0.02	-0.07				
	Dist. to POM	0.20	**-0.88****	-0.02			
	MBC	0.01	-0.14	**-0.83****	0.04		
	Soil C	**0.86****	0.19	0.36	-0.08	0.37	
Upland cultivars (n=16)	Very fine root						
	Medium pore	**0.45***					
	Dist. to pore	**-0.53***	**-0.61****				
	Dist. to POM	**-0.65****	**-0.49***	**0.57***			
	MBC	**0.48***	0.26	-0.12	-0.01		
	Soil C	**0.60****	0.17	**-0.45***	**-0.49***	**0.59****	

Note: Bolded values indicate statistical significances at $p < 0.05$, and the marked *, **, and ** denote coefficient levels at the $p < 0.05$, <0.01, and < 0.001 level, respectively.

3.3.4 Path analysis

The very fine roots (sum of 75 and 150 µm Ø size groups) had a direct positive impact on the fraction of medium pores (sum of 75 and 150 µm Ø size groups) (β = 0.41; p <0.01), MBC (β = 0.41; p <0.01), and soil C contents (β = 0.50; p <0.001), and negative impact on the distance to pores (β = -0.47; p <0.01) and POM (β = -0.52; p <0.001) (Figure 3.5). Additionally, such roots indirectly influenced MBC by increasing the fraction of medium pores (β = 0.19; p <0.05) and by decreasing the distances to pores (β = -0.28; p <0.05) and POM (β = -0.19; p <0.05). Soil C contents increased by a shorter distance to POM (β = -0.21; p <0.05), while neither the fraction of medium pores nor the distance to pores appeared to directly influence soil C. Yet, increases in medium pore fractions and decreases in distances to pores and POM indirectly fostered increases in soil C due to the rise in MBC (β = 0.30; p <0.05) (Figure 3.5).

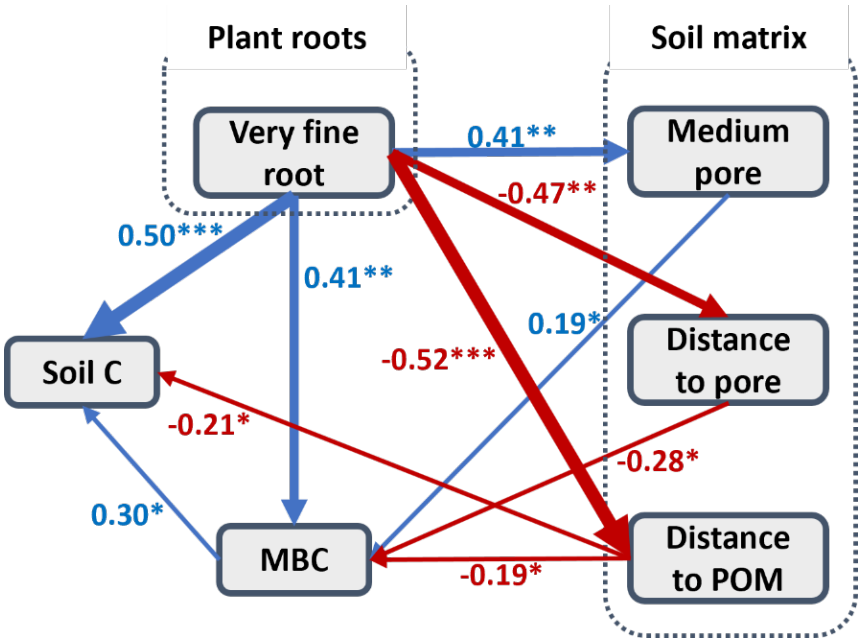

Figure 3.5. The outcome of the path analysis enumerating direct and indirect effects of very fine roots (sum of 75 and 150 µm Ø root fraction groups) on soil C contents through medium pores (sum of 75 and 150 µm Ø pore fraction groups), distance to pore and POM, and microbial biomass C (MBC) across six switchgrass cultivars. Numbers alongside arrows indicate standardized path coefficients. Blue and red arrows denote positive and negative relationships between variables, respectively, and thickness of arrows denote the significance of paths (marked *, **, and *** denote standardized coefficient levels at the p <0.05, <0.01, and <0.001 level, respectively). Non-significant paths are not shown in this figure.

3.4 Discussion

After seven years of continuous growth, variations were observed among the six switchgrass cultivars in volumes of very fine roots and of medium soil pores. Cultivars with a greater volume of very fine roots stimulated formation of medium soil pores compared to the cultivars with coarser root systems and led to a more ubiquitous spread of pores and POM within the soil matrix. Volumes of very fine roots were strongly positively associated with soil C and MBC. Abundance of the medium pores and spatial distribution patterns of the pore space were directly related to MBC, but not to soil C. While the cultivars of the lowland switchgrass ecotype increased soil MBC compared to that in the adjacent reference row crop agricultural soil, under none of the studied cultivars did soil C exceed that of the reference agriculture soil.

3.4.1 Influence of very fine roots

The abundance of very fine roots (<200 µm Ø) was the influential factor for microbial biomass and soil C (Figure 3.5). The very fine roots also indirectly affected them by contributing to volumes of medium (50-200 µm Ø) pores and spatial patterns in both pores and POM, the latter expressed via distances to pores and POM (Figure 3.5). Fine roots typically provide greater amounts of root exudates and rhizodeposits to soil (Xu and Juma, 1994; Paterson and Sim, 1999; Zhang et al., 2022). Such labile C sources as well as fine roots themselves can be preferentially used by soil microorganisms and contribute significantly to soil organic matter formation through their rapid turnover and subsequent decomposition (Ruess et al., 2003; Kalyn and Van Rees, 2006). While in the past many studies focused on a broadly defined size group of fine roots as those <1.0-2.5 mm Ø (Steinaker and Wilson, 2008; de Graaff et al., 2013; Sprunger et al., 2017; Sehgal et al., 2021), findings from our study indicate that in monoculture switchgrass systems, it is only the roots <200 µm Ø, i.e., very fine roots, that are particularly influential in promoting microbial biomass and concomitant soil C production (Figure 3.3 and 3.5).

Consistent with a meta-analysis demonstrating that phylogenetic characteristics can be the largest driver of root traits (Valverde-Barrantes et al., 2017), we found intraspecific variations in root size distributions among switchgrass cultivars, although primarily in the volumes of the very fine roots (Figure 3.2A). Earlier studies have shown that lowland cultivars such as Kanlow and Alamo tend to have more

extensive root systems than upland cultivars, whereas the latter tend to possess thicker root systems (de Graaff et al., 2013; Fike and Parrish, 2013; Ulbrich et al., 2021). We also found a greater volume of very fine roots in lowland than in the upland cultivars (Figure 3.2A and Table 3.2). A single exception was Cave-in-Rock, the upland cultivar with a volume of very fine roots comparable to that of lowland cultivars (Figure 3.2A and Table 3.2). Cave-in-Rock exceeds other upland cultivars in photosynthesis rates and biomass production (Ma et al., 2011; An et al., 2018), and its root biomass within the top 15 cm of soil has been reported to exceed that of Kanlow and Alamo (Ma et al., 2000). Moreover, Cave-in-Rock, as a relatively drought-sensitive cultivar, possibly extends its fine roots more aggressively to promote soil water access, thereby navigating this environmental challenge with its fine roots (McCully, 1999; Liu et al., 2015; Fort and Freschet, 2020).

These differences in very fine roots among our cultivars led to differences in formation of soil pores and different spatial distribution of the pores and POM through the soil matrix (Figure 3.2B, 3.4A, 3.4B, and 3.5). Root diameter can significantly influence a root's capacity to penetrate soil (Chimungu et al., 2015; Paez-Garcia et al., 2015), and differences in this trait are known to result in distinct pore structures, with prevalence of certain pore size classes (Bodner et al., 2014, 2021). Positive correlations between very fine roots and medium pores among six switchgrass cultivars support the notion that cultivars with greater volumes of very fine roots form greater volumes of medium pores (Figure 3.3A). Lowland cultivars possibly lead to the formation of more intricate soil pore networks through their fine roots (Gyssels et al., 2005; Reubens et al., 2007), and thus distances between individual pores are shorter than for those of upland cultivars (Figure 3.4A).

Roots are the major source of soil POM, thus shorter distances between the nearest POM fragments in soils under Kanlow and Cave-in-Rock (Figure 3.4B), which were the two cultivars with the greatest volumes of very fine roots (Figure 3.2A and Table 3.2), presumably resulted from a more uniform spread of root residues throughout the soil (Bengough et al., 2016; Bodner et al., 2021). Indeed, a significantly shorter distance was found in soils under prairie vegetation, which was known to have extensive root systems (Sprunger et al., 2017), compared to that under switchgrass (Cave-in-Rock) in a field adjacent to

this study (Figure 3.6). Negative correlations between volumes of very fine roots and distances to pores and POM further support this conclusion (Table 3.3).

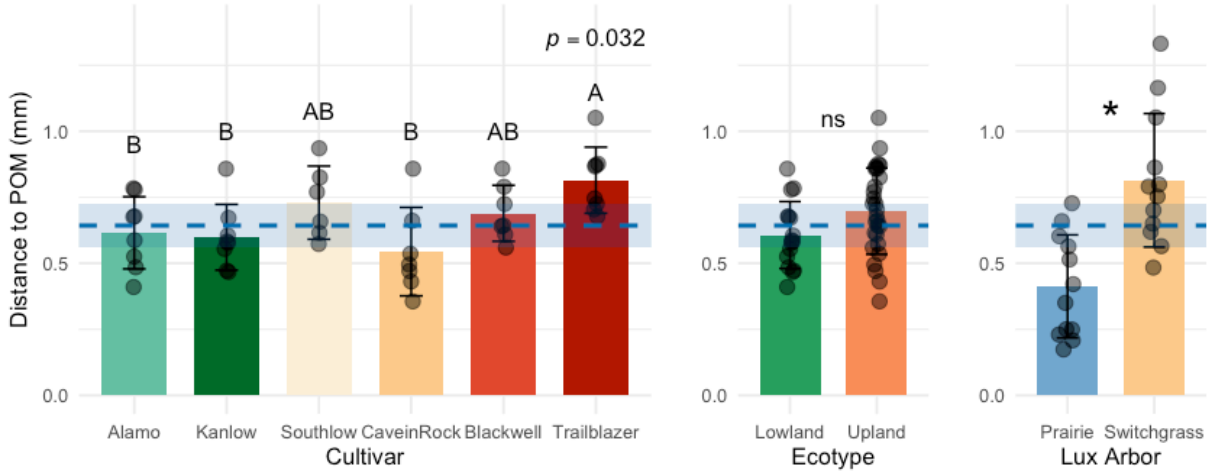

Figure 3.6. Distance to POM of six switchgrass cultivars individually, grouped by ecotypes, and taken by two vegetation of a former observation in the adjacent region (Lux Arbor, Michigan, USA) with soils classified as the same soil taxonomy and texture (Lee et al., 2023). The switchgrass cultivar in the former observation was Cave-in-Rock, and prairie vegetation included switchgrass as one of 18-species mixture. Error bars represent standard deviation, and dots represent individual data points. Different letters indicate significant differences at $p<0.05$ among six cultivars (n = 8), letter 'ns' indicates no significant difference between two ecotypes, and marks * indicate significant differences with $p<0.05$ between two vegetation in Lux Arbor site (n = 12). The blue dashed lines mark the average values of the distance to POM in the agricultural soil adjacent to this switchgrass variety experiment, assumed to be representative of the conditions prior to switchgrass cultivation, and shaded area indicate their 95% confidence intervals.

3.4.2 Influence of medium pores and their spatial distribution

My results demonstrate that medium pores and distances to pores did not directly impact measured soil C gains, even though they promoted soil microbial biomass, which was positively associated with soil C (Figure 3.5 and Table 3.3). This is consistent with a direct effect of medium pores on MBC and an indirect effect of such pores on soil C gains that were recently observed in monoculture switchgrass (Cave-in-Rock) cultivated across a wide range of low fertility soils of the U.S. Midwest (Lee et al., 2023). However, even though switchgrass cultivation greatly increased the proportion of medium pores as compared to the reference agricultural soil (Figure 3.2B), such increases did not translate into measured soil C gains (Figure 3.4D).

Pores in 30-180 μm Ø, which is very close to the range of medium pores in this study, are suggested as optimal microbial habitats (Kravchenko et al., 2019b), since such pores facilitate high microbial activity

by ensuring oxygen and water flows, while allowing for easy access to organic matter (Rawlins et al., 2016; Keiluweit et al., 2018). Since pores of this size range were also identified as the primary sites for rhizodeposition (Quigley and Kravchenko, 2022), the abundance of such pores likely facilitated the microbial growth in the soils under Kanlow and Alamo cultivars (Figures 3.2B and 3.4C).

Another two key links between very fine roots and microbial biomass were the distances from soil solid materials to the nearest pores and to the nearest POM fragments (Figure 3.5). The shorter distances to pores and POM likely benefited microbial habitats, because such distances imply closer proximity of microbes to water, oxygen, and C sources (Raynaud and Nunan, 2014; Rohe et al., 2021; Bickel and Or, 2023). Therefore, we can surmise that the indirect contribution of the extensive root systems in the two lowland cultivars as well as in Cave-in-Rock (Figure 3.2A) to increases in soil microbial biomass stemmed from decreasing distances to pores and POM (Figures 3.4A and 3.4B). Shorter distances to POM can allow easier translocation of the processed C during POM decomposition into surrounding soil (Védère et al., 2020; Schlüter et al., 2022), likely contributing to soil C gains (Figure 3.5).

3.4.3 Negligible soil C gains in switchgrass cropping systems

Neither the two lowland cultivars nor Cave-in-Rock, the cultivars that promoted several of the hypothesized drivers of soil C gains, including greater volumes of very fine roots and medium pores, higher MBC, and shorter distances to POM and pores (Figure 3.5 and Table 3.3), led to measurably greater soil C gains than other cultivars in this study (Figure 3.4D). Our results add to a substantial body of research reporting very slow to negligible soil C gains in monoculture switchgrass systems (Garten Jr. and Wullschleger, 2000; Liebig et al., 2005; Bates et al., 2022). In fact, a recent long-term study of switchgrass, conducted in a field adjacent to this experiment, also observed that switchgrass did not much increase soil C contents (~0.06 Mg C ha^{-1} yr^{-1}) (Perry et al., 2023). Another recent study, conducted in the same experimental site, showed that nine different switchgrass cultivars continuously grown for seven years had no significant impact on soil C contents (Mosier et al., 2024).

There is an apparent discrepancy between the lack of the detected increases in soil C contents and the implications of path analysis suggestions that such increases should have taken place, at least in the

cultivars with finer root systems (Figure. 3.5). I believe the discrepancy is due to lower statistical power of the experimental work, i.e., the attempts to detect relatively small changes in these soils C gains, given high variability, have been hampered by relatively small sample size. Note that the 4 replicated blocks, i.e., *n* of 4, of the current experiment is a common practice ubiquitously followed in field experimentation. Yet, *post-hoc* power analysis of the soil C data in this study suggests that at least three more replicated blocks, i.e., *n* of 7, would be required for detecting a significant difference with the power of 75%, and six more blocks, i.e., *n* of 10, with the power > 90% (Table 3.4). In other words, the nuanced relationship between switchgrass cultivars and C gains, as revealed by the path analysis with multifaceted factors, emphasizes the need to examine soil C gains with a greater number of replications to better test the effects of switchgrass cultivars on soil C. Alternatively, as these switchgrass stands mature and cultivars continue to differentially accumulate soil C, differences should become evident with fewer replicates in next few years. Expanding the replication size, as suggested by the power analysis, will also be important for better parameterizing process-level models that, like our path analysis, also predict significant soil C gains under long-term switchgrass cultivation (McLaughlin et al., 2002; McLaughlin and Adams Kszos, 2005; Martinez-Feria and Basso, 2020).

Table 3.4. Probability (power) of detecting statistically significant results at $\alpha = 0.05$ in the comparison of soil C contents among six switchgrass cultivars and the required number of replicated blocks under randomized complete block design.

Number of replicated blocks	*P* value	Power (%)
5	0.115	56.4
6	0.065	66.8
7	**0.035**	75.2
8	**0.018**	82.3
9	**0.009**	88.6
10	**0.003**	**94.4**

Note: The estimate of the variance was 0.046. Bolded values indicate statistical significances at $p < 0.05$ and the detecting probability > 90% for statistical differences.

3.5 Conclusions

This chapter elucidates complex yet pivotal relationships among root traits, soil pore structure, and microbial biomass for the potential accumulation of soil C using six switchgrass cultivars with different root traits, representing two distinct ecotypes. Results suggest that switchgrass cultivars with greater volumes of very fine roots have a greater capacity for soil C accumulation, mediated by increases in medium pores and decreases in distances to pore and POM that affect concomitant increases in MBC. However, seven years was insufficient to document measurable differences in soil C gains among cultivars. Overall, this study provides critical insights for the relative impacts of root traits and pore structure for soil C gains in bioenergy crop cultivation.

3.6 Acknowledgements

I thank Michelle Quigley for conducting X-ray μCT scanning and Maxwell Oerther for assistance with sample collection. Support for this research was provided by the Great Lakes Bioenergy Research Center, U.S. Department of Energy, Office of Science, Office of Biological and Environmental Research (Award DE-SC0018409), by the National Science Foundation Long-term Ecological Research Program (DEB 2224712) at the Kellogg Biological Station, and by Michigan State University AgBioResearch.

REFERENCES

Abadi, M., Barham, P., Chen, J., Chen, Z., Davis, A., Dean, J., Devin, M., Ghemawat, S., Irving, G., Isard, M., Kudlur, M., Levenberg, J., Monga, R., Moore, S., Murray, D.G., Steiner, B., Tucker, P., Vasudevan, V., Warden, P., Wicke, M., Yu, Y., and Zheng, X. (2016). TensorFlow: A System for Large-Scale Machine Learning. *Presented at the 12th USENIX Symposium on Operating Systems Design and Implementation* (OSDI 16), pp. 265–283.

Adkins, J., Jastrow, J.D., Morris, G.P., Six, J., and de Graaff, M.-A. (2016). Effects of switchgrass cultivars and intraspecific differences in root structure on soil carbon inputs and accumulation. *Geoderma* 262, 147–154. doi:10.1016/j.geoderma.2015.08.019

Adler, P.R., Grosso, S.J.D., and Parton, W.J. (2007). Life-Cycle Assessment of Net Greenhouse-Gas Flux for Bioenergy Cropping Systems. *Ecological Applications* 17, 675–691. doi:10.1890/05-2018

An, Q.-Q., Wang, S.-Q., Kang, J.-Y., Wang, Z., Chen, Y.-L., and Xu, B.-C. (2022). Fine root distribution and morphological characteristics of switchgrass under different row spacings on semi-arid Loess Plateau, China. *Archives of Agronomy and Soil Science* 68, 1–17. doi:10.1080/03650340.2020.1820490

An, Y., Gao, Y., and Ma, Y. (2018). Growth performance and weed control effect in response to nitrogen supply for switchgrass after establishment in the semiarid environment. *Field Crops Research* 221, 175–181. doi:10.1016/j.fcr.2018.02.032

An, Y., Ma, Y., and Shui, J. (2013). Switchgrass root exudates have allelopathic potential on lettuce germination and seedling growth. Acta Agriculturae Scandinavica, *Section B — Soil & Plant Science* 63, 497–505. doi:10.1080/09064710.2013.810770

Angers, D.A. and Caron, J. (1998). Plant-induced Changes in Soil Structure: *Processes and Feedbacks. Biogeochemistry* 42, 55–72. doi:10.1023/A:1005944025343

Assadollahi, H. and Nowamooz, H. (2020). Long-term analysis of the shrinkage and swelling of clayey soils in a climate change context by numerical modelling and field monitoring. *Computers and Geotechnics* 127, 103763. doi:10.1016/j.compgeo.2020.103763

Bacq-Labreuil, A., Crawford, J., Mooney, S.J., Neal, A.L., and Ritz, K. (2019). Cover crop species have contrasting influence upon soil structural genesis and microbial community phenotype. *Scientific Reports* 9, 7473. doi:10.1038/s41598-019-43937-6

Bates, C.T., Escalas, A., Kuang, J., Hale, L., Wang, Y., Herman, D., Nuccio, E.E., Wan, X., Bhattacharyya, A., Fu, Y., Tian, R., Wang, G., Ning, D., Yang, Y., Wu, L., Pett-Ridge, J., Saha, M., Craven, K., Brodie, E.L., Firestone, M., and Zhou, J. (2022). Conversion of marginal land into switchgrass conditionally accrues soil carbon but reduces methane consumption. *The ISME Journal* 16, 10–25. doi:10.1038/s41396-021-00916-y

Beare, R., Lowekamp, B., and Yaniv, Z. (2018). Image Segmentation, Registration and Characterization in R with SimpleITK. *Journal of Statistical Software* 86, 8. doi:10.18637/jss.v086.i08

Bengough, A.G., Loades, K., and McKenzie, B.M. (2016). Root hairs aid soil penetration by anchoring the root surface to pore walls. *Journal of Experimental Botany* 67, 1071–1078. doi:10.1093/jxb/erv560

Bentler, P.M. (1990). Comparative fit indexes in structural models. *Psychological Bulletin* 107, 238–246. doi:10.1037/0033-2909.107.2.238

Beschoren da Costa, P., Benucci, G.M.N., Chou, M.-Y., Van Wyk, J., Chretien, M., and Bonito, G. (2022). Soil Origin and Plant Genotype Modulate Switchgrass Aboveground Productivity and Root Microbiome Assembly. *mBio* 13, e00079-22. doi:10.1128/mbio.00079-22

Bickel, S. and Or, D. (2023). Aqueous habitats and carbon inputs shape the microscale geography and interaction ranges of soil bacteria. *Communications Biology* 6, 1–10. doi:10.1038/s42003-023-04703-7

Bodner, G., Leitner, D., and Kaul, H.-P. (2014). Coarse and fine root plants affect pore size distributions differently. *Plant and Soil* 380, 133–151. doi:10.1007/s11104-014-2079-8

Bodner, G., Mentler, A., and Keiblinger, K. (2021). Plant Roots for Sustainable Soil Structure Management in Cropping Systems, in: The Root Systems in Sustainable Agricultural Intensification. John Wiley & Sons, Ltd, pp. 45–90. doi:10.1002/9781119525417.ch3

Borgefors, G. (1996). On Digital Distance Transforms in Three Dimensions. *Computer Vision and Image Understanding* 64, 368–376. doi:10.1006/cviu.1996.0065

Buades, A., Coll, B., and Morel, J.-M. (2011). Non-Local Means Denoising. *Image Processing On Line* 1, 208–212. doi:10.5201/ipol.2011.bcm_nlm

Casler, M.D., Vogel, K.P., Taliaferro, C.M., Ehlke, N.J., Berdahl, J.D., Brummer, E.C., Kallenbach, R.L., West, C.P., and Mitchell, R.B. (2007). Latitudinal and Longitudinal Adaptation of Switchgrass Populations. *Crop Science* 47, 2249–2260. doi:10.2135/cropsci2006.12.0780

Casler, M.D., Vogel, K.P., Taliaferro, C.M., and Wynia, R.L. (2004). Latitudinal Adaptation of Switchgrass Populations. *Crop Science* 44, 293–303. doi:10.2135/cropsci2004.2930

Chimungu, J.G., Loades, K.W., and Lynch, J.P. (2015). Root anatomical phenes predict root penetration ability and biomechanical properties in maize (Zea Mays). *Journal of Experimental Botany* 66, 3151–3162. doi:10.1093/jxb/erv121

Darbon, J., Cunha, A., Chan, T.F., Osher, S., and Jensen, G.J. (2008). Fast nonlocal filtering applied to electron cryomicroscopy, in: 2008 5th IEEE International Symposium on Biomedical Imaging: From Nano to Macro. *Presented at the 2008 5th IEEE International Symposium on Biomedical Imaging* (ISBI 2008), IEEE, Paris, France, pp. 1331–1334. doi:10.1109/ISBI.2008.4541250

de Graaff, M.-A., Six, J., Jastrow, J.D., Schadt, C.W., and Wullschleger, S.D. (2013). Variation in root architecture among switchgrass cultivars impacts root decomposition rates. *Soil Biology and Biochemistry* 58, 198–206. doi:10.1016/j.soilbio.2012.11.015

Dungait, J.A.J., Hopkins, D.W., Gregory, A.S., and Whitmore, A.P. (2012). Soil organic matter turnover is governed by accessibility not recalcitrance. *Global Change Biology* 18, 1781–1796. doi:10.1111/j.1365-2486.2012.02665.x

Eisenhauer, N., Bowker, M.A., Grace, J.B., and Powell, J.R. (2015). From patterns to causal understanding: Structural equation modeling (SEM) in soil ecology. *Pedobiologia* 58, 65–72. doi:10.1016/j.pedobi.2015.03.002

Ekschmitt, K., Kandeler, E., Poll, C., Brune, A., Buscot, F., Friedrich, M., Gleixner, G., Hartmann, A., Kästner, M., Marhan, S., Miltner, A., Scheu, S., and Wolters, V. (2008). Soil-carbon preservation through habitat constraints and biological limitations on decomposer activity. *Journal of Plant Nutrition and Soil Science* 171, 27–35. doi:10.1002/jpln.200700051

Emmett, B.D., Youngblut, N.D., Buckley, D.H., and Drinkwater, L.E. (2017). Plant Phylogeny and Life History Shape Rhizosphere Bacterial Microbiome of Summer Annuals in an Agricultural Field. *Frontiers in Microbiology* 8.

Felzenszwalb, P.F. and Huttenlocher, D.P. (2012). Distance Transforms of Sampled Functions. *Theory of Computing* 8, 415–428. doi:10.4086/toc.2012.v008a019

Fike, J.H. and Parrish, D.J. (2013). Switchgrass. Biofuel Crops: Production, Physiology and Genetics, *CABI Books* 199–230. doi:10.1079/9781845938857.0199

Fort, F. and Freschet, G.T. (2020). Plant ecological indicator values as predictors of fine-root trait variations. *Journal of Ecology* 108, 1565–1577. doi:10.1111/1365-2745.13368

Franklin, S.M., Kravchenko, A.N., Vargas, R., Vasilas, B., Fuhrmann, J.J., and Jin, Y. (2021). The unexplored role of preferential flow in soil carbon dynamics. *Soil Biology and Biochemistry* 161, 108398. doi:10.1016/j.soilbio.2021.108398

Garten Jr., C.T. and Wullschleger, S.D. (2000). Soil Carbon Dynamics beneath Switchgrass as Indicated by Stable Isotope Analysis. *Journal of Environmental Quality* 29, 645–653. doi:10.2134/jeq2000.00472425002900020036x

Grace, J.B. (2006). Structural Equation Modeling and Natural Systems. Cambridge University Press, Cambridge. doi:10.1017/CBO9780511617799

Grandy, A.S. and Neff, J.C. (2008). Molecular C dynamics downstream: The biochemical decomposition sequence and its impact on soil organic matter structure and function. Science of The Total Environment, BIOGEOCHEMISTRY OF FORESTED ECOSYSTEM - Selected papers from BIOGEOMON, the 5th International Symposium on Ecosystem Behaviour, held at the University of California, Santa Cruz, on June 25–30, 2006 404, 297–307. doi:10.1016/j.scitotenv.2007.11.013

Gyssels, G., Poesen, J., Bochet, E., and Li, Y. (2005). Impact of plant roots on the resistance of soils to erosion by water: a review. Progress in Physical Geography: *Earth and Environment* 29, 189–217. doi:10.1191/0309133305pp443ra

Haque, M., Epplin, F.M., and Taliaferro, C.M. (2009). Nitrogen and Harvest Frequency Effect on Yield and Cost for Four Perennial Grasses. *Agronomy Journal* 101, 1463–1469. doi:10.2134/agronj2009.0193

Helliwell, J.R., Sturrock, C.J., Miller, A.J., Whalley, W.R., and Mooney, S.J. (2019). The role of plant species and soil condition in the structural development of the rhizosphere. *Plant, Cell & Environment* 42, 1974–1986. doi:10.1111/pce.13529

Henneron, L., Balesdent, J., Alvarez, G., Barré, P., Baudin, F., Basile-Doelsch, I., Cécillon, L., Fernandez-Martinez, A., Hatté, C., and Fontaine, S. (2022). Bioenergetic control of soil carbon dynamics across depth. *Nature Communications* 13, 7676. doi:10.1038/s41467-022-34951-w

Hildebrand, T. and Rüegsegger, P. (1997). A new method for the model-independent assessment of thickness in three-dimensional images. *Journal of Microscopy* 185, 67–75. doi:10.1046/j.1365-2818.1997.1340694.x

Hu, L. and Bentler, P.M. (1999). Cutoff criteria for fit indexes in covariance structure analysis: Conventional criteria versus new alternatives. Structural Equation Modeling: *A Multidisciplinary Journal* 6, 1–55. doi:10.1080/10705519909540118

Huang, X.-F., Chaparro, J.M., Reardon, K.F., Zhang, R., Shen, Q., and Vivanco, J.M. (2014). Rhizosphere interactions: root exudates, microbes, and microbial communities. *Botany* 92, 267–275. doi:10.1139/cjb-2013-0225

Jiang, Y., Li, S., Li, R., Zhang, J., Liu, Y., Lv, L., Zhu, H., Wu, W., and Li, W. (2017). Plant cultivars imprint the rhizosphere bacterial community composition and association networks. *Soil Biology and Biochemistry* 109, 145–155. doi:10.1016/j.soilbio.2017.02.010

Kallenbach, C.M., Grandy, A.S., Frey, S.D., and Diefendorf, A.F. (2015). Microbial physiology and necromass regulate agricultural soil carbon accumulation. *Soil Biology and Biochemistry* 91, 279–290. doi:10.1016/j.soilbio.2015.09.005

Kalyn, A.L. and Van Rees, K.C.J. (2006). Contribution of fine roots to ecosystem biomass and net primary production in black spruce, aspen, and jack pine forests in Saskatchewan. The Fluxnet-Canada Research Network: Influence of Climate and Disturbance on Carbon Cycling in Forests and Peatlands 140, 236–243. doi:10.1016/j.agrformet.2005.08.019

Keiluweit, M., Gee, K., Denney, A., and Fendorf, S. (2018). Anoxic microsites in upland soils dominantly controlled by clay content. *Soil Biology & Biochemistry*.

Kravchenko, A.N., Guber, A.K., Razavi, B.S., Koestel, J., Blagodatskaya, E.V., and Kuzyakov, Y. (2019a). Spatial patterns of extracellular enzymes: Combining X-ray computed micro-tomography and 2D zymography. *Soil Biology and Biochemistry* 135, 411–419. doi:10.1016/j.soilbio.2019.06.002

Kravchenko, A.N., Guber, A.K., Razavi, B.S., Koestel, J., Quigley, M.Y., Robertson, G.P., and Kuzyakov, Y. (2019b). Microbial spatial footprint as a driver of soil carbon stabilization. *Nature Communications* 10, 3121. doi:10.1038/s41467-019-11057-4

Kravchenko, A.N. and Robertson, G.P. (2011). Whole-Profile Soil Carbon Stocks: The Danger of Assuming Too Much from Analyses of Too Little. *Soil Science Society of America Journal* 75, 235–240. doi:10.2136/sssaj2010.0076

Kwan, J.L.Y. and Chan, W. (2011). Comparing standardized coefficients in structural equation modeling: a model reparameterization approach. *Behavior Research Methods* 43, 730–745. doi:10.3758/s13428-011-0088-6

Lee, J.H., Lucas, M., Guber, A.K., Li, X., and Kravchenko, A.N. (2023). Interactions among soil texture, pore structure, and labile carbon influence soil carbon gains. *Geoderma* 439, 116675. doi:10.1016/j.geoderma.2023.116675

Li, X., Sarma, S.J., Sumner, L.W., Jones, A.D., and Last, R.L. (2022). Switchgrass Metabolomics Reveals Striking Genotypic and Developmental Differences in Specialized Metabolic Phenotypes. *Journal of Agricultural and Food Chemistry* 70, 8010–8023. doi:10.1021/acs.jafc.2c01306

Liang, C., Amelung, W., Lehmann, J., and Kästner, M. (2019). Quantitative assessment of microbial necromass contribution to soil organic matter. *Global Change Biology* 25, 3578–3590. doi:10.1111/gcb.14781

Liang, J., Zhou, Z., Huo, C., Shi, Z., Cole, J.R., Huang, L., Konstantinidis, K.T., Li, X., Liu, B., Luo, Z., Penton, C.R., Schuur, E.A.G., Tiedje, J.M., Wang, Y.-P., Wu, L., Xia, J., Zhou, J., and Luo, Y. (2018). More replenishment than priming loss of soil organic carbon with additional carbon input. *Nature Communications* 9, 3175. doi:10.1038/s41467-018-05667-7

Liebig, M.A., Johnson, H.A., Hanson, J.D., and Frank, A.B. (2005). Soil carbon under switchgrass stands and cultivated cropland. *Biomass and Bioenergy* 28, 347–354. doi:10.1016/j.biombioe.2004.11.004

Liu, C., Lou, L., Deng, J., Li, D., Yuan, S., and Cai, Q. (2016). Morph-physiological responses of two switchgrass (*Panicum virgatum* L.) cultivars to cadmium stress. *Grassland Science* 62, 92–101. doi:10.1111/grs.12119

Liu, Y., Zhang, X., Tran, H., Shan, L., Kim, J., Childs, K., Ervin, E.H., Frazier, T., and Zhao, B. (2015). Assessment of drought tolerance of 49 switchgrass (Panicum virgatum) genotypes using physiological and morphological parameters. *Biotechnology for Biofuels* 8, 152. doi:10.1186/s13068-015-0342-8

Lovell, J.T., MacQueen, A.H., Mamidi, S., Bonnette, J., Jenkins, J., Napier, J.D., Sreedasyam, A., Healey, A., Session, A., Shu, S., Barry, K., Bonos, S., Boston, L., Daum, C., Deshpande, S., Ewing, A., Grabowski, P.P., Haque, T., Harrison, M., Jiang, J., Kudrna, D., Lipzen, A., Pendergast, T.H., Plott, C., Qi, P., Saski, C.A., Shakirov, E.V., Sims, D., Sharma, M., Sharma, R., Stewart, A., Singan, V.R., Tang, Y., Thibivillier, S., Webber, J., Weng, X., Williams, M., Wu, G.A., Yoshinaga, Y., Zane, M., Zhang, L., Zhang, J., Behrman, K.D., Boe, A.R., Fay, P.A., Fritschi, F.B., Jastrow, J.D., Lloyd-Reilley, J., Martínez-Reyna, J.M., Matamala, R., Mitchell, R.B., Rouquette, F.M., Ronald, P., Saha, M., Tobias, C.M., Udvardi, M., Wing, R.A., Wu, Y., Bartley, L.E., Casler, M., Devos, K.M., Lowry, D.B., Rokhsar, D.S., Grimwood, J., Juenger, T.E., and Schmutz, J. (2021). Genomic mechanisms of climate adaptation in polyploid bioenergy switchgrass. *Nature* 590, 438–444. doi:10.1038/s41586-020-03127-1

Lowry, D.B., Lovell, J.T., Zhang, L., Bonnette, J., Fay, P.A., Mitchell, R.B., Lloyd-Reilley, J., Boe, A.R., Wu, Y., Rouquette, F.M., Wynia, R.L., Weng, X., Behrman, K.D., Healey, A., Barry, K., Lipzen, A., Bauer, D., Sharma, A., Jenkins, J., Schmutz, J., Fritschi, F.B., and Juenger, T.E. (2019). QTL × environment interactions underlie adaptive divergence in switchgrass across a large latitudinal gradient. *Proceedings of the National Academy of Sciences* 116, 12933–12941. doi:10.1073/pnas.1821543116

Lucas, M., Nguyen, L.T.T., Guber, A., and Kravchenko, A.N. (2022). Cover crop influence on pore size distribution and biopore dynamics: Enumerating root and soil faunal effects. *Frontiers in Plant Science* 13, 928569. doi:10.3389/fpls.2022.928569

Ma, Y., An, Y., Shui, J., and Sun, Z. (2011). Adaptability evaluation of switchgrass (*Panicum virgatum* L.) cultivars on the Loess Plateau of China. *Bioenergy Plants in the United States and China* 181, 638–643. doi:10.1016/j.plantsci.2011.03.003

Ma, Z., Wood, C.W., and Bransby, D.I. (2000). Impacts of soil management on root characteristics of switchgrass. *Biomass and Bioenergy* 18, 105–112. doi:10.1016/S0961-9534(99)00076-8

Mahannopkul, K. and Jotisankasa, A. (2019). Influences of root concentration and suction on Chrysopogon zizanioides reinforcement of soil. *Soils and Foundations* 59, 500–516. doi:10.1016/j.sandf.2018.12.014

Makovetsky, R., Piche, N., and Marsh, M. (2018). Dragonfly as a Platform for Easy Image-based Deep Learning Applications. *Microscopy and Microanalysis* 24, 532–533. doi:10.1017/S143192761800315X

Martinez-Feria, R. and Basso, B. (2020). Predicting soil carbon changes in switchgrass grown on marginal lands under climate change and adaptation strategies. *GCB Bioenergy* 12, 742–755. doi:10.1111/gcbb.12726

McCully, M.E. (1999). ROOTS IN SOIL: Unearthing the Complexities of Roots and Their Rhizospheres. *Annual Review of Plant Physiology and Plant Molecular Biology* 50, 695–718. doi:10.1146/annurev.arplant.50.1.695

McLaughlin, S.B. and Adams Kszos, L. (2005). Development of switchgrass (*Panicum virgatum*) as a bioenergy feedstock in the United States. *Biomass and Bioenergy* 28, 515–535. doi:10.1016/j.biombioe.2004.05.006

McLaughlin, S.B., de la Torre Ugarte, D.G., Garten, C.T., Lynd, L.R., Sanderson, M.A., Tolbert, V.R., and Wolf, D.D. (2002). High-Value Renewable Energy from Prairie Grasses. *Environmental Science & Technology* 36, 2122–2129. doi:10.1021/es010963d

Miltner, A., Bombach, P., Schmidt-Brücken, B., and Kästner, M. (2012). SOM genesis: microbial biomass as a significant source. *Biogeochemistry* 111, 41–55. doi:10.1007/s10533-011-9658-z

Mitchell, R., Vogel, K.P., and Uden, D.R. (2012). The feasibility of switchgrass for biofuel production. *Biofuels* 3, 47–59. doi:10.4155/bfs.11.153

Mosier, S., Kelly, L., Ozlu, E., and Robertson, G.P. (2024). Switchgrass (*Panicum virgatum* L.) cultivars have similar impacts on soil carbon and nitrogen stocks and microbial function. *GCB Bioenergy* 16, e13125. doi:10.1111/gcbb.13125

Oates, L.G., Duncan, D.S., Gelfand, I., Millar, N., Robertson, G.P., and Jackson, R.D. (2016). Nitrous oxide emissions during establishment of eight alternative cellulosic bioenergy cropping systems in the North Central United States. *GCB Bioenergy* 8, 539–549. doi:10.1111/gcbb.12268

Oburger, E. and Schmidt, H. (2016). New Methods To Unravel Rhizosphere Processes. *Trends in Plant Science*, Special Issue: Unravelling the Secrets of the Rhizosphere 21, 243–255. doi:10.1016/j.tplants.2015.12.005

Paez-Garcia, A., Motes, C.M., Scheible, W.-R., Chen, R., Blancaflor, E.B., and Monteros, M.J. (2015). Root Traits and Phenotyping Strategies for Plant Improvement. *Plants* 4, 334–355. doi:10.3390/plants4020334

Panchal, P., Preece, C., Peñuelas, J., and Giri, J. (2022). Soil carbon sequestration by root exudates. *Trends in Plant Science* 27, 749–757. doi:10.1016/j.tplants.2022.04.009

Paterson, E. and Sim, A. (1999). Rhizodeposition and C-partitioning of Lolium perenne in axenic culture affected by nitrogen supply and defoliation. *Plant and Soil* 216, 155–164. doi:10.1023/A:1004789407065

Paul, E.A., Harris, D., Klug, M., and Ruess, R. (1999). The determination of microbial biomass, in: Standard Soil Methods for Long-Term Ecological Research. Oxford University Press, New York, NY, pp. 291–317.

Perry, S., Falvo, G., Mosier, S., and Robertson, G.P. (2023). Long-term changes in soil carbon and nitrogen fractions in switchgrass, native grasses, and no-till corn bioenergy production systems. *Soil Science Society of America Journal*. doi:10.1002/saj2.20575

Preacher, K.J. and Hayes, A.F. (2004). SPSS and SAS procedures for estimating indirect effects in simple mediation models. Behavior Research Methods, *Instruments, & Computers* 36, 717–731. doi:10.3758/BF03206553

Quigley, M.Y. and Kravchenko, A.N. (2022). Inputs of root-derived carbon into soil and its losses are associated with pore-size distributions. *Geoderma* 410, 115667. doi:10.1016/j.geoderma.2021.115667

Rawlins, B.G., Wragg, J., Reinhard, C., Atwood, R.C., Houston, A., Lark, R.M., and Rudolph, S. (2016). Three-dimensional soil organic matter distribution, accessibility and microbial respiration in macroaggregates using osmium staining and synchrotron X-ray computed tomography. *SOIL* 2, 659–671. doi:10.5194/soil-2-659-2016

Raynaud, X. and Nunan, N. (2014). Spatial Ecology of Bacteria at the Microscale in Soil. *PLOS ONE* 9, e87217. doi:10.1371/journal.pone.0087217

Reubens, B., Poesen, J., Danjon, F., Geudens, G., and Muys, B. (2007). The role of fine and coarse roots in shallow slope stability and soil erosion control with a focus on root system architecture: a review. *Trees* 21, 385–402. doi:10.1007/s00468-007-0132-4

Robertson, G.P., Hamilton, S.K., Barham, B.L., Dale, B.E., Izaurralde, R.C., Jackson, R.D., Landis, D.A., Swinton, S.M., Thelen, K.D., and Tiedje, J.M. (2017). Cellulosic biofuel contributions to a sustainable energy future: Choices and outcomes. *Science* 356, eaal2324. doi:10.1126/science.aal2324

Rohe, L., Apelt, B., Vogel, H.-J., Well, R., Wu, G.-M., and Schlüter, S. (2021). Denitrification in soil as a function of oxygen availability at the microscale. *Biogeosciences* 18, 1185–1201. doi:10.5194/bg-18-1185-2021

Roley, S.S., Ulbrich, T.C., and Robertson, G.P. (2021). Nitrogen Fixation and Resorption Efficiency Differences Among Twelve Upland and Lowland Switchgrass Cultivars. *Phytobiomes Journal* 5, 97–107. doi:10.1094/PBIOMES-11-19-0064-FI

Ronneberger, O., Fischer, P., and Brox, T. (2015). U-Net: Convolutional Networks for Biomedical Image Segmentation, in: Navab, N., Hornegger, J., Wells, W.M., Frangi, A.F. (Eds.), Medical Image Computing and Computer-Assisted Intervention – MICCAI 2015, Lecture Notes in Computer Science. Springer International Publishing, Cham, pp. 234–241. doi:10.1007/978-3-319-24574-4_28

Ruess, R.W., Hendrick, R.L., Burton, A.J., Pregitzer, K.S., Sveinbjornssön, B., Allen, M.F., and Maurer, G.E. (2003). COUPLING FINE ROOT DYNAMICS WITH ECOSYSTEM CARBON CYCLING IN BLACK SPRUCE FORESTS OF INTERIOR ALASKA. *Ecological Monographs* 73, 643–662. doi:10.1890/02-4032

Samson, R., Mani, S., Boddey, R., Sokhansanj, S., Quesada, D., Urquiaga, S., Reis, V., and Ho Lem, C. (2005). The Potential of C4 Perennial Grasses for Developing a Global BIOHEAT Industry. *Critical Reviews in Plant Sciences* 24, 461–495. doi:10.1080/07352680500316508

Sanford, G.R., Oates, L.G., Jasrotia, P., Thelen, K.D., Robertson, G.P., and Jackson, R.D. (2016). Comparative productivity of alternative cellulosic bioenergy cropping systems in the North Central USA. *Agriculture, Ecosystems & Environment* 216, 344–355. doi:10.1016/j.agee.2015.10.018

Sawyer, A., Staley, C., Lamb, J., Sheaffer, C., Kaiser, T., Gutknecht, J., Sadowsky, M.J., and Rosen, C. (2019). Cultivar and phosphorus effects on switchgrass yield and rhizosphere microbial diversity. *Applied Microbiology and Biotechnology* 103, 1973–1987. doi:10.1007/s00253-018-9535-y

Schindelin, J., Arganda-Carreras, I., Frise, E., Kaynig, V., Longair, M., Pietzsch, T., Preibisch, S., Rueden, C., Saalfeld, S., Schmid, B., Tinevez, J.-Y., White, D.J., Hartenstein, V., Eliceiri, K., Tomancak, P., and Cardona, A. (2012). Fiji: an open-source platform for biological-image analysis. *Nature Methods* 9, 676–682. doi:10.1038/nmeth.2019

Schlüter, S., Leuther, F., Albrecht, L., Hoeschen, C., Kilian, R., Surey, R., Mikutta, R., Kaiser, K., Mueller, C.W., and Vogel, H.-J. (2022). Microscale carbon distribution around pores and particulate organic matter varies with soil moisture regime. *Nature Communications* 13, 2098. doi:10.1038/s41467-022-29605-w

Schlüter, S., Sheppard, A., Brown, K., and Wildenschild, D. (2014). Image processing of multiphase images obtained via X-ray microtomography: A review. *Water Resources Research* 50, 3615–3639. doi:10.1002/2014WR015256

Schlüter, S. and Vogel, H.-J. (2016). Analysis of Soil Structure Turnover with Garnet Particles and X-Ray Microtomography. *PLOS ONE* 11, e0159948. doi:10.1371/journal.pone.0159948

Schlüter, S., Zawallich, J., Vogel, H.-J., and Dörsch, P. (2019). Physical constraints for respiration in microbial hotspots in soil and their importance for denitrification. *Biogeosciences* 16, 3665–3678. doi:10.5194/bg-16-3665-2019

Schumacker, R.E. and Lomax, R.G. (1996). A Beginner's Guide to Structural Equation Modeling: Fourth Edition, 2nd ed. Psychology Press, New York. doi:10.4324/9781410610904

Seethepalli, A., Dhakal, K., Griffiths, M., Guo, H., Freschet, G.T., and York, L.M. (2021). RhizoVision Explorer: open-source software for root image analysis and measurement standardization. *AoB PLANTS* 13, plab056. doi:10.1093/aobpla/plab056

Sehgal, A., Sita, K., Rehman, A., Farooq, M., Kumar, S., Yadav, R., Nayyar, H., Singh, S., and Siddique, K.H.M. (2021). Chapter 13 - Lentil, in: Sadras, V.O., Calderini, D.F. (Eds.), Crop Physiology Case Histories for Major Crops. Academic Press, pp. 408–428. doi:10.1016/B978-0-12-819194-1.00013-X

Semchenko, M., Xue, P., and Leigh, T. (2021). Functional diversity and identity of plant genotypes regulate rhizodeposition and soil microbial activity. *New Phytologist* 232, 776–787. doi:10.1111/nph.17604

Six, J., Frey, S.D., Thiet, R.K., and Batten, K.M. (2006). Bacterial and Fungal Contributions to Carbon Sequestration in Agroecosystems. *Soil Science Society of America Journal* 70, 555–569. doi:10.2136/sssaj2004.0347

Sokol, N.W., Kuebbing, Sara.E., Karlsen-Ayala, E., and Bradford, M.A. (2019). Evidence for the primacy of living root inputs, not root or shoot litter, in forming soil organic carbon. *New Phytologist* 221, 233–246. doi:10.1111/nph.15361

Sprunger, C.D., Oates, L.G., Jackson, R.D., and Robertson, G.P. (2017). Plant community composition influences fine root production and biomass allocation in perennial bioenergy cropping systems of the upper Midwest, USA. *Biomass and Bioenergy* 105, 248–258. doi:10.1016/j.biombioe.2017.07.007

Steinaker, D.F. and Wilson, S.D. (2008). Phenology of fine roots and leaves in forest and grassland. *Journal of Ecology* 96, 1222–1229. doi:10.1111/j.1365-2745.2008.01439.x

Strong, D.T., Wever, H.D., Merckx, R., and Recous, S. (2004). Spatial location of carbon decomposition in the soil pore system: Spatial location of carbon decomposition. *European Journal of Soil Science* 55, 739–750. doi:10.1111/j.1365-2389.2004.00639.x

Stroup, W.W. (2002). Power analysis based on spatial effects mixed models: A tool for comparing design and analysis strategies in the presence of spatial variability. *Journal of Agricultural, Biological, and Environmental Statistics* 7, 491–511. doi:10.1198/108571102780

Udawatta, R.P., Anderson, S.H., Gantzer, C.J., and Garrett, H.E. (2008). Influence of Prairie Restoration on CT-Measured Soil Pore Characteristics. *Journal of Environmental Quality* 37, 219–228. doi:10.2134/jeq2007.0227

Ulbrich, T.C., Friesen, M.L., Roley, S.S., Tiemann, L.K., and Evans, S.E. (2021). Intraspecific Variability in Root Traits and Edaphic Conditions Influence Soil Microbiomes Across 12 Switchgrass Cultivars. *Phytobiomes Journal* 5, 108–120. doi:10.1094/PBIOMES-12-19-0069-FI

Valverde-Barrantes, O.J., Freschet, G.T., Roumet, C., and Blackwood, C.B. (2017). A worldview of root traits: the influence of ancestry, growth form, climate and mycorrhizal association on the functional trait variation of fine-root tissues in seed plants. *New Phytologist* 215, 1562–1573. doi:10.1111/nph.14571

Védère, C., Vieublé Gonod, L., Pouteau, V., Girardin, C., and Chenu, C. (2020). Spatial and temporal evolution of detritusphere hotspots at different soil moistures. *Soil Biology and Biochemistry* 150, 107975. doi:10.1016/j.soilbio.2020.107975

Vogel, H.-J., Weller, U., and Schlüter, S. (2010). Quantification of soil structure based on Minkowski functions. *Computers & Geosciences* 36, 1236–1245. doi:10.1016/j.cageo.2010.03.007

Vogel, K.P., Schmer, M.R., and Mitchell, R.B. (2005). Plant Adaptation Regions: Ecological and Climatic Classification of Plant Materials. *Rangeland Ecology and Management* 58, 315–319. doi:10.2111/1551-5028(2005)58[315:PAREAC]2.0.CO;2

Xu, J.G. and Juma, N.G. (1994). Relations of shoot C, root C and root length with root-released C of two barley cultivars and the decomposition of root-released C in soil. *Canadian Journal of Soil Science* 74, 17–22. doi:10.4141/cjss94-002

Zhang, P., Wang, Y., Xu, L., Sun, H., Li, R., and Zhou, J. (2022). Factors controlling the spatial variability of soil aggregates and associated organic carbon across a semi-humid watershed. *Science of The Total Environment* 809, 151155. doi:10.1016/j.scitotenv.2021.151155

Zhang, Y., Zalapa, J., Jakubowski, A.R., Price, D.L., Acharya, A., Wei, Y., Brummer, E.C., Kaeppler, S.M., and Casler, M.D. (2011). Natural Hybrids and Gene Flow between Upland and Lowland Switchgrass. *Crop Science* 51, 2626–2641. doi:10.2135/cropsci2011.02.0104

CHAPTER 4: Belowground carbon and nitrogen plant transfer and its association with soil carbon and nitrogen inputs and pore structure formation

Abstract

Belowground transfers of carbon (C) and nitrogen (N) can promote soil C gains and plant N availability, and both transfers can take place via root-based or mycorrhizae-based mechanisms. Yet, roles and magnitudes of such mechanisms in C and N transfers among different plant combinations and in the structure formation of soil pores remain unexplored. Three North American prairie species: switchgrass (*Panicum virgatum* L.), bush clover (*Lespedeza capitata* Michx.), and black-eyed Susan (*Rudbeckia hirta* L.), were grown as neighbors of the central SG within three-compartment rhizoboxes, and the central switchgrass was always the source of the transfers. Half of the boxes had mesh barriers to disallow root branching but allow fungal interactions, while another half was open to allow both root and fungal interactions. The central switchgrass was labelled by ^{13}C and ^{15}N to trace their transfers. After four months, (1) roots and surrounding rhizosphere soils were collected to analyze their ^{13}C and ^{15}N levels, (2) aboveground and root biomass of plants and inorganic N of soils were measured, and (3) intact soil cores were taken from soils between the source and recipients and scanned using X-ray computed tomography to analyze changes in pore structure and presence of root residues. Root-based mechanism predominantly facilitated C transfers from the source switchgrass to neighboring recipient switchgrass and bush clover, while N transfers occurred through both mechanisms. The presence of bush clover promoted C and N transfer from source switchgrass to co-planted black-eyed Susan. The observed C and N transfers through root-based mechanism were positively associated with those in rhizosphere soils, and such transfer mechanism led to greater formation of finer pores (8-30µm diameter) between the source and recipient plants. Conclusively, the presence of bush clover promotes root-based transfers, and this can release more C into soil, allowing more chances to store C within the newly formed finer pores.

4.1 Introduction

In diverse perennial vegetation, belowground transfer of nutrients among plant neighbors is expected to be one of the potential drivers of beneficial synergies for soil carbon (C) accumulation and plant productivity by sharing their nutrients and fostering soil microbial environment (Thilakarathna et al., 2012; Lange et al., 2015; Yang et al., 2019). Belowground C transfer to roots of adjacent plants was first documented in 1960s (Björkman, 1960; Reid and Woods, 1969) and was reported both between plants of the same as well as disparate species (Ren et al., 2013; Gorzelak et al., 2020; Cahanovitc et al., 2022), with extents of the transfer depending on the species involved (Carey et al., 2004; Walder and van der Heijden, 2015). Belowground intra- and inter-specific transfers of nitrogen (N) have also been commonly reported (Høgh-Jensen and Schjoerring, 2000; Shao et al., 2020; Reay et al., 2022).

The transfer of both elements primarily takes place via two key routes: through direct involvement of roots and through mycorrhizal networks (Robinson and Fitter, 1999; Thilakarathna et al., 2016; Hupe et al., 2021). The transfer via root-driven mechanisms takes place when C and N are released from roots of the source plant as exudates and rhizodeposits, and then are absorbed by the roots of neighboring recipient plants (Jones et al., 2004; Segonzac et al., 2007; Badri and Vivanco, 2009). Such absorption can take place both when there is a direct contact between roots of source and recipient plants or when roots of the recipient plant encounter the released C and N somewhere within the soil. Hereafter we will refer to this mechanism as root-based transfer.

C and N transfer via mycorrhizal networks occurs when symbiotic fungi utilize C and N obtained from roots to develop their hyphae (Rillig, 2004a; Parniske, 2008). Plant-derived C and N are transported to the symbiotic fungi and their hyphae (Smith et al., 2009; Smith and Smith, 2011; Roth and Paszkowski, 2017), and roots of a neighboring plant are interconnected through the same mycorrhizal networks (Wipf et al., 2019). Mycorrhizal networks serve as pathways for the movement or transfer of C and N (Martins, 1993; Martins and Cruz, 1998; He et al., 2003) and enable plants to share nutrients among interconnected plants (Walder et al., 2012; Walder and van der Heijden, 2015). Hereafter we will refer to this mechanism as fungal-based transfer.

Belowground transfers of nutrients, especially N, are expected to depend on the identity of the involved plants and on the overall availability of soil N, since both factors can substantially impact root growth and mycorrhizae development (Stober et al., 2000; López-Bucio et al., 2003; Cox et al., 2010). For example, root development responds to the proximity of neighboring plants, adjusting their root growth to optimize nutrient uptake (McNickle, 2020). Several studies had shown that roots respond to adjacent roots in a manner contingent on the specific identity of the neighboring plant (Maina et al., 2002; Falik et al., 2003; de Kroon, 2007). Moreover, spatial variability of soil N is known to influence the root development in response to its immediate availability (Aibara and Miwa, 2014; Kellermeier et al., 2014; Boer et al., 2020). However, as of now there is no experimental evidence of how the spatial variability of soil N, altered by the identity of neighboring plants, affects C and N transfer.

Plant roots influence soil structure through direct penetration of the soil matrix, water extraction, and root exudation (Bengough et al., 2016; Oburger and Schmidt, 2016). Most roots grow into relatively large (e.g., > 100 μm diameter) pores within the soil matrix (Bauhus and Messier, 1999; An et al., 2022), where they deposit a variety of root-released C compounds as well as leave root residues upon senescence (Jones et al., 2004; Badri and Vivanco, 2009). Organic inputs into such pores are subsequently susceptible to decomposition and loss as carbon dioxide (CO_2) (Ruamps et al., 2011; Kravchenko et al., 2019).

Fungi release C and N-containing compounds into the soil as glomalin-related proteins, extracellular enzymes, and other secondary metabolites (Rillig, 2004b; Karlovsky, 2008; Burns et al., 2013), while C and N from senescent and decomposed hyphae further add to soil organic matter (Treseder and Holden, 2013). Unlike compounds of root origin, the fungi-originated organics can be expected to be located not only in the large but also in the very fine (e.g., ~ 10 μm diameter) pores accessible to fungal hyphae (Carlile, 1995). Organic C in such fine pores tends to be better protected from further microbial decomposition (Keiluweit et al., 2016; Kravchenko et al., 2019; Zheng et al., 2022).

Recently, Kravchenko et al. (2021) demonstrated that belowground C transfer can influence the quantities of plant-derived C inputs added to the soil, potentially influencing soil pore structure, thus suggesting that interplant C transfer may stimulate soil C gains. While numerous studies examined the

relative contributions of the two transfer mechanisms, i.e., root-based vs. fungal-based, to C and N transfers (Carey et al., 2004; Ren et al., 2013; Shao et al., 2020; Cahanovitc et al., 2022), our understanding of how these transfers contribute to alterations in soil pore structure remains limited.

Switchgrass (*Panicum virgatum* L.) is one of the dominant grass species of the North American prairie and is also a promising perennial bioenergy crop (Parrish and Fike, 2005; Sanderson and Adler, 2008; Gelfand et al., 2020). This deep-rooted perennial grass is known to promote soil C accumulation when it is grown in diverse plant communities (Sanford, 2014; Sprunger and Robertson, 2018; Lee et al., 2023a; Perry et al., 2023) with a mitigating impact on global warming (Gelfand et al., 2020). However, which plant neighbors might be particularly effective in stimulating switchgrass-derived C inputs into the soil and what role C and N transfers might play in such stimulation remains unknown.

The first objective of this chapter is to quantify C and N transfers from switchgrass source plants to recipient switchgrass plants or to two other species common in prairie communities: a legume bush clover (*Lespedeza capitata* Michx) and a forb black-eyed-Susan (*Rudbeckia hirta* L.). We specifically focus on assessing the transfers taking place via mycorrhizae-only vs. root-based plus fungal-based mechanisms. The second objective is to assess whether C and N is released into the soil during these transfer processes. The third objective is to explore the associations of C and N transfers with inputs of plant-derived C into the soil and with alterations in soil pore structure.

4.2 Materials and Methods

4.2.1 Overview of the experiment

The study was conducted as a greenhouse experiment where plants of three species were grown in rhizoboxes filled with soils from two different sources (Table 4.1). In half of all rhizoboxes the plants could contact neighbors via their roots through shared soil, while in the rhizoboxes, plants were separated by root-impenetrable 35 μm mesh accessible to fungal hyphae (Figure 4.1). Each rhizobox consisted of three compartments, with one plant grown per compartment. The central compartment plants of each rhizobox, further referred to as source plants, were subjected to ^{13}C and ^{15}N labeling. The side compartment plants,

referred to as recipient plants, were not purposely labeled themselves and could have become ^{13}C and ^{15}N enriched only through belowground C and N transfer.

Table 4.1. Taxonomy and physical and chemical characteristics of two soil types.

Soil type	Taxonomy	Texture	Total C (%)	Total N (%)	Inorganic P (ppm)
Hickory Corners (HC)	Typic Hapludalf (Alfisol)	Loam	1.17	0.10	17.6
Escanaba (ESC)	Inceptic Hapludalf (Alfisol)	Sandy loam	2.27	0.19	8.4

At the end of the plant growth stage of the experiment, we opened the front panel of each rhizobox, and aboveground biomass, roots, and rhizosphere soils were destructively sampled for ^{13}C and ^{15}N analyses. In addition, intact soil cores were collected from each rhizobox and subjected to X-ray computed micro-tomography (μCT) for soil pore structure characterization and particulate organic matter (POM) segmentation (Figure 4.1B). A representative picture of a rhizobox is in the Figure 4.1C, and detailed descriptions of all experimental, sampling, and analyses components of the study are provided in subsequent sections.

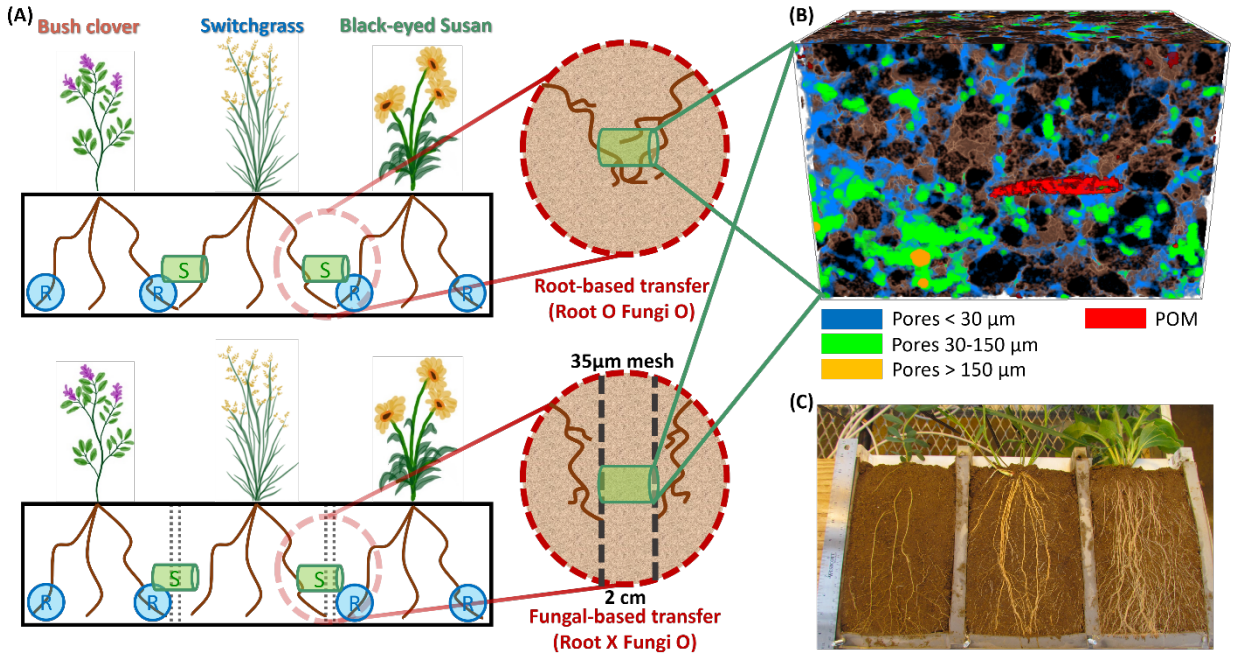

Figure 4.1. Schematic setting of rhizoboxs (A), showing the arrangement of plants, soil sampling locations, and two barrier treatments: open on both sides or wrapped in 35 µm mesh. Blue "R" circles indicate sampling locations for roots of recipient plants and the adjacent rhizosphere soils to explore C and N transfers from the source switchgrass. Green cylinders labeled as "S" indicate locations for intact soil core sampling to explore the alteration of soil structure and particulate organic matter (POM), which is considered as residues of newly grown roots. Soil cores collected from "S" locations were scanned, segmented into solid, pore, and POM classes (B), and size distributions of soil pores were analyzed separating pores into three size classes: < 30 µm, 30-150 µm, and > 150 µm in diameter (B). One example picture of rhizobox representative to BC-SG-BES plant combination (Table 4.2) is in (C).

4.2.2 Soil and rhizobox preparation

Two Alfisol soils with disparate characteristics were used in this study (Table 4.1): a loam Typic Hapludalf and a sandy loam Inceptic Hapludalf. The Typic Hapludalf soil originated from Biofuel Cropping System Experiment at Kellogg Biological Station in Hickory Corners, Michigan, which will be referred to as HC soil (42° 40'N, 85°37'W), and the Inceptic Hapludalf soil from the Great Lake Bioenergy Research Center Marginal Land Experiment site in Escanaba, Michigan, as ESC soil (45°76'N, -87°19'W). At each site the soil was collected from Ap horizon (5-20 cm) from conventionally managed agricultural fields. The collected soil was air-dried, sieved (2 mm), and thoroughly mixed, with small stones and visible plant residues removed.

A total of 88 rhizoboxes were constructed for the study. Each rhizobox (30 cm deep, 54 cm wide, and 4 cm thick) had three equally sized compartments with each compartment hosting a single plant (Figure

4.1). Three sides of the rhizobox were made from non-transparent plastic, while one side was transparent, which enabled visual monitoring of root growth during the study. The transparent side was also removable to facilitate root and soil sampling at the end of the study. The three compartments were separated by plastic dividers (30 cm deep, 2 cm wide, and 4 cm thick). The dividers were either open between the compartments or covered by mesh barriers (35 μm, ELKO Filtering Co., Tamarac, FL, USA), restricting root-to-root contact while still permitting passage of fungal hyphae (Figure 4.1A). The rhizobox compartments as well as dividers were filled with prepared soils ensuring consistent bulk density of 1.3 g/cm^3 throughout the rhizobox, at a volumetric water content of 20%.

4.2.3 Plant growth

The three studied plants were switchgrass (SG), bush clover (BC), and black-eyed Susan (BES). A total of four plant combinations were explored (Table 4.2), with all of them having SG as the source plant, i.e., the plant that received ^{13}C and ^{15}N labeling, growing in the central compartment. The side compartments were occupied either by two SG plants, two BC plants, two BES plants (one per compartment), or with one of each non-SG plants, i.e., BC and BES, in each compartment. The latter combination aimed at exploring the potential impact of a more diverse, i.e., three-species plant community. The recipient plant species were randomly assigned to each side of each rhizobox (Figure 4.1). Six replicated boxes with HC soil and five replicated boxes with ESC soil were constructed for each of the four plant combinations. Additionally, boxes containing all three species were prepared as non-isotope-labeled controls, and another set of boxes without plants for non-plant controls.

Table 4.2. Composition of the studied plant combination treatments. Each combination consisted of switchgrass (SG), growing in the central compartment and serving as the labeled source of ^{13}C and ^{15}N, and two neighboring plants, serving as recipients of ^{13}C and ^{15}N transfer. The recipient plants were of three species: SG, bush clove (BC), and black-eyed Susan (BES).

Combination	Recipient 1	Source	Recipient 2
SG-SG-SG	Switchgrass (SG)	Switchgrass (SG)	Switchgrass (SG)
BC-SG-BC	Bush clover (BC)	Switchgrass (SG)	Bush clover (BC)
BES-SG-BES	Black-eyed Susan (BES)	Switchgrass (SG)	Black-eyed Susan (BES)
BC-SG-BES	Bush clover (BC)	Switchgrass (SG)	Black-eyed Susan (BES)

Note: Recipient plant species were randomly placed in left and right compartments of rhizoboxes.

Seeds of each plant species were first germinated in seed starter trays for three weeks, and the seedlings that developed their leaves were transplanted to the center of each compartment in the rhizoboxes, one plant per compartment. The plants were grown for three months in the rhizoboxes with HC soil and for four months in the rhizoboxes with ESC soil. All plants were fertilized using Hoagland's solution after transplanting and then, again, one month later to promote growth. Two months after transplanting, the plants in ESC soil boxes showed signs of phosphorous deficiency, and hence, were additionally fertilized with 134 mg of KH_2PO_4 per box (equivalent to 56 kg P/ha). Initially, the boxes were kept tilted at a 60° angle with the transparent side down to stimulate root growth towards the transparent side and to enable visual observations of the root growth. After two months the boxes were moved to a vertical (90°) position to ensure that roots explored the rest of the soil and to promote root interactions through the dividers. Each plant in its own compartment was separately watered with 0.5 L of reverse osmosis water every day. The temperature in the greenhouse was regulated to maintain a maximum of 29°C during daylight hours and a minimum of 20°C during the night, accompanied by 16 hours of artificial fluorescent light.

4.2.4 ^{13}C pulse and ^{15}N foliage labeling

In order to trace the belowground C and N transfer from the source plants, all SG plants in the central compartment were pulse-labeled with $^{13}CO_2$ and foliage-labelled with $^{15}NH_4NO_3$. The labeling for both elements was performed three times for the rhizoboxes with HC soil and four times for those with ESC soil. In all cases the last labeling event took place one month before plant termination.

Pulse labeling for ^{13}C enrichment of the source plants took place in labeling chambers. Before placing the rhizoboxes into the labeling chambers, the recipient plants of each rhizobox were covered with light-impenetrable plastic bags, while the central SG remained uncovered. This setup ensured that only the uncovered source SG plant was able to photo-assimilate ^{13}C from the produced $^{13}CO_2$, and the recipient plants were not conducting photosynthesis. This setup has been successfully implemented by our team in the past (Kravchenko et al., 2021; Zheng et al., 2022). For the pulse labeling, we utilized 98% ^{13}C-enriched $NaHCO_3$ solution. The solution was mixed with H_2SO_4 to produce $^{13}CO_2$, releasing 88 mg of ^{13}C per pulse event per labeling chamber. Upon H_2SO_4 administration, the chamber was sealed for six hours in each pulse labeling event. The chamber was equipped with ventilators to facilitate even distribution of $^{13}CO_2$, and thermometers were installed to continuously monitor the internal temperature. To eliminate any potential heat stress, the lower portions of the chamber exteriors were insulated with ice. Upon opening the chamber, rhizoboxes were immediately moved to the environment with controlled lighting and ample ventilation to support normal plant photosynthesis and to protect the recipient plants from potential ^{13}C assimilation through $^{13}CO_2$ respiration of the source plants.

For ^{15}N enrichment of the source plants, we conducted foliage labeling with 45% ^{15}N-enriched NH_4NO_3 (Chu et al., 2004; Shao et al., 2020). One undamaged leaf of each source SG plant was gently inserted into a 2-ml tube containing 1.5 ml of 5% (v/w) $^{15}NH_4NO_3$ solution (6.38 g ^{15}N per L). We aimed to synchronize the ^{13}C and ^{15}N labeling events, thus, the ^{15}N labeling events took place at the same time as ^{13}C labeling events. The ^{15}N labeling started 48 hours before each $^{13}CO_2$ pulse-labeling event and ended 72 hours after inserting the leaf, providing sufficient time for the leaf of the source SG plant to absorb the $^{15}NH_4NO_3$ solution. The inserted SG leaf, along with the labeling tube, was carefully removed to avoid any dripping of $^{15}NH_4NO_3$ from the leaf and contaminating the soil.

4.2.5 Sampling and analyses of roots and of rhizosphere soil

Root and surrounding rhizosphere soil samples were collected from four locations on the transparent panel side in each box, two per each neighboring compartment (Figure 4.1A). One of the sampling locations was ~2 cm while the other was ~15 cm from the border of the central compartment; we

refer to them, respectively, as locations close and far from the source SG plant (location "R" in Figure 4.1A). Between each location's sampling, the sampling tools were thoroughly cleaned and sanitized by 70% ethanol to eliminate cross contamination. All collected root and soil samples were stored in 5 ml tubes at 4°C before the preparation for ^{13}C and ^{15}N analyses.

Root sample preparation consisted of cleaning the attached soil from the roots and drying them. For that, 1.8 ml of 0.05M $CaCl_2$ was added to each tube containing the root and the tube was sonicated for 5 minutes. Then, the roots were brushed to remove any remaining soil particles, and dark-brownish old roots were excluded from the tube. The roots were then oven-dried at 30°C for 2 days before further analyses. Rhizosphere soil sample preparation consisted of cleaning, drying and grinding the soil. For cleaning we manually removed visible roots and organic debris from each tube containing rhizosphere soil. The soil samples from the tubes were oven-dried at 30°C for 2 days, and then ground using an iron-ball mill.

An elemental analyzer (Vario ISOTOPE CUBE, Elementar Americas Inc., Ronkonkoma, NY, USA) coupled to an isotope ratio mass spectrometer (Isoprime Vision, Elementar Americas Inc., Ronkonkoma, NY, USA) was utilized for ^{13}C and ^{15}N analysis. The atom % of isotope ratios ($^{13}C/^{12}C$ and $^{15}N/^{14}N$) in the root and soil samples were calculated using the measured ^{13}C and ^{15}N enrichment expressed as $\delta^{13}C$ and $\delta^{15}N$ (‰) and total ^{13}C and ^{15}N contents using the PeeDee Belemnite and air standard, respectively (Fry, 2006). Then, the atom % excess values were obtained by subtracting the ^{13}C and ^{15}N atom % in the non-labeled root and rhizosphere soil samples.

4.2.6 Plant biomass and soil measurements

After collecting roots and rhizosphere soil samples, the entire aboveground biomass was clipped and collected. Due to the extensive branching of roots across the three rhizobox compartments, it was not feasible to collect the total belowground biomass. Instead, the biomass of major roots was collected by plucking out the crown of roots from the opened panel of each rhizobox and then by gently washing away the soil with DI water. The collected aboveground and major root biomass were oven-dried at 60°C for three days and weighed.

After the biomass removal, bulk soil from all three compartments of each rhizobox was collected and used for measurements of total C, total N, and inorganic N (NH_4^+ and NO_3^-) contents in soils. For total C and N, soils were homogenized, 2mm-sieved, ground, and analyzed by a CHNSO Elemental Analyzer (Costech Analytical Technologies, Valencia, CA, USA). For the NH_4^+ and NO_3^-, salicylate-cyanurate method (Sinsabaugh et al., 2000) and vanadium method (Doane and Horwáth, 2003) were used for 10 g of the homogenized soils with spectrophotometry (Victor3 1420 Multilabel Counter, Perkin Elmer, Waltham, MA, USA) at 630 and 540 nm, respectively.

4.2.7 Intact soil cores: sampling, μCT scanning, and μCT image analysis

Intact soil micro-cores (2 cm height and 0.8 cm diameter) were taken from the dividers in between the rhizobox compartments at 15 cm depth (Location "S" in Figure 4.1A). In the plant combinations with the same two recipient species (Table 4.2), the core was collected only from one (randomly selected) rhizobox side. In the plant combination with BC and BES recipients, two cores, one per each rhizobox side, were collected. A total of 104 intact cores were obtained and subjected to μCT scanning.

Prior to scanning, the cores were air-dried and then scanned at the 13-BM-D station of the GeoSoilEnviroCARS sector, Advanced Photon Source, Argonne National Laboratory (Lemont, IL, USA), with an energy of 30 keV and the scanning resolution of 5.7 μm. Original images were cropped to focus on the central portions of the cores, avoiding areas potentially subjected to scanning and sampling artifacts. The stack of the cropped images was 4.6 × 4.6 × 8.0 mm (800 × 800 ×1400 pixels) in size. Then, the cropped images were denoised using 3D non-local mean filter ($\sigma = 0.08$) (Darbon et al., 2008; Buades et al., 2011) implemented in scikit-image of Python (Walt et al., 2014).

The filtered images were used to identify POM and pores. The POM was segmented using a U-Net (convolutional neural network) model under the deep learning engine pre-built in Dragonfly software (Ronneberger et al., 2015; Abadi et al., 2016; Makovetsky et al., 2018). The segmentation model was trained using 16 cores randomly selected from the entire set of 104 cores. I used five slices with representative POM fragments in each of the selected cores as training inputs, and two slices directly below and above the selected frames were also considered for generating segmentation outcomes. Then, the

trained model was applied to the entire set of cores. The segmented POM images were visually inspected to ensure the integrity and accuracy of the process. The outcome of POM segmentation was denoised by removing clusters having voxels less than four from the images. I will refer the segmented POM fragments to here as root residues, because such fragments were derived from newly grown roots as I removed plant residues from soils and sieved and homogenized them prior to the rhizobox construction.

The pores were segmented using the filtered images via Otsu method in SimpleITK of Python (Yaniv et al., 2018; Lucas et al., 2022), and then the previously identified POM was subtracted from pore images to ensure that only air-filled pores were part of the finalized images of soil pore space (Figure 4.1C). The scanning resolution and the applied image filtering allow us to reliably identify pores with >8 μm diameters (Ø).

The finalized pore images were used to compute pore size distributions using 'Local Thickness' tool in Image-Fiji software (Schindelin et al., 2012), an approach based on the maximum inscribed sphere method (Hildebrand and Rüegsegger, 1997; Vogel et al., 2010). We decided to classify the segmented pores into three Ø size ranges, namely 8-30 μm, 30-150 μm, >150 μm Ø, because pores 30-150 μm are often found to be associated with high microbial abundance and activity (Nunan et al., 2003; Strong et al., 2004; Li et al., 2024). For each size range, pore fractions were determined by dividing the pore volumes (mm^3) by the total cropped soil (pore + POM + solid) volumes (mm^3).

4.2.8 Statistical analysis

Data analyses were conducted using SAS 9.4 (SAS Institute Inc., Cary, NC, USA), and statistical models were fitted using PROC MIXED. The models for measures of atom % ^{13}C and ^{15}N excess in roots and rhizosphere soils of recipient plants included fixed effects of barrier treatments for two transfer mechanisms (root-based vs. mycorrhizae-based), four plant combinations of recipient plant species (Table 4.2), two sampling locations (close vs. far from the source plant), and their interactions. Statistical models for aboveground and major root biomass, image-based root residue and soil porosity, atom % ^{13}C and ^{15}N excess in shoots, and soil inorganic N contents (NO_3^- and NH_4^+) included the fixed effects of barrier treatments, recipient plant species, and their interactions. Statistical models for pore fractions in different

size ranges additionally included the fixed effect of size ranges, which were treated as a repeated measure factor. In all models, replicated rhizoboxes nested within soils, barrier treatments, and recipient species were used as an error term for testing their effects and as a subject of the repeated measurement.

Note that we regarded the two studied soils as a source of random variation, representing soil variability among Alfisols under agricultural land use in the studied region. Thus, a random effect of the soil was included in all statistical models.

The assumptions of normality and variance homogeneity were assessed by examining histograms, normal probability plots, and side-by-side box plots of the residuals, and by conducting Levene's test for variances. Except for atom % ^{13}C and ^{15}N excess in roots, the residuals were found to be normally distributed and the equal variance assumption not violated for all studied variables. As the normality assumption for ^{13}C and ^{15}N excess in roots and rhizosphere soils was not met, the variables were log transformed, and due to the negative values in the excesses, a constant value was added to the data prior to the transformation.

When the interactions between the studied factors were found statistically significant, we used simple F-tests (aka slicing) followed by multiple comparisons with t-tests. The effects and differences were reported as statistically significant at $p < 0.05$. Additionally, to determine the enrichment of ^{13}C and ^{15}N in recipient roots, soils, and shoots and changes in pore and root residue fractions between the source and recipients, we performed another series of t-tests to compare them with those of non-isotope-labelled controls and in non-planted controls, respectively. Linear associations among the studied response variables were assessed using Pearson's correlation coefficients via PROC CORR procedure in SAS.

4.3 Results

4.3.1 Plant growth and soil inorganic N

As expected, the three studied recipient species differed in their aboveground and major root biomass with much greater foliage and root systems of SG and BES plant species as compared to those of BC ($p < 0.001$) (Figure 4.2). The presence of barriers did not affect aboveground and root biomass for any of the recipient species (Table 4.3), and different recipient species or presence of barriers did not affect

aboveground and the root biomass for the source SG (Figure 4.3). Aboveground and the root biomass for recipient BES and BC plants in the two-species treatments, i.e., BES-SG-BES and BC-SG-BC combinations, were not different from their respective counterparts in the three species BC-SG-BES combination (Figure 4.2).

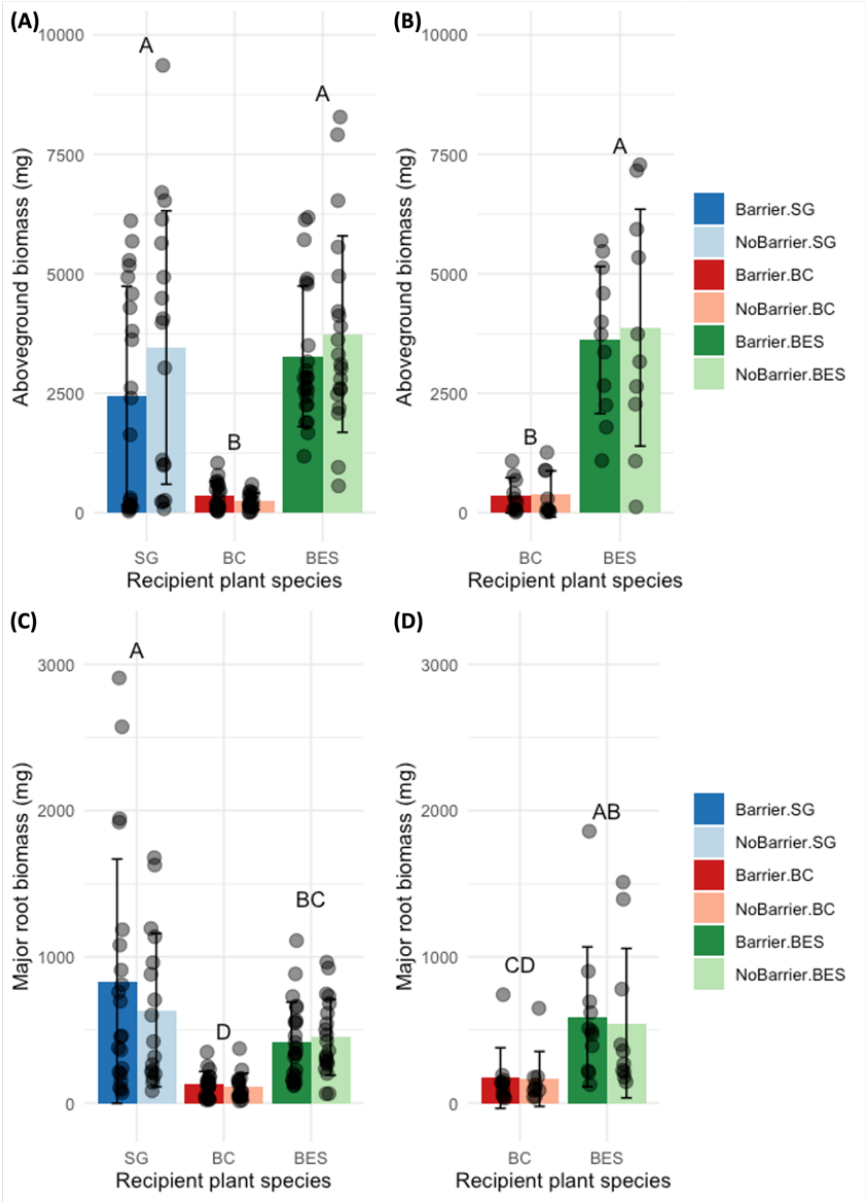

Figure 4.2. Aboveground (A and B) and major root (C and D) biomass of recipient plant species in the four studied plant combinations (Table 4.2): SG-SG-SG, BC-SG-BC, and BES-SG-BES, which had the same species at both sides (A and C), and BC-SG-BES with BC and BES presented at each side of rhizoboxes, separately (B and D). Error bars and dots represent standard deviations and individual data points, respectively. Different letters on the bars indicate significant differences in above or major root biomass of recipient species in four plant combinations at p <0.05. Differences between two barrier conditions were not significant (p >0.05) (Table 4.3), thereby not shown.

Table 4.3. ANOVA F-test results with *p*-values for effects of recipient plant species, barrier conditions, and their interaction on aboveground and major root biomass in four plant combinations. Significant effects ($p < 0.05$) in the ANOVA table are shown in bold.

	Aboveground biomass		Major root biomass	
Effect	F-value	*p*-value	F-value	*p*-value
Recipient	**13.94**	**<0.001**	**4.44**	**0.008**
Barrier	0.69	0.416	0.19	0.668
Recipient × Barrier	0.19	0.940	0.12	0.975

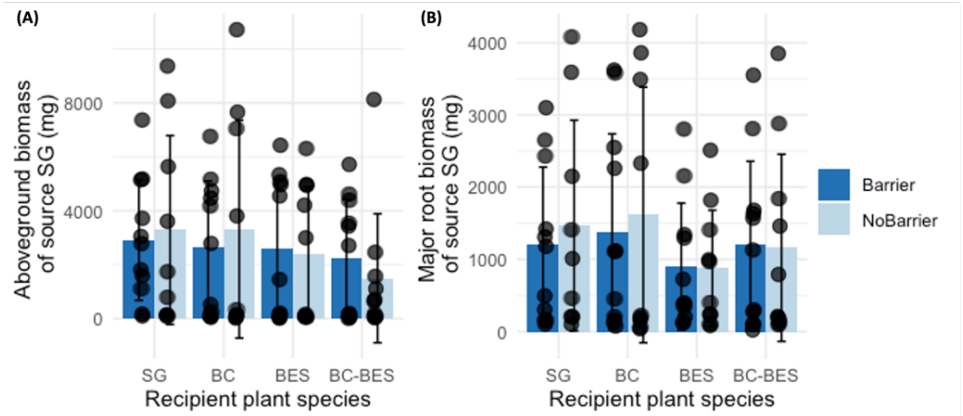

Figure 4.3. Aboveground (A) and major root (B) biomass of source SG plants in the four studied plant combinations (Table 4.2): SG-SG-SG, BC-SG-BC, and BES-SG-BES, which had the same species at both sides, and BC-SG-BES with BC and BES presented at each side of rhizoboxes, separately. Error bars and dots represent standard deviations and individual data points, respectively. Neither difference between two barrier conditions nor among four plant combinations were not significant ($p > 0.05$), thereby not shown.

Root residues within the rhizobox dividers were identified in X-ray μCT images of soil cores in no barrier rhizoboxes (Figure 4.4). However, root residues in the cores taken from the rhizoboxes with barriers were not greater than those in the control soil cores taken from unplanted control rhizoboxes (Figure 4.4). The results point out that the mesh barriers were effective in keeping away the roots, eliminating direct root interactions as needed for testing the study's hypotheses. The volume of root residues in the SG-SG-SG plant combination tended to be above that in all other treatments ($p < 0.1$) (Figure 4.4 and Table 4.4).

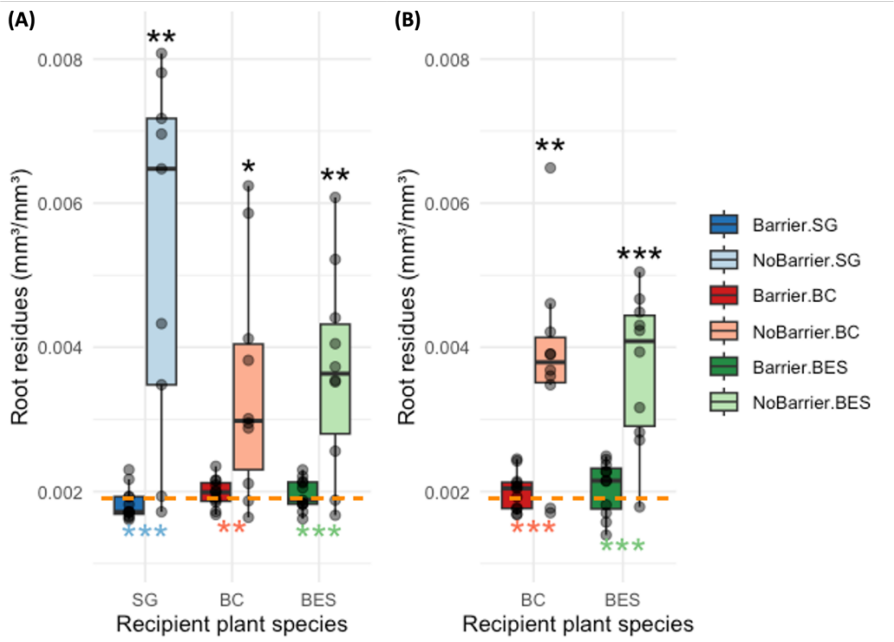

Figure 4.4. Fractions of root residues detected using X-ray µCT within the rhizobox dividers between source SG and recipient plant species in the four plant combinations (Table 4.2): SG-SG-SG, BC-SG-BC, and BES-SG-BES, which had the same species at both sides (A), and BC-SG-BES with BC and BES presented at each side of rhizoboxes, separately (B). Black *, **, and *** marks on the box plots denote that root residue fractions were significantly greater than the fractions of non-planted controls (orange-colored dashed lines) at p <0.05, 0.01, and 0.001 level, respectively. Marked ** and *** with corresponding colors to the boxes of recipient species and located below the adjacent two boxes indicate significant differences between barrier and non-barrier treatments within the species at p <0.01 and 0.001 level, respectively. Differences among recipient plants in the four combinations were not significant (p >0.05) (Table 4.4), thereby not shown.

Table 4.4. ANOVA F-test results with p-values for effects of recipient plant species, barrier conditions, and their interaction on root residues detected using X-ray µCT within the rhizobox dividers. Significant effects (p < 0.05) in the ANOVA table are shown in bold.

	Root residues	
Effect	F-value	p-value
Recipient	2.10	0.087
Barrier	**90.82**	**<0.001**
Recipient × Barrier	**3.02**	**0.021**

Presence of barriers did not affect either inorganic N (NO_3^- and NH_4^+) contents in soils (Table 4.5), while soils in BC recipient compartments had greater inorganic N contents compared to those in SG and BES compartments (Figure 4.5). Such N contents in BC recipient soils in BC-SG-BC plant combination were not different from their respective counterparts in BC-SG-BES combination (Figure 4.5).

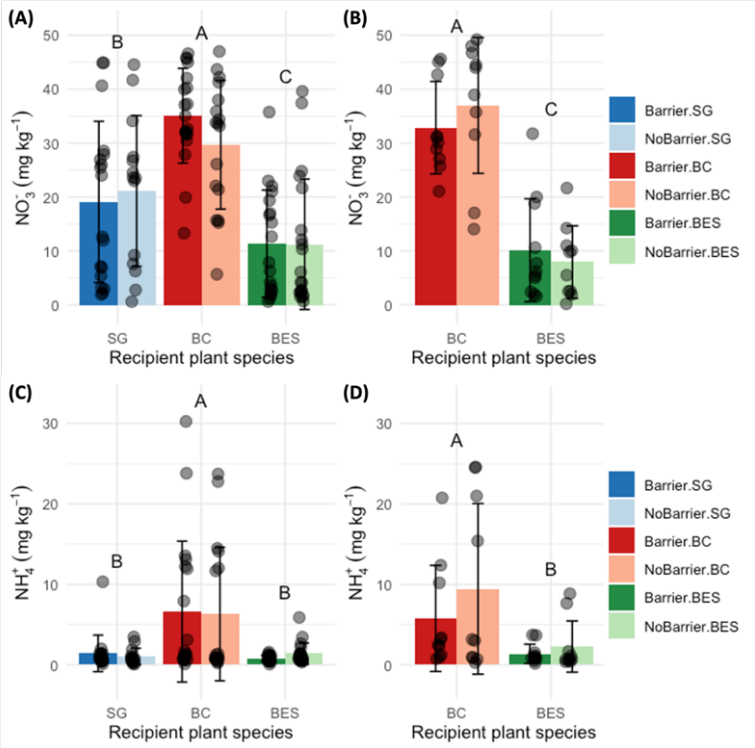

Figure 4.5. Nitrate (NO_3^-) (A and B) and ammonium (NH_4^+) (C and D) contents in soils of recipient plants in the four studied plant combinations (Table 4.2): SG-SG-SG, BC-SG-BC, and BES-SG-BES, which had the same species at both sides (A and C), and BC-SG-BES with BC and BES presented at each side of rhizoboxes, separately (B and D). Error bars and dots represent standard deviations and individual data points, respectively. Different letters on the bars indicate significant differences in NO_3^- and NH_4^+ contents in soils of recipient species across four plant combinations at p <0.05. Differences between two barrier conditions were not significant (p >0.05) (Table 4.5), thereby not shown.

Table 4.5. ANOVA F-test results with p-values for effects of recipient plant species, barrier conditions, and their interaction on NO_3^- and NH_4^+ contents in soils of four plant combinations. Significant effects (p < 0.05) in the ANOVA table are shown in bold.

	NO_3^-		NH_4^+	
Effect	F-value	p-value	F-value	p-value
Recipient	**43.10**	**<0.001**	**9.85**	**<0.001**
Barrier	0.15	0.697	0.99	0.322
Recipient × Barrier	1.01	0.405	0.56	0.691

4.3.2 ^{13}C and ^{15}N excesses in roots of recipient plants

^{13}C enrichment of recipient roots at the close location was generally greater than that at the far location (p <0.001), and likewise, the presence of the barrier led to overall lower ^{13}C enrichment (p <0.01) (Table 4.6). However, significant interactions were observed between the effects of the barriers and the recipient plant combinations. Specifically, in SG-SG-SG combination, i.e., when SG was both the source and the recipient species, in the absence of barriers, the roots of the recipient SG were ^{13}C enriched at both close and far locations (p <0.01) (Figure 4.6A). In the presence of the barrier, the recipient's roots were enriched only at the close location (p <0.01) (Figure 4.6A). In BC-SG-BC combination, i.e., when BC was the recipient species of the source SG, the ^{13}C root enrichment was detected in both close and far locations, both in the presence and in the absence of the barrier (p <0.05-0.01) (Figure 4.6A). In contrast, in BES-SG-BES combination, the roots of BES recipient plant were not ^{13}C enriched at either close or far locations, whether in the presence or absence of the barrier (p >0.05) (Figure 4.6A).

Table 4.6. ANOVA F-test results with p-values for effects of recipient plant species, barrier conditions, sampling locations, and their interaction on ^{13}C and ^{15}N atom % excesses in roots of recipient plants in four plant combinations. Significant effects (p < 0.05) in the ANOVA table are shown in bold.

	^{13}C excess		^{15}N excess	
Effect	F-value	p-value	F-value	p-value
Recipient	**5.05**	**0.001**	**3.62**	**0.007**
Barrier	**5.44**	**0.009**	2.53	0.088
Location	**12.96**	**<0.001**	**9.88**	**0.002**
Recipient × Barrier	**4.50**	**0.021**	1.67	0.156
Recipient × Location	1.60	0.175	0.48	0.747
Barrier × Location	**9.34**	**0.002**	2.15	0.144
Recipient × Barrier × Location	1.83	0.123	0.37	0.829

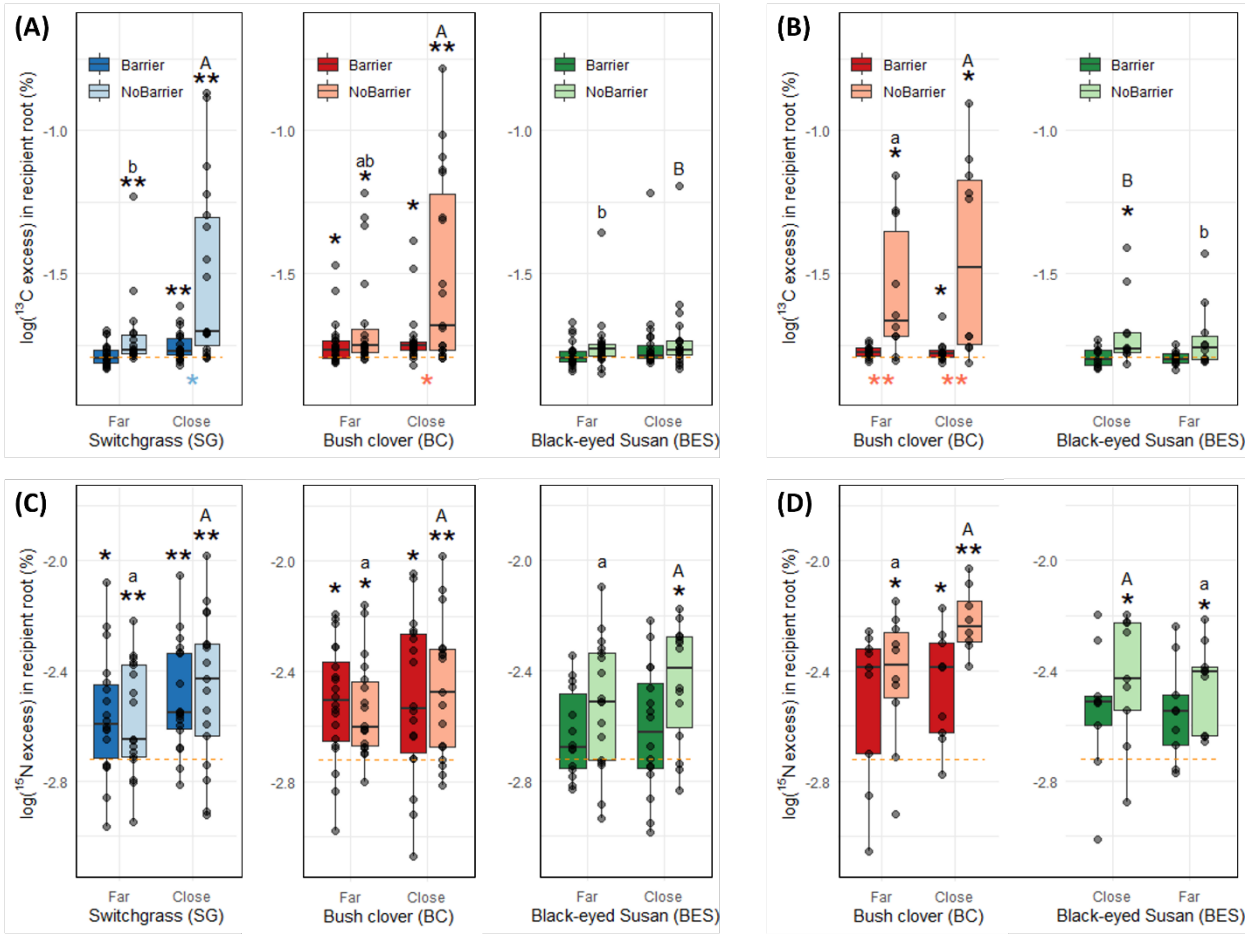

Figure 4.6. Atom % ^{13}C (A and B) and ^{15}N (C and D) excesses in the roots of recipient plants neighboring the ^{13}C labeled, thereby the source SG in the four studied plant combinations (Table 4.2): SG-SG-SG, BC-SG-BC, and BES-SG-BES, which have the same species of the non-labeled plants at both sides (A and C) and BC-SG-BES with BC and BES sides presented separately (B and D). Results obtained at close and far distances from the source plants are reported separately. Note that to ensure that data from all distances and plant combinations are clearly visible on the same graph we show the data in a log scale, and due to the negative values in % ^{13}C and ^{15}N excess, a constant value was added to the data prior to the log transformation. Dots represent individual data points. The black * and ** marks above the box plots denote that ^{13}C and ^{15}N excesses significantly exceed non-labelled controls (yellow dashed line) at p <0.05 and 0.01 level, respectively. Colored * and ** marks under the adjacent two boxes within each sampling location indicate significant differences between barrier and non-barrier treatments within the location at p <0.05 and 0.01 level, respectively. Different uppercase letters on the boxes indicate significant differences among three recipient species across four plant combinations within non-barrier treatments in the close location (p <0.05), and different lowercase letters indicate significant differences in the far location (p <0.05). Letters are not shown within barrier treatments, as differences were not statistically significant among the species (p >0.05).

When two different species were co-planted alongside the source SG in each rhizobox, i.e., in BC-SG-BES plant combination (Table 4.2), the ^{13}C excess results in the roots of BC and BES recipients (Figure 4.6B) were overall similar to those of their respective two-species combinations (Figure 4.6A). For example, just as in the two-species combinations, the ^{13}C excess in BC recipients was greater than that of the BES recipients, and the sizes of the barrier effects were comparable. Yet, notably, roots of BES recipients in the three-species BC-SG-BES combination were ^{13}C enriched at the close location (Figure 4.6B) unlikely to those in the BES-SG-BES combination (Figure 4.6A). In addition, at the far location, the ^{13}C excess in the roots of BC recipients was greater than that in far locations of any other recipients.

Similar to ^{13}C results, the ^{15}N enrichment of the recipient roots at the close location was somewhat higher than at the far (p <0.001). Yet, the strength of the barrier effect was much weaker and significant only at p <0.1 level (Table 4.6), and the root ^{15}N enrichment of all recipient plants tended to be more pronounced than the ^{13}C enrichment (Figure 4.6). For both SG and BC recipients, significant ^{15}N enrichment of the roots was observed at both close and far locations not only with the absence but also with the presence of the barrier (p <0.05-0.01) (Figure 4.6C). Even roots of BES recipients were ^{15}N enriched at the close location without barriers (p <0.05) (Figure 4.6C), while their ^{13}C enrichment was negligible (p >0.05) (Figure 4.6A). Again, similar to ^{13}C results, the BES ^{15}N enrichment in the three-species rhizoboxes (BC-SG-BES combination) tended to be stronger than that in the BES-SG-BES. Specifically, ^{15}N enrichment of BES roots was detected even at the far location of the BES side (p <0.05) (Figure 4.6D), while it was only found at the close location in the BES recipient of the BES-SG-BES combination (Figure 4.6C).

^{13}C enrichment in the shoots of the recipient plants was not observed in any of the studied combinations or barrier treatments (Figure 4.7A and 4.7B). However, the shoots of recipient plants were significantly enriched with ^{15}N in most combinations and barrier treatments (Figure 4.7C and 4.7D). BES recipient plants in the barrier treatments of both BES-SG-BES and BC-SG-BES combinations were the only ones where ^{15}N enrichments in shoots was not statistically significant.

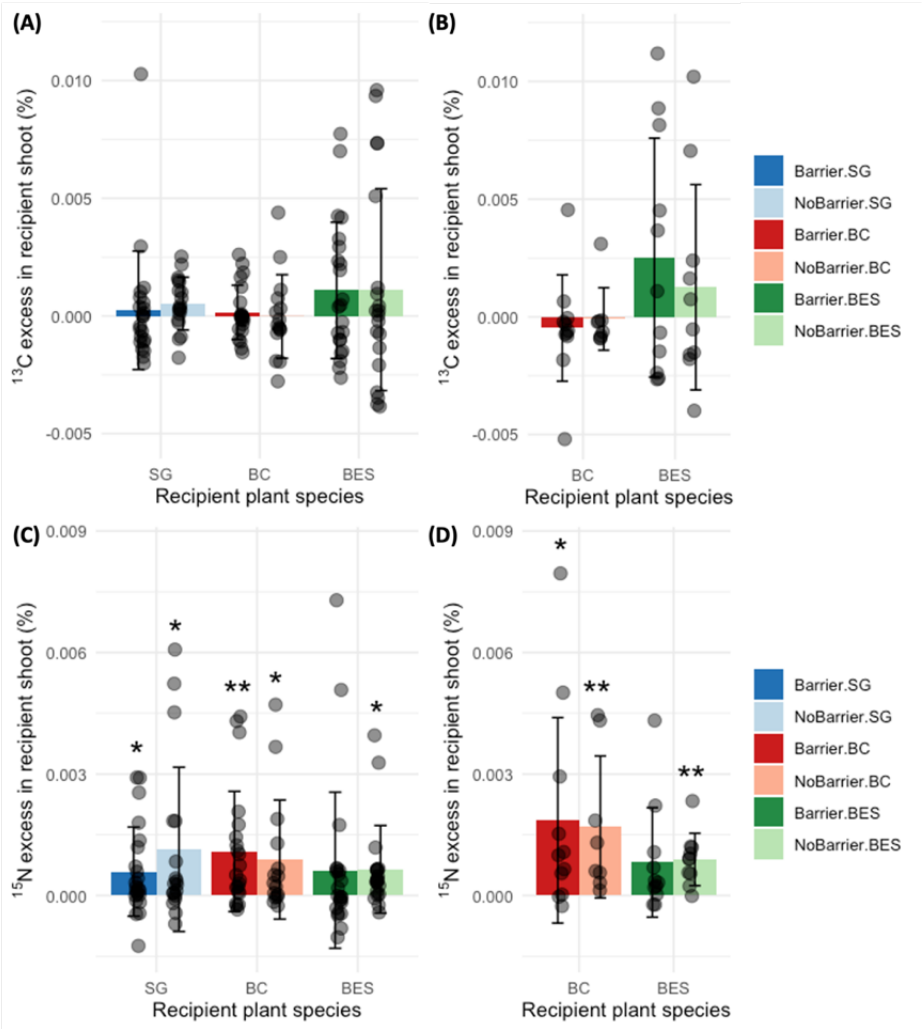

Figure 4.7. Atom % ^{13}C (A and B) and ^{15}N excesses in shoots of recipient plant species in the four plant combinations (Table 4.2): SG-SG-SG, BC-SG-BC, and BES-SG-BES, which had the same species at both sides (A and C), and BC-SG-BES with BC and BES presented at each side of rhizoboxes, separately (B and D). Error bars and dots represent standard deviations and individual data points, respectively. The black * and ** marks above the bar plots denote that ^{13}C and ^{15}N excesses significantly exceed non-labelled controls, which are all 0 %, at p <0.05 and 0.001 level, respectively. Differences between two barrier conditions or among recipient species were not significant (p >0.05), thereby not shown.

Significant correlations between ^{13}C and ^{15}N excesses in the roots of the recipient plants were observed only in SG neighbors in the absence of barrier (p <0.05), and in the BC neighbors in both presence and absence of the barriers (p <0.05-0.01), both at close locations (Figure 4.8A). The ^{13}C and ^{15}N excesses in the roots of BES plants were not significantly correlated to each other. In none of the plants there were significant correlations between ^{13}C and ^{15}N excesses at the far locations (p >0.05).

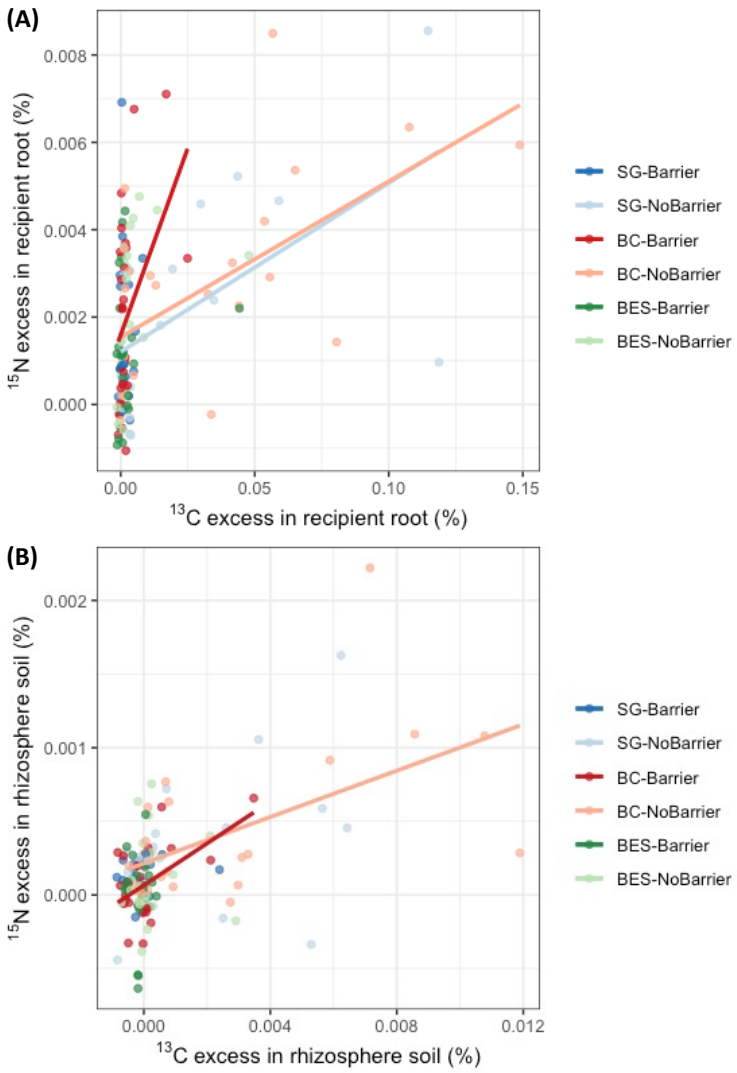

Recipient	Barrier	Roots		Rhizo. soils	
		r^2	p-value	r^2	p-value
SG	Barrier	0.01	0.960	0.02	0.594
	NoBarrier	**0.35**	**0.012**	0.19	0.079
BC	Barrier	**0.20**	**0.023**	**0.28**	**0.005**
	NoBarrier	**0.36**	**0.002**	**0.31**	**0.004**
BES	Barrier	0.03	0.432	0.01	0.985
	NoBarrier	0.13	0.097	0.01	0.888

Figure 4.8. Relationships between atom % ^{13}C and ^{15}N excesses in the roots (A) and the rhizosphere soils (B) adjacent to the roots of recipient SG, BC, and BES at close location from the source SG. The table presents coefficients (r^2) and p-values of linear regression models, and models significant at p <0.05 are in bold. Shown on figures are observations from barrier and non-barrier treatments (darker and lighter dots, respectively) and the linear regressions fitted to the data (darker and lighter lines, respectively). Fitted lines are not shown on the figures when regressions were not statistically significant (p >0.05).

4.3.3 ^{13}C and ^{15}N excesses in rhizosphere soils of recipient plants

The presence of the barrier led to lower ^{13}C enrichment of rhizosphere soils (p <0.001) (Table 4.7). The ^{13}C enrichment at the close location was generally greater than that at the far location (p <0.001) (Table S6), and when SG and BC were the recipient species, in the absence of barriers, rhizosphere soils were ^{13}C enriched only at the close location (p < 0.01) (Figure 4.9A). On the contrary, rhizosphere soils of BES recipient plant were not ^{13}C enriched at either close or far locations (p >0.05) (Figure 4.9A), similar to the trend of the ^{13}C enrichment in their roots (Figure 4.6A). When two different species were co-planted alongside the source SG, i.e., in BC-SG-BES plant combination (Table 4.2), the results of ^{13}C excess in the rhizosphere soils of BC and BES recipients (Figure 4.9B) were very similar to those of their respective two-species combinations (Figure 4.9A), having greater ^{13}C excess in BC recipients than that of the BES recipients at the close location.

Table 4.7. ANOVA F-test results with p-values for effects of recipient plant species, barrier conditions, sampling locations, and their interaction on ^{13}C and ^{15}N atom % excesses in rhizosphere soils of recipient plants in four plant combinations. Significant effects (p < 0.05) in the ANOVA table are shown in bold.

	^{13}C excess		^{15}N excess	
Effect	F-value	p-value	F-value	p-value
Recipient	**3.21**	**0.013**	**6.93**	**<0.001**
Barrier	**24.28**	**<0.001**	**9.53**	**0.002**
Location	**18.24**	**<0.001**	**9.00**	**0.003**
Recipient × Barrier	**2.41**	**0.049**	1.59	0.178
Recipient × Location	**3.44**	**0.009**	0.28	0.890
Barrier × Location	**11.81**	**0.001**	3.72	0.065
Recipient × Barrier × Location	2.29	0.069	2.23	0.085

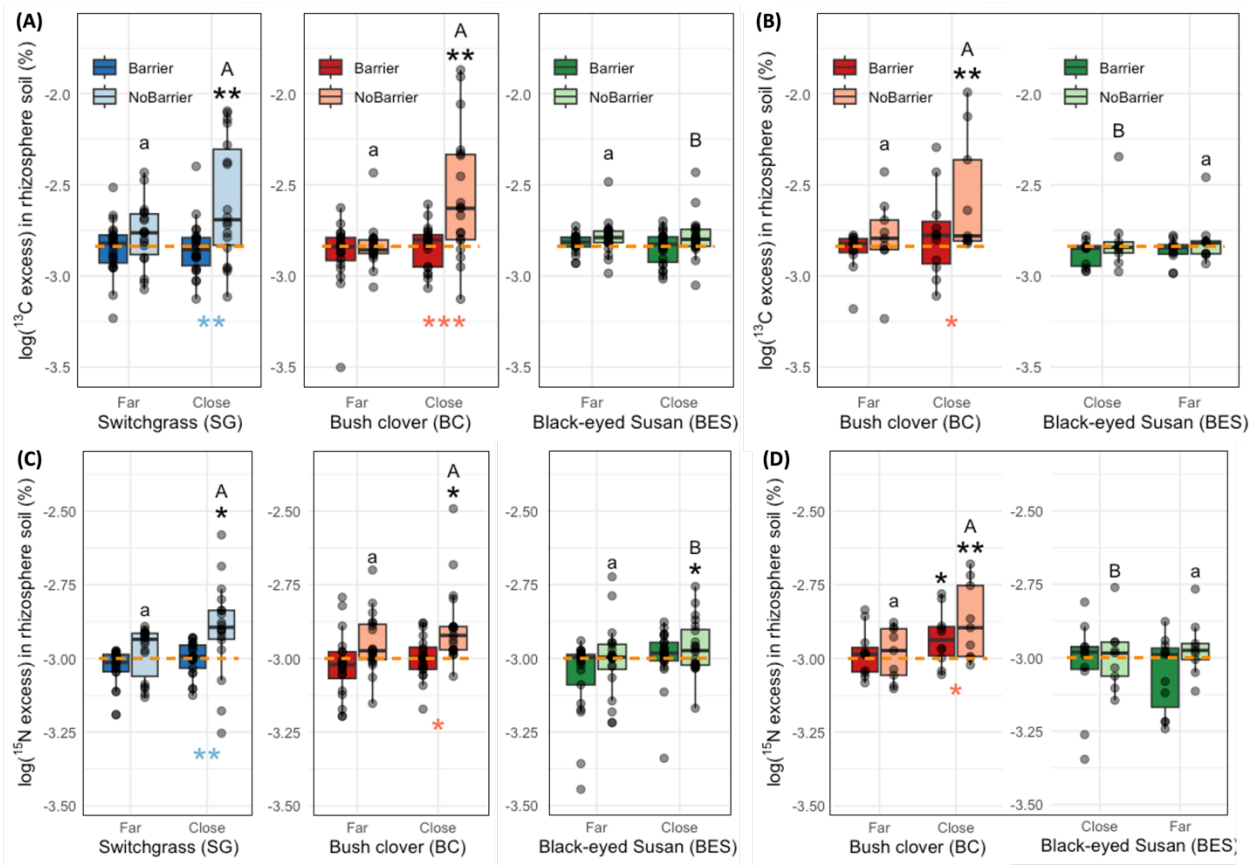

Figure 4.9. Atom % ^{13}C (A and B) and ^{15}N (C and D) excesses in rhizosphere soils of recipient plants neighboring the ^{13}C labeled, thereby the source SG in the four studied plant combinations (Table 4.2): SG-SG-SG, BC-SG-BC, and BES-SG-BES, which have the same species of the non-labeled plants at both sides (A and C) and BC-SG-BES with BC and BES sides presented separately (B and D). Results obtained at close and far distances from the source plants are reported separately. Note that to ensure that data from all distances and plant combinations are clearly visible on the same graph we show the data in a log scale, and due to the negative values in % ^{13}C and ^{15}N excess, a constant value was added to the data prior to the log transformation. Dots represent individual data points. The black * and ** marks above the box plots denote that ^{13}C and ^{15}N excesses significantly exceed non-labelled controls (yellow dashed line) at p <0.05 and 0.01 level, respectively. Colored *, **, and *** marks under the adjacent two boxes within each sampling location indicate significant differences between barrier and non-barrier treatments within the location at p <0.05, 0.01, and 0.001 level, respectively. Different uppercase letters on the boxes indicate significant differences among three recipient species across four plant combinations within non-barrier treatments in the close location (p <0.05), and different lowercase letters indicate significant differences in the far location (p <0.05). Letters are not shown within barrier treatments, as differences were not statistically significant among the species (p >0.05).

The ^{15}N enrichment of the rhizosphere soils at the close location was also higher than at the far (p <0.01) (Table 4.7). Similar to the ^{13}C enrichment in rhizosphere soils, ^{15}N enrichment was detected at the close location with the absence of barriers in the two-species combinations (p <0.05) (Figure 4.9C), i.e., SG-SG-SG and BC-SG-BC (Table 4.2). The presence of the barrier generally led to lower soil ^{15}N enrichment compared to its absence (p <0.01) (Table 4.7), and one exception was BES recipients having comparable barrier effects (p >0.05) (Figure 4.9C). Notably, in BC-SG-BES plant combination, the ^{15}N enrichment of BC rhizosphere soils was detected with the presence of barriers (p <0.05) (Figure 4.9D), while it was not found in BC soils of the BC-SG-BC combination (Figure 4.9C).

At the close location, ^{13}C excesses in rhizosphere soils were positively associated with ^{13}C excesses in roots in all three recipient species, when there were no barriers between the source and recipients (p <0.05-0.001) (Figure 4.10A). In the presence of barrier, significant positive association between the rhizosphere soil and root ^{13}C excesses was observed only in SG recipient (p <0.001). The ^{15}N excess in rhizosphere soils from the close location were also positively associated with the ^{15}N excess in roots in both barrier conditions in all three recipient species (p <0.05-0.01) (Figure 4.10B). An exception with no significant correlation was SG recipients in the presence of barriers (p >0.05).

Significant correlations between ^{13}C and ^{15}N excesses in the rhizosphere soil of the recipient plants were observed only in BC recipient both in the presence and the absence of barriers (p <0.01) (Figure 4.8B). The ^{13}C and ^{15}N excesses in the rhizosphere of SG and BES plants were not significantly correlated to each other (p >0.05), and in none of the recipient plants, there were significant correlations observed at the far locations (p >0.05).

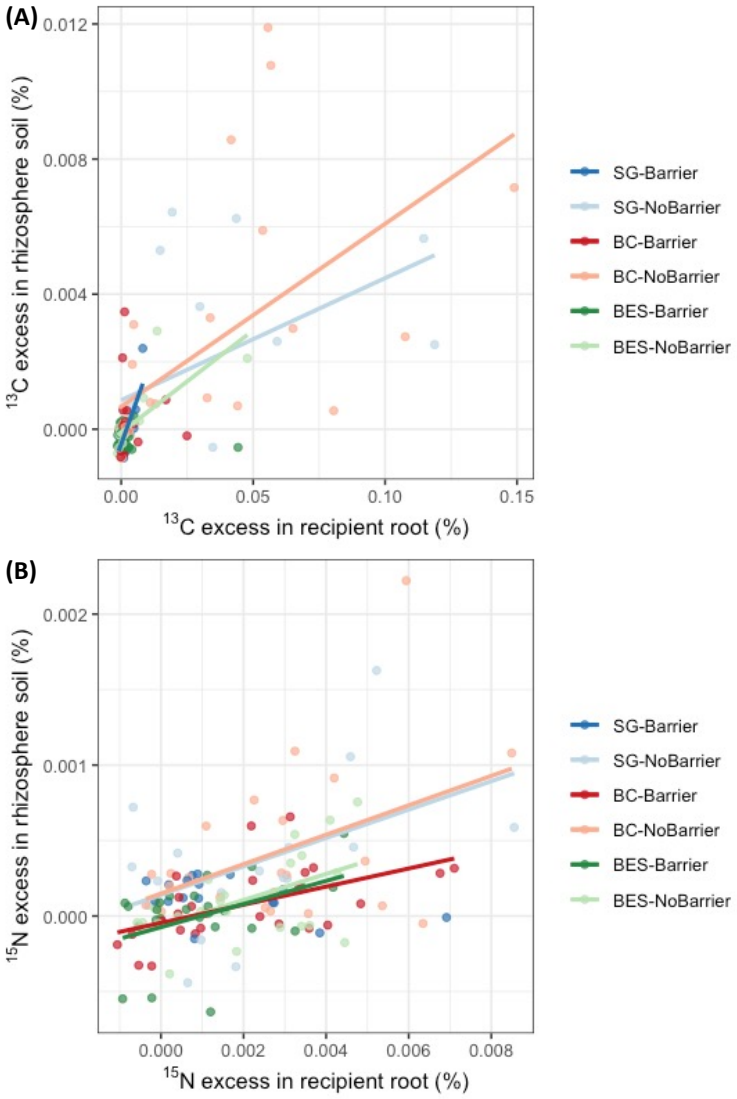

Recipient	Barrier	^{13}C excess		^{15}N excess	
		r^2	p-value	r^2	p-value
SG	Barrier	**0.57**	**<0.001**	0.17	0.089
	NoBarrier	**0.28**	**0.013**	**0.23**	**0.018**
BC	Barrier	0.01	0.73	**0.29**	**0.005**
	NoBarrier	**0.34**	**0.001**	**0.20**	**0.026**
BES	Barrier	0.05	0.194	**0.20**	**0.026**
	NoBarrier	**0.56**	**<0.001**	**0.28**	**0.012**

Figure 4.10. Relationships of atom % ^{13}C (A) and ^{15}N (B) excesses between the roots and the rhizosphere soils adjacent to the roots of recipient SG, BC, and BES at close location from the source SG. The table presents coefficients (r^2) and p-values of linear regression models, and models significant at p <0.05 are in bold. Shown on figures are observations from barrier and non-barrier treatments (darker and lighter dots, respectively) and the linear regressions fitted to the data (darker and lighter lines, respectively). Fitted lines are not shown on the figures when regressions were not statistically significant (p >0.05).

4.3.4 Soil pores between source SG and recipient plants

When SG and BC were recipient species, fractions of finer pores (8-30 µm Ø) in soils between the source and recipients with the absence of the barrier were approximately 70% and 50% greater than that in soils with its presence (p <0.01), respectively, and approximately 75% greater than that in control soils without plants (p <0.001) (Figure 4.11A and 4.11B). In contrast, fractions of medium (30-150 µm Ø) and coarser pores (>150 µm Ø) in such soils were approximately 20% (p <0.01) and 60% (p <0.001) smaller than those in the non-planted control soils, respectively. Notably, with the presence of the barrier between the source and recipient BC, finer pore and coarser pore fractions were slightly greater (p <0.01) and smaller (p <0.01) than those of the non-planted control, respectively (Figure 4.11B). When BES plants were the recipient species, pore fractions in three size ranges were not significantly different from those of the non-planted control in both barrier conditions (p >0.05) (Figure 4.11C).

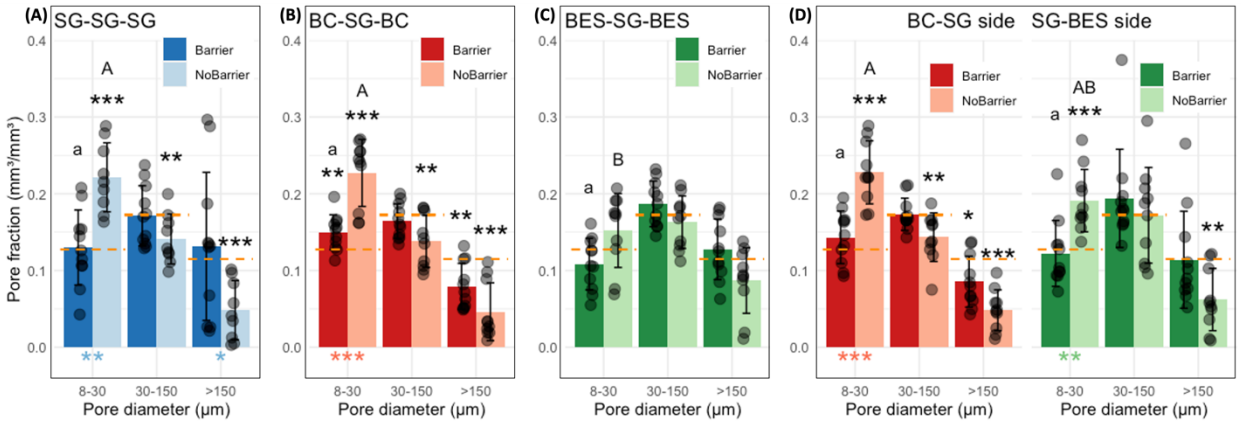

Figure 4.11. Fractions of pores of three size ranges (8-30, 30-150, and >150 µm Ø) in the soils between source SG and recipient SG (A), BC (B), and BES (C) in SG-SG-SG, BC-SG-BC, and BES-SG-BES plant combination (Table 4.2), and between source SG and BC side or between source SG and BES side in BC-SG-BES plant combination (D). Error bars and dots represent standard deviations and individual data points, respectively. Black *, **, and *** marks above the bar graphs denote that pore fractions were significantly greater or less than the fractions of non-planted controls (yellow dashed lines) at p <0.05, 0.01, and 0.001 level, respectively. Marked *, **, and *** with corresponding colors to the bars of recipient species and located below the adjacent two bars within each size range indicate significant differences between barrier and non-barrier treatments within the size at p <0.05, 0.01, and 0.001 level, respectively. Different uppercase letters on the bars indicate significant differences at p <0.05 among recipient plants in the four plant combinations without barriers, and different lowercase letters indicate differences with barriers. Marks and letters are not shown when differences were not statistically significant (p >0.05).

When BES was co-planted with the BC in BC-SG-BES plant combination, finer and coarser pore fractions between the source SG and BES recipient side became greater (p <0.001) and smaller (p <0.01) than those of the non-planted control, respectively (Figure 4.11D). For the BC recipient side, the trend was similar to that in the BC-SG-BC combination (Figure 4.11B and 4.11D), while for the BES recipient side, the deviations from the non-planted control were much more pronounced in BC-SG-BES than in BES-SG-BES combination (p <0.001 in finer pore and p <0.01 in coarser pore fractions) (Figure 4.11C and 4.11D).

The finer pores showed differences in pore fractions among four plant combinations in the absence of barriers, and fractions of these pores followed the trend: SG-SG-SG ~ BC-SG-BC ~ BC side of BC-SG-BES > BES side of BC-SG-BES > BES-SG-BES (Fig. 4.11). Since soil porosities measured using the images were not significantly different among all plant combinations and between two barrier conditions, given differences were derived by changes in soil structure (Figure 4.12).

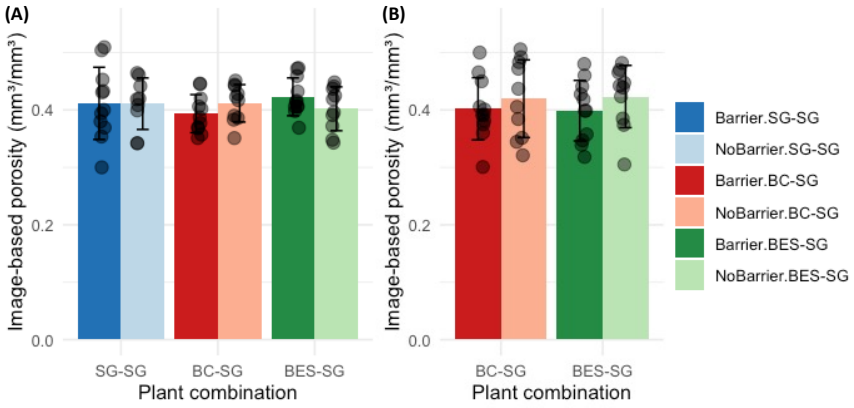

Figure 4.12. Image-based porosity of soils between source SG and recipient SG, BC, and BES (A) in SG-SG-SG, BC-SG-BC, and BES-SG-BES plant combination, and between source SG and BC side or between source SG and BES side in BC-SG-BES plant combination (B) (Table 4.2). Error bars and dots represent standard deviations and individual data points, respectively. Differences between two barrier conditions or among recipient species were not significant (p >0.05), thereby not shown.

In the absence of the barrier, the root residues were positively associated with fractions of finer pores for all three recipient plants (r^2 = 0.47 and p <0.01; r^2 = 0.38 and p <0.05; r^2 = 0.41 and p <0.05 in SG, BC, and BES, respectively). Alternatively, they were negatively associated with fractions of coarser pores (r^2 = 0.45 and p <0.001; r^2 = 0.34 and p <0.05; r^2 = 0.33 and p <0.05 in SG, BC, and BES, respectively) (Figure 4.13).

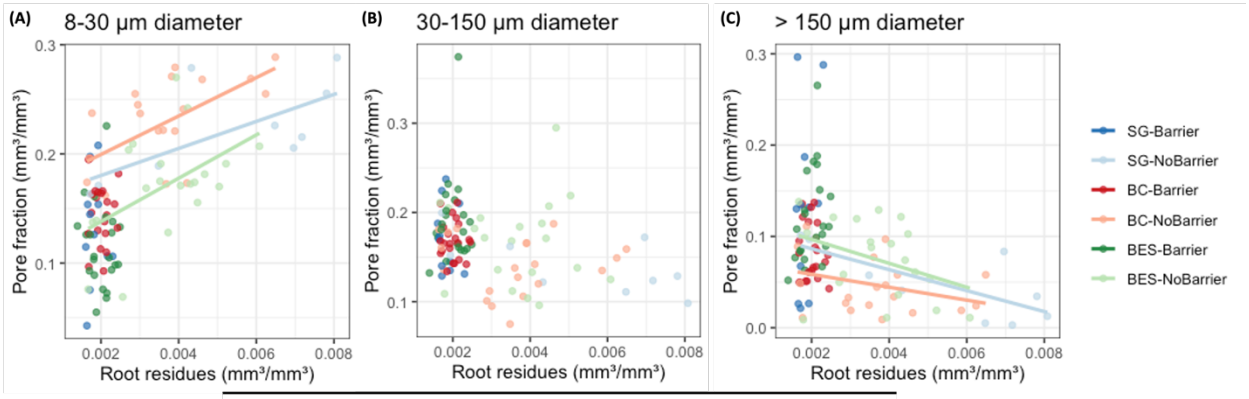

Recipient	Barrier	8-30 µm pores		30-150 µm pores		> 150 µm pores	
		r^2	*p*-value	r^2	*p*-value	r^2	*p*-value
SG	Barrier	0.01	0.918	0.02	0.644	0.11	0.329
	NoBarrier	**0.47**	**0.004**	0.34	0.052	**0.45**	**0.009**
BC	Barrier	0.01	0.700	0.01	0.742	0.02	0.562
	NoBarrier	**0.38**	**0.038**	0.01	0.692	**0.34**	**0.046**
BES	Barrier	0.01	0.669	0.01	0.819	0.12	0.112
	NoBarrier	**0.41**	**0.025**	0.01	0.890	**0.33**	**0.048**

Figure 4.13. Relationships betweem fractions of root residues and fractions of pores in 8-30 (A), 30-150 (B), and > 150 µm (C) diameter size ranges. The table presents coefficients (r^2) and *p*-values of linear regression models, and models significant at $p < 0.05$ are in bold. Shown on figures are observations from barrier and non-barrier treatments (darker and lighter dots, respectively) and the linear regressions fitted to the data (darker and lighter lines, respectively). Fitted lines are not shown on the figures when regressions were not statistically significant ($p > 0.05$).

4.4 Discussion

SG-assimilated C was transferred via belowground mechanisms to neighboring plants. However, the extent of the transfer varied depending on the identity of the neighboring recipient (s), and the transfer in the presence of barriers (via fungal-only mechanism) was markedly lower than in the presence of barriers (via a combination of root-based and fungal-based mechanisms). The transfer of SG-assimilated N was more pronounced than that of C. It occurred through both fungal-only and the root-based mechanisms, and the transfer through the root-based ways was present regardless of the identity of the recipient plants. SG-assimilated C and N in the rhizosphere of the recipients were positively associated with those in the recipients' roots. Patterns in modifications in soil pore-size distributions were consistent with the C transfer patterns, demonstrating formation of fine pores where root-based C transfer occurred.

4.4.1 Mechanisms of C and N transfer

Rhizoboxes without barriers allowed C and N transfers through both root-based and fungal-based mechanisms (Figure 4.1A), and the installation of mesh barriers successfully restricted such transfers

through root contacts. This can be supported by the absence of root residues within the mesh barriers while significantly greater root residues were found without barriers compared to the non-planted control in all plant combinations (Figure 4.4).

^{13}C and ^{15}N enrichment in recipient roots revealed that fungal-based C and N transfers could occur (Figure 4.6). However, the extent of the fungal-based C transfer was significantly less compared to that of the root-based C transfer, whereas N transfer remained comparable between the two mechanisms. This phenomenon can be explained by the molecular size and complexity of C and N compounds that mycorrhizal networks obtain from source roots and transport to their recipients. Mycorrhizal fungi efficiently transport smaller molecules such as amino acids, NH_4^+, and NO_3^- through their extensive hyphal networks (López-Pedrosa et al., 2006; Parniske, 2008; Whiteside et al., 2012). This contrasts with larger C compounds such as glycogen granules and lipid droplets, which are synthesized from hexoses obtained from the source plant (Pfeffer et al., 1999; Keymer et al., 2017). Such C-rich molecules can have greater challenges for transport through hyphal networks due to their relatively large size and structural complexity, while smaller compounds are more readily transported through these networks (Wang et al., 2018; Salvioli di Fossalunga and Novero, 2019). This implies that the movement of the C-rich compounds may require more direct pathway, i.e., root-based transfer mechanisms, and this differential transport capability likely influenced the discrepancy in this study, particularly between extents of C and N transfers to SG and BES recipients (Figure 4.6).

The discrepancy in barrier effects between C and N transfers may also be attributed to the high demand and rapid uptake of N by soil microorganisms. Once N is released into the soil, it tends to be immediately assimilated by soil microorganisms (Jones et al., 2005; Kuzyakov and Xu, 2013), leaving little available N in the soil for transfer to recipient roots (Luo et al., 2006). This rapid microbial uptake may lead to N transfers through more direct and specified pathways such as the mycorrhizae-based mechanism, which facilitate the efficient delivery of N directly to the recipient plants.

Pfeffer et al. (2004) reported a case of the unidirectional C flow within arbuscular mycorrhizal symbiosis and implied C transfer from the plant to the fungus, not being assimilated back into recipient

plants but largely retained within the intraradical mycelium of fungi in their symbiotic roots. This unidirectional flow, possibly occurred in our study, could restrict fungal-based C transfer, thus the root-based C transfer was predominant (Figure 4.6). This phenomenon might also elucidate very little extents of the C transfer detected at far locations of recipient SG and BC (Figure 4.6A). Recipient shoots, which were not ^{13}C enriched, can support that the shoot biomass of recipient plants did not assimilate the transferred C from the source SG (Figure 4.7A and 4.7B), thereby could not have capability to redistribute C to the other sides of recipient roots. On the contrary, mycorrhizal symbiotic roots could utilize forms of the transferred N for their further growth (Govindarajulu et al., 2005; Parniske, 2008), having enriched ^{15}N in their shoot biomass (Figure 4.7C and 4.7D), and such N was able to be moved to the other sides.

The potential reach of mycorrhizal hyphae was reported to extend up to 15 cm from their symbiotic root (Muneer et al., 2020a, 2020b; Shen et al., 2020) with the spread of up to 111 m cm^{-3} hyphae in soil (Miller et al., 1995). This could be a plausible reason for the fungal-based C transfers to the BC recipient within the 13 cm distance from the source to the far location of recipient roots (Figure 4.8A), as legume species are known to promote the development of mycorrhizal hyphae due to their strong rhizobium symbiotic relationship (de Novais et al., 2020; Liu et al., 2020, 2021).

4.4.2 C and N input into rhizosphere while their transfer

Root can release C compounds as exudates and rhizodeposits (Jones et al., 2009), and such root-derived C compounds and decomposed root and fungal biomass substantially contribute to soil organic C pools (Jones et al., 2004; Badri and Vivanco, 2009). Indeed, ^{13}C enrichment in rhizosphere soils was detected with the absence of the barrier in recipient plant species of the one- and two-species plant combinations, i.e., SG-SG-SG and BC-SG-BC, where the root-based C transfer occurred (Figure 4.6A and 4.9A). This also aligns with the recent finding by Kravchenko et al. (2021), demonstrating the plant-derived C input, which was promoted by the C transfer. Positive associations of ^{13}C excesses between roots and rhizosphere soils can support the plant-derived C input during the root-based C transfer (Figure 4.10A).

Notably, unlikely to the trend of ^{15}N enrichment in roots (Figure 4.6), the presence of the barrier led to lower ^{15}N enrichment in rhizosphere soils in SG and BC recipients of the one- and two-species

combination and BC recipients of the three-species combination, i.e., BC-SG-BES, compared to the absence of the barrier (Figure 4.9). This implies that the amount of the released N in rhizosphere soils was not significant, while transferred to the corresponding roots through the fungal-based mechanism. Although N is taken up as forms of NO_3^- and NH_4^+ by fungal hyphae (López-Pedrosa et al., 2006), it is transported as arginine, which is relatively stable against release, during the transfer to the connected roots (Govindarajulu et al., 2005).

4.4.3 Influence of recipient species on C and N transfer

Roots are known to grow towards N-enriched locations within the soil, and legumes enrich soil N (Ruffel et al., 2011; Guan et al., 2014; Mounier et al., 2014). Indeed, NO_3^- and NH_4^+ contents in soils under BC recipient plants were greater than those under BES recipients in the BC-SG-BES combination (Figure 4.5B and 4.5D). This implies more root branching possibly occurred towards this legume plant due to the soil N enrichment, potentially facilitating closer proximity and enhanced element exchange between the source and the legume plant (Figure 4.6A and 4.6B).

Interestingly, in the BC-SG-BES combination containing the legume plant, ^{13}C enrichment was found in BES roots (Figure 4.6B), while BES roots were not ^{15}N enriched in the BES-SG-BES combination (Figure 4.6A). Moreover, ^{15}N excess in BES roots in the combination with the presence of the legume exceeded that of the non-labeled BES at the more distant locations in (Figure 4.6D), in contrast to the exceeded ^{15}N within the close location in the BES-SG-BES combination without the legume (Figure 4.6C). Non-legume plants involved in a plant community plays roles for rapidly depleting the available N in soil and resulting in higher N_2 fixation in companion legumes (Viera-Vargas et al., 1995). Such stimulatory interactions between legumes and non-legumes enhanced the total N uptake by plants in the community (Nyfeler et al., 2011). Moreover, legumes synergistically interact with non-legume species that often have more fibrous root systems, enhancing soil nutrient dynamics (Mahieu et al., 2009; Chapagain and Riseman, 2014), and such mixture can promote efficient N transfer, facilitated by arbuscular mycorrhizal fungi, which form symbiotic relationships possibly with non-leguminous plants in their plant community (Mahieu et al., 2009; Chapagain and Riseman, 2015; Suter et al., 2015).

4.4.4 Fine pore formation and potential for C storage

The response of pore size distributions within the rhizobox dividers to plant neighbor and barrier effects followed the same pattern as that of ^{13}C transfer. Specifically, changes in pore size distributions compared to those of the no-plant controls were observed in SG and BC, but not BES recipients, and were more pronounced in the absence of the barriers.

In the observed plant combinations, there were notable increases in the volume of finer pores (8-30 μm Ø) and decreases in that of coarser pores (>150 μm Ø) within soils (Figure 4.11) where greater root-based transfers of C and N occurred (Figure 4.6). Since image-based porosity did not differ among the plant combinations and was not affected by the presence of the barrier (Figure 4.12), such modifications in the pore structure could be attributed to the reorganization of soil particles via root activity of different plant combinations. Root growth can lead to soil compaction as well as the subsequent formation of air-gaps in close proximity to the root, after its senescence and shrinking (Lucas et al., 2019; Phalempin et al., 2021; Lee et al., 2023b), and such air-gaps can form finer pores around the root (Aravena et al., 2011; Liu et al., 2022). The physical compaction can also lead either full or partial collapsing of coarser pores (Aravena et al., 2011; Pandey et al., 2021). Moreover, root exudates and rhizodeposits together with fluctuations in the soil moisture due to root's water uptake could have led to enhanced formation of finer pores and rearrangement of the pore space (Oburger and Schmidt, 2016; Jin et al., 2017). The observed positive correlations between root residues and the formation of finer pores, alongside the reduction in coarser pores, in all plant combinations support the potential influence of roots on fine pore formation (Figure 4.13).

One notable observation was that there were increases in finer pores and decreases in coarser pores with the presence of the barrier in BC recipient soils (Figure 4.11B and 4.11D) where significant fungal-based transfers occurred (Figure 4.6). Fungi are known to substantially impact the pore structure as well, and in the soils accessible by fungi, the volume of >10 μm Ø pores doubled compared to that in fungi-inaccessible soils separated by barriers (Feeney et al., 2006; Hallett et al., 2009).

Such finer pores play a critical role in long-term soil C storage due in part to their not sufficient size to accommodate a large microbial community and limited oxygen supplies, potentially hinder

microbial activity and subsequent decomposition of organic matter (Bailey et al., 2017; Kravchenko et al., 2019; Franklin et al., 2021). Plant combinations that facilitated greater C transfers might enhance C accumulation within such newly-formed fine pores (Figure 4.6 and 4.11), because the root-based transfers released C into the soil (Figure 4.10A), and pores in this size are readily accessible to fungal hyphae (2-20 μm Ø) from the roots (Smith and Smith, 2011). Quigley and Kravchenko (2022) recently found positive correlations between root-derived C and fine pores, which were not accessible to roots, suggesting fungal-derived C could enter such pores and be protected from further decomposition.

4.5 Conclusions

This greenhouse experiment with ^{13}C and ^{15}N isotope labeling and tracing reveals that fungal-based C and N transfer occur from SG to recipient BC and BES, native prairie species, as well as to the other SG that was grown together. The root-based C transfer was the predominant mechanism, while N was effectively transferred via mycorrhizal networks. Notably, the presence of BC plants, legume species, enhanced the transfer of both C and N not only to their side but also to co-planted BES side. Both transfer mechanisms led to notable increases in C and N within the rhizosphere soils, and newly formed fine pores via the root growth could possibly provide the protective storage for the rhizosphere C inputs. These findings suggest that root interactions, aided by mycorrhizal networks, are likely to play a critical role in C and N exchanges and concomitant soil C accumulation in native prairie vegetation.

4.6 Acknowledgements

I appreciate Mark Rivers for conducting soil core scanning at Argonne National Laboratory and Maxwell Oerther and Tayler Ulbrich for assistance with sample collection. Support for this research was provided by the Great Lakes Bioenergy Research Center, U.S. Department of Energy, Office of Science, Office of Biological and Environmental Research (Award DE-SC0018409), by the National Science Foundation Long-term Ecological Research Program (DEB 2224712) at the Kellogg Biological Station, and by Michigan State University AgBioResearch.

REFERENCES

Abadi, M., P. Barham, J. Chen, Z. Chen, A. Davis, J. Dean, M. Devin, et al. (2016). TensorFlow: A System for Large-Scale Machine Learning. 265–283.

Aibara, I., and K. Miwa. 2014. Strategies for Optimization of Mineral Nutrient Transport in Plants: Multilevel Regulation of Nutrient-Dependent Dynamics of Root Architecture and Transporter Activity. *Plant and Cell Physiology* 55: 2027–2036.

An, Q.-Q., S.-Q. Wang, J.-Y. Kang, Z. Wang, Y.-L. Chen, and B.-C. Xu. (2022). Fine root distribution and morphological characteristics of switchgrass under different row spacings on semi-arid Loess Plateau, China. *Archives of Agronomy and Soil Science* 68: 1–17.

Aravena, J. E., M. Berli, T. A. Ghezzehei, and S. W. Tyler. (2011). Effects of Root-Induced Compaction on Rhizosphere Hydraulic Properties - X-ray Microtomography Imaging and Numerical Simulations. *Environmental Science & Technology* 45: 425–431.

Badri, D. V., and J. M. Vivanco. 2009. Regulation and function of root exudates. *Plant, Cell & Environment* 32: 666–681.

Bailey, V. L., A. P. Smith, M. Tfaily, S. J. Fansler, and B. Bond-Lamberty. (2017). Differences in soluble organic carbon chemistry in pore waters sampled from different pore size domains. *Soil Biology and Biochemistry* 107: 133–143.

Bauhus, J., and C. Messier. (1999). Soil exploitation strategies of fine roots in different tree species of the southern boreal forest of eastern Canada. *Canadian Journal of Forest Research* 29: 260–273.

Bengough, A. G., K. Loades, and B. M. McKenzie. (2016). Root hairs aid soil penetration by anchoring the root surface to pore walls. *Journal of Experimental Botany* 67: 1071–1078.

Björkman, E. (1960). Monotropa Hypopitys L. — an Epiparasite on Tree Roots. *Physiologia Plantarum* 13: 308–327.

Boer, M. D., J. Santos Teixeira, and K. H. Ten Tusscher. (2020). Modeling of Root Nitrate Responses Suggests Preferential Foraging Arises From the Integration of Demand, Supply and Local Presence Signals. *Frontiers in Plant Science* 11.

Buades, A., B. Coll, and J.-M. Morel. (2011). Non-Local Means Denoising. *Image Processing On Line* 1: 208–212.

Burns, R. G., J. L. DeForest, J. Marxsen, R. L. Sinsabaugh, M. E. Stromberger, M. D. Wallenstein, M. N. Weintraub, and A. Zoppini. (2013). Soil enzymes in a changing environment: Current knowledge and future directions. *Soil Biology and Biochemistry* 58: 216–234.

Cahanovitc, R., S. Livne-Luzon, R. Angel, and T. Klein. (2022). Ectomycorrhizal fungi mediate belowground carbon transfer between pines and oaks. *The ISME Journal* 16: 1420–1429.

Carey, E. V., M. J. Marler, and R. M. Callaway. (2004). Mycorrhizae transfer carbon from a native grass to an invasive weed: evidence from stable isotopes and physiology. *Plant Ecology* 172: 133–141.

Carlile, M. J. 1995. The Success of the Hypha and Mycelium. *In* N. A. R. Gow, and G. M. Gadd [eds.], The Growing Fungus, 3–19. Springer Netherlands, Dordrecht.

Chapagain, T., and A. Riseman. (2014). Barley–pea intercropping: Effects on land productivity, carbon and nitrogen transformations. *Field Crops Research* 166: 18–25.

Chapagain, T., and A. Riseman. (2015). Nitrogen and carbon transformations, water use efficiency and ecosystem productivity in monocultures and wheat-bean intercropping systems. *Nutrient Cycling in Agroecosystems* 101: 107–121.

Chu, G., Q. Shen, Y. Li, J. Zhang, and S. Wang. (2004). Researches on Bi-directional N transfer between the intercropping system of groundnut with rice cultivated in aerobic soil using ^{15}N foliar labelling metho. *Acta Ecologica Sinica* 24: 278–284.

Cox, F., N. Barsoum, E. A. Lilleskov, and M. I. Bidartondo. (2010). Nitrogen availability is a primary determinant of conifer mycorrhizas across complex environmental gradients. *Ecology Letters* 13: 1103–1113.

Darbon, J., A. Cunha, T. F. Chan, S. Osher, and G. J. Jensen. (2008). Fast nonlocal filtering applied to electron cryomicroscopy. 2008 5th IEEE International Symposium on Biomedical Imaging: From Nano to Macro, 1331–1334. IEEE, Paris, France.

Doane, T. A., and W. R. Horwáth. (2003). Spectrophotometric Determination of Nitrate with a Single Reagent. *Analytical Letters* 36: 2713–2722.

Falik, O., P. Reides, M. Gersani, and A. Novoplansky. (2003). Self/Non-Self Discrimination in Roots. *Journal of Ecology* 91: 525–531.

Feeney, D. S., J. W. Crawford, T. Daniell, P. D. Hallett, N. Nunan, K. Ritz, M. Rivers, and I. M. Young. (2006). Three-dimensional Microorganization of the Soil–Root–Microbe System. *Microbial Ecology* 52: 151–158.

Franklin, S. M., A. N. Kravchenko, R. Vargas, B. Vasilas, J. J. Fuhrmann, and Y. Jin. (2021). The unexplored role of preferential flow in soil carbon dynamics. *Soil Biology and Biochemistry* 161: 108398.

Fry, B. (2006). Isotope Notation and Measurement. *In* B. Fry [ed.], Stable Isotope Ecology, 21–39. Springer, New York, NY.

Gelfand, I., S. K. Hamilton, A. N. Kravchenko, R. D. Jackson, K. D. Thelen, and G. P. Robertson. (2020). Empirical Evidence for the Potential Climate Benefits of Decarbonizing Light Vehicle Transport in the U.S. with Bioenergy from Purpose-Grown Biomass with and without BECCS. *Environmental Science & Technology* 54: 2961–2974.

Gorzelak, M. A., B. H. Ellert, and L. Tedersoo. (2020). Mycorrhizas transfer carbon in a mature mixed forest. *Molecular Ecology* 29: 2315–2317.

Govindarajulu, M., P. E. Pfeffer, H. Jin, J. Abubaker, D. D. Douds, J. W. Allen, H. Bücking, et al. (2005). Nitrogen transfer in the arbuscular mycorrhizal symbiosis. *Nature* 435: 819–823.

Guan, P., R. Wang, P. Nacry, G. Breton, S. A. Kay, J. L. Pruneda-Paz, A. Davani, and N. M. Crawford. (2014). Nitrate foraging by Arabidopsis roots is mediated by the transcription factor TCP20 through the systemic signaling pathway. *Proceedings of the National Academy of Sciences* 111: 15267–15272.

Hallett, P. D., D. S. Feeney, A. G. Bengough, M. C. Rillig, C. M. Scrimgeour, and I. M. Young. (2009). Disentangling the impact of AM fungi versus roots on soil structure and water transport. *Plant and Soil* 314: 183–196.

He, X. H., C. Critchley, and C. Bledsoe. (2003). Nitrogen transfer within and between plants through common mycorrhizal networks (CMNs). *Critical Reviews In Plant Sciences* 22: 531–567.

Hildebrand, T., and P. Rüegsegger. (1997). A new method for the model-independent assessment of thickness in three-dimensional images. *Journal of Microscopy* 185: 67–75.

Høgh-Jensen, H., and J. K. Schjoerring. (2000). Below-ground nitrogen transfer between different grassland species: Direct quantification by 15N leaf feeding compared with indirect dilution of soil 15N. *Plant and Soil* 227: 171–183.

Hupe, A., F. Naether, T. Haase, C. Bruns, J. Heß, J. Dyckmans, R. G. Joergensen, and F. Wichern. (2021). Evidence of considerable C and N transfer from peas to cereals via direct root contact but not via mycorrhiza. *Scientific Reports* 11: 11424.

Jin, K., P. J. White, W. R. Whalley, J. Shen, and L. Shi. (2017). Shaping an Optimal Soil by Root–Soil Interaction. *Trends in Plant Science* 22: 823–829.

Jones, D. L., J. R. Healey, V. B. Willett, J. F. Farrar, and A. Hodge. (2005). Dissolved organic nitrogen uptake by plants—an important N uptake pathway? *Soil Biology and Biochemistry* 37: 413–423.

Jones, D. L., A. Hodge, and Y. Kuzyakov. (2004). Plant and mycorrhizal regulation of rhizodeposition. *New Phytologist* 163: 459–480.

Jones, D. L., C. Nguyen, and R. D. Finlay. (2009). Carbon flow in the rhizosphere: carbon trading at the soil–root interface. *Plant and Soil* 321: 5–33.

Karlovsky, P. (2008). Secondary Metabolites in Soil Ecology. *In* P. Karlovsky [ed.], Secondary Metabolites in Soil Ecology, Soil Biology, 1–19. Springer, Berlin, Heidelberg.

Keiluweit, M., P. S. Nico, M. Kleber, and S. Fendorf. (2016). Are oxygen limitations under recognized regulators of organic carbon turnover in upland soils? *Biogeochemistry* 127: 157–171.

Kellermeier, F., P. Armengaud, T. J. Seditas, J. Danku, D. E. Salt, and A. Amtmann. (2014). Analysis of the Root System Architecture of Arabidopsis Provides a Quantitative Readout of Crosstalk between Nutritional Signals. *The Plant Cell* 26: 1480–1496.

Keymer, A., P. Pimprikar, V. Wewer, C. Huber, M. Brands, S. L. Bucerius, P.-M. Delaux, et al. (2017). Lipid transfer from plants to arbuscular mycorrhiza fungi G. Stacey [ed.],. *eLife* 6: e29107.

Kravchenko, A. N., A. K. Guber, B. S. Razavi, J. Koestel, E. V. Blagodatskaya, and Y. Kuzyakov. (2019). Spatial patterns of extracellular enzymes: Combining X-ray computed micro-tomography and 2D zymography. *Soil Biology and Biochemistry* 135: 411–419.

Kravchenko, A. N., H. Zheng, Y. Kuzyakov, G. P. Robertson, and A. K. Guber. (2021). Belowground interplant carbon transfer promotes soil carbon gains in diverse plant communities. *Soil Biology and Biochemistry* 159.

de Kroon, H. (2007). How Do Roots Interact? *Science* 318: 1562–1563.

Kuzyakov, Y., and X. Xu. (2013). Competition between roots and microorganisms for nitrogen: mechanisms and ecological relevance. *New Phytologist* 198: 656–669.

Lal, R. 2016. Soil health and carbon management. *Food and Energy Security* 5: 212–222.

Lange, M., N. Eisenhauer, C. A. Sierra, H. Bessler, C. Engels, R. I. Griffiths, P. G. Mellado-Vázquez, et al. (2015). Plant diversity increases soil microbial activity and soil carbon storage. *Nature Communications* 6: 6707.

Lange, M., E. Koller-France, A. Hildebrandt, Y. Oelmann, W. Wilcke, and G. Gleixner. (2019). Chapter Six - How plant diversity impacts the coupled water, nutrient and carbon cycles. *In* N. Eisenhauer, D. A. Bohan, and A. J. Dumbrell [eds.], Advances in Ecological Research, Mechanisms underlying the relationship between biodiversity and ecosystem function, 185–219. Academic Press.

Lee, J. H., M. Lucas, A. K. Guber, and A. N. Kravchenko. (2023a). Pore structure in detritusphere of soils under switchgrass and restored prairie vegetation community. *TechRxiv*.

Lee, J. H., M. Lucas, A. K. Guber, X. Li, and A. N. Kravchenko. (2023b). Interactions among soil texture, pore structure, and labile carbon influence soil carbon gains. *Geoderma* 439: 116675.

Lee, T. D., P. B. Reich, and M. G. Tjoelker. (2003). Legume presence increases photosynthesis and N concentrations of co-occurring non-fixers but does not modulate their responsiveness to carbon dioxide enrichment. *Oecologia* 137: 22–31.

Li, Z., A. N. Kravchenko, A. Cupples, A. K. Guber, Y. Kuzyakov, G. Philip Robertson, and E. Blagodatskaya. (2024). Composition and metabolism of microbial communities in soil pores. *Nature Communications* 15: 3578.

Liu, A., Y.-S. Ku, C. A. Contador, and H.-M. Lam. (2020). The Impacts of Domestication and Agricultural Practices on Legume Nutrient Acquisition Through Symbiosis With Rhizobia and Arbuscular Mycorrhizal Fungi. *Frontiers in Genetics* 11.

Liu, H., Y. Wu, H. Xu, Z. Ai, J. Zhang, G. Liu, and S. Xue. (2021). N enrichment affects the arbuscular mycorrhizal fungi-mediated relationship between a C4 grass and a legume. *Plant Physiology* 187: 1519–1533.

Liu, Y.-F., L.-C. Meng, Z. Huang, Z.-H. Shi, and G.-L. Wu. (2022). Contribution of fine roots mechanical property of Poaceae grasses to soil erosion resistance on the Loess Plateau. *Geoderma* 426: 116122.

López-Bucio, J., A. Cruz-Ramírez, and L. Herrera-Estrella. (2003). The role of nutrient availability in regulating root architecture. *Current Opinion in Plant Biology* 6: 280–287.

López-Pedrosa, A., M. González-Guerrero, A. Valderas, C. Azcón-Aguilar, and N. Ferrol. (2006). *GintAMT1* encodes a functional high-affinity ammonium transporter that is expressed in the extraradical mycelium of *Glomus intraradices*. *Fungal Genetics and Biology* 43: 102–110.

Lucas, M., L. T. T. Nguyen, A. Guber, and A. N. Kravchenko. (2022). Cover crop influence on pore size distribution and biopore dynamics: Enumerating root and soil faunal effects. *Frontiers in Plant Science* 13: 928569.

Lucas, M., S. Schlüter, H.-J. Vogel, and D. Vetterlein. (2019). Roots compact the surrounding soil depending on the structures they encounter. *Scientific Reports* 9: 16236.

Luo, Y., C. B. Field, and R. B. Jackson. (2006). Does Nitrogen Constrain Carbon Cycling, or Does Carbon Input Stimulate Nitrogen Cycling?1. *Ecology* 87: 3–4.

Mahieu, S., F. Germon, A. Aveline, H. Hauggaard-Nielsen, P. Ambus, and E. S. Jensen. (2009). The influence of water stress on biomass and N accumulation, N partitioning between above and below ground parts and on N rhizodeposition during reproductive growth of pea (Pisum sativum L.). *Soil Biology and Biochemistry* 41: 380–387.

Maina, G. G., J. S. Brown, and M. Gersani. (2002). Intra-plant versus Inter-plant Root Competition in Beans: avoidance, resource matching or tragedy of the commons. *Plant Ecology* 160: 235–247.

Makovetsky, R., N. Piche, and M. Marsh. (2018). Dragonfly as a Platform for Easy Image-based Deep Learning Applications. *Microscopy and Microanalysis* 24: 532–533.

Martins, M. A. (1993). The role of the external mycelium of arbuscular mycorrhizal fungi in the carbon transfer process between plants. *Mycological Research* 97: 807–810.

Martins, M. A., and A. F. Cruz. (1998). The Role of the external mycelial network of arbuscular mycorrhizal fungi: III. a study of nitrogen transfer between plants interconnected by a common mycelium. *Revista de Microbiologia* 29: 289–294.

McNickle, G. G. (2020). Interpreting plant root responses to nutrients, neighbours and pot volume depends on researchers' assumptions. *Functional Ecology* 34: 2199–2209.

Miller, R. M., J. D. Jastrow, and D. R. Reinhardt. (1995). External hyphal production of vesicular-arbuscular mycorrhizal fungi in pasture and tallgrass prairie communities. *Oecologia* 103: 17–23.

Mounier, E., M. Pervent, K. Ljung, A. Gojon, and P. Nacry. (2014). Auxin-mediated nitrate signalling by NRT1.1 participates in the adaptive response of Arabidopsis root architecture to the spatial heterogeneity of nitrate availability. *Plant, Cell & Environment* 37: 162–174.

Mulder, C., A. Jumpponen, P. Högberg, and K. Huss-Danell. (2002). How plant diversity and legumes affect nitrogen dynamics in experimental grassland communities. *Oecologia* 133: 412–421.

Muneer, M. A., P. Wang, Zaib-un-Nisa, C. Lin, and B. Ji. (2020a). Potential role of common mycorrhizal networks in improving plant growth and soil physicochemical properties under varying nitrogen levels in a grassland ecosystem. *Global Ecology and Conservation* 24: e01352.

Muneer, M. A., P. Wang, J. Zhang, Y. Li, M. Z. Munir, and B. Ji. (2020b). Formation of Common Mycorrhizal Networks Significantly Affects Plant Biomass and Soil Properties of the Neighboring Plants under Various Nitrogen Levels. *Microorganisms* 8: 230.

de Novais, C. B., C. Sbrana, E. da Conceição Jesus, L. F. M. Rouws, M. Giovannetti, L. Avio, J. O. Siqueira, et al. (2020). Mycorrhizal networks facilitate the colonization of legume roots by a symbiotic nitrogen-fixing bacterium. *Mycorrhiza* 30: 389–396.

Nunan, N., K. Wu, I. M. Young, J. W. Crawford, and K. Ritz. (2003). Spatial distribution of bacterial communities and their relationships with the micro-architecture of soil. *FEMS Microbiology Ecology* 44: 203–215.

Oburger, E., and H. Schmidt. (2016). New Methods To Unravel Rhizosphere Processes. *Trends in Plant Science* 21: 243–255.

Pandey, B. K., G. Huang, R. Bhosale, S. Hartman, C. J. Sturrock, L. Jose, O. C. Martin, et al. (2021). Plant roots sense soil compaction through restricted ethylene diffusion. *Science* 371: 276–280.

Parniske, M. (2008). Arbuscular mycorrhiza: the mother of plant root endosymbioses. *Nature Reviews Microbiology* 6: 763–775.

Parrish, D. J., and J. H. Fike. (2005). The Biology and Agronomy of Switchgrass for Biofuels. *Critical Reviews in Plant Sciences* 24: 423–459.

Perry, S., G. Falvo, S. Mosier, and G. P. Robertson. (2023). Long-term changes in soil carbon and nitrogen fractions in switchgrass, native grasses, and no-till corn bioenergy production systems. *Soil Science Society of America Journal* n/a.

Pfeffer, P. E., D. D. Douds Jr., G. Bécard, and Y. Shachar-Hill. (1999). Carbon Uptake and the Metabolism and Transport of Lipids in an Arbuscular Mycorrhiza1. *Plant Physiology* 120: 587–598.

Pfeffer, P. E., D. D. Douds Jr, H. Bücking, D. P. Schwartz, and Y. Shachar-Hill. (2004). The fungus does not transfer carbon to or between roots in an arbuscular mycorrhizal symbiosis. *New Phytologist* 163: 617–627.

Phalempin, M., E. Lippold, D. Vetterlein, and S. Schlüter. (2021). Soil texture and structure heterogeneity predominantly governs bulk density gradients around roots. *Vadose Zone Journal* 20.

Quigley, M. Y., and A. N. Kravchenko. (2022). Inputs of root-derived carbon into soil and its losses are associated with pore-size distributions. *Geoderma* 410: 115667.

Reay, M. K., K. A. Pears, A. Kuhl, R. P. Evershed, P. J. Murray, L. M. Cardenas, J. A. J. Dungait, and I. D. Bull. (2022). Mechanisms of nitrogen transfer in a model clover-ryegrass pasture: a 15N-tracer approach. *Plant and Soil* 480: 369–389.

Reid, C. P. P., and F. W. Woods. (1969). Translocation of C^{14}-Labeled Compounds in Mycorrhizae and It Implications in Interplant Nutrient Cycling. *Ecology* 50: 179–187.

Ren, L., Y. Lou, N. Zhang, X. Zhu, W. Hao, S. Sun, Q. Shen, and G. Xu. (2013). Role of arbuscular mycorrhizal network in carbon and phosphorus transfer between plants. *Biology and Fertility of Soils* 49: 3–11.

Rillig, M. C. (2004a). Arbuscular mycorrhizae and terrestrial ecosystem processes. *Ecology Letters* 7: 740–754.

Rillig, M. C. (2004b). Arbuscular mycorrhizae, glomalin, and soil aggregation. *Canadian Journal of Soil Science* 84: 355–363.

Robinson, D., and A. Fitter. (1999). The magnitude and control of carbon transfer between plants linked by a common mycorrhizal network. *Journal of Experimental Botany* 50: 9–13.

Ronneberger, O., P. Fischer, and T. Brox. (2015). U-Net: Convolutional Networks for Biomedical Image Segmentation. *In* N. Navab, J. Hornegger, W. M. Wells, and A. F. Frangi [eds.], Medical Image Computing and Computer-Assisted Intervention – MICCAI 2015, Lecture Notes in Computer Science, 234–241. Springer International Publishing, Cham.

Roth, R., and U. Paszkowski. (2017). Plant carbon nourishment of arbuscular mycorrhizal fungi. *Current Opinion in Plant Biology* 39: 50–56.

Ruamps, L. S., N. Nunan, and C. Chenu. (2011). Microbial biogeography at the soil pore scale. *Soil Biology and Biochemistry* 43: 280–286.

Ruffel, S., G. Krouk, D. Ristova, D. Shasha, K. D. Birnbaum, and G. M. Coruzzi. (2011). Nitrogen economics of root foraging: Transitive closure of the nitrate–cytokinin relay and distinct systemic signaling for N supply vs. demand. *Proceedings of the National Academy of Sciences* 108: 18524–18529.

Salvioli di Fossalunga, A., and M. Novero. (2019). To trade in the field: the molecular determinants of arbuscular mycorrhiza nutrient exchange. *Chemical and Biological Technologies in Agriculture* 6: 12.

Sanderson, M. A., and P. R. Adler. (2008). Perennial Forages as Second Generation Bioenergy Crops. *International Journal of Molecular Sciences* 9: 768–788.

Sanford, G. R. (2014). Perennial Grasslands Are Essential for Long Term SOC Storage in the Mollisols of the North Central USA. *In* A. E. Hartemink, and K. McSweeney [eds.], Soil Carbon, Progress in Soil Science, 281–288. Springer International Publishing, Cham.

Schindelin, J., I. Arganda-Carreras, E. Frise, V. Kaynig, M. Longair, T. Pietzsch, S. Preibisch, et al. (2012). Fiji: an open-source platform for biological-image analysis. *Nature Methods* 9: 676–682.

Segonzac, C., J.-C. Boyer, E. Ipotesi, W. Szponarski, P. Tillard, B. Touraine, N. Sommerer, et al. (2007). Nitrate Efflux at the Root Plasma Membrane: Identification of an Arabidopsis Excretion Transporter. *The Plant Cell* 19: 3760–3777.

Shao, Z., X. Wang, Q. Gao, H. Zhang, H. Yu, Y. Wang, J. Zhang, et al. (2020). Root Contact between Maize and Alfalfa Facilitates Nitrogen Transfer and Uptake Using Techniques of Foliar 15N-Labeling. *Agronomy* 10: 360.

Shen, K., J. H. C. Cornelissen, Y. Wang, C. Wu, Y. He, J. Ou, Q. Tan, et al. (2020). AM Fungi Alleviate Phosphorus Limitation and Enhance Nutrient Competitiveness of Invasive Plants via Mycorrhizal Networks in Karst Areas. *Frontiers in Ecology and Evolution* 8.

Sinsabaugh, R. L., H. Reynolds, and T. M. Long. (2000). Rapid assay for amidohydrolase (urease) activity in environmental samples. *Soil Biology and Biochemistry* 32: 2095–2097.

Smith, F. A., E. J. Grace, and S. E. Smith. (2009). More than a carbon economy: nutrient trade and ecological sustainability in facultative arbuscular mycorrhizal symbioses. *New Phytologist* 182: 347–358.

Smith, S. E., and F. A. Smith. (2011). Roles of Arbuscular Mycorrhizas in Plant Nutrition and Growth: New Paradigms from Cellular to Ecosystem Scales. *Annual Review of Plant Biology* 62: 227–250.

Sprunger, C. D., and G. Philip Robertson. 2018. Early accumulation of active fraction soil carbon in newly established cellulosic biofuel systems. *Geoderma* 318: 42–51.

Stober, C., E. George, and H. Persson. (2000). Root Growth and Response to Nitrogen. *In* E.-D. Schulze [ed.], Carbon and Nitrogen Cycling in European Forest Ecosystems, 99–121. Springer, Berlin, Heidelberg.

Strong, D. T., H. D. Wever, R. Merckx, and S. Recous. (2004). Spatial location of carbon decomposition in the soil pore system: Spatial location of carbon decomposition. *European Journal of Soil Science* 55: 739–750.

Suter, M., J. Connolly, J. A. Finn, R. Loges, L. Kirwan, M.-T. Sebastià, and A. Lüscher. (2015). Nitrogen yield advantage from grass–legume mixtures is robust over a wide range of legume proportions and environmental conditions. *Global Change Biology* 21: 2424–2438.

Thilakarathna, M. S., M. S. McElroy, T. Chapagain, Y. A. Papadopoulos, and M. N. Raizada. (2016). Belowground nitrogen transfer from legumes to non-legumes under managed herbaceous cropping systems. A review. *Agronomy for Sustainable Development* 36: 58.

Thilakarathna, R. M. M. S., Y. A. Papadopoulos, A. V. Rodd, A. N. Gunawardena, S. A. E. Fillmore, and B. Prithiviraj. (2012). Characterizing nitrogen transfer from red clover populations to companion bluegrass under field conditions. *Canadian Journal of Plant Science* 92: 1163–1173.

Treseder, K. K., and S. R. Holden. (2013). Fungal Carbon Sequestration. *Science* 339: 1528–1529.

Vogel, H.-J., U. Weller, and S. Schlüter. (2010). Quantification of soil structure based on Minkowski functions. *Computers & Geosciences* 36: 1236–1245.

Walder, F., and M. G. A. van der Heijden. (2015). Regulation of resource exchange in the arbuscular mycorrhizal symbiosis. *Nature Plants* 1: 1–7.

Walder, F., H. Niemann, M. Natarajan, M. F. Lehmann, T. Boller, and A. Wiemken. (2012). Mycorrhizal Networks: Common Goods of Plants Shared under Unequal Terms of Trade. *Plant Physiology* 159: 789–797.

Walt, S. van der, J. L. Schönberger, J. Nunez-Iglesias, F. Boulogne, J. D. Warner, N. Yager, E. Gouillart, and T. Yu. (2014). scikit-image: image processing in Python. *PeerJ* 2: e453.

Wang, R., M. Wang, K. Chen, S. Wang, L. A. J. Mur, and S. Guo. (2018). Exploring the Roles of Aquaporins in Plant–Microbe Interactions. *Cells* 7: 267.

Whiteside, M. D., M. O. Garcia, and K. K. Treseder. (2012). Amino Acid Uptake in Arbuscular Mycorrhizal Plants. *PLOS ONE* 7: e47643.

Wipf, D., F. Krajinski, D. van Tuinen, G. Recorbet, and P.-E. Courty. (2019). Trading on the arbuscular mycorrhiza market: from arbuscules to common mycorrhizal networks. *New Phytologist* 223: 1127–1142.

Yang, Y., D. Tilman, G. Furey, and C. Lehman. (2019). Soil carbon sequestration accelerated by restoration of grassland biodiversity. *Nature Communications* 10: 718.

Yaniv, Z., B. C. Lowekamp, H. J. Johnson, and R. Beare. (2018). SimpleITK Image-Analysis Notebooks: a Collaborative Environment for Education and Reproducible Research. *Journal of Digital Imaging* 31: 290–303.

Zheng, H., A. K. Guber, Y. Kuzyakov, W. Zhang, and A. N. Kravchenko. (2022). Plant species and plant neighbor identity affect associations between plant assimilated C inputs and soil pores. *Geoderma* 407: 115565.

CHAPTER 5: Root distributions altered by spatial nitrogen availability affects belowground carbon and nitrogen transfer and soil pore structure

Abstract

Belowground carbon (C) and nitrogen (N) transfer takes place via root-based or fungal-based mechanisms, and the mechanisms depend on the development of roots and fungal hyphae, which can be affected by soil N availability. Yet, magnitudes of the two mechanisms in the transfer and their contributions to pore structure formation remain unexplored under the spatial N variability. Objectives of this study were (i) to identify root- and mycorrhizae-based C and N transfer in response to the soil N variability and subsequent root distribution in soil, and (ii) to assess the alteration in pore structure derived by the transfer mechanisms. Black-eyed Susan (BES, *Rudbeckia hirta* L.) was grown at both sides of the source switchgrass (SG, *Panicum virgatum* L.) as neighbors, or BES was co-planted with bush clover (BC, *Lespedeza capitata* Michx), a legume species. Half boxes had meshed barriers not to allow root contacts but mycorrhizal interactions, and another half was opened to allow both mechanisms. Source SG was labelled by ^{13}C and ^{15}N to trace their transfers, and NH_4NO_3 was only applied to one side of BES neighboring recipients to create the spatial N enrichment. After four months, (i) SG roots were photographed to estimate their preferential distributions, (ii) roots and rhizosphere soils of recipient plants were collected to analyze their ^{13}C and ^{15}N enrichment, and (iii) intact cores were taken from soils between the source and recipients and scanned using X-ray CT to analyze pore size distributions. Source SG roots grew towards the N applied BES and the co-planted BC plants, and particularly, root-based mechanism facilitated C transfers to both sides of BES when N was applied. The two mechanisms led to greater formation of 8-30μm diameter pores in the vicinity of the N applied BES and the BC roots in soils spatially N enriched. Conclusively, spatial N enrichment attracts recipient plant roots, facilitating C and N transfers, fine pore formation, and enhancing root-based transfer in the plant community.

5.1 Introduction

Diverse perennial vegetation is known to enhance soil carbon (C) accumulation and increase overall nitrogen (N) availability (Mulder et al., 2002; Sprunger and Robertson, 2018; Lange et al., 2019), thereby improving soil health and promoting plant growth (Lal, 2016; Sainju et al., 2017). The beneficial synergy of high plant diversity in C accumulation and plant productivity is particularly pronounced in grassland ecosystems (Tilman et al., 2001; Lange et al., 2015; Yang et al., 2019).

One potential driver of this synergy is the belowground transfer of water, C, and nutrients among individual plants within the community (Ayres et al., 2007; Thilakarathna et al., 2012; Kravchenko et al., 2021). The transfers improve efficiency of nutrient cycles and resilience against environmental stresses, thereby contributing to plant growth and productivity (Luo et al., 2023). Belowground C and N transfers are driven either by root interactions or by mycorrhizal networks (Robinson and Fitter, 1999; Thilakarathna et al., 2016; Hupe et al., 2021). Root-based transfers take place when C and N are released from the source plant's roots as rhizodeposits and exudates (Badri and Vivanco, 2009; De Sena et al., 2023), which are then absorbed by the roots of neighboring recipient plants (Jones et al., 2004; Segonzac et al., 2007). This absorption can occur either through direct root contact between source and recipient plants or when the recipient plant roots encounter the released C and N within the soil. Fungal-based transfer involves fungi utilizing C and N obtained from plant roots to develop their hyphae (Rillig, 2004a; Parniske, 2008). When plants are interconnected through common mycorrhizal networks, the symbiotic fungi and their hyphae transport the obtained C and N to roots of the neighboring plants (Smith et al., 2009; Roth and Paszkowski, 2017; Wipf et al., 2019). Fungal-based transfer can be particularly strong in perennial grass species (Martins, 1993; He et al., 2003; Walder and van der Heijden, 2015).

One hypothesis in drivers of these transfers is that C transfer occurs alongside N transfer as a side effect, driven by the plants' need for N. This process can be influenced by soil N availability, which affect root growth and mycorrhizal development (Stober et al., 2000; López-Bucio et al., 2003; Cox et al., 2010). Particularly, the root development and the direction of root foraging are known to be determined by the spatial variability of available N within the soil (Aibara and Miwa, 2014; Kellermeier et al., 2014; Boer et

al., 2020). This hypothesized driver is especially relevant in systems where legumes enrich the soil with N, promoting non-leguminous plants to extend their roots towards these N enriched zones (Temperton et al., 2007; Weidlich et al., 2018), thereby possibly facilitating C and N transfer towards legume plants.

Both root- and fungal-based transfer are expected to be heavily impacted by soil structural characteristics, which, in turn, are affected by the roots. Roots play a crucial role in the formation of soil structure through direct penetration, cracks via water extraction, and aggregations of soil particles via root exudation (Bengough et al., 2016; Oburger and Schmidt, 2016). Roots typically grow into soil pores > 50 µm diameter (Ø) (Bauhus and Messier, 1999; Grierson et al., 2014; An et al., 2022), where they release various C compounds, such as root exudates and rhizodeposits, and leave behind senesced root residues (Farrar and Jones, 2000; Jones et al., 2004; Badri and Vivanco, 2009). Carbon inputs from the residues are then decomposed by ample microbial communities residing in such pores and are lost to the atmosphere as CO_2 (Ruamps et al., 2011; Kravchenko et al., 2019b).

In contrast, fungal hyphae can access much smaller pores (~10µm Ø) than roots (Carlile, 1995; Smith and Smith, 2011), leaving there the organic materials from fungal extracellular enzymes, glomalin-related proteins, secondary metabolites, and senesced hyphae (Rillig, 2004b; Karlovsky, 2008; Burns et al., 2013). Organic C within these small pores is more likely to be protected from further microbial decomposition and stabilized (Keiluweit et al., 2016; Kravchenko et al., 2019a; Zheng et al., 2022), contributing to soil organic matter accrual (Treseder and Holden, 2013). Despite numerous studies examining the relative contributions of root-based and mycorrhizae-based mechanisms to C and N transfers (Carey et al., 2004; Ren et al., 2013; Shao et al., 2020; Cahanovitc et al., 2022), there is still a limited understanding of how spatial variability of soil N may affect these transfers and their impact on soil C processing and accrual.

I used three-compartment plant boxes, hereafter rhizoboxes, to grow plants of three species common in prairie communities: a grass, Switchgrass (*Panicum virgatum* L.), a forb, Black-eyed Susan (*Rudbeckia hirta* L.), and a legume, Bush clover (*Lespedeza capitata* Michx). Switchgrass, one of dominant grass species of North American prairie, known for promoting soil C accumulation when grown in diverse

plant communities (Sanford, 2014; Lee et al., 2023b; Perry et al., 2023), was the focal plant of the study. The first objective is to examine how spatial variability in available N, created either via mineral fertilization or via legume planting, affects the spatial distribution of switchgrass roots in prairie communities. The second objective is to identify how the spatial distribution of switchgrass roots influences C and N transfers to the recipient forb plants or legumes, with a focus on comparing the fungal-based transfer mechanism to the root-based one. The third objective is to explore associations of C and N transfers with inputs of plant-derived C and N into the soil and with alterations in soil pore structure.

5.2 Materials and Methods

5.2.1 Soil collection and rhizobox preparation

Soils used in this study were collected from two experimental sites located in Hickory Corners (42° 40'N, 85°37'W) and Escanaba (45°76'N, -87°19'W), Michigan, United States. Both sites are part of the Great Lake Bioenergy Research Center and will be referred to as HC and ESC sites hereafter. Both soils are classified as Alfisols but have disparate physical and chemical properties (Table 5.1). At each site, the soils were collected from Ap horizon (2-20 cm), air-dried, sieved (2 mm), and thoroughly mixed. Small stones and visible plant residues were removed.

Table 5.1. Taxonomy and physical and chemical characteristics of two soil types.

Soil type	Taxonomy	Texture	Total C (%)	Total N (%)	Inorganic P (ppm)
Hickory Corners (HC)	Typic Hapludalf (Alfisol)	Loam	1.17	0.10	17.6
Escanaba (ESC)	Inceptic Hapludalf (Alfisol)	Sandy loam	2.27	0.19	8.4

The greenhouse experiment consisted of a total of 66 rhizoboxes. Each rhizobox (30 cm x 54 cm x 4 cm) had three equally sized compartments, which were separated by two plastic 2 cm-wide dividers. Open dividers were installed in the half (33) of the rhizoboxes, while dividers covered by mesh barriers (35 μm, ELKO Filtering Co., Tamarac, FL, USA) were installed in the other half to restrict root-to-root contact, while still allowing passage of fungal hyphae (Figure 5.1A). One side of each rhizobox was transparent and removable, thereby enabling visual monitoring of root growth during the growing period and facilitating root and soil sampling at the end of the period. The three compartments and two dividers of each rhizobox

were filled with the prepared soils at consistent volumetric water content of 20% and bulk density of 1.3 g/cm^3. Six replicated boxes with HC soil and five replicated boxes with ESC soil were prepared for each of the three treatments. Additionally, rhizoboxes containing all three species were prepared as non-isotope-labeled controls, and another set of the boxes without plants to serve as non-plant controls. Due to time and labor restrictions to process large quantities of the rhizoboxes and plants, the experiment with HC soil was conducted first, followed by the experiment with ESC soil.

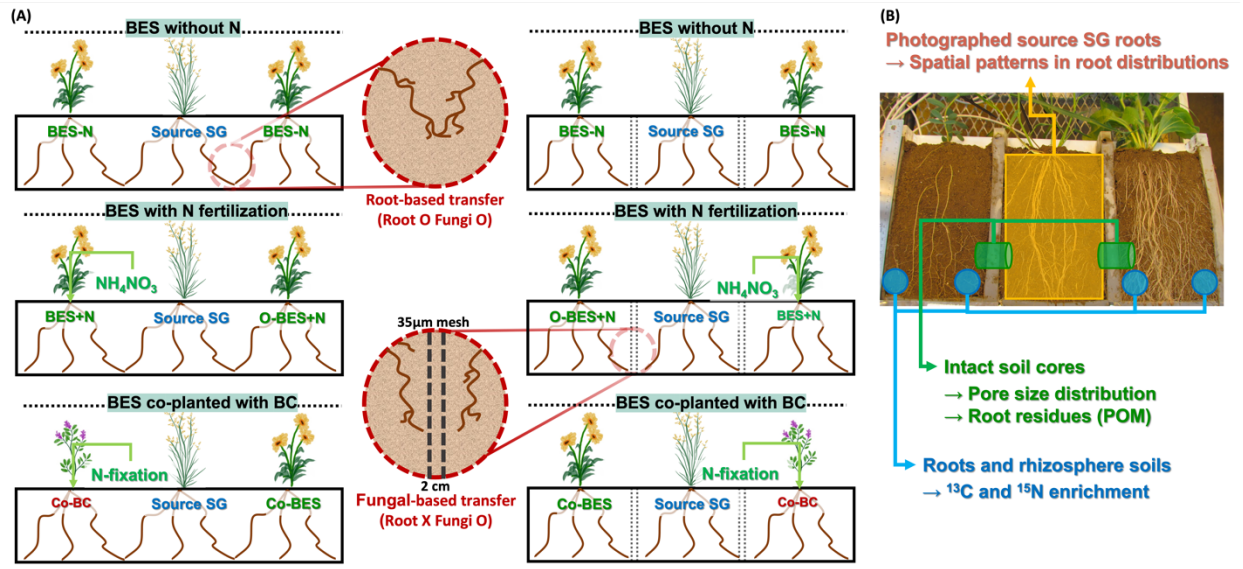

Figure 5.1. Schematic setting of rhizoboxs **(A)**, showing the arrangement of plants, three neighboring N status (without N, with N fertilization, and co-planted with BC), and two barrier treatments (left = open on both sides or right = wrapped in 35 µm mesh), and one example picture of the opened rhizobox **(B)**, showing schematic sampling locations. A yellow rectangle in the center marks the area that was photographed to explore spatial patterns in distribution of source switchgrass (SG) roots. Blue circles mark sampling locations for roots of recipient plants and the adjacent rhizosphere soils for ^{13}C and ^{15}N analyses. Green cylinders mark locations of intact soil core samples to explore soil pore structure and particulate organic matter (POM).

5.2.2 Experimental treatments and greenhouse experiment

Switchgrass (SG), black-eyed Susan (BES), and bush clover (BC) were used in the study. Each compartment of rhizoboxes contained one plant, with switchgrass positioned in the center compartment, and there were three types of rhizobox setting with the center SG (Figure 5.1A): BES with N fertilization, BES without N, and BES co-planted with BC. In the BES without N, none of BES sides received N (BES-N). In the BES with N fertilization, NH_4NO_3 solution was applied to one BES side (BES+N), while the other side of BES did not received N (O-BES+N). In the BES co-planted with BC, one side planted BES

(Co-BES) while the other side had BC (Co-BC), an N-fixing legume. Those three sets consisted of five N status, thereby aimed to explore the impact of natural N application through legume plants. The compartments receiving N and the legume plants were randomly assigned to each side of the rhizoboxes.

Two different N application methods were utilized for the two studied soils: a variation of a split-root approach was employed in HC soil and direct additions of small quantities of the fertilizer were used in ESC soil. For the split-root approach, the compartments of the BES+N side were outfitted with auxiliary boxes separated from the main compartments, where we directed some of the BES roots. The NH_4NO_3 solution was applied into the auxiliary boxes and was only available to the roots located within the auxiliary box. This approach aimed at ensuring high N available for the BES plant itself, while not affecting the N availability within the soil. Unfortunately, in several of the rhizoboxes the roots within the auxiliary boxes died, thus for ESC soils, we decided to modify the N application approach. In ESC soil, the NH_4NO_3 solution was applied directly at the crown of the BES+N plant. Each application consisted of 1 ml of 100 ppm NH_4NO_3 solution. Small quantities and direct application to the plant's crown minimized the spread of the applied N throughout the compartment soil. The N application for both soils was conducted at six times across two weeks and terminated before the plant labeling.

Seeds of each plant species were germinated in seed starter trays for three weeks. Seedlings that had developed leaves were transplanted into the center of each compartment in the rhizoboxes and grown there for either three (HC soil) or four (ESC soil) months. Plants in ESC soil developed much slower than in HC soil, likely due to its low levels of plant available soil phosphorus (Table 5.1), prompting the decision to extend the growth period for them. All plants were fertilized using Hoagland's solution immediately after transplanting and again one month later to promote plant growth. Two months after transplanting, since the plants in ESC soil showed signs of phosphorus deficiency, 134 mg of KH_2PO_4 was added to each ESC rhizobox (equivalent to 56 kg P/ha).

Initially, the rhizoboxes were tilted at a 60° angle with the transparent side down to encourage root growth towards the transparent side, facilitating visual observation of root development. After two months, the boxes were set up in the vertical standing position to ensure that the roots more evenly explored the

compartment's soil and to promote root interactions through the dividers. Each plant was watered daily with 0.5 liters of reverse osmosis water. The greenhouse temperature was maintained at a maximum of 29°C during daylight hours and a minimum of 20°C at night, with 16 hours of artificial fluorescent light provided daily.

5.2.3 ^{13}C pulse and ^{15}N foliage labeling

To trace belowground C and N transfer from the source plants, all SG plants in the center compartments were subjected to pulse labeling with $^{13}CO_2$ and foliage labeling with $^{15}NH_4NO_3$. The labeling for both elements was conducted three times for the source plants in HC soil and four times for those in ESC soil, with the final labeling event one month before root and soil sampling.

For ^{13}C enrichment of the source SG plants, first, the recipient plants in each rhizobox were covered with light-impermeable plastic bags, leaving only the central source SG exposed to the light. This ensured that only the exposed source SG could photosynthesize and assimilate ^{13}C from the produced $^{13}CO_2$, preventing photosynthesis in the covered recipient plants. Then, rhizoboxes were placed into the labeling chambers. The pulse labeling process involved using 98 % ^{13}C-enriched $NaHCO_3$ solution mixed with H_2SO_4 to produce $^{13}CO_2$, releasing 88 mg of ^{13}C per labeling event per chamber. Each labeling event involved sealing the chamber for six hours, with ventilators ensuring even distribution of $^{13}CO_2$ throughout the chamber and with thermometers monitoring the internal temperature. When the internal temperature increased above 35°C, the lower parts of the chambers were insulated with ice to prevent heat stress. After each labeling event, the rhizoboxes were moved to a controlled environment with proper lighting and high ventilation to support photosynthesis and to prevent the potential ^{13}C assimilation by the recipient plants from the $^{13}CO_2$ respired by the source SG plants. This procedure has successfully worked in previous greenhouse studies (Kravchenko et al., 2021; Zheng et al., 2022).

For ^{15}N enrichment, foliage labeling was conducted using 45% ^{15}N-enriched NH_4NO_3 (Chu et al., 2004; Shao et al., 2020). One undamaged leaf of each source SG plant was inserted into a 2-ml tube containing 1.5 ml of 5% (w/v) the ^{15}N-enriched NH_4NO_3 solution (6.38 g ^{15}N per L). After five days the leaf was carefully removed from the tube while ensuring that no $^{15}NH_4NO_3$ dripped on the soil. ^{15}N labeling

events were synchronized with the ^{13}C labeling, starting 2 days before and ending 3 days after the ^{13}C labeling.

5.2.4 Spatial patterns in root distributions of the source plants

At the end of the growing period, the transparent side of each rhizobox was opened, and the exposed panel of the central compartment, i.e., the one containing the source SG, was photographed (Figure 5.1B). The camera (Canon EOS, Tokyo, Japan) was positioned at 50 cm distance from the panel. The photos were used to segment the roots and to assess preferential directions of root growth.

The central compartment was cropped from the entire image and converted into 8-bit gray scale. MaxEntropy threshold method was applied to differentiate potential root area from the soil. To remove noise, Gaussian Blur ($\sigma = 2$) was applied to the binary image, and then the image was re-thresholded using Otsu method to enhance the root area segmentation. The segmented root pixel clusters were subsequently identified using Particle Analyzer plugin in BoneJ (Doube, 2021).

Each root image was bisected vertically based on the center of the crown of the SG plant, dividing the panel into two sections (Figure 5.2A). The proportion of roots in each section was calculated, and the ratio of those proportions between the two sections was used to determine the preferential direction of root growth between adjacent neighboring compartments. Ratio 1.0 indicates an equal distribution among the two compartments, and ratio >1.0 denotes preferential root growth towards right vs. left side of BES-N plants in BES without N status, or towards BES+N vs. O-BES+N sides in BES with N fertilization status, or towards Co-BC vs. Co-BES sides in BES co-planted with BC status.

5.2.5 Root and rhizosphere soil sampling and analysis

After the source SG roots were photographed, roots and surrounding rhizosphere soils of the recipient plants were collected from four locations on the opened side of each rhizobox (Figure. 5.1B). One sampling location was approximately 2 cm from the border of the divider, and the other was approximately 15 cm away, and those will be referred to as close and far locations from the source SG, respectively. The collected recipient root and soil samples were stored in 5 ml tubes at 4°C until preparation for ^{13}C and ^{15}N enrichment analyses.

For root sample preparation, first, 1.8 ml of 0.05M $CaCl_2$ was added to each tube containing roots, and tubes were sonicated for five minutes to detach the soil. Roots were then brushed to remove any remaining soil particles, and the cleaned roots were oven-dried at 30°C for two days. For rhizosphere soil sample preparation, visible roots and organic debris were manually removed from the tubes, and the cleaned soil samples were oven-dried at 30°C fir two days. The prepared roots and soils were subsequently ground using iron-ball mill for further analyses.

An elemental analyzer (Vario ISOTOPE CUBE, Elementar Americas Inc., Ronkonkoma, NY) coupled to an isotope ratio mass spectrometer (Isoprime Vision, Elementar Americas Inc., Ronkonkoma, NY) was utilized to measure ^{13}C and ^{15}N enrichment expressed as $\delta^{13}C$ and $\delta^{15}N$ (‰). Total ^{13}C and ^{15}N contents, $\delta^{13}C$ and $\delta^{15}N$, and PeeDee Belemnite and AIR standard were used to calculate atom % of isotope rations ($^{13}C/^{12}C$ and $^{15}N/^{14}N$) in the prepared root and rhizosphere soil samples (Fry, 2006). Then, ^{13}C and ^{15}N atom % in roots and soils of the non-labeled controls were subtracted from the obtained atom % in samples to calculate atom % excess values.

5.2.6 Plant biomass and soil inorganic N measurements

After collecting root and rhizosphere soil samples from recipient plants, the entire aboveground biomass was clipped, oven-dried at 60°C for three days, and weighed. Given the extensive root branching across the three rhizobox compartments, collecting the total belowground biomass was not feasible. Instead, the main root biomass was obtained by plucking out the crown of roots from the opened side of each rhizobox and by gently washing the soil off with deionized water. The cleaned root biomass was also oven-dried at 60°C for three days and weighed.

After removing the biomass, bulk soils from all three compartments of each rhizobox were collected and homogenized. 10 g of the prepared soil was taken for soil inorganic N measurements, ammonium (NH_4^+) and nitrate (NO_3) contents, using alicylate-cyanurate method (Sinsabaugh et al., 2000) and vanadium method (Doane and Horwáth, 2003), with spectrophotometry (Victor3 1420 Multilabel Counter, Perkin Elmer, Waltham, MA, USA) at 630 and 540 nm, respectively.

5.2.7 Intact soil core sampling, μCT scanning, and image analysis

Intact soil cores (2 cm height and 0.8 cm Ø) were collected from the dividers at depth of 15 cm (Figure 5.1B). For the status of BES without N containing BES-N plants at both sides of the source SG, a core was collected from one randomly selected side. For the other two status: BES with N fertilization and BES co-planted with BC, which contained two different conditions at both sides, i.e., O-BES+N vs. BES+N and Co-BES vs. Co-BC, respectively, two cores were collected, one from each side. A total of 70 cores were obtained for μCT scanning.

The cores were air-dried and then scanned at the 13-BM-D station of the GeoSoilEnviroCARS sector, Advanced Photon Source, Argonne National Laboratory (Lemont, IL, USA), with an energy of 30 keV and a scanning resolution of 5.7 μm. The scanned images were cropped into 4.6 × 4.6 × 8.0 mm (800 × 800 × 1400 pixels) stack to focus on the central portions of the cores, avoiding volumes potentially subjected to sampling and scanning artifacts. The images were denoised using 3D non-local mean filter (σ = 0.08) (Darbon et al., 2008; Buades et al., 2011), which was performed with scikit-image library in Python (Walt et al., 2014).

The filtered images were used to identify soil particulate organic matter (POM) and pores. POM was segmented using U-Net convolutional neural network model within the Dragonfly software's deep learning engine (Ronneberger et al., 2015; Abadi et al., 2016; Makovetsky et al., 2018). The segmentation model was trained using 16 randomly selected cores from the total of 70, and five slices containing representative POM fragments and two additional slices above and below the selected slices were used as inputs for training the model. The segmented POM images were visually inspected for accuracy, and clusters with fewer than four voxels were removed to denoise the segmentation results. Since pre-existing plant residues were removed from the soil before constructing the rhizoboxes, we interpret the POM fragments identified within the studied cores as remnants of the new roots grown during the greenhouse experiment. Thus, we will interchangeably refer to them either as POM or as root residues. Soil pores were segmented from the filtered images using Otsu method in SimpleITK of Python (Beare et al., 2018; Yaniv et al., 2018). The previously identified POM fragments were subtracted from the pore images to ensure that

only air-filled pores were included in the final images of soil pore space. The resolution of the processed POM and pore images was 8 μm.

The segmented pore images were used to conduct pore size distribution analysis using Local Thickness tool in ImageJ-Fiji software (Schindelin et al., 2012). Pores were classified into three pore size ranges, namely 8-30 μm, 30-150 μm, >150 μm Ø, as pores in the 30-150 μm range are known to be associated with high microbial abundance and activity (Nunan et al., 2003; Strong et al., 2004; Li et al., 2024). Volume-based pore fractions were determined by dividing the pore volumes (mm^3) by the total cropped soil (solid + POM + pore) volumes (mm^3).

5.2.8 Statistical analysis

Statistical analyses were performed using SAS 9.4 (SAS Institute Inc., Cary, NC, USA), with statistical models fitted via PROC MIXED procedure. Statistical models for atom % ^{13}C and ^{15}N excess data in the roots and rhizosphere soils of recipient plants included fixed effects of three factors (Fig. 1A): barrier treatments (root-based vs. mycorrhizae-based transfers), five N status (BES-N, O-BES+N, BES+N, Co-BES, and Co-BC), two sampling locations (close vs. far from the source SG), and their interactions. Models for the response variables not measured at multiple sampling locates included fixed effects of barrier treatments, five N status, and their interactions. Models for pore fractions of different size ranges additionally included the fixed effect of size ranges, treated as a repeated measure factor. Replicated rhizoboxes nested within soil types (HC and ESC soils), barrier treatments, and plant treatments served as an error term and as the subject of repeated measurements in all models. In all statistical models, the two soils were considered as a random blocking effect, representing soil variability among Alfisols in the region as well as variations in experimental procedures of the study.

When interactions among studied factors were significant, slicing for F-tests followed by multiple comparisons with t-tests were conducted. Effects and differences were reported as statistically significant at $p < 0.05$ level. To determine ^{13}C and ^{15}N enrichment in recipient roots, rhizosphere soils, and shoots, and the changes in pores and root residues between compartments, additional t-tests were performed comparing them with non-isotope-labelled controls and non-planted controls, respectively.

Normality and variance homogeneity assumptions were assessed by examining histograms, normal probability plots, and side-by-side box plots of the residuals, as well as by conducting Levene's test for variances. Residuals for all studied variables, except for atom % ^{13}C and ^{15}N excesses in roots and rhizosphere soils, were normally distributed and met the equal variance assumption. The atom % ^{13}C and ^{15}N excess data that did not meet normality assumptions were log-transformed, and to handle negative excess data, a constant value was added to all data points before the transformation.

Pearson's correlation coefficients were used to assess linear associations among the studied response variables via PROC CORR procedure in SAS.

5.3 Results

5.3.1 Plant biomass, root growth, and soil inorganic N

The presence/absence of the barrier did not affect aboveground and root biomass for any of N status treatments (Table 5.2 and 5.3). In the absence of barriers, the aboveground biomass of BES+N was greater than that of O-BES+N, and also higher than that of BES-N (Figure 5.2A and 5.2B), while the aboveground biomass of Co-BES was comparable to that of BES+N (Figure 5.2B and 5.2C). In the presence of the barrier the means followed similar numeric trends to those observed in the absence of the barrier, however, were not statistically significant (Figure 5.2A, 5.2B, and 5.2C). In the absence of barriers, root biomass of O-BES+N was comparable to that of BES+N sides (Figure 5.2E), which had greater biomass than BES-N and Co-BES (Figure 5.2D, 5.2E, and 5.2F). Interestingly, with its presence, the root biomass of BES+N was greater than O-BES+N (Figure 5.2D and 5.2E), and the Co-BES had comparable root biomass to that of BES+N (Figure 5.2E and 5.2F).

Table 5.2. ANOVA F-test results with *p*-values for effects of N status treatments, barrier treatments, and their interaction on aboveground and major root biomass of recipient plants. Significant effects (p <0.05) in the ANOVA table are shown in bold.

	Aboveground biomass		Major root biomass	
Effect	F-value	*p*-value	F-value	*p*-value
N status	**18.01**	**<0.001**	**8.37**	**<0.001**
Barrier	2.13	0.149	1.35	0.304
N status × Barrier	0.41	0.804	1.71	0.159

Table 5.3. ANOVA F-test results with *p*-values for effects of N status treatments, barrier treatments, and their interaction on aboveground and major root biomass of source SG.

	Aboveground biomass		Major root biomass	
Effect	F-value	*p*-value	F-value	*p*-value
N status	1.65	0.211	1.38	0.268
Barrier	0.28	0.601	1.24	0.276
N status × Barrier	3.53	0.043	0.79	0.463

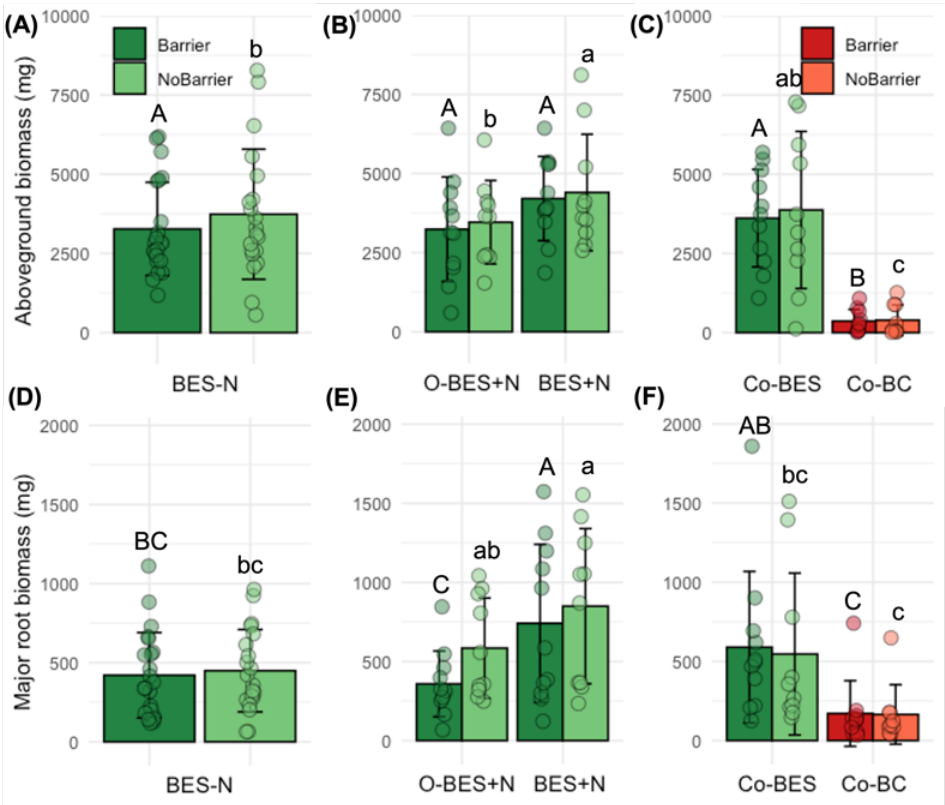

Figure 5.2. Aboveground **(A, B, and C)** and major root **(D, E, and F)** biomass of BES-N **(A and D)**, O-BES+N and BES+N **(B and E)**, and Co-BES and Co-BC plants **(C and F)**. Error bars and dots represent standard deviations and individual data points, respectively. Different uppercase letters on the bars indicate significant differences in aboveground or major root biomass of N status treatments within barrier treatments, and different lowercase letters indicate significant differences within non-barrier treatments at p <0.05 level. Differences between barrier and non-barrier treatments were not statistically significant (p >0.05) (Table 5.2).

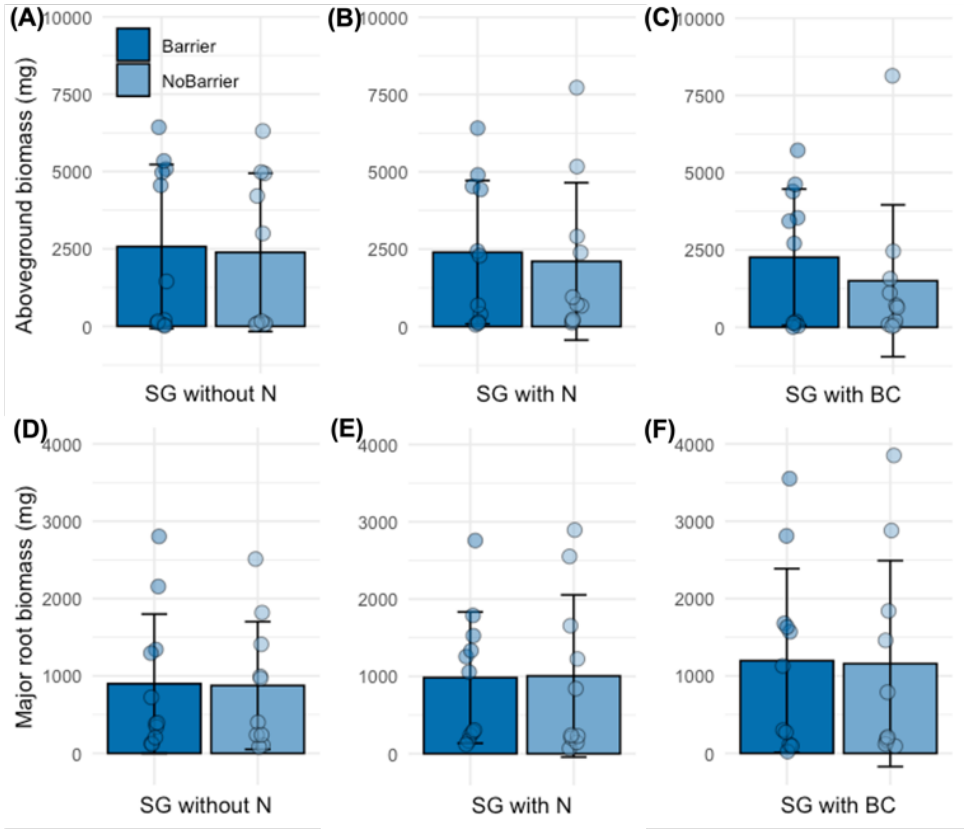

Figure 5.3. Aboveground **(A, B, and C)** and major root **(D, E, and F)** biomass of source SG plants neighboring BES-N **(A and D)**, O-BES+N and BES+N **(B and E)**, and Co-BES and Co-BC plants **(C and F)**. Error bars and dots represent standard deviations and individual data points, respectively. Any of differences among N status treatments or barrier treatments were not statistically significant (p >0.05) (Table 5.3).

Different recipient conditions did not influence the aboveground and root biomass for the source SG plants (Figure 5.3 and Table 5.3). The two studied recipient species, i.e., BES and BC plants, differ greatly in their aboveground biomass in both barrier treatments, reflecting inherently greater foliage and root systems of BES compared to those of BC plants (Figure 5.2).

The barrier treatments did not affect soil inorganic N (NO_3^- and NH_4^+) contents (Table 5.4). However, soils in BES+N and Co-BC had greater NO_3^- contents compared to those under BES plants in their opposite side, O-BES+N and Co-BES, respectively, with and without barriers (Figure 5.4A, 5.4B, and 5.4C). Soil NH_4^+ contents in BES+N and O-BES+N showed similar trend to the NO_3^- contents, while NH_4^+ contents in Co-BES were comparable to those in Co-BC when there were barriers (Figure 5.4D, 5.4E, and 5.4F).

Table 5.4. ANOVA F-test results with *p*-values for effects of N status treatments, barrier treatments, and their interaction on NO_3^- and NH_4^+ contents in soils. Significant effects (p <0.05) in the ANOVA table are shown in bold.

	NO_3^-		NH_4^+	
Effect	F-value	*p*-value	F-value	*p*-value
N status	**24.51**	**<0.001**	**8.57**	**<0.001**
Barrier	0.12	0.732	1.30	0.256
N status × Barrier	0.27	0.896	0.70	0.590

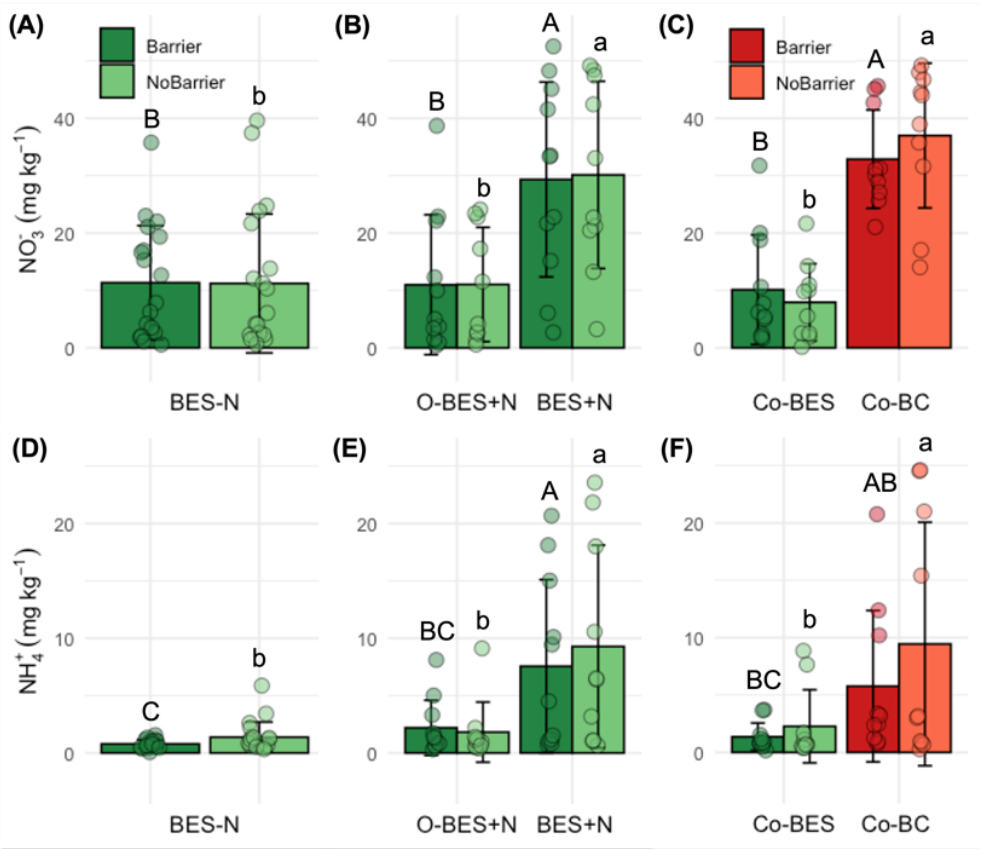

Figure 5.4. Nitrate (NO_3^-) **(A, B, and C)** and ammonium (NH_4^+) **(D, E, and F)** contents in soils of BES-N **(A and D)**, O-BES+N and BES+N **(B and E)**, and Co-BES and Co-BC plants **(C and F)**. Error bars and dots represent standard deviations and individual data points, respectively. Different uppercase letters on the bars indicate significant differences in NO_3^- or NH_4^+ contents in soils of N status treatments within barrier treatments, and different lowercase letters indicate significant differences within non-barrier treatments at p <0.05 level. Differences between barrier and non-barrier treatments were not statistically significant (p >0.05) (Table 5.4).

When the source SG plant had BES neighboring recipients without N application, its roots were equally abundant in soils of both side compartments (Figure 5.5B). However, when N was applied to BES+N plants, SG roots grew preferentially towards BES+N even with the presence of barriers (p <0.01)

(Figure 5.5C). Its roots also grew towards Co-BC than towards Co-BES without barriers (p <0.01), while the preferential growth was not significant when barriers blocked the root contact (p >0.05) (Figure 5.5D).

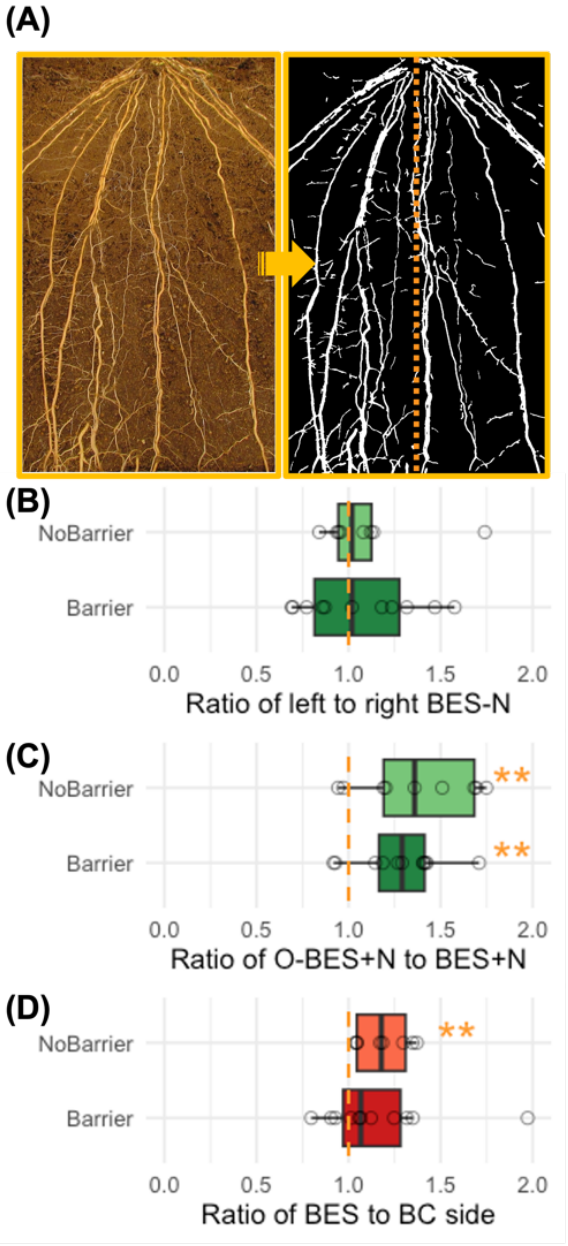

Figure 5.5. Representative photo taken from the source switchgrass (SG) root areas, its segmented binary image into root and background **(A)**, and distributions of source SG roots located next to roots of BES-N **(B)**, O-BES+N and BES+N **(C)**, and Co-BES and Co-BC plants **(D)**. Darker and lighter boxes represent barrier and non-barrier treatments, and dots represent individual data points. Orange dashed line at 1.0 ratio indicates that roots were equally distributed at right and left sides of BES-N, at both sides of O-BES+N and BES+N, or at both sides of Co-BES and Co-BC. Higher than 1.0 indicates the skewed growth of roots toward the right side of BES-N, BES+N, or Co-BC plant side. Marked ** denotes that the ratio was significantly higher than 1.0 at p <0.01 level.

In the absence of barriers, POM in the soil cores from the compartment dividers was significantly higher than that in the control unplanted rhizoboxes (p <0.01-0.001) (Figure 5.6 and Table 5.5). In the presence of barriers, POM did not exceed that in the unplanted control soil supporting our interpretation of the detected POM as the residues of the plant roots newly grown during the experiment. The highest POM was observed in the soil from the BES+N treatment (Figure 5.6).

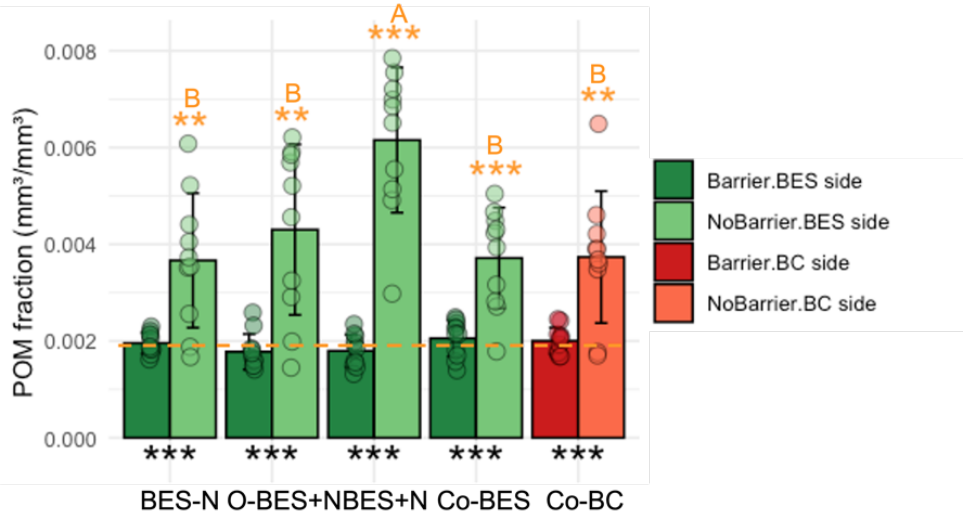

Figure 5.6. Fractions of particulate organic matter (POM) detected using X-ray µCT within the rhizobox dividers between soils in source SG and BES-N, O-BES+N, BES+N, Co-BES, and Co-BC plants. Orange **, and *** marks on the bar graphs denote that root residue fractions were significantly greater than the fractions of non-planted controls (orange dashed lines) at p <0.01 and 0.001 level, respectively. Black *** located below the adjacent two boxes indicate significant differences between barrier and non-barrier treatments within each of N status treatments at p <0.001 level, respectively. Letters are not shown within barrier treatments, as differences were not statistically significant among the N status (p >0.05).

Table 5.5. ANOVA F-test results with p-values for effects of N status treatments, barrier treatments, and their interaction on particulate organic matter (POM) fractions detected using X-ray µCT within the rhizobox dividers. Significant effects (p < 0.05) in the ANOVA table are shown in bold.

	Root residues	
Effect	F-value	p-value
N status	**4.55**	**0.010**
Barrier	**137.07**	**<0.001**
N status × Barrier	**6.33**	**0.002**

5.3.2 ^{13}C and ^{15}N excesses in recipient roots and rhizosphere soils

The presence of the barrier led to overall lower ^{13}C enrichment (p <0.001), and likewise, ^{13}C enrichment of recipient roots at the close location was generally greater than that at the far location (p <0.001) (Table 5.6). In the absence of barriers, the recipient's roots were enriched at the close location in all recipient N status (p <0.05) (Figure 5.7B and 5.7C), except for roots of BES-N (Figure 5.7A). Notably, in the presence of barriers, Co-BC's roots at the close location were only enriched (p <0.05), and the Co-BC was the only plants that the ^{13}C enrichment was found at the far location with the absence of barriers (p <0.05) (Figure 5.7C). However, the ^{13}C excess in roots of the Co-BC was smaller than that of BES+N (Figure 5.7B and 5.7C), while it was greater than that of BES in the other N status, i.e., O-BES+N and Co-BES (Figure 5.7A, 5.7B, and 5.7C).

Table 5.6. ANOVA F-test results with p-values for effects of N status treatments, barrier treatments, sampling locations, and their interaction on ^{13}C and ^{15}N atom % excesses in roots of recipient plants. Significant effects (p <0.05) in the ANOVA table are shown in bold.

	^{13}C excess		^{15}N excess	
Effect	F-value	p-value	F-value	p-value
N status	**6.26**	**<0.001**	**4.38**	**0.002**
Barrier	**21.10**	**<0.001**	**19.88**	**<0.001**
Location	**5.12**	**0.025**	**9.61**	**0.002**
N status × Barrier	**6.37**	**<0.001**	1.90	0.112
N status × Location	1.88	0.114	1.92	0.108
Barrier × Location	**4.34**	**0.038**	**6.35**	**0.013**
N status × Barrier × Location	2.04	0.090	1.65	0.162

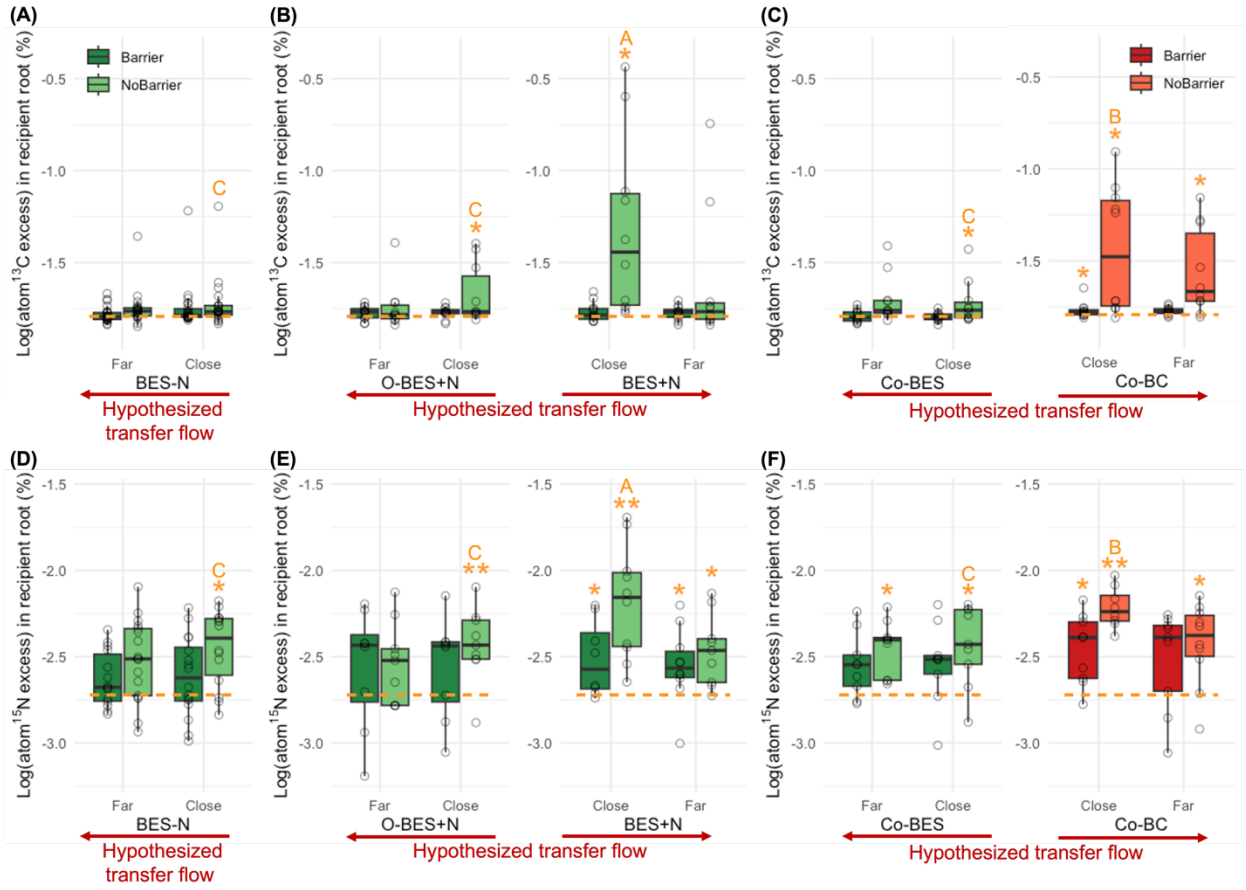

Figure 5.7. Atom % ^{13}C **(A, B, and C)** and ^{15}N **(D, E, and F)** excesses in the roots of BES-N **(A and D)**, O-BES+N and BES+N **(B and E)**, and Co-BES and Co-BC plants **(C and F)**, which were recipients of ^{13}C and ^{15}N labelled, thereby source SG. Results obtained at close and far distances from the source SG plants are reported separately. Note that to ensure that data from all distances and N status are clearly visible on the same graph we show the data in a log scale, and due to the negative values in % ^{13}C and ^{15}N excess, a constant value was added to the data prior to the log transformation. Dots represent individual data points. Orange * and ** marks above the box plots denote that ^{13}C and ^{15}N excesses significantly exceed non-labelled controls (orange dashed line) at p <0.05 and 0.01 level, respectively. Black ** and *** marks under the adjacent two boxes within each sampling location indicate significant differences between barrier and non-barrier treatments within the location at p <0.01 and 0.001 level, respectively. Different letters on the boxes indicate significant differences among N status treatments within non-barrier treatments in the close location (p <0.05), and letters are not shown within barrier treatments or within far locations, as differences were not statistically significant among the conditions (p >0.05).

Similar to ^{13}C results, the presence of the barriers led to overall lower ^{15}N enrichment (p <0.001), and the enrichment at the close location was generally greater than that at the far (p <0.01) (Table 5.6). With the absence of barriers, roots of all recipient N status were ^{15}N enriched at the close location (p <0.05-0.01), while with its presence, only roots of BES+N and Co-BC were ^{15}N enriched at the location (p <0.05) (Figure 5.7D, 5.7E, and 5.7F). Notably, ^{15}N enrichment was found at the far location only in the two recipient N statuses as well as Co-BES (p <0.05). Again, similar to ^{13}C results with the absence of barriers, the ^{15}N excess in roots of BES+N was the greatest and followed by those of Co-BC, while the excess was the least in roots of O-BES+N, Co-BES, and BES-N (Figure 5.7D, 5.7E, and 5.7F).

Likewise, the presence of barriers generally led to lower ^{13}C and ^{15}N enrichment in rhizosphere soils (p <0.05-0.001) (Table 5.7), and this enrichment was only detected at the close location in few of recipient N status. Specifically, in the absence of barriers, rhizosphere soils were ^{13}C enriched only at the close location of BES+N and Co-BC (Figure 5.8B and 5.8C). In the absence of barriers, the ^{13}C excesses of the two N statuses were greater than those with the presence of barriers in the same status as well as those of other status with the absence of barriers (Fig. 5.8A, 5.8B and 5.8C). ^{15}N of rhizosphere soils was also enriched at the close location of the BES+N and the Co-BC with the absence of barriers, while the enrichment was also detected at their close location with the barrier absence and at the close location of Co-BC with the barrier presence (Figure 5.8D, 5.8E, and 5.8F). Similar to ^{13}C results in rhizosphere soils, ^{15}N excesses in the BES+N and the Co-BC were greater than those with the presence of barriers in the same N status and those of the other statuses with the absence of barriers.

Table 5.7. ANOVA F-test results with *p*-values for effects of N status treatments, barrier treatments, sampling locations, and their interaction on ^{13}C and ^{15}N atom % excesses in rhizosphere soils of recipient plants. Significant effects ($p < 0.05$) in the ANOVA table are shown in bold.

	^{13}C excess		^{15}N excess	
Effect	F-value	*p*-value	F-value	*p*-value
N status	**12.65**	**<0.001**	**6.90**	**0.002**
Barrier	**20.16**	**<0.001**	**5.95**	**0.045**
Location	**14.30**	**<0.001**	**13.44**	**<0.001**
N status × Barrier	**6.84**	**<0.001**	1.83	0.170
N status × Location	**5.84**	**<0.001**	1.54	0.192
Barrier × Location	**6.42**	**0.012**	0.91	0.342
N status × Barrier × Location	2.42	0.056	1.23	0.185

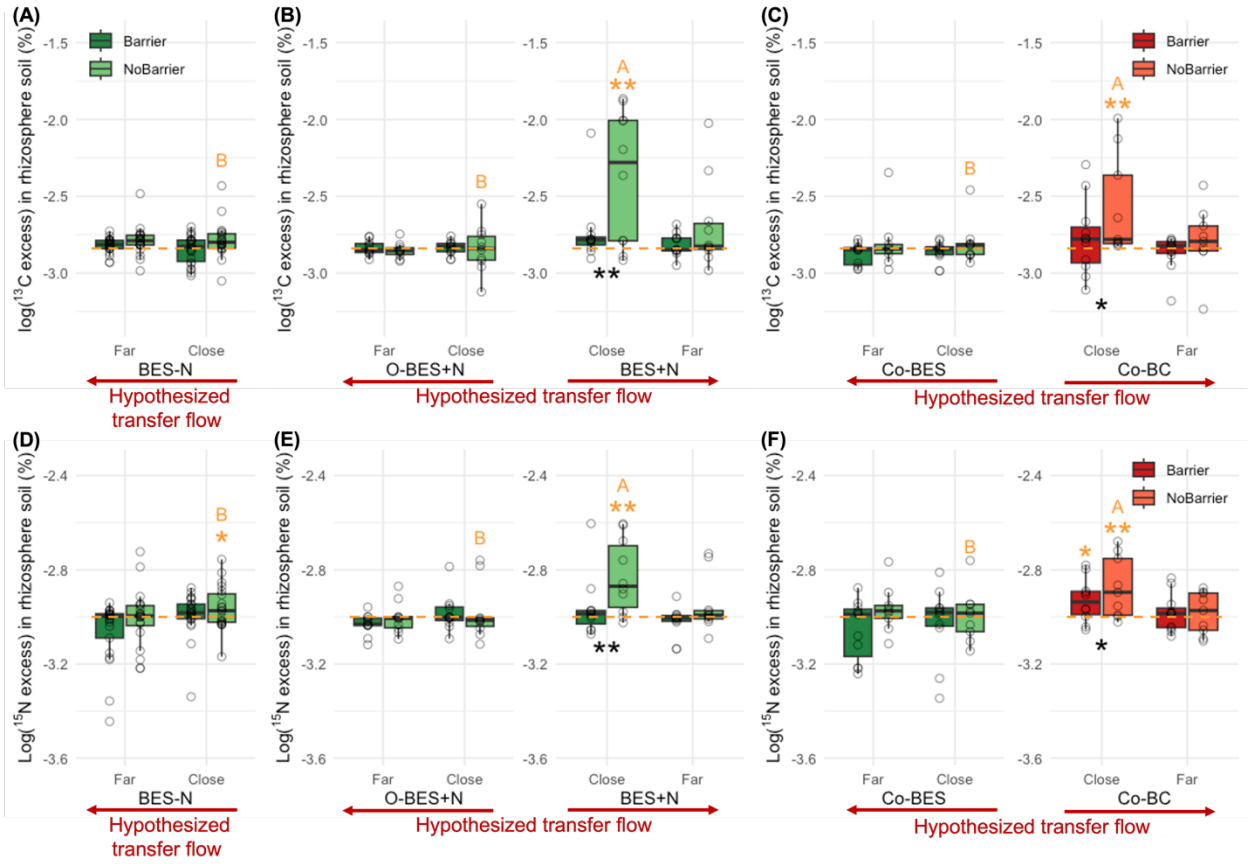

Figure 5.8. Atom % ^{13}C **(A, B, and C)** and ^{15}N **(D, E, and F)** excesses in the rhizosphere soils of BES-N **(A and D)**, O-BES+N and BES+N **(B and E)**, and Co-BES and Co-BC plants **(C and F)**, which were recipients of ^{13}C and ^{15}N labelled, thereby source SG. Results obtained at close and far distances from the source SG plants are reported separately. Note that to ensure that data from all distances and N status are clearly visible on the same graph we show the data in a log scale, and due to the negative values in % ^{13}C and ^{15}N excess, a constant value was added to the data prior to the log transformation. Dots represent individual data points. Orange * and ** marks above the box plots denote that ^{13}C and ^{15}N excesses significantly exceed non-labelled controls (orange dashed line) at p <0.05 and 0.01 level, respectively. Black * and ** marks under the adjacent two boxes within each sampling location indicate significant differences between barrier and non-barrier treatments within the location at p <0.05 and 0.01 level, respectively. Different letters on the boxes indicate significant differences among the N status treatments within non-barrier treatments in the close location (p <0.05), and letters are not shown within barrier treatments or within far locations, as differences were not statistically significant among the N status (p >0.05).

At the close location, ^{13}C excesses in rhizosphere soils were positively associated with ^{13}C excesses in roots in overall, when there were no barriers between the source and recipients ($r^2 = 0.52$ and $p < 0.001$), while those were not associated in the presence of barriers ($r^2 = 0.01$ and $p > 0.05$) (Figure 5.9A). The ^{15}N excess in rhizosphere soils from the close location were also positively associated with the ^{15}N excess in roots in both barrier treatments ($r^2 > 0.29$ and $p < 0.001$) (Figure 5.9B).

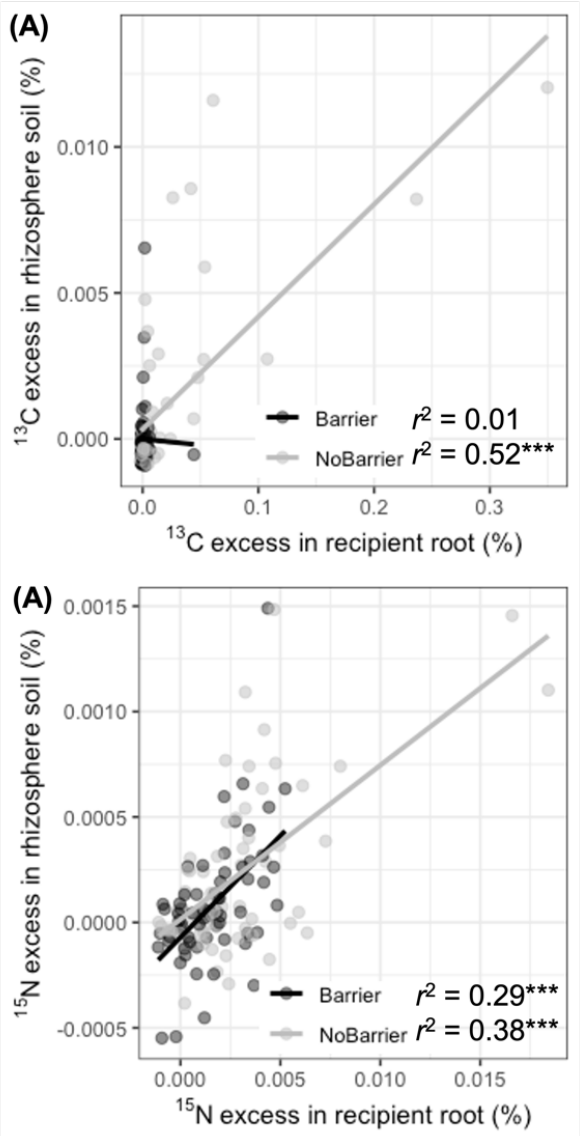

Figure 5.9. Relationships of atom % ^{13}C **(A)** and ^{15}N **(B)** excesses between the roots and the rhizosphere soils at close location from the source SG across all recipient conditions. Shown on figures are observations from barrier and non-barrier treatments (dark and light grey dots, respectively) and the linear regressions fitted to the data (dark and light grey lines, respectively). *** marks indicate r^2 significant at $p < 0.001$.

5.3.3 Soil pores between source SG and recipients

When BES plants were the recipient species without any N application, i.e., BES-N, soil pore fractions in three size ranges (8-30, 30-150, and >150 µm Ø) were not significantly different from those of the non-planted control in both barrier conditions (p >0.05) (Figure 5.10A). However, in the N fertilization status, fractions of finer pores (8-30 µm Ø) between the source and BES+N with the absence of barriers were approximately 70% and 40% greater than that in soils without plants (p <0.01) and with plants and barriers (p <0.05), respectively (Figure 5.10B). Notably, such N fertilization also led to 40% and 35% greater fractions of the finer pores in O-BES+N compared to those without plants (p <0.01) and with plants and barriers (p <0.05), respectively (Figure 5.10B). In contrast, fractions of coarser pores (>150 µm Ø) in soils adjacent to the BES+N and O-BES+N were approximately 50% and 45% smaller than those in the non-planted control soils when the barriers did not block the root-to-root contacts (p <0.001).

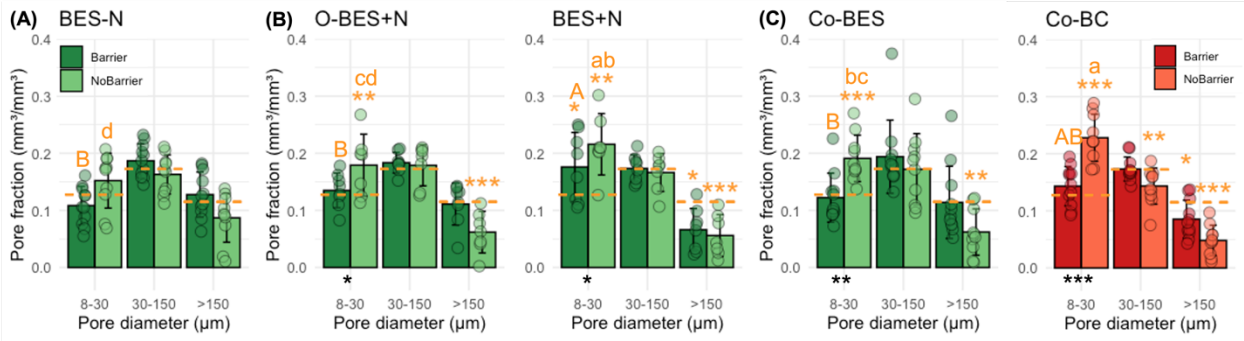

Figure 5.10. Fractions of pores of three size ranges (8-30, 30-150, and >150 µm Ø) in the soils between source and five N status treatments: BES-N **(A)**, O-BES+N and BES+N **(B)**, and Co-BES and Co-BC **(C)**. Error bars and dots represent standard deviations and individual data points, respectively. Orange *, **, and *** marks above the bar graphs denote that pore fractions were significantly greater or less than the fractions of non-planted controls (orange dashed lines) at p <0.05, 0.01, and 0.001 level, respectively. Black *, **, and *** located below the adjacent two bars within each size range indicate significant differences between barrier and non-barrier treatments within the size at p <0.05, 0.01, and 0.001 level, respectively. Different uppercase letters on the bars indicate significant differences at p <0.05 among N status treatments with the presence of barriers, and different lowercase letters indicate differences with the absence of barriers. Marks and letters are not shown when differences were not statistically significant (p >0.05).

In the status of BES co-planted with BC, finer pore fractions between the source and Co-BC as well as Co-BES were approximately 80% and 50% greater with the absence of barriers than those in soils without plants, respectively (p <0.01-0.001) (Figure 5.10C). Moreover, such pores were also 60% and 55% greater than those in Co-BC and Co-BES having barriers, respectively (p <0.01-0.001). Notably, in the

absence of barriers, the Co-BC led to smaller fractions of medium (30-150 µm Ø) and coarser pores compared to those in soils without plants (p <0.01-0.001) (Figure 5.10C).

The finer pores showed differences in pore fractions among the recipient N statuses in both barrier treatments. With the presence of barriers, fractions of such pores were greater in BES+N compared to any of other recipient In the absence of barriers, soils in BES+N had 20% greater finer pore fractions than those in its opposite side, i.e., O-BES+N, and such pores in Co-BC was also 20% greater than those in its opposite side, i.e., Co-BES (Figure 5.10B and 5.10C). Since soil porosities measured using the images were not significantly different among all recipient N statuses and between two barrier treatments, given differences were derived by changes in soil structure (Figure 5.11).

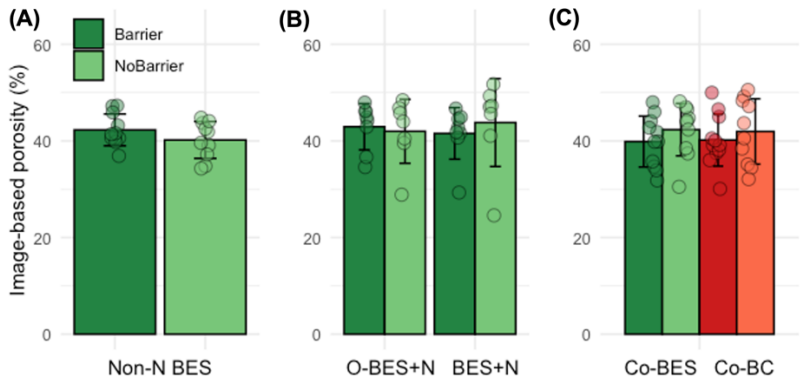

Figure 5.11. Image-based porosity of soils between source SG and BES-N **(A)**, O-BES+N and BES+N **(B)**, and Co-BES and Co-BC plants **(C)**. Error bars and dots represent standard deviations and individual data points, respectively. Differences between two barrier treatments or N status treatments were not significant (p >0.05), thereby not shown.

In the absence of barriers, the root residues were positively associated with fractions of finer pores in soils between the source SG and recipients (r^2 = 0.28 and p <0.001), and alternatively, they were negatively associated with fractions of coarser pores (r^2 = 0.11 and p <0.05) (Figure 5.12). There were any of relationships with the presence of barriers, and medium pores were not associated with fractions of root residues even without barriers.

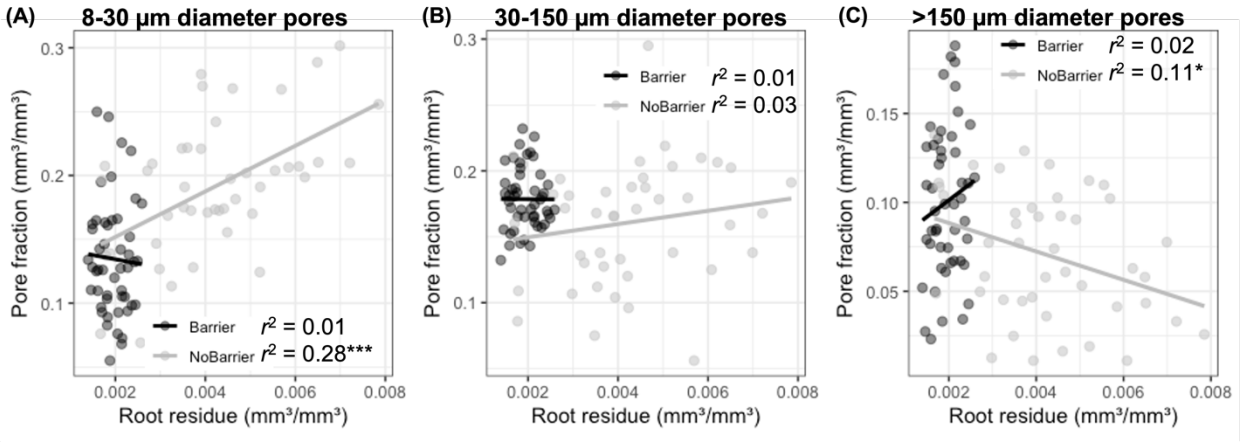

Figure 5.12. Relationships betweem fractions of root residues and fractions of pores in 8-30 **(A)**, 30-150 **(B)**, and > 150 µm **(C)** diameter size ranges. Shown on figures are observations from barrier and non-barrier treatments (darker and lighter dots, respectively) and the linear regressions fitted to the data (darker and lighter lines, respectively). * and *** marks indicate r^2 significant at p <0.05 and 0.001, respectively.

5.4 Discussion

Roots of source SG plants tended to grow towards the neighboring plants with higher N availability, i.e., both towards fertilized BES and legume BC plants. Greater root growth towards the N-enriched neighbor apparently modified soil pore structure, reducing the volume of large (>150 um) while increasing the volume of fine (8-30 um) pores. C and N of SG origin were found in the roots of the neighboring plants, but only in the cases of enhanced N availability. SG-assimilated N was transported to the roots of the N-enriched neighbors both via direct/close root contact and via fungal-based mechanism. Transport of SG-assimilated C to BES occurred via root-based mechanism only, while both mechanisms seemed to be involved in the C transfer to BC plants. Interestingly, in the presence of a N-enriched neighbor, the SG plants had greater root-based interactions, as indicated by C and N transfers, even with their non-N-enriched neighbors. When the transfers occurred through direct/close root interactions mechanism, both SG-assimilated C and N in the roots of the neighbor plants were positively associated with those in the rhizosphere soils, supporting the notion that N availability impacts the quantities of plant-assimilated inputs into the soil. Yet, in case of the fungal-based transport such relationships were only found for N.

5.4.1 Plant growth in response to soil inorganic N

It is well known that legume plant species can increase plant-available N in soil via N fixation (Kakraliya et al., 2018; Tian et al., 2021), and indeed, soils under Co-BC had greater soil inorganic N (NO_3^-

and NH_4^+) contents compared to those in the Co-BES within the same rhizobox (Figure 5.4C and 5.4F). Expectedly, greater inorganic N contents were also found in BES+N than other side of the soil, O-BES+N (Figure 5.4). This N application to plants could enhance soil plant-available inorganic N by increasing root biomass and exudation. The root exudates serve as C sources for soil microorganisms, promoting microbial activity and stimulating N mineralization and thus converting organic N into the plant-available forms (Meier et al., 2017; Liu et al., 2022a). This could be supported by the greater root biomass of N applied BES side compared to that of another BES side, which had no N application in this study (Figure 5.2D and 5.2E).

Spatial variability of soil N is known to influence the root development and the foraging direction in response to immediate availability of soil N (Aibara and Miwa, 2014; Kellermeier et al., 2014; Boer et al., 2020), and specifically plant roots tend to grow towards N-enriched locations within the soil (Ruffel et al., 2011; Guan et al., 2014; Mounier et al., 2014). This aligns with our findings that roots of source SG plants grew towards BES+N or Co-BC instead of O-BES+N or C-BES within their rhizoboxes (Figure 5.5C and 5.5D), leaving greater amount of root residues between the source SG and the two N-enriched status (Figure 5.6).

Interestingly, even though greater N availability increased the belowground biomass of BES (Figure 5.2), SG biomass did not respond to higher N availability in its neighborhood. This result is consistent with a weak response of SG to N fertilization in the field studies reported in the past (Mulkey et al., 2006; Ruan et al., 2016; Wang et al., 2020). However, given the strong preferential patterns towards N sources in SG root growth (Figure 5.5C and 5.5D), such lack of impact on its biomass is still surprising.

5.4.2 C and N transfers

Rhizoboxes without barriers allowed C and N transfers through both root-based and fungal-based mechanisms, while only fungal-based transfers were possible in the presence of the mesh barriers (Figure 5.1A). As evident from the absence of POM, i.e., root residues, in the soil cores (Figure 5.6), the barriers indeed successfully restricted direct/close root contacts. Unsurprisingly, the C and N transfers in all root-

exclusive barrier treatments were lower than those observed in the absence of the barriers (Figure 5.7 & Table 5.6).

Fungal-based transfer of both C and N could occur when the source roots were relatively close (< 4 cm) to the recipient roots, i.e., at close locations (Figure 5.5 and 5.7), but only N could be transferred to the far locations, i.e., ~13 cm away from the source SG (Figure 5.7). This phenomenon can be explained by differences in mobility of C and N within the framework of the fungal-based transfer. Mycorrhizal fungi can efficiently transport N-containing smaller molecules such as amino acids, NH_4^+, and NO_3^- through their extensive hyphal networks (López-Pedrosa et al., 2006; Parniske, 2008; Whiteside et al., 2012). Meanwhile, relatively large C compounds such as glycogen granules and lipid droplets involved in mycorrhizal transfer (Pfeffer et al., 1999; Keymer et al., 2017) can have greater challenges being moved through hyphal networks (Wang et al., 2018; Salvioli di Fossalunga and Novero, 2019).

Moreover, this discrepancy between the ^{13}C and ^{15}N enrichment at the far location (Figure 5.7) may also be attributed to the unidirectional C flow, which is the C transport only from the host plants for fungal hyphae development within arbuscular mycorrhizal symbiosis. This implies that the transferred C to the recipient plants were not assimilated but largely retained within their symbiotic roots (Pfeffer et al., 2004). In this study, recipient shoots were not ^{13}C enriched (Figure 5.13A, 5.13B, and 5.13C), and this can support that the shoots of recipient plants did not assimilate the transferred C from the source, thereby could not have capability to redistribute C to the other sides of recipient roots. On the contrary, mycorrhizal symbiotic roots could utilize the transferred N compounds for their further growth (Govindarajulu et al., 2005; Parniske, 2008), having ^{15}N-enriched shoot biomass (Figure 5.13D, 5.13E, and 5.13F), thereby enable to move them to the far location from the source.

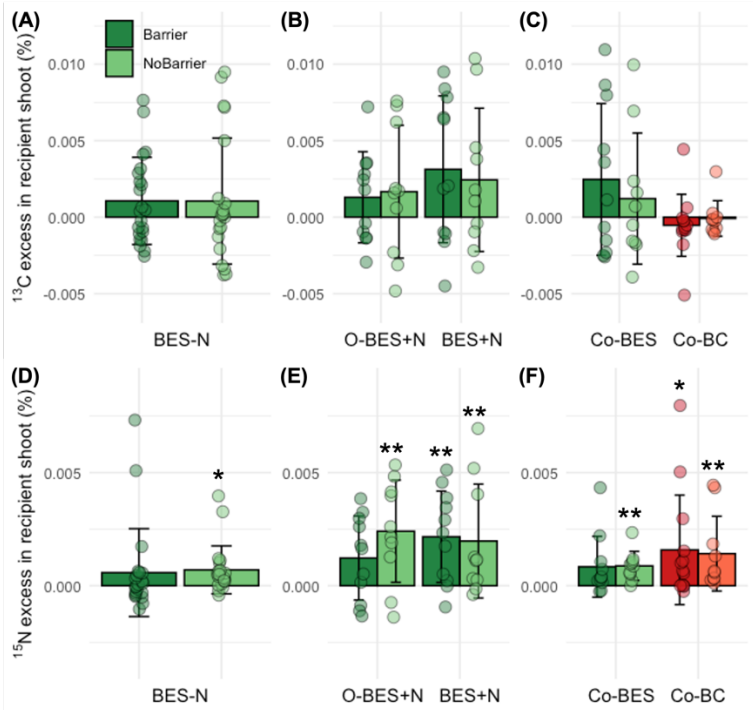

Figure 5.13. Atom % ^{13}C **(A, B, and C)** and ^{15}N **(D, E, and F)** excesses in shoots of BES-N **(A and D)**, O-BES+N and BES+N **(B and E)**, and Co-BES and Co-BC plants **(C and F)**. Error bars and dots represent standard deviations and individual data points, respectively. The black * and ** marks above the bar plots denote that ^{15}N excesses significantly exceed non-labelled controls, which are all 0 %, at p <0.05 and 0.001 level, respectively.

Despite the unidirectional C flow within arbuscular mycorrhizal symbiosis, the fungal-based C transfers to the far location of the BC recipients were observed (Figure 5.7C). The potential reach of mycorrhizal hyphae was reported to extend up to 15 cm from their symbiotic root (Muneer et al., 2020a, 2020b; Shen et al., 2020) with the spread of up to 111 m cm-3 hyphae in soil (Miller et al., 1995). This could be a plausible reason for the observed long-distance C transfers to the 13 cm away from the source, as legume species are known to promote the development of mycorrhizal hyphae due to their strong symbiotic relationship (de Novais et al., 2020; Liu et al., 2020, 2021). Burrows and Pfleger (2002) reported that BC species increased arbuscular-mycorrhizal fungal species richness and spore density within the diverse plant community.

5.4.3 C and N transfers vs. C and N in rhizosphere

Interplant interactions via direct/close root contacts led to greater quantities of interplant C transfer, which were positively correlated with C in the rhizosphere soil surrounding the roots (Figure 5.9). Roots

are the main source of soil C inputs, and a substantial share of such inputs are added as a variety of exudates (Jones et al., 2009). Thus, we can surmise that greater extents of interplant C transfer and subsequent higher quantities of recently plant-assimilated C ending up in the rhizosphere soil are beneficial for soil C gains. This finding also aligns with the recently reported plant-derived C input, which was promoted by the C transfer in the similar prairie plant community (Kravchenko et al., 2021). The ^{13}C excesses in recipient roots were not associated with those in rhizosphere soils in the presence of barriers (Figure 5.9A), suggesting that an availability of direct/close root contacts is instrumental to this type of soil enrichment with recently assimilated plant C.

The trend of plant-derived N input was similar to that of the C input, as input sources were expected to be shared as rhizodeposits, exudates, decomposed root, and symbiotic fungal biomass (Jones et al., 2004; Badri and Vivanco, 2009). However, unlike the negligible fungal-based C transfer and its subsequent soil input, the substantial N transfer to the N-enriched statuses through mycorrhizal networks could release N into soil while the transfer (Figure 5.8E and 5.8F). Positive associations of ^{15}N excesses between roots and rhizosphere soils can support the plant-derived N input while the fungal-based transfer (Figure 5.9B).

5.4.4 Changes in pore size distributions

The response of pore size distributions within the rhizobox dividers to recipient conditions and barrier effects followed the pattern of root-based C transfer. Specifically, increases in the volume of finer pores (8-30 μm Ø) and decreases in that of coarser pores (>150 μm Ø) compared to those of the no-plant controls were pronounced with two N-enriched statuses, i.e., BES+N and Co-BC (Figure 5.10B and 5.10C). Such modifications in the pore structure could be attributed to the reorganization of soil particles, as image-based porosity did not differ among all recipient conditions or between the presence and absence of barriers (Figure 5.11). Root activity was possibly the major factor for the modification in the pore structure. Root growth is known to lead soil compaction, and after its senescence and shrinking, air gaps were subsequently formed in close proximity to the root (Lucas et al., 2019; Phalempin et al., 2021; Lee et al., 2023b). Such air gaps can contribute to the formation of finer pores around the root (Aravena et al., 2011; Liu et al., 2022b). This physical compaction also leads either full or partial collapsing of coarser pores, possibly

converting them into finer pores (Aravena et al., 2011; Pandey et al., 2021). Moreover, root exudates and rhizodeposits, combined with soil moisture fluctuations by root water uptake, likely enhance the formation of finer pores and rearrange the coarse pore space (Oburger and Schmidt, 2016; Jin et al., 2017). Indeed, recipient BES root biomass was greater under the N fertilization (Figure 5.2D, 5.2E, and 5.2F), and the source SG roots were also grown towards the N-enriched statuses (Figure 5.5C and 5.5D). The observed positive correlations between root residues and the formation of finer pores, alongside the reduction in coarser pores, can strongly support the influence of root growth in the pore structure modification (Figure 5.12).

Fungi are also known to influence the pore structure in soil, and approximately doubled volume of pores > 10 μm Ø was reported when fungi were accessible to soil as compared to that in fungal-inaccessible soils (Feeney et al., 2006; Hallett et al., 2009). This aligns with the increases in finer pores and decreases in coarser pores with root-exlcusive barriers between the source SG and BES+N (Figure 5.10B), where roots of the source plant were located close to the barrier (Figure 5.5C).

Such pores < 30 μm Ø are known to have a smaller microbial community size and oxygen supply due to their size limit (Bailey et al., 2017; Kravchenko et al., 2019a; Franklin et al., 2021), while pores in 30-150 μm size are often found to be associated with high microbial abundance and activity (Nunan et al., 2003; Strong et al., 2004; Li et al., 2024). In this study, root-based transfers included the transfer mechanism through mycorrhizae (Figure 5.1A), and such finer pores are accessible to fungal hyphae grown from roots (Smith and Smith, 2011). Therefore, soils with artificial and natural N enrichment, i.e., under BES+N and Co-BC status, that enhance C transfers, may promote C accumulation in those newly formed finer pores (Figure 5.7B, 5.7C, 5.10B, and 5.10C). A recent study by Quigley and Kravchenko (2022) demonstrated positive associations between root-derived C and fine pores, which were not accessible to roots, suggesting fungi-derived C could enter these pores and be protected from further decomposition.

5.5 Conclusions

This study reveals that root-based C and N transfer to recipient roots were strongly affected by spatial variability of soil N, as roots of source plants were grown towards to this N-enriched location, which could be achieved by applying N directly into plants or growing legume plants. Only root-based transfer mechanism led to notable increases in C within the rhizosphere soils, while N in rhizosphere soils increased even by fungal-based transfer mechanism. The preferential root growth of the source plants towards the available soil N led to the formation of fine pores there, and those newly formed fine pores could possibly provide the protective storage for the rhizosphere C inputs. Even though N fertilization promoted greater C and N exchanges compared to the legume plant growing, this is not the usual case for native prairie. Therefore, this study suggests legume species involved in the prairie vegetation could be promising to promote C and N exchanges and concomitant soil C accumulation within the prairie community.

5.6 Acknowledgements

I appreciate Mark Rivers for conducting soil core scanning at Argonne National Laboratory and Maxwell Oerther and Tayler Ulbrich for assistance with sample collection. Support for this research was provided by the Great Lakes Bioenergy Research Center, U.S. Department of Energy, Office of Science, Office of Biological and Environmental Research (Award DE-SC0018409), by the National Science Foundation Long-term Ecological Research Program (DEB 2224712) at the Kellogg Biological Station, and by Michigan State University AgBioResearch.

REFERENCES

Abadi, M., P. Barham, J. Chen, Z. Chen, A. Davis, J. Dean, M. Devin, et al. (2016). TensorFlow: A System for Large-Scale Machine Learning. 265–283.

Aibara, I., and K. Miwa. (2014). Strategies for Optimization of Mineral Nutrient Transport in Plants: Multilevel Regulation of Nutrient-Dependent Dynamics of Root Architecture and Transporter Activity. *Plant and Cell Physiology* 55: 2027–2036.

An, Q.-Q., S.-Q. Wang, J.-Y. Kang, Z. Wang, Y.-L. Chen, and B.-C. Xu. (2022). Fine root distribution and morphological characteristics of switchgrass under different row spacings on semi-arid Loess Plateau, China. *Archives of Agronomy and Soil Science* 68: 1–17.

Aravena, J. E., M. Berli, T. A. Ghezzehei, and S. W. Tyler. (2011). Effects of Root-Induced Compaction on Rhizosphere Hydraulic Properties - X-ray Microtomography Imaging and Numerical Simulations. *Environmental Science & Technology* 45: 425–431.

Ayres, E., K. M. Dromph, R. Cook, N. Ostle, and R. D. Bardgett. (2007). The influence of below-ground herbivory and defoliation of a legume on nitrogen transfer to neighbouring plants. *Functional Ecology* 21: 256–263.

Badri, D. V., and J. M. Vivanco. (2009). Regulation and function of root exudates. *Plant, Cell & Environment* 32: 666–681.

Bailey, V. L., A. P. Smith, M. Tfaily, S. J. Fansler, and B. Bond-Lamberty. (2017). Differences in soluble organic carbon chemistry in pore waters sampled from different pore size domains. *Soil Biology and Biochemistry* 107: 133–143.

Bauhus, J., and C. Messier. (1999). Soil exploitation strategies of fine roots in different tree species of the southern boreal forest of eastern Canada. *Canadian Journal of Forest Research* 29: 260–273.

Beare, R., B. Lowekamp, and Z. Yaniv. (2018). Image Segmentation, Registration and Characterization in R with SimpleITK. *Journal of Statistical Software* 86: 8.

Bengough, A. G., K. Loades, and B. M. McKenzie. (2016). Root hairs aid soil penetration by anchoring the root surface to pore walls. *Journal of Experimental Botany* 67: 1071–1078.

Boer, M. D., J. Santos Teixeira, and K. H. Ten Tusscher. (2020). Modeling of Root Nitrate Responses Suggests Preferential Foraging Arises From the Integration of Demand, Supply and Local Presence Signals. *Frontiers in Plant Science* 11.

Buades, A., B. Coll, and J.-M. Morel. (2011). Non-Local Means Denoising. *Image Processing On Line* 1: 208–212.

Burns, R. G., J. L. DeForest, J. Marxsen, R. L. Sinsabaugh, M. E. Stromberger, M. D. Wallenstein, M. N. Weintraub, and A. Zoppini. (2013). Soil enzymes in a changing environment: Current knowledge and future directions. *Soil Biology and Biochemistry* 58: 216–234.

Burrows, R. L., and F. L. Pfleger. (2002). Host responses to AMF from plots differing in plant diversity. *Plant and Soil* 240: 169–180.

Cahanovitc, R., S. Livne-Luzon, R. Angel, and T. Klein. (2022). Ectomycorrhizal fungi mediate belowground carbon transfer between pines and oaks. *The ISME Journal* 16: 1420–1429.

Carey, E. V., M. J. Marler, and R. M. Callaway. (2004). Mycorrhizae transfer carbon from a native grass to an invasive weed: evidence from stable isotopes and physiology. *Plant Ecology* 172: 133–141.

Carlile, M. J. (1995). The Success of the Hypha and Mycelium. *In* N. A. R. Gow, and G. M. Gadd [eds.], The Growing Fungus, 3–19. Springer Netherlands, Dordrecht.

Chu, G., Q. Shen, Y. Li, J. Zhang, and S. Wang. (2004). Researches on Bi-directional N transfer between the intercropping system of groundnut with rice cultivated in aerobic soil using ~(15)N foliar labelling metho. *Acta Ecologica Sinica* 24: 278–284.

Cox, F., N. Barsoum, E. A. Lilleskov, and M. I. Bidartondo. (2010). Nitrogen availability is a primary determinant of conifer mycorrhizas across complex environmental gradients. *Ecology Letters* 13: 1103–1113.

Darbon, J., A. Cunha, T. F. Chan, S. Osher, and G. J. Jensen. (2008). Fast nonlocal filtering applied to electron cryomicroscopy. 2008 5th IEEE International Symposium on Biomedical Imaging: From Nano to Macro, 1331–1334. IEEE, Paris, France.

De Sena, A., C. A. Madramootoo, and J. K. Whalen. (2023). Nitrogen transfer from root exudates to the rhizobiome: A 15N stem feeding method. *Soil Biology and Biochemistry* 186: 109159.

Doane, T. A., and W. R. Horwáth. (2003). Spectrophotometric Determination of Nitrate with a Single Reagent. *Analytical Letters* 36: 2713–2722.

Doube, M. (2021). Multithreaded two-pass connected components labelling and particle analysis in ImageJ. *Royal Society Open Science* 8: 201784.

Farrar, J. F., and D. L. Jones. (2000). The control of carbon acquisition by roots. *New Phytologist* 147: 43–53.

Feeney, D. S., J. W. Crawford, T. Daniell, P. D. Hallett, N. Nunan, K. Ritz, M. Rivers, and I. M. Young. (2006). Three-dimensional Microorganization of the Soil–Root–Microbe System. *Microbial Ecology* 52: 151–158.

Franklin, S. M., A. N. Kravchenko, R. Vargas, B. Vasilas, J. J. Fuhrmann, and Y. Jin. (2021). The unexplored role of preferential flow in soil carbon dynamics. *Soil Biology and Biochemistry* 161: 108398.

Fry, B. (2006). Isotope Notation and Measurement. *In* B. Fry [ed.], Stable Isotope Ecology, 21–39. Springer, New York, NY.

Govindarajulu, M., P. E. Pfeffer, H. Jin, J. Abubaker, D. D. Douds, J. W. Allen, H. Bücking, et al. (2005). Nitrogen transfer in the arbuscular mycorrhizal symbiosis. *Nature* 435: 819–823.

Grierson, C., E. Nielsen, T. Ketelaarc, and J. Schiefelbein. (2014). Root Hairs. *The Arabidopsis Book / American Society of Plant Biologists* 12: e0172.

Guan, P., R. Wang, P. Nacry, G. Breton, S. A. Kay, J. L. Pruneda-Paz, A. Davani, and N. M. Crawford. (2014). Nitrate foraging by Arabidopsis roots is mediated by the transcription factor TCP20 through the systemic signaling pathway. *Proceedings of the National Academy of Sciences* 111: 15267–15272.

Hallett, P. D., D. S. Feeney, A. G. Bengough, M. C. Rillig, C. M. Scrimgeour, and I. M. Young. (2009). Disentangling the impact of AM fungi versus roots on soil structure and water transport. *Plant and Soil* 314: 183–196.

He, X. H., C. Critchley, and C. Bledsoe. (2003). Nitrogen transfer within and between plants through common mycorrhizal networks (CMNs). *Critical Reviews In Plant Sciences* 22: 531–567.

Hupe, A., F. Naether, T. Haase, C. Bruns, J. Heß, J. Dyckmans, R. G. Joergensen, and F. Wichern. (2021). Evidence of considerable C and N transfer from peas to cereals via direct root contact but not via mycorrhiza. *Scientific Reports* 11: 11424.

Jin, K., P. J. White, W. R. Whalley, J. Shen, and L. Shi. (2017). Shaping an Optimal Soil by Root–Soil Interaction. *Trends in Plant Science* 22: 823–829.

Jones, D. L., A. Hodge, and Y. Kuzyakov. (2004). Plant and mycorrhizal regulation of rhizodeposition. *New Phytologist* 163: 459–480.

Jones, D. L., C. Nguyen, and R. D. Finlay. (2009). Carbon flow in the rhizosphere: carbon trading at the soil–root interface. *Plant and Soil* 321: 5–33.

Kakraliya, S. K., U. Singh, A. Bohra, K. K. Choudhary, S. Kumar, R. S. Meena, and M. L. Jat. (2018). Nitrogen and Legumes: A Meta-analysis. *In* R. S. Meena, A. Das, G. S. Yadav, and R. Lal [eds.], Legumes for Soil Health and Sustainable Management, 277–314. Springer, Singapore.

Karlovsky, P. (2008). Secondary Metabolites in Soil Ecology. *In* P. Karlovsky [ed.], Secondary Metabolites in Soil Ecology, Soil Biology, 1–19. Springer, Berlin, Heidelberg.

Keiluweit, M., P. S. Nico, M. Kleber, and S. Fendorf. (2016). Are oxygen limitations under recognized regulators of organic carbon turnover in upland soils? *Biogeochemistry* 127: 157–171.

Kellermeier, F., P. Armengaud, T. J. Seditas, J. Danku, D. E. Salt, and A. Amtmann. (2014). Analysis of the Root System Architecture of Arabidopsis Provides a Quantitative Readout of Crosstalk between Nutritional Signals. *The Plant Cell* 26: 1480–1496.

Keymer, A., P. Pimprikar, V. Wewer, C. Huber, M. Brands, S. L. Bucerius, P.-M. Delaux, et al. (2017). Lipid transfer from plants to arbuscular mycorrhiza fungi G. Stacey [ed.],. *eLife* 6: e29107.

Kravchenko, A. N., A. K. Guber, B. S. Razavi, J. Koestel, E. V. Blagodatskaya, and Y. Kuzyakov. (2019a). Spatial patterns of extracellular enzymes: Combining X-ray computed micro-tomography and 2D zymography. *Soil Biology and Biochemistry* 135: 411–419.

Kravchenko, A. N., A. K. Guber, B. S. Razavi, J. Koestel, M. Y. Quigley, G. P. Robertson, and Y. Kuzyakov. (2019b). Microbial spatial footprint as a driver of soil carbon stabilization. *Nature Communications* 10: 3121.

Kravchenko, A. N., H. Zheng, Y. Kuzyakov, G. P. Robertson, and A. K. Guber. (2021). Belowground interplant carbon transfer promotes soil carbon gains in diverse plant communities. *Soil Biology and Biochemistry* 159.

Lal, R. (2016). Soil health and carbon management. *Food and Energy Security* 5: 212–222.

Lange, M., N. Eisenhauer, C. A. Sierra, H. Bessler, C. Engels, R. I. Griffiths, P. G. Mellado-Vázquez, et al. (2015). Plant diversity increases soil microbial activity and soil carbon storage. *Nature Communications* 6: 6707.

Lange, M., E. Koller-France, A. Hildebrandt, Y. Oelmann, W. Wilcke, and G. Gleixner. (2019). Chapter Six - How plant diversity impacts the coupled water, nutrient and carbon cycles. *In* N. Eisenhauer, D. A. Bohan, and A. J. Dumbrell [eds.], Advances in Ecological Research, Mechanisms underlying the relationship between biodiversity and ecosystem function, 185–219. Academic Press.

Lee, J. H., M. Lucas, A. K. Guber, and A. N. Kravchenko. (2023a). Pore structure in detritusphere of soils under switchgrass and restored prairie vegetation community. *TechRxiv*.

Lee, J. H., M. Lucas, A. K. Guber, X. Li, and A. N. Kravchenko. (2023b). Interactions among soil texture, pore structure, and labile carbon influence soil carbon gains. *Geoderma* 439: 116675.

Li, Z., A. N. Kravchenko, A. Cupples, A. K. Guber, Y. Kuzyakov, G. Philip Robertson, and E. Blagodatskaya. (2024). Composition and metabolism of microbial communities in soil pores. *Nature Communications* 15: 3578.

Liu, A., Y.-S. Ku, C. A. Contador, and H.-M. Lam. (2020). The Impacts of Domestication and Agricultural Practices on Legume Nutrient Acquisition Through Symbiosis With Rhizobia and Arbuscular Mycorrhizal Fungi. *Frontiers in Genetics* 11.

Liu, H., Y. Wu, H. Xu, Z. Ai, J. Zhang, G. Liu, and S. Xue. (2021). N enrichment affects the arbuscular mycorrhizal fungi-mediated relationship between a C4 grass and a legume. *Plant Physiology* 187: 1519–1533.

Liu, Y., S. E. Evans, M. L. Friesen, and L. K. Tiemann. (2022a). Root exudates shift how N mineralization and N fixation contribute to the plant-available N supply in low fertility soils. *Soil Biology and Biochemistry* 165: 108541.

Liu, Y.-F., L.-C. Meng, Z. Huang, Z.-H. Shi, and G.-L. Wu. (2022b). Contribution of fine roots mechanical property of Poaceae grasses to soil erosion resistance on the Loess Plateau. *Geoderma* 426: 116122.

López-Bucio, J., A. Cruz-Ramírez, and L. Herrera-Estrella. (2003). The role of nutrient availability in regulating root architecture. *Current Opinion in Plant Biology* 6: 280–287.

López-Pedrosa, A., M. González-Guerrero, A. Valderas, C. Azcón-Aguilar, and N. Ferrol. (2006). *GintAMT1* encodes a functional high-affinity ammonium transporter that is expressed in the extraradical mycelium of *Glomus intraradices*. *Fungal Genetics and Biology* 43: 102–110.

Lucas, M., S. Schlüter, H.-J. Vogel, and D. Vetterlein. (2019). Roots compact the surrounding soil depending on the structures they encounter. *Scientific Reports* 9: 16236.

Luo, X., Y. Liu, S. Li, and X. He. (2023). Interplant carbon and nitrogen transfers mediated by common arbuscular mycorrhizal networks: beneficial pathways for system functionality. *Frontiers in Plant Science* 14.

Makovetsky, R., N. Piche, and M. Marsh. (2018). Dragonfly as a Platform for Easy Image-based Deep Learning Applications. *Microscopy and Microanalysis* 24: 532–533.

Martins, M. A. (1993). The role of the external mycelium of arbuscular mycorrhizal fungi in the carbon transfer process between plants. *Mycological Research* 97: 807–810.

Meier, I. C., A. C. Finzi, and R. P. Phillips. (2017). Root exudates increase N availability by stimulating microbial turnover of fast-cycling N pools. *Soil Biology and Biochemistry* 106: 119–128.

Miller, R. M., J. D. Jastrow, and D. R. Reinhardt. (1995). External hyphal production of vesicular-arbuscular mycorrhizal fungi in pasture and tallgrass prairie communities. *Oecologia* 103: 17–23.

Mounier, E., M. Pervent, K. Ljung, A. Gojon, and P. Nacry. (2014). Auxin-mediated nitrate signalling by NRT1.1 participates in the adaptive response of Arabidopsis root architecture to the spatial heterogeneity of nitrate availability. *Plant, Cell & Environment* 37: 162–174.

Mulder, C., A. Jumpponen, P. Högberg, and K. Huss-Danell. (2002). How plant diversity and legumes affect nitrogen dynamics in experimental grassland communities. *Oecologia* 133: 412–421.

Mulkey, V. R., V. N. Owens, and D. K. Lee. (2006). Management of Switchgrass-Dominated Conservation Reserve Program Lands for Biomass Production in South Dakota. *Crop Science* 46: 712–720.

Muneer, M. A., P. Wang, Zaib-un-Nisa, C. Lin, and B. Ji. (2020a). Potential role of common mycorrhizal networks in improving plant growth and soil physicochemical properties under varying nitrogen levels in a grassland ecosystem. *Global Ecology and Conservation* 24: e01352.

Muneer, M. A., P. Wang, J. Zhang, Y. Li, M. Z. Munir, and B. Ji. (2020b). Formation of Common Mycorrhizal Networks Significantly Affects Plant Biomass and Soil Properties of the Neighboring Plants under Various Nitrogen Levels. *Microorganisms* 8: 230.

de Novais, C. B., C. Sbrana, E. da Conceição Jesus, L. F. M. Rouws, M. Giovannetti, L. Avio, J. O. Siqueira, et al. (2020). Mycorrhizal networks facilitate the colonization of legume roots by a symbiotic nitrogen-fixing bacterium. *Mycorrhiza* 30: 389–396.

Nunan, N., K. Wu, I. M. Young, J. W. Crawford, and K. Ritz. (2003). Spatial distribution of bacterial communities and their relationships with the micro-architecture of soil. *FEMS Microbiology Ecology* 44: 203–215.

Oburger, E., and H. Schmidt. (2016). New Methods To Unravel Rhizosphere Processes. *Trends in Plant Science* 21: 243–255.

Pandey, B. K., G. Huang, R. Bhosale, S. Hartman, C. J. Sturrock, L. Jose, O. C. Martin, et al. (2021). Plant roots sense soil compaction through restricted ethylene diffusion. *Science* 371: 276–280.

Parniske, M. (2008). Arbuscular mycorrhiza: the mother of plant root endosymbioses. *Nature Reviews Microbiology* 6: 763–775.

Perry, S., G. Falvo, S. Mosier, and G. P. Robertson. (2023). Long-term changes in soil carbon and nitrogen fractions in switchgrass, native grasses, and no-till corn bioenergy production systems. *Soil Science Society of America Journal* n/a.

Pfeffer, P. E., D. D. Douds Jr., G. Bécard, and Y. Shachar-Hill. (1999). Carbon Uptake and the Metabolism and Transport of Lipids in an Arbuscular Mycorrhiza1. *Plant Physiology* 120: 587–598.

Pfeffer, P. E., D. D. Douds Jr, H. Bücking, D. P. Schwartz, and Y. Shachar-Hill. (2004). The fungus does not transfer carbon to or between roots in an arbuscular mycorrhizal symbiosis. *New Phytologist* 163: 617–627.

Phalempin, M., E. Lippold, D. Vetterlein, and S. Schlüter. (2021). Soil texture and structure heterogeneity predominantly governs bulk density gradients around roots. *Vadose Zone Journal* 20.

Quigley, M. Y., and A. N. Kravchenko. (2022). Inputs of root-derived carbon into soil and its losses are associated with pore-size distributions. *Geoderma* 410: 115667.

Ren, L., Y. Lou, N. Zhang, X. Zhu, W. Hao, S. Sun, Q. Shen, and G. Xu. (2013). Role of arbuscular mycorrhizal network in carbon and phosphorus transfer between plants. *Biology and Fertility of Soils* 49: 3–11.

Rillig, M. C. (2004a). Arbuscular mycorrhizae and terrestrial ecosystem processes. *Ecology Letters* 7: 740–754.

Rillig, M. C. (2004b). Arbuscular mycorrhizae, glomalin, and soil aggregation. *Canadian Journal of Soil Science* 84: 355–363.

Robinson, D., and A. Fitter. (1999). The magnitude and control of carbon transfer between plants linked by a common mycorrhizal network. *Journal of Experimental Botany* 50: 9–13.

Ronneberger, O., P. Fischer, and T. Brox. (2015). U-Net: Convolutional Networks for Biomedical Image Segmentation. *In* N. Navab, J. Hornegger, W. M. Wells, and A. F. Frangi [eds.], Medical Image Computing and Computer-Assisted Intervention – MICCAI 2015, Lecture Notes in Computer Science, 234–241. Springer International Publishing, Cham.

Roth, R., and U. Paszkowski. (2017). Plant carbon nourishment of arbuscular mycorrhizal fungi. *Current Opinion in Plant Biology* 39: 50–56.

Ruamps, L. S., N. Nunan, and C. Chenu. (2011). Microbial biogeography at the soil pore scale. *Soil Biology and Biochemistry* 43: 280–286.

Ruffel, S., G. Krouk, D. Ristova, D. Shasha, K. D. Birnbaum, and G. M. Coruzzi. (2011). Nitrogen economics of root foraging: Transitive closure of the nitrate–cytokinin relay and distinct systemic signaling for N supply vs. demand. *Proceedings of the National Academy of Sciences* 108: 18524–18529.

Sainju, U. M., B. L. Allen, A. W. Lenssen, and R. P. Ghimire. (2017). Root biomass, root/shoot ratio, and soil water content under perennial grasses with different nitrogen rates. *Field Crops Research* 210: 183–191.

Salvioli di Fossalunga, A., and M. Novero. (2019). To trade in the field: the molecular determinants of arbuscular mycorrhiza nutrient exchange. *Chemical and Biological Technologies in Agriculture* 6: 12.

Sanford, G. R. (2014). Perennial Grasslands Are Essential for Long Term SOC Storage in the Mollisols of the North Central USA. *In* A. E. Hartemink, and K. McSweeney [eds.], Soil Carbon, Progress in Soil Science, 281–288. Springer International Publishing, Cham.

Schindelin, J., I. Arganda-Carreras, E. Frise, V. Kaynig, M. Longair, T. Pietzsch, S. Preibisch, et al. (2012). Fiji: an open-source platform for biological-image analysis. *Nature Methods* 9: 676–682.

Segonzac, C., J.-C. Boyer, E. Ipotesi, W. Szponarski, P. Tillard, B. Touraine, N. Sommerer, et al. (2007). Nitrate Efflux at the Root Plasma Membrane: Identification of an Arabidopsis Excretion Transporter. *The Plant Cell* 19: 3760–3777.

Shao, Z., X. Wang, Q. Gao, H. Zhang, H. Yu, Y. Wang, J. Zhang, et al. (2020). Root Contact between Maize and Alfalfa Facilitates Nitrogen Transfer and Uptake Using Techniques of Foliar 15N-Labeling. *Agronomy* 10: 360.

Shen, K., J. H. C. Cornelissen, Y. Wang, C. Wu, Y. He, J. Ou, Q. Tan, et al. (2020). AM Fungi Alleviate Phosphorus Limitation and Enhance Nutrient Competitiveness of Invasive Plants via Mycorrhizal Networks in Karst Areas. *Frontiers in Ecology and Evolution* 8.

Sinsabaugh, R. L., H. Reynolds, and T. M. Long. (2000). Rapid assay for amidohydrolase (urease) activity in environmental samples. *Soil Biology and Biochemistry* 32: 2095–2097.

Smith, F. A., E. J. Grace, and S. E. Smith. (2009). More than a carbon economy: nutrient trade and ecological sustainability in facultative arbuscular mycorrhizal symbioses. *New Phytologist* 182: 347–358.

Smith, S. E., and F. A. Smith. (2011). Roles of Arbuscular Mycorrhizas in Plant Nutrition and Growth: New Paradigms from Cellular to Ecosystem Scales. *Annual Review of Plant Biology* 62: 227–250.

Sprunger, C. D., and G. Philip Robertson. (2018). Early accumulation of active fraction soil carbon in newly established cellulosic biofuel systems. *Geoderma* 318: 42–51.

Stober, C., E. George, and H. Persson. (2000). Root Growth and Response to Nitrogen. *In* E.-D. Schulze [ed.], Carbon and Nitrogen Cycling in European Forest Ecosystems, 99–121. Springer, Berlin, Heidelberg.

Strong, D. T., H. D. Wever, R. Merckx, and S. Recous. (2004). Spatial location of carbon decomposition in the soil pore system: Spatial location of carbon decomposition. *European Journal of Soil Science* 55: 739–750.

Temperton, V. M., P. N. Mwangi, M. Scherer-Lorenzen, B. Schmid, and N. Buchmann. (2007). Positive interactions between nitrogen-fixing legumes and four different neighbouring species in a biodiversity experiment. *Oecologia* 151: 190–205.

Thilakarathna, M. S., M. S. McElroy, T. Chapagain, Y. A. Papadopoulos, and M. N. Raizada. (2016). Belowground nitrogen transfer from legumes to non-legumes under managed herbaceous cropping systems. A review. *Agronomy for Sustainable Development* 36: 58.

Thilakarathna, R. M. M. S., Y. A. Papadopoulos, A. V. Rodd, A. N. Gunawardena, S. A. E. Fillmore, and B. Prithiviraj. (2012). Characterizing nitrogen transfer from red clover populations to companion bluegrass under field conditions. *Canadian Journal of Plant Science* 92: 1163–1173.

Tian, Y., W. Sun, M. Song, Y. Zhao, S. Wen, Y. Cui, X. Li, and X. Xu. (2021). Effects of grass-legume mixture on plant production and inorganic nitrogen acquisition. *Rhizosphere* 20: 100447.

Tilman, D., P. B. Reich, J. Knops, D. Wedin, T. Mielke, and C. Lehman. (2001). Diversity and Productivity in a Long-Term Grassland Experiment. *Science* 294: 843–845.

Treseder, K. K., and S. R. Holden. (2013). Fungal Carbon Sequestration. *Science* 339: 1528–1529.

Walder, F., and M. G. A. van der Heijden. (2015). Regulation of resource exchange in the arbuscular mycorrhizal symbiosis. *Nature Plants* 1: 1–7.

Walt, S. van der, J. L. Schönberger, J. Nunez-Iglesias, F. Boulogne, J. D. Warner, N. Yager, E. Gouillart, and T. Yu. (2014). scikit-image: image processing in Python. *PeerJ* 2: e453.

Wang, R., M. Wang, K. Chen, S. Wang, L. A. J. Mur, and S. Guo. (2018). Exploring the Roles of Aquaporins in Plant–Microbe Interactions. *Cells* 7: 267.

Wang, S., G. R. Sanford, G. P. Robertson, R. D. Jackson, and K. D. Thelen. (2020). Perennial Bioenergy Crop Yield and Quality Response to Nitrogen Fertilization. *BioEnergy Research* 13: 157–166.

Weidlich, E. W. A., V. M. Temperton, and M. Faget. (2018). Neighbourhood stories: role of neighbour identity, spatial location and order of arrival in legume and non-legume initial interactions. *Plant and Soil* 424: 171–182.

Whiteside, M. D., M. O. Garcia, and K. K. Treseder. (2012). Amino Acid Uptake in Arbuscular Mycorrhizal Plants. *PLOS ONE* 7: e47643.

Wipf, D., F. Krajinski, D. van Tuinen, G. Recorbet, and P.-E. Courty. (2019). Trading on the arbuscular mycorrhiza market: from arbuscules to common mycorrhizal networks. *New Phytologist* 223: 1127–1142.

Yang, Y., D. Tilman, G. Furey, and C. Lehman. (2019). Soil carbon sequestration accelerated by restoration of grassland biodiversity. *Nature Communications* 10: 718.

Yaniv, Z., B. C. Lowekamp, H. J. Johnson, and R. Beare. (2018). SimpleITK Image-Analysis Notebooks: a Collaborative Environment for Education and Reproducible Research. *Journal of Digital Imaging* 31: 290–303.

Zheng, H., A. K. Guber, Y. Kuzyakov, W. Zhang, and A. N. Kravchenko. (2022). Plant species and plant neighbor identity affect associations between plant assimilated C inputs and soil pores. *Geoderma* 407: 115565.

Conclusion

Soil is an important terrestrial compartment acting as a major role in the cycling of carbon (C) in bioenergy cropping systems. This study explored the complex relationships among plant roots, soil physical structure, and microbial interactions and their implications in soil C processing and subsequent accumulation in monoculture switchgrass and polyculture prairie. By utilizing advanced experimental techniques such as flatbed root scanning, X-ray micro-computed tomography (μCT), stable isotope labeling, and *in-situ* root growth analysis, this research provided insights into strategic approaches for optimizing soil C sequestration in switchgrass-based bioenergy cropping systems.

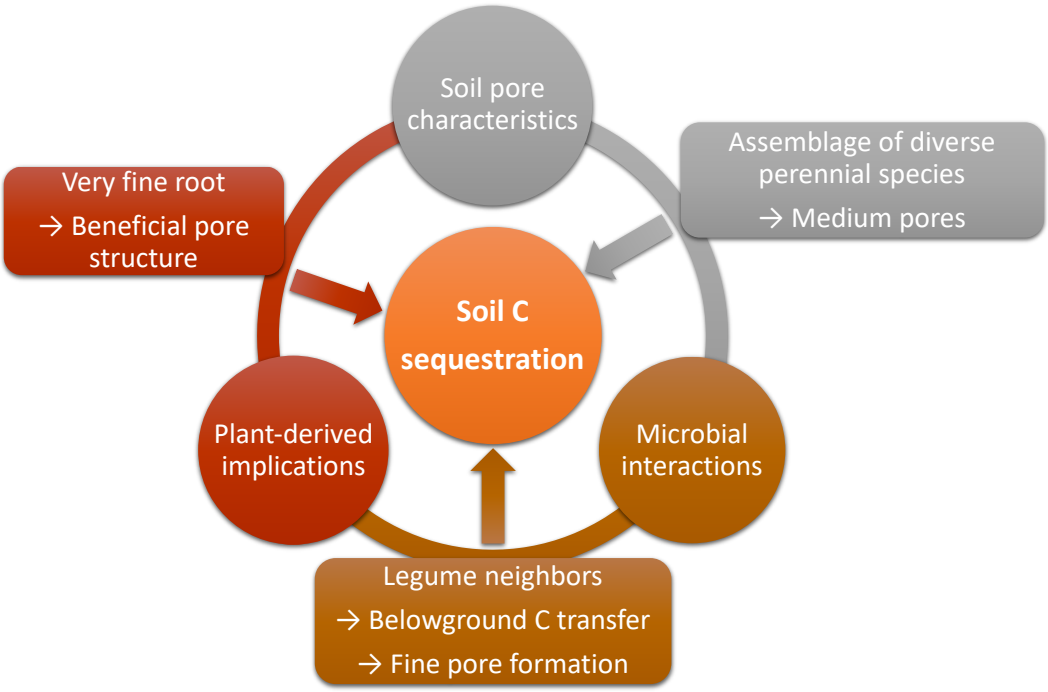

Figure 7.1. Diagram of interconnected factors influencing soil C sequestration in switchgrass-based bioenergy cropping systems.

Key findings of my dissertation research demonstrated that bioenergy crops, particularly the assemblage of diverse perennial species, significantly enhance soil C sequestration by promoting medium-sized pore formation and microbial biomass (Figure 7.1). Results highlighted that prairie vegetation with extensive root system promoted microbial biomass and concomitantly led to soil C accrual. Soil texture and mineralogy played a pivotal role in forming soil pore structures conducive to C sequestration, offering

optimal microbial habitats and facilitating soil C processing. Moreover, switchgrass cultivars with greater volumes of very fine roots positively impacted the formation of the beneficial pore structure, leading to increases in soil microbial biomass and potential C accrual (Figure 7.1). The importance of legume plant species was revealed in belowground root-soil interactions within prairie plant species. Root growth towards N-enriched locations enhanced C and N exchanges within the switchgrass-based perennial plant community, possibly promoting soil C accumulation through the formation of fine pores (Figure 7.1).

In conclusion, my dissertation research advanced the understanding of how bioenergy cropping systems should be managed to enhance soil C sequestration through detailed examination of root traits, soil structure, microbial C processes, and their interactions. It emphasizes the need for in-depth understanding of root-soil interactions to optimize bioenergy cropping systems, maximizing their contribution to soil C sequestration to achieve their ultimate goal, mitigating climate change.

There is a need for further studies on root-soil-microbial interactions to optimize bioenergy cropping systems for maximum soil C sequestration. Field experiments are required focusing on incorporating legume species into switchgrass-based cropping systems to enhance nutrient exchanges without decreases in cellulosic biomass for biofuel production. Additionally, breeding efforts should emphasize developing switchgrass cultivars with root traits that can promote beneficial pore structures.